THE ACTIVE CRYOCUBESAT TECHNOLOGY: ACTIVE THERMAL CONTROL FOR SMALL SATELLITES

by

Lucas S. Anderson

A dissertation submitted in partial fulfillment
of the requirements for the degree

of

DOCTOR OF PHILOSOPHY

in

Electrical Engineering

Approved:

Charles Swenson, Ph.D. Major Professor	Todd Moon, Ph.D. Committee Member
Jacob Gunther, Ph.D. Committee Member	Reyhan Baktur, Ph.D. Committee Member
Thomas Fronk, Ph.D. Committee Member	D. Richard Cutler, Ph.D. Vice Provost of Graduate Studies

UTAH STATE UNIVERSITY
Logan, Utah

2023

ABSTRACT

The Active CryoCubeSat Technology: Active Thermal Control for Small Satellites

by

Lucas S. Anderson, Doctor of Philosophy

Utah State University, 2023

Major Professor: Charles Swenson, Ph.D.
Department: Electrical and Computer Engineering

This research will detail the design and development of the Active CryoCubeSat (ACCS) technology. An advanced active thermal control (ATC) system for CubeSat and Small Satellite platforms. The ACCS is based on a two-stage design, where an integrated tactical cryocooler forms the first stage and a single-phase mechanically pumped fluid loop (MPFL) heat exchanger forms the second. The first stage cryocooler provides cryogenic level cooling to science payloads and advanced LWIR electro-optical detectors, while the second stage MPFL provides bulk thermal power rejection and set-point temperature control. The ACCS leverages advanced 3D printing technologies to form multi-function structures within the satellite bus. This research has developed a ground based prototype of the ACCS system and demonstrated and characterized its performance it in a relevant thermal vacuum environment, raising the ACCS TRL to ∼5. The ACCS team has also developed new systems engineering design methodologies and procedures, along with model-based design tools for the rapid development of ATC's. Ultimately, the ACCS technology will help to enable a new generation of high-powered Small Satellite missions in earth-science, Heliophysics, and deep space.

(306 pages)

PUBLIC ABSTRACT

The Active CryoCubeSat Technology: Active Thermal Control for Small Satellites

Lucas S. Anderson

Modern CubeSats and Small Satellites have advanced in capability to tackle science and technology missions that would usually be reserved for more traditional, large satellites. However, this rapid growth in capability is only possible through the fast-to-production, low-cost, and advanced technology approach used by modern small satellite engineers. Advanced technologies in power generation, energy storage, and high-power density electronics have naturally led to a thermal bottleneck, where CubeSats and Small Satellites can generate more power than they can easily reject. The Active CryoCubeSat (ACCS) is an advanced active thermal control technology (ATC) for Small Satellites and CubeSats, which hopes to help solve this thermal problem. The ACCS technology is based on a two-stage design. An integrated miniature cryocooler forms the first stage, and a single-phase mechanically pumped fluid loop heat exchanger the second. The ACCS leverages advanced 3D manufacturing techniques to integrate the ATC directly into the satellite structure, which helps to improve the performance while simultaneously miniaturizing and simplifying the system. The ACCS system can easily be scaled to mission requirements and can control zonal temperature, bulk thermal rejection, and dynamic heat transfer within a satellite structure. The integrated cryocooler supports cryogenic science payloads such as advanced LWIR electro-optical detectors. The ACCS hopes to enable future advanced CubeSat and Small Satellite missions in earth science, heliophysics, and deep space operations. This dissertation will detail the design, development, and testing of the ACCS system technology.

I would like to dedicate this dissertation to my family and my beloved wife, Sarah.
Without their love and patience, none of this would have been possible.
Thank you...

ACKNOWLEDGMENTS

I would like to thank and acknowledge the ACCS team...

Dr. Swenson for his mentorship throughout all the years,

A.J. Mastropietro and the JPL team for their innovation and support,

The Center for Space Engineering students & faculty for their hard work and help,

I would also like to thank NASA and the Science Technology Mission Directorate (STMD) for funding and believing in this work.

Lucas S. Anderson

CONTENTS

LIST OF TABLES

LIST OF FIGURES

MPFL	Mechanically Pumped Fluid Loop
ISS	International Space Station
CC	Cryocooler
LEO	Low Earth Orbit
ACCS	Active CryoCubeSat
UV	Ultra Violet
IR	Infrared
SWIR	Short Wave IR)
MWIR	Mid-Wave IR
LWIR	Long-Wave IR
UAM	Ultrasonics Additive Manufacturing
UC	Ultrasonic Consolidation
TRL	Technology Readiness Level
HX	Heat Exchanger
PID	Proportional Integral Derivative
COTS	Common Off The Shelf)
ADCS	Atitude Determination And Control
EPS	Electrical Power Systems)
GEVs	General Environmental Verification
CONOP	Concept of Operations
BOM	Bill Of Material
GUI	Graphical User Interface
TVAC	Thermal Vacuum
STMD	Science Technology Mission Directorate
STP	Small Satellite Technology Partnership
USU	Utah State University
JPL	Jet Propulsions Laboratory
MLI	Multi Layer Insulation
SLA	Stereolithography
FDM	Fused Deposition Modeling
DLP	Digital Light Processing
SLS	Selective Laser Sintering
PLA	Polylactic Acid
PEEK	Poly Ether Ketone

CHAPTER 1

The Active CryoCubeSat Project: Introduction, Objectives, Requirements, & Background

We cannot predict the future, but we can invent it

Dennis Gabor

1.1 Thesis Statement

This research proposes a solution to the stated CubeSat "thermal problem" through systems engineering methodologies, model-based design, and the development of innovative technologies.

1.2 Research Overview

Modern CubeSats and Small Satellites have repeatedly proven their worth as scientific testbeds and technology platforms. In fact, there are many current examples of cutting-edge CubeSat missions in heliophysics, earth science, deep space, and lunar operations. In many ways, low-cost, low-risk, fast-to-launch CubeSats are dominating the LEO environment. These advanced CubeSat and Small Satellite platforms employ the latest cutting-edge technologies, including power generation and energy storage, naturally leading to a sharp increase in the overall power density of these small spacecraft. These high-power technologies have directly led to a series of thermal roadblocks. As mission-capable spacecraft sizes shrink and power levels increase, thermal control and rejection capabilities must grow to match the challenge. Equally advanced thermal support technologies are required for the next generation of CubeSats and Small Satellites. Including advancements in passive and active thermal control, single-phase and two-phase heat transfer, and radiator technology. NASA's 2015 Technology roadmap lists thermal management as a critical area of technology development for CubeSats and Small Satellites [4].

This dissertation will detail the design and development of the Active CryoCubeSat (ACCS) technology. An advanced active thermal control technology intended for thermal control and support of high-power payloads as well as zonal and bus-wide temperature management of SmallSat and CubeSat platforms. The ACCS is a single-phase mechanically pumped fluid loop (Closed-Loop MPFL) heat exchanger. A working fluid transports thermal energy from an internal heat exchanger to an external, deployed radiator driven by an advanced micro-pump. Temperatures are maintained by PID control of the relative flow rate, power load, and radiator view factor. The ACCS is a two-stage design with an integrated miniature cryocooler providing direct payload support and cryogenic level cooling to advanced SWIR, MWIR & LWIR electro-optics (2-18 μm). The ACCS also leverages advanced 3D fabrication methods such as Ultrasonic Additive Manufacturing (UAM) [2] and an innovative deployable/tracking radiator. The ACCS technology represents a unique and novel approach to SmallSat thermal control and management. This research will fully characterize the performance of the ACCS system and demonstrate the integrated technology through relevant ground-based testing and raise the NASA Technology Readiness Level (TRL) to ~ 5. This research will leverage contemporary systems engineering methodologies in the development of the ACCS and advance those methodologies to include fundamental thermal analysis and dedicated thermal support subsystems as primary design considerations for future CubeSats and SmallSats. This research will develop high-level analytical tools for rapid-iterative mission design, analysis, and performance prediction. An advanced Thermal Desktop numerical model will also be built to add fidelity to the ACCS design. Ultimately, each of these is critical to the successful development of advanced applications of ACCS technology.

The ACCS development team hopes to enable the next generation of CubeSat and SmallSat spacecraft science by advancing the state-of-the-art in thermal control technology, paving the road for future thermal control technology development. Such as active two-phase systems, advanced radiator technologies, and ultimately, the dynamic end-to-end control of a spacecraft's thermal profile. This chapter will introduce the broader subject of

satellite thermal control and give a background on the various technologies upon which the ACCS is built. Finally, an overview of modern space systems engineering methodologies will be presented, and a discussion of how these practices can be modified to enable advanced smallsat missions through dedicated thermal control.

1.3 Introduction

Satellite technology has been evolving since Sputnik, and while traditional satellites have helped to bring the human era into the modern age, it's very possible that a new generation of advanced small satellites might take us even further. CubeSats, first coined in 1999 [5,6] as an academic learning tool, are limited in volume to multiples of a standard 1U volume (1 liter or 10 cm on a side). CubeSats can range in size from 1U to 12U and beyond, see figure 1.1, and rely on modern miniaturized technology, a standard layout, COTS parts, and a system's engineering low-cost/fast development model. Another advantage for CubeSats is utilizing a standardized launch package and rideshare approach, which helps lead to a low-cost launch industry. In the last 20 years, CubeSats have developed into a thriving and rapidly evolving industry, with modern CubeSats taking on advanced missions previously only thought possible with large, costly, traditional satellites. As of May 2018, more than $\sim$ 2100 CubeSats [7] are currently flying low earth missions in observation, communication, remote earth and helio science, and in situ atmospheric measurements. Recently CubeSats have been taking deep space by storm [8] with proposed lunar missions such as the Lunar Flashlight and IceCube missions [9, 10] and the success of the Martian Mars Cube One, or MarCO-A & MarCO-B CubeSats [11, 12].

CubeSats technology advancements include an array of powerful and miniaturized systems, including onboard propulsion, communications and radar, miniaturized cryogenic cryocoolers, and a relative suite of advanced scientific instruments. Chief among these new technologies are large multi-axis deployable solar arrays with greatly improved efficiencies and high-density energy storage methods. Because of this, a modern 6U CubeSat, or larger, is more than capable of generating over 100 W of power [13,14]. As CubeSats tackle more diverse power-intensive missions and advanced payloads require strict thermally sta-

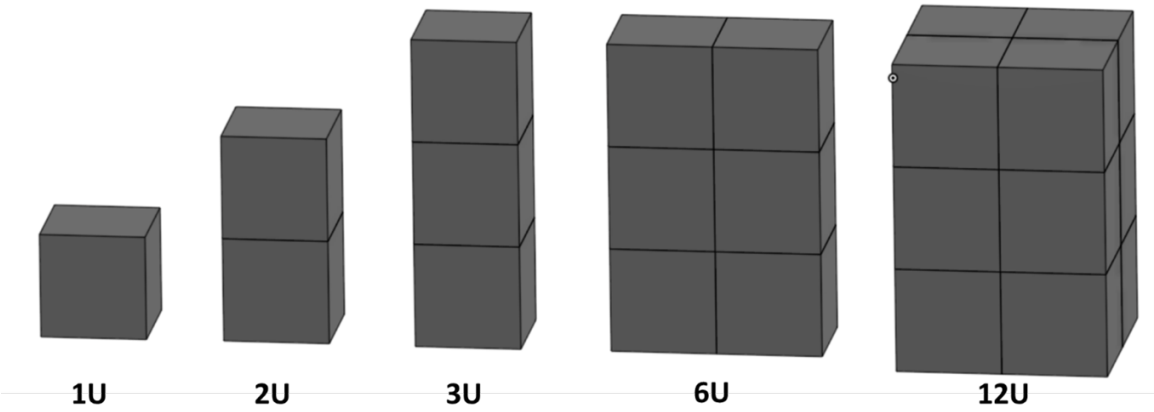

Fig. 1.1: CubeSat Standard size reference. 1U to 12U.

ble onboard environments, a *"Thermal Problem"* is quickly developing within the CubeSat industry.

Traditional techniques of satellite thermal control often rely on passive methods, in that no additional energy is required to operate the systems or manage and reject thermal energy. These passive methods include optical surface properties, special paints, louvers, internal conductive paths, and two-phase heat pipe technologies [15]. While these technologies have been miniaturized from more traditional satellite applications, they are, in many ways, inadequate for the new generation of high-power CubeSats. A potential solution lies in the realm of active thermal control. Active thermal management utilizes power to reject and control thermal energy. These technologies include electric heaters, fluid loop heat exchangers (both single-phase & two-phase), and thermoelectric coolers [16]. Active thermal control has many advantages over traditional passive methods, the biggest of which is scaled and feedback-controlled thermal management. Power rejection can be tuned with active thermal control, and onboard thermal environments can be continuously adjusted to meet mission requirements. In addition, thermal energy can be transported over large distances from internal sources to external radiators while minimizing and controlling thermal gradients.

While active thermal control systems offer a promising solution to advanced power-intensive CubeSat missions, they exist as complex standalone systems while simultaneously

interacting with the satellite as a whole. Because of this, they offer their own unique challenges and require a new design paradigm to implement successfully. This research will explore the design of these complex systems and provide a roadmap for their development.

1.4 ACCS Operational Concept

Fundamentally, the ACCS is an active thermal control technology designed to support advanced high-power CubeSat missions. Based on a single-phase, closed-loop MPFL heat exchanger design and a dedicated radiator, the ACCS leverages advanced COTS technologies such as miniaturized "Canned" micro-pumps, ultra-low viscosity thermal heat transfer fluids, and novel 3D printing techniques. As an active system, the ACCS offers controlled thermal management and scalable performance in support of SmallSat payloads as well as bus-wide thermal and temperature control. The ACCS is capable of rejecting more than 115 W of thermal load from a 6U radiator at temperatures below the electronic operational limit of 60 C. The power cost of the ACCS system can be as low as 1-2.5 W. A power input to output ratio of up to 1/100. This iteration of the ACCS is composed of a two-stage design. The first stage of the ACCS is formed by an integrated miniature cryocooler, which provides direct cryogenic cooling to an analog LWIR/MWIR electro-optical detector. The second stage consists of the MPFL, which provides direct thermal support to the integrated cryocooler and maintains an ideal rejection temperature for the cryocooler. The ACCS is designed to operate as a thermal support utility to the spacecraft avionics system. Similar to ADCS, EPS, and Comms. A block diagram of the ACCS operational concept is given below in figure 1.2.

The miniature Ricor K508N tactical cryocooler forms the first stage of the ACCS system. The K508N is a Stirling cycle-based cryogenic cooler capable of cold tip rejections of more than 500 mW at cryogenic temperatures of 77K [17, 18]. This miniature cryocooler is an ideal low-cost, low-power, high-performance SmallSat solution for onboard cryogenic instrumentation. It is also suitable for integration with the ACCS system as they both represent a distinct design methodology for low-cost, rapid design and direct support of CubeSat payloads. The second stage of the ACCS operates as a closed-loop liquid heat

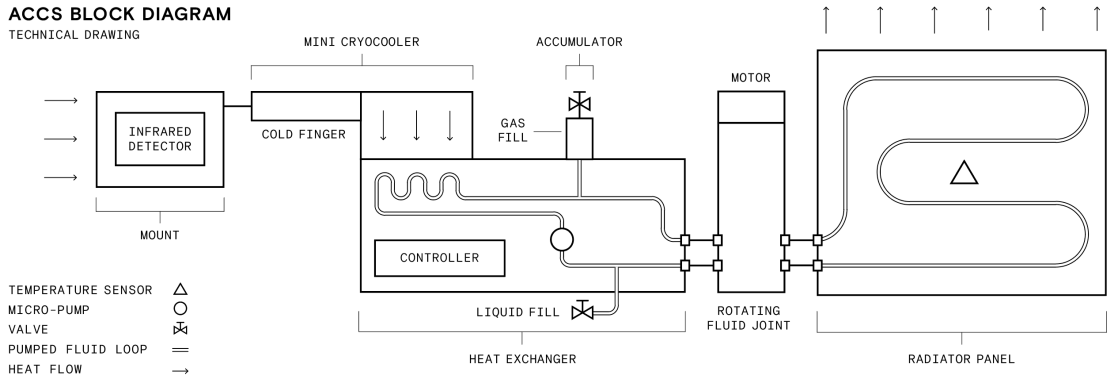

Fig. 1.2: High-level ACCS operational concept.

exchange system. A TCS M510 centrifugal micro-pump circulates a low-viscosity thermal transfer fluid, 3M's Novec 7000, in a closed loop between an internal cold plate heat exchanger and a dedicated radiator. A fluid accumulator compensates for the incompressible expansion/contraction of the fluid as the thermal system varies in temperature and provides a fluid reservoir for any long-term small leaks. The baseline temperature of the system is defined by the physical size of the radiator, its optical properties, and the total thermal power rejected by the ACCS system. The MPFL operates as a variable thermal resistor. By varying the flow rate of the working fluid and by toggling between laminar, transitional, and turbulent flow regimes, the internal rejection temperature of the ACCS heat exchanger can be set at some consistent point above that of the radiator, which operates as the coldest point within the ACCS loop. The ACCS ideally operates in a hot-biased fashion. The radiator and MPFL system is designed for the hottest scenario. Integrated guard heaters provide additional thermal support to the ACCS system as needed. In addition, the pump itself can be operated in a high-power mode to provide additional thermal support. Dual pumps can be used for redundancy and to improve mission lifetime. The second stage ACCS MPFL provides thermal support and an ideal operating environment to the integrated, first-stage Ricor K508N cryocooler.

The ACCS utilizes advanced 3D UAM [19], which has made the integration of an MPFL into a SmallSat platform possible. UAM is uniquely capable of embedding channels and

voids directly into a solid metallic body. This allows for the creation of designs that would otherwise be impossible with traditional fabrication and 3D printing techniques. UAM is used to embed the ACCS MPFL working fluid channels directly into the heat exchanger, spacecraft chassis/structure, and radiator, helping to significantly miniaturize and simplify the system while reducing the overall number of seals (soft & hard) and hard welds. UAM enables an overall more leak-tight system. These custom, multifunction thermal support structures reduce the overall cost and development time for the ACCS technology and allow for rapid design iteration, which is an ideal methodology for CubeSat and Small Satellite system engineering. Because UAM results in a solid metallic body of aluminum, copper, etc., the overall thermal performance and heat transfer efficiency of UAM is also greatly improved.

1.5 Funding & Support

The ACCS research began with an original proposal by Dr. Charles Swenson of Utah State University (USU) and A.J. Mastropietro, Jet Propulsions Laboratory (JPL). This proposal outlined a new and innovative active thermal control technology for CubeSats and Small Satellites as defined by NASA's 2015 technology roadmap, TX14: "Thermal Management Systems." Funded through NASA's Space Technology Mission Directorate (STMD) and the SmallSat Technology Partnership (STP) program, the ACCS is a collaborative project between USU and JPL. Utah State University provided primary development, facilities, and student support, while JPL provided expertise on space-based MPFLs and UAM manufacturing.

1.6 Research Objectives

The high-level objectives of the ACCS research stem directly from NASA's 2015 technology roadmap taxonomy section 14, "Thermal Management Systems" [20]:

"This area (TX:14) covers technologies for acquiring, transporting, and rejecting heat, as well as insulating and controlling the flow of heat to maintain temperatures within specified limits."

This roadmap and the subsequent ACCS objectives are based on the current state of the industry and the anticipated future needs of the SmallSat community. The high-level "qualitative" objectives of the Active CryoCubeSat are given below in Table 1.1. The quantitative goals and requirements of the ACCS project are shown in Table 1.2.

ACCS Qualitative Objectives	
1.	*To advance the capabilities of Small Satellites by developing novel active thermal control technologies.* • *Develop a miniaturized single-phase mechanically pumped fluid loop heat transfer system for CubeSats 6U or larger.* • *Advance the TRL of COTS low-power, high-flow micro-pumps appropriate for aerospace applications.* • *Advance the use of COTS thermal transfer fluids (3M Novec 7000) for CubeSat MPFL applications.* • *Demonstrate dynamic & static soft-rubber O-rings for spacecraft sealing applications.* • *Utilize advanced UAM 3D fabrication techniques to create novel multifunctional structural elements, miniature flow paths, and thermal, structural components for CubeSats.* • *Develop an internal UAM multifunctional heat exchanger and a deployable UAM radiator.* • *Demonstrate the thermal accommodation of a miniature cryocooler for advanced CubeSat LWIR & MWIR electro-optical instrumentation.*
2.	*Integrate novel technologies into a relevant ground-based test bench and demonstrate/characterize the system to GEVS standards and an overall TRL level of ~5.* • *Relevant thermal vacuum characterization and technology demonstration.*
3.	*To develop aerospace systems engineering methodologies for the design and implementation of space-vehicle active thermal control* • *To develop analytical and numerical tools for the rapid design & iteration of aerospace & SmallSat single-phase MPFL based heat transfer systems*
4.	• *Enable a new generation of advanced CubeSats and Small Satellites for earth science, heliophysics, deep space, and lunar missions through active thermal control.*

Table 1.1: Proposed ACCS Research Objectives.

Simply put, the ACCS hopes to develop a new family of active thermal control technology for CubeSats and Small Satellites, as well as the tools and methodologies for their design and development.

1.7 ACCS Significance & Developed Technologies

The ACCS technology is the first of its kind and represents a significant improvement over the current state of the art for CubeSat and Small Satellite thermal management. In

ACCS Quantitative Project Objectives & Requirements	
Required Performance	**Performance Goal**
MPFL	
Thermal Load: > 30 W Interface: 20-30°C Power: < 4 W Mass: < 2 kg Volume: < 1U	Thermal Load: > 60 W Interface: 10-30°C Power: < 0.3 W Mass: < 0.5 kg Volume: < 0.3U
Additive Manufacturing	
10cm x 10cm HX Panel 20cm x 30cm Radiator Panel	10cm x 10cm HX Panel 20cm x 30cm Radiator Panel
Cryocooler	
Temperature: < 100K Thermal Load: > 50 mW Power: < 15 W Mass: < 1 kg Volume: < 1U	Temperature: < 75K Thermal Load: > 250 mW Power: < 5 W Mass: < 0.2 kg Volume: < 0.3U

Table 1.2: ACCS "Quantitative" Research Objectives & Goals.

addition, as an active thermal control technology, the ACCS promises to provide a direct, scalable and controllable solution to CubeSat thermal management and a unique addition to NASA's thermal management taxonomy. Traditionally, satellite thermal control is often overlooked. Therefore, by developing a dedicated active thermal control subsystem that can be integrated directly into the spacecraft bus and be considered an integrated component of the space vehicle's onboard subsystems, the ACCS offers a critical contribution to SmallSat technology and capabilities. The ACCS represents a thermal first approach to spacecraft design. Including active thermal control as a fundamental technology service in Phase-A design, will help to improve mission success and prevent costly redesigns later in a satellite's life cycle. The system engineering design methodologies developed in this work and the first-principle analytical design tools and thermal desktop numerical models are innovative and represent an important addition to aerospace systems engineering and model-based design.

Mechanically pumped fluid loops are standard and relatively straightforward in design and implementation on the ground. However, MPFL's are rare and incredibly difficult to implement in space and are unheard of on Small Satellites. In fact, until recently, the very concept of a CubeSat MPFL did not exist [21–25]. The difficulty is in miniaturizing and simplifying the fluid flow path to such an extent that it does not represent a significant

impact on the SmallSat internal system. Additive manufacturing, specifically UAM, offers a unique solution to this problem along with multifunctional thermal design and novel CubeSat structural development. Appropriate COTS components, including a CANNED low-power, high-flow micro-pump, a miniaturized fluid accumulator, purge and fill system, and a suitable low-viscosity thermal heat transfer fluid, are also required. Each represents a significant effort in COTS trade studies and down selection. The COTS technologies selected for the ACCS represent some of the best and most appropriate technologies currently available for SmallSat applications. Ultimately, this work has the potential to inform a new family of advanced active thermal management technologies for CubeSats and will help to enable a new generation of advanced CubeSat missions.

The ACCS features several innovative technologies for Small Spacecraft systems, summarized below. These technologies represent a novel and essential step in CubeSat/SmallSat development.

- Closed-loop Single-Phase MPFL heat exchanger systems..
  - A unique heat transfer fluid. 3M's Novec 7000 series liquids.
  - A TCS low-power, high-flow CANNED Centrifugal Micro-Pump (M510).
  - Integration and UAM-HX thermal accommodation of an advanced miniature Stirling Ricor K508N tactical cryocooler.
- Advanced UAM fabrication technology.
  - Miniaturize and simplify the MPFL fluid system.
  - Multifunctional thermal structures.

1.8 Research Scope & Methodology

This research aims to design, develop, and validate the ACCS active thermal control technology. Including a NASA GEV's demonstration of the technology in a relevant ground-based thermal vacuum environment, which will raise the ACCS technology to a TRL of ~ 5. The deliverables of the ACCS research are given below and are driven by the ACCS

objectives, the section above. The development process and research methodology for the ACCS system are laid out below as a step-by-step process. This dissertation represents the culmination of the ACCS technology development. Numerous papers and presentations have been published as supplemental material for this dissertation, see the vitae at the end of this dissertation.

Research Deliverables:

- Design and develop the ACCS active thermal control technology.
  - Built a highly instrumented test-cube for relevant ground-based characterization.
  - Performed relevant TVAC ground testing to TRL ~ 5.
  - Analyzed the performance and behavior data of the ACCS system.
    - Created ACCS data products.
  - Validated model-based tools from experimental data.
- System's engineering design methodologies for Active MPFL thermal control systems.
  - Created several new and innovative systems engineering methodologies, procedures, and processes for the development of active thermal control technologies like the ACCS.
  - Created Model-based design tools.
    - Excel (VBA) based analytical design tools.
      - Rapid, iterative tool for pre-phase-A design.
    - Numerical Thermal Desktop model.
      - Detailed analysis of performance and behavior for Phase-A design.

The ACCS research process began with an in-depth review of the current state-of-the-art in thermal management technologies for CubeSats. This literature review helped inform the design, objectives, and scope of the ACCS project. From this review, a series of design methodologies were developed and used to create a basic concept of operations

for the ACCS system. These methodologies were based on classical systems engineering principles and the concepts of model-based design. Next, the performance goals of the ACCS system were defined to best solve the stated CubeSat thermal problem. The ACCS objectives, requirements, and deliverables were extrapolated from the basic CONOPS and defined into a coherent framework. From the ACCS CONOPS, a series of first principle, interconnected, steady-state, thermal analytical models were developed in excel to predict the performance of the ACCS system and provide a rapid, iterative design tool for the ACCS system. These models can predict the performance of each of the ACCS technology's major subsystems and provide a simple design tool for many of the components. This analytical model consists of a detailed space environment model, a flat plate orbital radiator model, 1-D & 2-D conduction models, convective transport models, radiation and view factor calculators, resistive networks, near and far-field parasitic models, as well as insulation and contactor models. Each of these models will be coupled with various optical and thermal databases and integrated into a set of excel tools. This allows for any change within one model or a database to be tracked and propagated through the entire system. Excel is uniquely fitted for the task of model-based design due to its GUI interface and widespread use. A Thermal Desktop numerical model was also created to explore the behavior of the ACCS in more detail. This numerical model included transient, steady-state, radiative, and 2D/3D modeling of the ACCS system and provided far greater detail and insight into the characteristics of the ACCS system.

An essential aspect of CubeSat design is the use of Common Off The Shelf (COTS) parts. Many of the critical components of the ACCS system are COTS. These include the Miniaturized Ricor K508N tactical cryocooler, the TCS M510 Micro-pump, and the 3M Novec 7000 working fluid. A comprehensive and detailed trade study on the various critical COTS components for the ACCS system was performed. Parts that satisfied all requirements were down-selected and formed into Bills of Materials (BOMs). Next, a detailed test plan for the NASA GEV's TVAC technology demonstration was outlined, and the lab-based experimental test cube was designed and built. Additional trade studies were performed

for the development of this highly instrumented testbed. USU's Center for Space Engineering KJL TVAC chamber was re-purposed for this technology demonstration. A custom, dedicated electronics box was fabricated for the system-level control of the ACCS system and overall instrumentation data acquisition. The ACCS test cube was manufactured by USU personnel and supported by JPL staff. Ultimately, the ACCS system underwent three different TVAC tests. These tests raised the ACCS technology to a TRL of ~ 5. The TVAC test conducted in June of 2018 represented the first exploration of the ACCS system and demonstrated its behavior and performance benchmarks. A more thorough and systematic test was held in September of that year, supported by JPL staff. This data represents the critical characterization of the ACCS system. Finally, in January, the ACCS was re-tested for the development of a PID feedback & control algorithm. Each of the active and controllable parameters of the ACCS system was impulse tested throughout its total available range. This data was used to develop a PID control algorithm for the ACCS system [26]. A custom MATLAB data analysis code was created to break down the "test-cube" telemetry and create modeling products of the ACCS's performance. This data was also used to validate the model-based design tools developed for the ACCS, including the analytical design tool and the Thermal Desktop numerical model.

This research is a technology development effort and is constrained in both funding and development time. Because of this, the overall scope of the project was limited. The ACCS does not represent a final flight-ready technology, nor has it undergone a complete set of GEV's testing and has not been qualified for flight. In addition, due to the substantial effort required to perform TVAC testing, the ACCS system has not been exercised through all possible performance envelopes. Instead, the limits and extremes of performance have been studied and used to qualify the analytical and numerical design tools. These tools can then be used to further explore the predicted performance of the ACCS system. This dissertation will detail the design, fabrication, and relevant testing/characterization of the ACCS system as well as the development of model-based systems engineering tools. The basic outline of this dissertation is given below.

CHAPTER 2

ACCS Background & Literature Review

To understand our future, we must first understand our past

2.1 Introduction

The Active CryoCubeSat is built on a foundation of existing research, technology, and aerospace experience. This chapter will review the history, background, and relevant literature of the ACCS system, as well as the underlying scientific and engineering theories and methodologies that led to its development. Topics will cover several broad categories beginning with the history and definition of CubeSats & Small Satellites, the fundamental mechanisms and governing laws of heat transfer, and the best practices of aerospace thermal control design. Next, the impact of the thermal space environment on satellite design and the underlying differences between passive and active heat transfer technologies will be discussed, along with how they apply to modern CubeSats and Small Satellites. The fundamental technologies that enabled the ACCS system will also be covered; these include the basics of heat transfer, single-phase MPFLs, closed-loop heat exchangers, cryocooler technology, and advanced next-generation additive 3D printing techniques. Finally, a review of past, current, and future CubeSat/SmallSat missions that would benefit from a convective heat transfer technology like the ACCS will be presented.

In conclusion, this literature review will place the ACCS system within the larger field of thermal management and demonstrate how the current state of the art for Small Satellite thermal control is inadequate to address the next-generation thermal burden of modern CubeSat power generation and storage technologies.

2.2 CubeSat Background

Satellite technology has been evolving since Sputnik, and while traditional satellites have helped to bring the human era into the modern age, the new generation of advanced small satellites and CubeSats might take us even further. CubeSats, First coined in 1999 [27], began as an academic learning tool with limited mission capabilities and scope. The term CubeSat refers to a classification of NanoSatallite that adheres to a strict standard in terms of size, shape, and weight. CubeSats are limited to multiples of 1U (1 liter or 10 cm on a side) and masses of approximately 2 kg per U [5, 28]. CubeSat typically ranges from 1U to 12U, with 24U and larger possible. At a certain point, usually, when the total wet mass exceeds 500 kg [29], CubeSats become classified as Small Satellites. CubeSats are known for their low-cost, high-risk, fast-to-development approach and state-of-the-art modern miniaturized solid-state technologies. CubeSats rely on standardized launch packages called canisters and ride-share opportunities to help reduce the overall cost of development and launch.

The first CubeSats launched in 2003 consisted of a swarm of six 1U satellites. These CubeSats were produced by various universities and government entities with missions ranging from technology demonstrations to amateur radio, tether research, and earthquake detection. In the last 20 years, CubeSats have developed into a thriving and rapidly evolving industry, with modern CubeSats taking on advanced missions previously only thought possible with large, costly, traditional satellites. As of 2018, more than 2100 CubeSats [7] have been launched. Flying low earth missions in Earth observation, communication, remote earth science, and heliophysics. Notable CubeSat missions include: the Earth-observing swarms of Planetary Labs [30], the dual deep space Martian CubeSat's MarCO-A & MarCO-B [11, 12], Lunar-Ice Cube [9, 10], which is monitoring lunar surface ice, and RainCube, an earth-rain monitoring CubeSat with a deployable Ka-band radar [31]. CubeSats are ideal platforms for scientific payloads. Capable of advanced remote (limb & nadir viewing) and in-situ missions for observations of the Earth's surface and atmosphere, CubeSats are also promising for deep space operations to study asteroids and celestial bodies.

Currently, CubeSats are undergoing a revolution in terms of advanced technology development. This includes miniaturized onboard computing, as demonstrated by the new UniBap Onboard Computer system [32, 33], powerful FPGAs, high-data-rate telemetry transceivers, complex deployable solar arrays, and next-generation batteries. CubeSats are also pioneering onboard propulsion, electric, cold gas, and solid state. Currently, CubeSats are limited in mission scope by net power and thermal rejection/control capabilities. However, the next generation of advanced CubeSat buses will generate hundreds of Watts of onboard power and, with the inclusion of Active Thermal Control technologies, be more than capable of matching and managing these thermal loads. The fundamental reason for CubeSat's and Small Satellite's success and track record is the modern systems engineering methodologies used by designers to push the boundaries of technology and mission capabilities.

2.3 Basic Heat Transfer: Theory & Modeling

Thermal energy is a fundamental measurement of a system's internal enthalpy [34]. It is represented by a system's heat or as an absolute temperature. Conversely, heat transfer refers to the exchange of thermal energy between systems and is governed by the laws of thermodynamics. There are five primary types of heat transfer: Conduction, Convection, Radiation, Advection, and Mass Transfer. Each of these is briefly explained below [35, 36].

- Conduction or thermal diffusion is the transfer of thermal energy within and between solid bodies due to the kinetic transfer of energy at a particle/molecular level [37].
- Convection transfers thermal energy between solid and liquid materials due to material heterogeneity and internal body forces [38].
- Radiation is the transfer of thermal energy by electromagnetic waves. Thermal motion of charged particles (protons & electrons) with non-zero temperature generates electromagnetic radiation [39].

- Advection & Mass Transfer is the exchange of thermal energy by the bulk movement of a fluid or a thermal mass.

The ACCS is a closed loop heat transfer system that is governed by the first and second laws of thermodynamics and utilizes all of these heat transfer methods [40, 41]:

- First Law: Energy is conserved. Energy gained or lost by a system is retained by its surroundings.
  - The energy absorbed by the ACCS system must be equally rejected to maintain a stable thermal environment.
- Second Law: The entropy of A closed system must either stay the same or increase.
  - Thermal energy within the ACCS system must flow from hot to cold.

The thermal zones of satellite are connected to the ACCS via high conductivity thermal paths that form boundary inputs. Convective heat transfer couples the ACCS HX body to the MPFL working fluid. Thermal resistors can be used to insulate the system from the satellite bus as a whole, enabling payload-specific thermal zones. The sink for the ACCS system is a deployable radiator used to reject the thermal load of the ACCS system to cold space. An advective link is formed between the internal heat exchanger source and the external radiator sink [42, 43]. The various theories and governing laws of heat transfer are readily available. Numerous texts are dedicated to each of the given methods of heat transfer. For this research, these include, but are not limited to [44–46]. The ACCS system is modeled as a simplified, steady-state, nodal system with conductive, convective, advective, and radiative transfers occurring at each node. The heat transfer equations for the ACCS technology are covered in the theory chapter of this dissertation.

A series of heat transfer model-based tools were created for this research. These include a simplified analytical model for the early-phase rapid iterative design of MPFL ATC systems like the ACCS and a Thermal Desktop (TD) numerical model. The TD model provides high-fidelity, transient heat transfer analysis and predicts the standalone behavior

of the system and the on-orbit performance of a satellite flying the ACCS technology. These systems engineering simulations, when combined, provide an end-to-end set of model-based design tools for the design of ATC's like the ACCS. The ACCS analytical model is created in Excel using VBA as a backbone code source. The TD numerical model uses Sinda Fluent as a heat transfer solver and AutoCAD as a 3D simulation environment. TD also offers an advanced radiative heat transfer and view factor package, which leverages ray tracing and Monte Carlo Techniques [47].

2.4 Satellite Thermal Control

Due to the harsh thermal environment of space, thermal control & management was one of the first subsystems incorporated into satellites. In fact, Sputnik featured the first active thermal control technology as one of its primary subsystems. A dual thermal switch would turn on or off a cooling fan, circulating the pressurized internal atmosphere of the bus to maintain the primary payload's temperature—the iconic radio "beep" transmitter [48]. Since then, thermal control has been an integral part of satellite design. Almost all space vehicles feature some form of thermal control technology, including the pumped fluid loops and deployable tracking radiators of the ISS [49], the cooling bay doors of the space shuttle [50], and even something as simple as the careful selection of a 1U CubeSat's surface properties. There are many excellent examples of satellite thermal design—however, two recent missions stand out. The first is the Parker Solar probe launched in 2018 on a mission to touch the sun. Parker's mission is to sample the outer Corona of the sun directly, a feat that requires an incredible thermal design. The solar probe is shielded from the extreme environment of the sun by an innovative Carbon Composite heat shield, which can withstand temperatures of up to 2,500 F [51]. Without this incredible thermal design, no man-made satellite could withstand the solar environment.

Another example is the James Webb Space Telescope (JWST) [52]. The James Webb is a dual MWIR & LWIR electro-optical telescope for the 0.6 to 28 μm spectral range [53]. With a 6.5 m primary, segmented, hexagonal mirror. The JWST can image distant celestial objects to an incredible level of resolution. The JWST also features an advanced

low-vibration Joule-Thomson cycle Pulse Tube cryocooler which is capable of cooling the primary focal plane detector to as low as 7 K [54]. Because of the JWST's strict thermal requirements; a shadowed L2 orbit was selected with a dedicated radiation shield to prevent any incident solar or IR thermal radiation from effecting the sensitive imaging payloads. The JWST sun-shield is composed of a five-layer deployable multi-layer insulation (MLI) shield that can practically eliminate the environmental load of the earth space environment. The JWST sun-shield can maintain almost a 350 K thermal gradient across its five layers [55]. Both of these are incredible examples of how thermal design can enable otherwise impossible scientific missions and help humanity to explore our universe further. Thermal control for CubeSats and Small Satellites has generally followed a similar pattern to more traditional satellites. Typical CubeSat thermal control techniques include conductive links between internal components and passive radiative surfaces to reject thermal loads [56]. In some cases, heat pipes are integrated to manage areas of high thermal density, such as payload sources, onboard computing, and radio transceivers. Advanced passive techniques such as micro-louvers have even been adapted to CubeSat platforms [57, 58]

The purpose of a satellite's thermal management subsystem is to control the temperature and environment of the bus and payload to an ideal operating range. Despite variations in the space environment, long periods of eclipse, or shifts in the thermal generation as mission parameters change. Both mechanical and electrical systems often require a relatively narrow temperature range to operate effectively, often qualified as a survival range of -40 C to 85 C with an operational range of -20 C to 60 C [59]. Usually, a balance must be struck between the resources and complexity required to maintain a satellite's thermal environment and the mission benefits that control provides. A typical design process for a satellite is outlined in the SMAD text [60], page 691, and in the space systems engineering handbooks [61, 62]. These design methods are considered traditional [63, 64]. However, it is the overall opinion of this research that a new era of dedicated active thermal technologies can rewrite these procedures and methodologies. That modern CubeSat power generation has reached a level that now requires more advanced active thermal control technologies. This

dissertation includes a detailed systems-level review of classic and contemporary thermal control design.

This research has developed a single-phase, closed-loop MPFL-based heat exchanger system capable of rejecting more than 100 W of thermal load from a CubeSat platform. The ACCS technology represents the first step in creating an advanced next-generation CubeSat bus capable of game-changing power generation/storage. A Small Satellite like this would usher in a new era of technology and payload development that would rocket CubeSats and Small Satellites into the forefront of scientific exploration.

2.5 The Space Thermal Environment

The thermal space environment is quite complex, consisting of atmospheric chemistry and dynamics, ionizing radiation, solar and IR electromagnetic radiation, etc [65]. In addition, the lack of atmosphere or connection to other bodies prohibits traditional thermal management methods such as conduction and natural/forced convection. Because of these limitations, the space environment offers several truly unique engineering and design challenges. However, for this research, the space environment will be simplified to a series of three approximate sources and a single sink. These boundaries are defined below. Each source/sink is described in the literature [1, 66–68]. Cassandra Belle VanOutryve From University of San Jose [1], provides an excellent review of the space environment and establishes the thermal space environment for a floating plate in low earth orbit. This article is of particular value to the development of the ACCS system because it provides a simplified model for the deployed ACCS radiator.

- Solar Flux: The sun's electromagnetic, thermal radiation output, given as a flux or power per area. This value depends on the radial distance from the sun, the season, and the solar cycle.

- Earth IR: Also called planet-shine, this is the blackbody IR electromagnetic radiation emitted by a planetary body, typically the Earth. Often defined as an absolute

temperature, this can be converted to flux or a total thermal load via radiation heat transfer equations and geometric view factors.

- Albedo: The solar flux reflected by a celestial body. This value is determined by surface radiative properties and can be converted to flux or total thermal load by geometric calculation.

- Deep Space: The primary method of thermal rejection for a satellite is IR radiation to cold dark space. The radiation heat transfer equations and the total area/surface properties of the satellite's radiating surfaces determine the net value and rate of thermal rejection.

Orbiting satellites experience a thermal balance or equilibrium that is defined by the power/generation of the satellite's thermal/mechanical configuration and the space environment. The structure of the satellite includes its mechanical design, thermal mass, heat capacity, and internal thermal resistance. The radiator design: surface properties, effective area, view factor, equivalent conductance, and isothermallity define the satellite's thermal link to deep space. The zonal temperature of the satellite is a transient to steady-steady state problem that can be solved by an interconnected nodal analysis of the fundamental heat transfer equations and the energy balance defined by the satellite's power generation, sources, and sinks. An essential concept for satellite thermal design is Prevost's law of exchanges, which states, "Every material body, at any temperature above absolute zero, radiates heat to the surroundings and at the same time absorbs heat from the surrounding" [69]. This statement outlines the radiative behavior of multiple interactive bodies in a cold void. It states that a body's radiative heat is defined only by its properties and absolute temperature. The radiative connection to other bodies will determine a body's net thermal load, input vs. output. A satellite's thermal strategy is complicated by large transients introduced by variations in the power profile of the satellite or payload, the heat capacity and mass of the satellite, changes in mission parameters, and long eclipse times as defined by a given orbit. Overall, space thermal design is challenging and quite complex, often requiring a great deal of insight into the systems-level design of the entire satellite,

payload, and mission. Traditionally, thermal design on CubeSats or Small Satellites is left to a late stage of the development effort; this is often a mistake. The thermal design of a satellite should take place early in the design phase, include dedicated technology, and be incorporated into the satellite bus as an avionics subsystem.

2.6 Active vs. Passive Thermal Control

Satellite thermal control can broadly be broken down into two categories: passive vs. active. Traditional satellite thermal design often relies on passive methods, which date back to the very beginning of space thermal design. Passive thermal control techniques require no input energy to operate, manage, or reject thermal energy from within the satellite system. These passive methods include optical surface properties, special paints, louvers, phase-change materials/thermal inertia, internal conductive paths, and two-phase heat pipe technologies [16]. While many of these technologies have been miniaturized from more traditional satellite applications and offer advantages, including simplicity and reliability, they are, in many ways, inadequate for the new generation of high-power CubeSats. In addition, passive thermal control techniques do not often scale up or down easily. A potential solution lies in the realm of active thermal control. Active thermal management utilizes power to reject and control thermal energy. These technologies include electric heaters, fluid loop heat exchangers (both single-phase & two-phase), and thermoelectric coolers. Active thermal control has many advantages over traditional passive methods, the biggest of which is scaled and feedback-controlled thermal management. Power rejection can be scaled to mission requirements with active thermal control, and onboard thermal environments can be continuously tuned to match ideal operating temperatures. In addition, thermal energy can be transported over large distances from internal sources to external radiators while minimizing and controlling thermal gradients [70].

2.7 Mechanically Pumped Fluid Loops In Space

At its heart, the ACCS is a single-phase, closed-loop, mechanically pumped fluid heat exchanger. This type of technology is quite common for terrestrial applications but rare for

traditional space platforms and, until recently, unheard of for CubeSats or Small Satellites. Only in the last few years have MPFL and single-phase ATC technologies for CubeSats been featured in scientific and technology journals [22–25]. Selvadurai [21] provides an overview of the significant engineering challenges associated with adapting MPFLs and ATCS to Small Satellites. The ACCS represents a novel adaptation of MPFL/ATC technology and one of the first practical designs/adaptations for CubeSat and Small Satellite applications.

The underlying physics and governing behavior of pumped fluid loops are well understood and adapt well to microgravity and the space environment. While many design resources exist to aid in the engineering of MPFL ACT systems, the *Design of Fluid Thermal Systems* [71] provides a systematic overview of the working theories and practical considerations of designing a single-phase ATCS, while Selvadurai and Pradeep provide insight into adaptations for the space environment [21, 72]. Several space-based single-phase pumped fluid loops have been previously implemented. These include a dual parallel loop MPFL on the International Space Station [73] in the 1980s. The ISS's internal waste heat is routed through a water-based MPFL to an external loop connected to the ISS's deployed tracking radiator system. The external loop is isolated due to the toxic nature of the Ammonia working fluid and its danger to the crew. The Jet Propulsions Laboratory has pioneered MPFL systems for many of its flagship missions. These include the Mars Path Finder [74], Mars Exploration Rover [75], and Mars Science Laboratory [76]. Each single-phase MPFL ATCS have operated flawlessly and helped enable their missions. The upcoming Europa Clipper mission features a truly astonishing MPFL capable of rejecting more than 500 W during inner cruise flybys and conversely isolate the clipper Heat Rejection System (HRS) to less than 10 W during cold cycles [77, 78]. The European Space Agency is currently developing a high-power, 3 to 6-kW technology demonstration mission flying on the Alphasat satellite featuring an advanced MPFL [79]. Pradeep Bhandari is considered the grandfather of aerospace MPFL systems, and JPL's thermal fluids technology team has pioneered many of the most important and groundbreaking ATCS missions [70, 80].

An important aspect of MPFL design is the choice of working heat transfer fluid. A

great deal of research has been done on heat transfer and convective/advection processes in vacuum and zero/microgravity environments. These include single-phase and two-phase mechanisms, phase-change and open vs. closed loop systems. Aerospace fluids range from water to phase change materials such as liquid metals, paraffin waxes, and refrigerants, solvents, alcohol, and modern engineered heat transfer fluids such as silicone-based oils, dielectric hydrofluorocarbons, and many others [81–83]

2.8 UAM & 3D Printing In Space

The history of additive manufacturing and 3D printing dates back to the 1980s with Hideo Kodama [84], who developed a layer-by-layer printing technique with UV-cured resin. The first 3D technology patent featured the foundation of Stereolithography (SLA) and appeared in 1986 by Charles Hull [85]. Since then, the field of 3D printing has blossomed, with a diverse range of technologies and possible materials. The most common types of non-metallic 3D printing include Fused Deposition Molding (FDM), Stereolithography/Digital Light Processing (DLP), PolyJet, Selective Laser Sintering (SLS), and Multi-Jet Fusion. Each of these technologies is ideal for a wide variety of applications and print in non-metallic materials such as Polylactic Acid (PLA), Acrylonitrile butadiene styrene (ABS), Resin, and Poly Ether Ketone (PEEK) [86, 87]. Metal and mixed metal 3D printing is often ideal for space applications and allow for the design and fabrication of multi-function structures that would otherwise be impossible to produce without additive manufacturing. Metallic 3D printing technologies can broadly be categorized as one of the following: Powder Bed Fusion, Binder Jetting, Direct Energy Deposition, or Metallic Extrusion [88]. Each offers unique advantages. However, this research will focus on Ultrasonic Additive Manufacturing (UAM) and Direct Metal Laser Sintering Techniques (DMLS) technologies. UAM is ideal for creating high-precision internal features, voids, and channels within mixed metal media, while DMLS offers unprecedented design flexibility for producing complex parts and structures that would be impossible or prohibitively expensive with traditional subtractive machining techniques. Ultrasonic additive manufacturing or Ultrasonic Consolidation (UC) was first invented and patented by Dawn White in 1999 [19]. UAM is a combination of

subtractive and additive technology. Traditional milling techniques are used to pre-form a solid metal block. This subtractive step includes the formation of internal voids. Next, a thin metallic foil is compressed and formed over the pre-machined voids with an ultrasonic sonotrode. Ultrasonic vibrations create a lateral scrubbing force at the intermetallic contact point, which breaks up the surface oxide layers exposing the pure metallic surfaces. This creates a atomic level bond at the interface under cold weld conditions [2, 89]. UAM technology features heavily in the design and implementation of the ACCS system. The field of additive manufacturing/3D printing is still relatively new. However, 3D printing has already proven to be a disruptive technology, with rapid progress being made in the last few years. Ultimately, 3D printing promises to feature prominently in the future of space technologies.

There are many current and future applications within the space industry for 3D printing and additive manufacturing. These include 3D printed satellite frames, rocket bodies, nozzles, satellite components, Lunar/Martian habitats, tools, medical devices, and many others [90]. Another critical area of study is 3D printing in space directly, which could significantly reduce the time and cost to launch parts/products to and allow for the creation of remote orbital fabrication and manufacturing facilities [91]. Technologies such as this are critical to NASA's decadal technology development plan, the Artemis moon missions, and the future colonization of Mars. 3D printing is an ongoing area of research, but several current examples exist of 3D printing for CubeSat applications. These include the TubePOD 3U satellite [92] and OGMS-SA, a 3D printed carbon fiber CubeSat [93]. Ultimately, 3D printing and additive manufacturing are ideal for rapid iterative systems engineering design and offer a fast, reliable, low-cost method to create complex engineering products.

2.9 Miniaturized Cryocoolers

Cryocoolers (CC) are cryogenic refrigeration systems capable of producing localized temperatures below 4 K [94, 95]. CC's often operate via the Gifford McMahon cycle [96]. A cryogenic gas, usually pressurized Helium, is cycled within a cold finger/cold head assembly by a compressor. High-pressure gas is forced through a regeneration material and

into a heat exchanger. The gas is allowed to expand, thus reducing the thermal energy and lowering the fluid temperature. The He is drawn back through the regenerator, which conductively removes heat from the expander. This cycle is repeated at high frequencies to incrementally lower the temperature of the working He gas and the cryocooler cold tip [97]. R.G. Ross provides an excellent review of the last 50 years' of cryocooler technology in space. Aerospace applications that require onboard cryocoolers include infrared photodetectors and x-ray/gamma-ray detectors. From 1985 to 1995, long-life, reliable cryocoolers became a reality and ushered in a new era of space satellite-based miniaturized cryogenic instrumentation. Notable missions included the Mariner 6 & 7 missions, which featured the first cryocoolers in space. With Air Force Sponsorship, Northrop Grumman developed the first long-life Pulse-Tube cryocooler between 1989 and 1992 as a derivative of the highly successful Oxford-Stirling design. By 1995, space-based cryocooler designs had matured with flagship missions such as SABER (Mini-PT NGST TRW cryocooler), ODIN, and MIPAS (Oxford Stirling cryocooler) [98]. The military and industry have developed miniaturized cryocoolers for a variety of applications. A notable mission is the James Webb space telescope which features a cryocooler derived from the TRW ACTDP that cools the primary LWIR detector to an operational temperature of 7 K [99]. As of 2018, no CubeSat has flown a cryocooler of any type. Many future missions plan to, but none have launched.

Cryocoolers, while unique in their operation and ability to produce cryogenic level cooling, are highly inefficient. They require significant input power to reject small thermal loads from the cold expander tip. Because of this, cryocoolers require dedicated thermal accommodation to implement on a CubeSat effectively. High conductivity mounting interfaces and thermally stable/regulated rejection zones are required. Several miniature tactical cryocoolers were considered for this research. The Lockheed Martin miniature Pulse Tube cryocooler [100] is a remarkable technology. With no moving parts, the LM PT cryocooler can achieve cold tip temperatures of 125 to 150 K with a total mass of less than 328 grams. Because this cryocooler is a no-moving parts Pulse Tube, the LM PT cryocooler produces almost no exported vibration to the payload or optical instrument, making it an ideal cry-

ocooler for many CubeSat applications. The ACCS system currently integrates the Ricor K508N miniature tactical cryocooler. An ideal low-cost, high-performance CC capable of 70 K cold tip temperatures of thermal loads greater than 0.5 W [17]. As a Stirling system, however, induced vibrations are a concern with these cryocoolers. Ricor USA, Ball, Raytheon and AIM produce more common Stirling-based miniature cryocoolers [101, 102]. These cryocoolers are capable of cold tip temperatures down to 60 K and are low-cost and reliable for a shorter mission, typically less than 2 to 5 years.

2.10 Relevant High-Powered CubeSat Missions

Several advanced and next-generation CubeSat missions were considered reference sources for this research and used as design examples. The first was a CubeSat replacement for the Sounding of the Atmosphere in Broadband Emission Radiometry (SABER) instrument on the TIMED satellite [103–106]. This CubeSat mission was proposed as the SABER-Cube mission. Launched in 2001, SABER is a multispectral LWIR (1.27 to 17 μm) limb imager for 15 to over 100 km altitude. SABER's mission was to study the chemistry and dynamics of the thermosphere/ionosphere MLTI region. The original SABER instrument was used as a primary design source and inspiration for the ACCS research [107–109]. SABER-Cube would be proposed as a solid-state, no-moving parts CubeSat replacement for the SABER instrument. Ideally, SABER-Cube would be capable of providing the same spectral wavelength, bands, and spatial resolution.

CIRAS is a proposed JPL InVEST 6U CubeSat mission aimed at studying the Earth's upwelling infrared radiation in the spectrum's MWIR region (4-5 micrometers). This data can be assimilated into weather forecast models and used to retrieve the lower tropospheric temperature and water vapor profiles [110, 111]. JPL has also proposed a contemporary mission called the Earth-Observing Nanosatellite (EON-IR) CubeSat, which would serve as a follow on mission to CIRAS. EON-IR would improve the thermal-mechanical design of CIRAS, enable full-swath scanning, and extend the MWIR range to CrLS sensor technology [112]. Each of these CubeSat missions would benefit from a dedicated active thermal control technology and have served as design inspiration and reference for the ACCS technology.

2.11 Space Systems Engineering

The ACCS technology design is based on modern space systems engineering principles as outlined by the Space Mission Analysis and Design text (SMAD) [60] and the NASA principles of engineering an elegant system by MD. Watson [113]. Additional resources include Fundamentals of Space Systems, 2nd edition by Pisacane [61], Spacecraft Systems Engineering by Fortescue et al [62], and Elements of Spacecraft Design by Charles D. Brown [114]. In addition, the naturally gained industry experience of the research team (USU & JPL) has proven invaluable to the development of the ACCS technology.

2.12 Conclusions

Modern CubeSats can generate more power (thermal power) than they can easily reject. Based on this, the ACCS technology represents a novel addition to the Small Satellite thermal control taxonomy. The ACCS fulfills a current industry need as an active thermal control technology capable of rejecting modern power loads within advanced next-generation CubeSats and SmallSats. This dissertation will describe in detail the design, modeling, characterization, and ground testing of the ACCS technology.

CHAPTER 3

SPACE SYSTEMS ENGINEERING: DESIGN FOR SPACECRAFT THERMAL CONTROL

There is safety in numbers & a good plan

Euripide (Modified)

3.1 Introduction

NASA defines Space Systems Engineering as a "*Methodical, multidisciplinary approach for the design, realization, technical management, operations, and retirement of a system*". Taking this definition one step further, space systems engineering is a handshake between technical experts, designers, engineers, and scientists of all kinds to form interactive, fully duplexed communication networks to efficiently and effectively design complex space systems. Dominique Luzeaux said that,"Systems engineering should be, first and foremost, a state of mind and an attitude taken when dealing with complexity. "This is a crucial distinction. Systems Engineering is not simply a set of methodologies, a technical approach to design, or a recipe for successfully designing complex systems. It is a mentality to continually look at the bigger picture and understand a system's interactions, trade-offs, and natural complexity. To trace and understand a system from the tiniest component to the end of its mission life and to treat a system as a whole, a sum of its parts, and a derivative of each one. When done correctly, systems engineering can help to create systems of true beauty, elegant designs, and true effect. Simply put, when applied correctly, systems engineering can enable a level of engineering capability and perfection that would otherwise be impossible.

3.2 Space Systems Engineering

The field of systems engineering is quite large, with more methodologies and techniques added daily. In addition, systems engineering is somewhat topic dependent. Therefore, this chapter will limit our discussion to a few essential processes and techniques used in developing the ACCS technology. This chapter will focus specifically on the systems engineering methodologies, model-based design tools, and procedures developed by the ACCS team to help in the future design of Active Thermal Control technologies.

3.2.1 Methodologies, Techniques, Tools, and Procedures

Modern systems engineering techniques, procedures, methodologies, and tools were critical to the development of the ACCS system. These include progressive hierarchal design, concurrent engineering, iterative spiral design, model-based tools, and many more. Each will be discussed in the following sections, along with how they were modified and updated to better serve the development of future advanced active thermal control systems and technologies. However, a few definitions are required before any kind of systems engineering can be discussed with respect to the ACCS technology.

3.2.2 What is a System

Engineering defines a system as "A collection of elements/components organized for a common purpose" [115]. Another way to think of it is that a system takes: inputs performs some processes and provides useful outputs. For this discussion, space systems can broadly be broken down into three subcategories. These categories include the ground service, the launch service, and the satellite. This breakdown is shown below in figure 3.1. As previously mentioned, each system is integrated and cross-communicate throughout a space mission's lifetime.

The satellite system is generally broken down further into two broad categories: the spacecraft bus and the payload. The payload is defined by the mission scope and is broadly tasked with accomplishing whatever the mission objectives are. Examples would include scientific, communications, earth-observing, or human exploration payloads. The payload

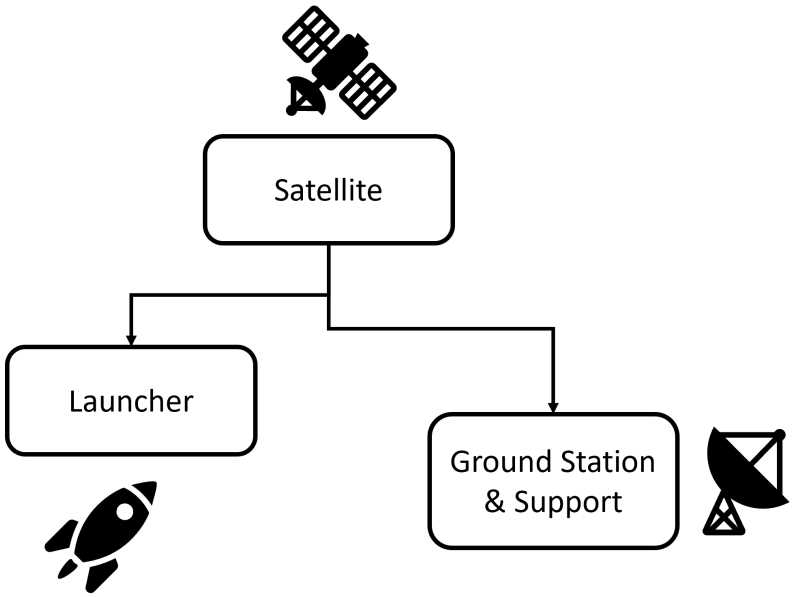

Fig. 3.1: Breakdown of the various standard space systems and their interactions.

is often an incredibly complex and detailed system within itself. However, payloads are mission specific and do not necessarily follow a standard pattern. On the other hand, satellite buses follow a pattern and can be broken down into a series of onboard avionics/subsystems. The purpose of the satellite bus/avionics is to enable the payload operation and mission. It does this by providing the environment and capabilities required by the mission. These include satellite power, deployable mechanisms, attitude and orientation, propulsion, communication, onboard processing, etc. Figure 3.2 below shows a simplified breakdown of a satellite system with the major avionics groupings labeled.

In this work, we are calling attention to satellite thermal control and management—a topic with a great deal of existing heritage. However, we are specifically focusing on developing satellite-wide climate control via active thermal control technologies. These satellite and payload thermal subsystems are highlighted in figure 3.2. It should be noted that while independent technologies can be used for the bus and payload, an integrated bus thermal control system, by default, can provide thermal power rejection and basic temperature control to the payload. The reverse is often not true. A final note is that generally, a complex system like a satellite is itself built from systems. These subsystems can, in turn, be built

from systems and so on. Eventually, individual components, parts, and materials will form the basic units. For this work, the distinction of system vs. subsystem will be made from context.

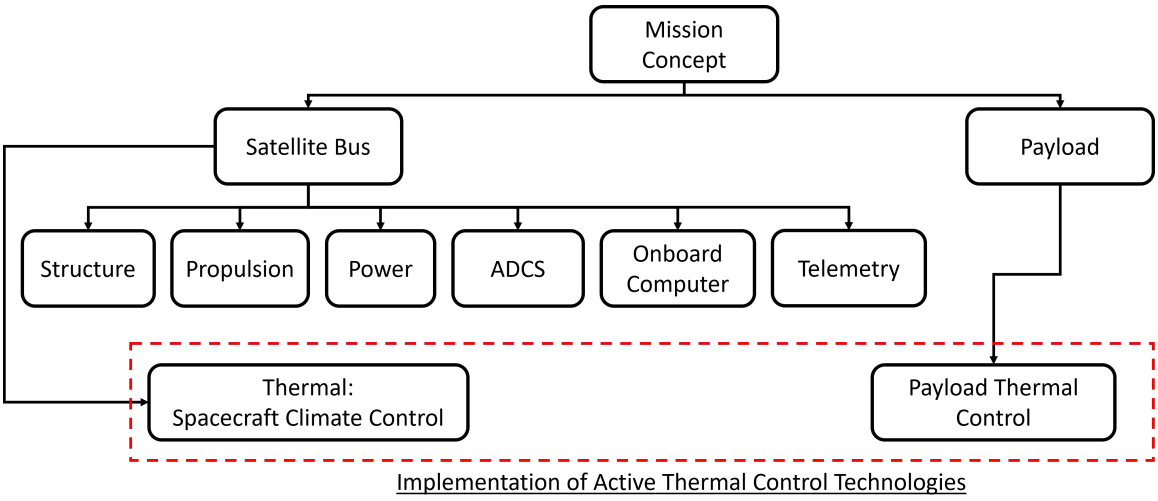

Fig. 3.2: Satellite system breakdown.

3.2.3 Goals vs. Objectives vs. Requirements

When systems engineers communicate, they do so on three distinct levels: Goals, Objectives, and Requirements. These levels of design hierarchy represent an essential distinction within systems engineering. Requirements and objectives form the foundation of systems engineering. They are flexible, dynamic, and can compromise and evolve as required with trade-offs. Goals, however, cannot. Goals are why a system exists and cannot change without fundamentally altering the system. Without each of these levels being clearly defined, a system cannot capture the intent of its creators, nor can the system's inputs, processes, and outputs be clearly defined. Figure 3.3 shows these levels as a pyramid with goals as the peak and requirements as the foundation.

The first level of design hierarchy is that of goals. Goals define the overall intent of a system, or simply put, why it exists. Goals are high-level and far-reaching, often existing many years into the future and spanning a wide and complex set of ideas and concepts.

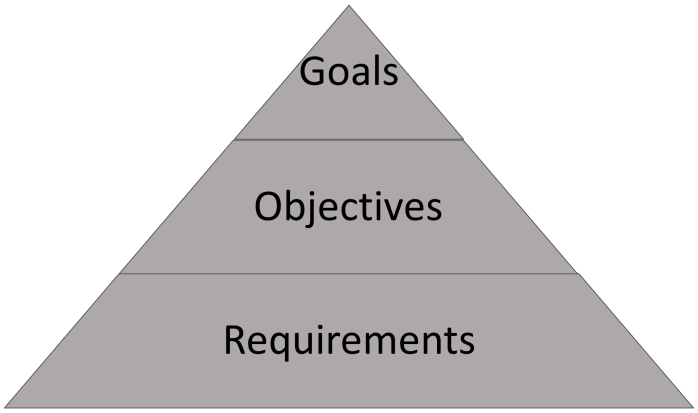

Fig. 3.3: Levels of design hierarchy.

Furthermore, the commitment to a goal allows a system to be created in the first place and provides the necessary guidance throughout its lifetime. Effective communication of goals can be difficult. In many situations, goals can be nebulous, fuzzy, hard to explain, and more akin to feelings, what-ifs, or gut instinct. However, if a system's goals cannot be communicated, then there can be no meaningful discussion at lower, more precise levels. Simon Sinek provides an excellent example of how to define a goal in his TedTalk on "WHY" and the Golden Circle [116]. A system can accomplish many things and have several goals. However, goals should be simplified and ranked until only a single, overall, concise goal exists. Ideally, the goals of a project or system should be defined early in the process and communicated to the entire team as thoroughly and quickly as possible.

Objectives form the next layer of the design hierarchy and are the stepwise process of how goals become a reality. They are the bridge between goals and requirements and share qualities of both. In general, objectives can be broken into three broad categories: strategic, tactical, and operational [117]. Strategic objectives are purpose-driven and help create and define the overall vision of a system. They provide design guidance and help form the system's development plan and procedural map. Tactical objectives are focused on actionable, short-term deliverables and numerous design milestones. These objectives inform the system's performance-driven design targets. Operational objectives are action-oriented and define how a team progresses towards a goal. These objectives determine how

a team organizes, schedules, operates, and achieves. Ultimately, objectives allow a team to discuss a system or design at a high level without becoming bogged down. Good objectives should be short-term, achievable, and measurable. Objectives should be directly translated into requirements.

Requirements form the base of the systems engineering triangle. They are the foundation of aerospace design and, when combined with objectives, form the fundamental layer of communication within systems engineering. Requirements are the universal metric of aerospace engineering and provide a convenient set of design parameters for system and subsystem performance and interaction. NASA provides an excellend resource for writing requirements in Appendix C of the Systems engineering handbook [118]. Fundamentally, any number of designs can satisfy the requirements of a given system. Without requirements, however, any number of designs would technically be acceptable. Whether they satisfied the objectives and goals or not. In addition, without reasonable requirements, many systems will fall short of performance benchmarks and objectives, other systems will not integrate properly, and design creep can set in. The proper definition of requirements forms a system's fundamental blueprints and ensures that higher-level goals and objectives are met irrespective of specific requirements or design.

Whereas goals and objectives can and should be high-level, requirements should be simple, concise, easy to understand, and extremely low level. Often describing the performance or necessary condition of a single component or behavior. The definition, tracking, and fulfillment of requirements is one of the critical responsibilities of a system's engineer. Any set of requirements can and often needs to be communicated in two distinct ways. Quantitative and Qualitative.

- Qualitative requirements are plainly written and speak directly to the objectives of a given system. They should not contain specific numbers or metrics, instead focusing on capturing the overall heart and why of a given requirement.

- Quantitative requirements are entirely numeric. Each quantitative requirement should be represented by a short, simple, and exact design metric.

Requirements are a direct statement of a system's capabilities, performance, and behavior. Good requirements should follow the five C's: correct, complete, clear, concise, and consistent. Requirements should also be achievable, traceable, and measurable/verifiable. The clear and concise definition and communication of a system's goals, objectives, and requirements are critical to its success. The overall design hierarchy of the ACCS system is given below as a long-term goal and three short-term objectives. The requirements for the ACCS system were given in the original NASA proposal and in the first chapter of this dissertation.

ACCS Goal:

- To innovate and develop active thermal climate control technologies for Small Satellites to enable and advance the next generation of space missions in science and exploration.

ACCS Objectives:

- Develop an innovative active thermal control technology for Small Satellites.
  - Develop a single-phase, mechanically pumped fluid loop heat exchanger system for 6U CubeSat platforms and larger.
  - Utilize advanced 3D fabrication techniques to form multi-functional systems.
  - Enable the thermal accommodation of integrated miniature tactical cryocoolers for space-based science instrumentation and payloads.
  - Demonstrate & characterize the ACCS technology through relevant ground-based testing.
- Develop system's engineering design methodologies and model-based tools for the rapid development of active thermal control technologies.

To have any real meaning, requirements need to be traceable. A reasonable requirement will be based on a solid foundation of systems engineering logic and math, which will inform the wording and metrics of that requirement. Therefore, requirements need to point back to

the logical flow of thought on which they are based. It is a systems engineer's job to not only support the requirement but to trace that requirement through whatever supporting data exists. This process becomes critical when a conflict between requirements arises. A good design trade-off cannot be made without traceability and without being able to examine the logic behind each conflicting requirement.

Objectives and requirements can exist at multiple levels, interacting and directly informing each other. The system level flow of objectives to requirements at a system and subsystem level is shown below in figure 3.4. One of the key benefits of defining a systems design hierarchy early is that of budget allocation. Budgets can include funding, personnel, time, equipment, and facilities. By allocating early, a team can strategically apply their resources, budgets, personnel, and supplies where they will do the most good at any given time.

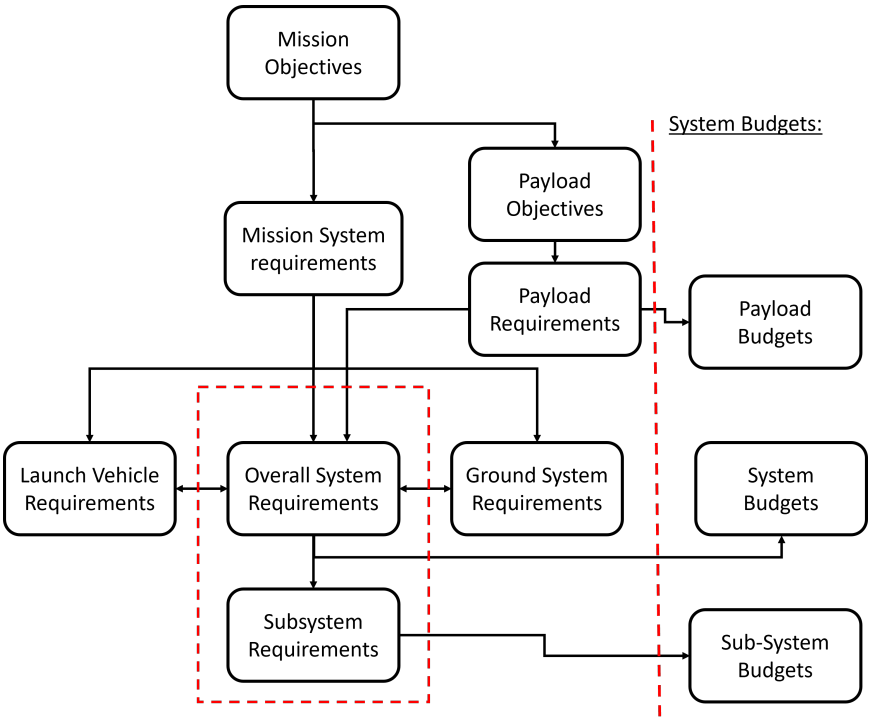

Fig. 3.4: Objectives & Requirements Breakdown and Budget Allocation.

3.2.4 Concurrent Design Engineering

The space systems engineering design team is a modern marvel of management and multidisciplinary engineering. Teams include leaders, technical experts, systems engineers, and managers. The top level of any given project team within the space industry is the Principle Investigator (PI). The PI provides leadership as well as technical and scientific expertise. The PI is also tasked with making the final decision on any matter pertaining to the project or system. PI's are backed by a team of Co-Investigators (CO-I), often industry experts and scientists. These two groups define and maintain the system's goals and vision. Often, a deputy PI is assigned to supervise the project's day-to-day operations and ensure that each step of the development is synchronous, peer-reviewed, and in line with the set project goals. Next, a project manager (PM) is assigned to provide management and oversight of the project. The PM ensures that the project's schedule, budget, and deliverables are met throughout the development process. The PM also serves as an overall team manager and ensures that the various teams work harmoniously.

At this point, team configurations can vary drastically. NASA defines three primary team layouts for system development: sequential, centralized, and concurrent [62]. Sequential systems engineering relies on a linear progression of design. Each team or discipline takes a turn at the system's design, in isolation, one at a time. Progress is made through design cycles and iteration. This traditional, tried and true approach offers several advantages, mainly flexibility in budget and personnel allocation. However, sequential systems engineering has many disadvantages, including lengthy development times, a lack of innovation, and a tendency to allow subsystem and sub-discipline interference and mistakes to propagate. Conversely, centralized systems engineering is characterized by simultaneous parallel design efforts and a centralized core of systems engineers who act as intermediaries for the various teams and disciplines. All communications are routed through the central systems team, who monitor, record, and coordinate all of the critical data. The systems engineering team is also tasked with maintaining the big picture and ensuring that all of the subsystems are coherent and meet requirements. Centralized design is a marked improve-

ment due to the parallel workflow and the inclusion of a dedicated core of systems engineers. Development speed and design accuracy are both improved. However, due to the lack of direct inter-team communication, a bottleneck can once again slow down the team's overall progress. In addition, without inter-team brainstorming, innovation is limited.

Concurrent engineering represents the latest development in space systems engineering. Like centralized design, concurrent utilizes a simultaneous and parallel development methodology backed by a core team of systems engineers. However, concurrent engineering expands the parallel effort of the design teams by enabling direct communication between individual teams and experts. This allows a free and continuous flow of information, requirements, innovation, and design. This level of communication is only possible with modern integrated technology. Concurrent engineering combines the advantages of parallel design with the coherent management of systems engineering and the rapid dissemination of ideas and concepts through direct person-to-person communication. Concurrent engineering has many advantages, including true multidisciplinary design collaboration, the fastest development timeframe of any of the three methods, a reduction in cost/budget, increased productivity, a free space for innovation, problem-solving, and troubleshooting, and an increase in the quality of the product. Concurrent engineering is naturally a chaotic experience and has several disadvantages; namely, it is problematic from a management perspective and requires excellent and straightforward communication across all teams and disciplines. In addition, systems engineers need to work much harder to coordinate and record all of the parallel communications and flows of information. Despite these drawbacks, concurrent systems engineering is the modern method of choice for rapid space system and mission concept development.

Many aerospace companies and governments have formed their own dedicated teams of concurrent engineers for rapid pre-phase A and Phase-A mission/technology developments. Two notable examples include NASA JPL's Team-X and the European Space Agencies (ESA) Concurrent Design Facility (CDF). JPL's Team-X is a cross-functional, multidisciplinary team of engineers who use concurrent systems engineering methodologies

to complete rapid design, analysis, and evaluation of mission concept designs [119]. The European CDF has championed concurrent design and utilizes state-of-the-art facilities and telecommunication systems to coordinate and connect teams of specialists and experts. The CDF's primary mission is to rapidly assess the feasibility of future missions, spacecraft, new technologies, payload instrumentation, etc. [120]. Figure 3.5 below represents a typical concurrent systems engineering team layout for a project like the ACCS; note the interconnected communication paths.

The ACCS system has wholly relied on concurrent engineering for its development. Dr. Charles Swenson is the director of the Center for Space Systems Engineering at Utah State University and served as the ACCS project's PI. CO-I's from JPL provided technical expertise and design assistance. The remaining roles of Deputy-PI, PM, systems engineers, and technical teams were formed by USU graduate and undergraduate students. The interconnected methodologies of concurrent engineering were critical to the development of the ACCS system. Without direct communication, systems engineering support, and parallel multidisciplinary design, the ACCS would not have been possible.

3.2.5 Iterative Spiral Design & Model-Based Design

Two final key systems engineering techniques utilized by the ACCS system are iterative spiral design and model-based design. Iterative spiral design is a hybrid methodology created for the ACCS project, which combines the concepts and procedures of incremental (Kaizen), iterative, and spiral design into one basic technique. The key concept is that any complex system can be broken down into small, easier-to-handle subsystems. These systems can then be iteratively changed and adapted with progressively tighter and better-defined requirements until a design emerges that satisfies the systems requirements, objectives, and goals. The advantages of this approach are numerous but specifically include rapid design iteration, early-stage conceptualization, and basic modeling/analysis at an early phase of development. In addition, it is relatively simple to change requirements or scope, reduces risk, and large complex systems can be broken down into easier manageable bite-size pieces. The critical steps of incremental, iterative, and spiral design are outlined below in Table 1.

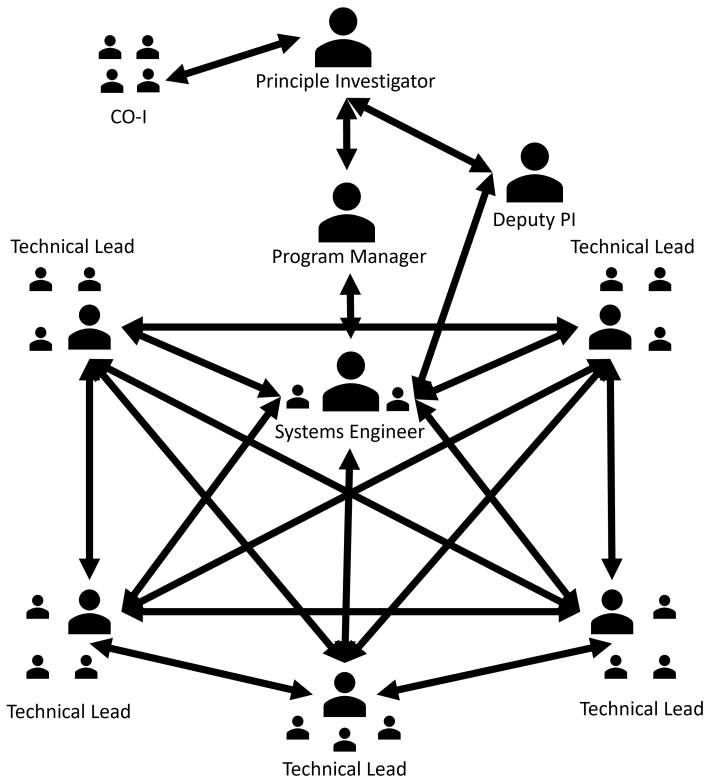

Fig. 3.5: Concurrent Systems Engineering Network Model.

Incremental design or Kaizen (Japanese for: "improvement" or "change for better") is a design methodology developed by the Toyota corporation to improve assembly line production [121]. The Kaizen method is closely linked to iterative design and can be summarized by a simple statement. Continuous improvement through slow, positive, incremental change. Kaizen has many forms, but the primary techniques used by the ACCS program were: to break each system, subsystem, or problem down into small bite-sized pieces. To solve problems as quickly and efficiently as possible, employ the five why's technique and embrace creative problem solving and progressive design methodologies. Kaizen also teaches to reject the status quo and to look outside the box for inspiration. Iterative and spiral design methodologies are closely related. The primary difference between them is that iterative design outlines the design actions, while spiral design defines the thought process behind those actions. This can be seen by spiral design's emphasis on planning, risk analysis, and evaluation.

The spiral iterative methodology is shown graphically below in figure 3.6. The design process begins with the conceptualization of the mission, including defining the mission goals, objectives, and requirements. Next, model-based tools are used to simulate the system's behavior and performance. These tools are used to inform good design decisions which meet the previously defined requirements. The current iteration design is then prototyped and tested in relevant ground-based characterizations. Detailed analysis is performed between these two stages to validate the current model and design with the prototype and test data. This analysis is reviewed, and risk analysis is performed. Finally, the design is iterated back to refining the concept and requirements of the mission. This creates an iterative design evolution, which can be repeated until the design loop closes. Ultimately, this process spirals to an ideal design.

The final key methodology to the ACCS system's success is that of model-based design (MBD). MBD utilizes mathematical models, numerical approximations, CAD simulations, and simplified/scaled prototypes to predict the performance and behavior of a physical system that does not exist yet. MBDs allow engineers and designers to explore a design before

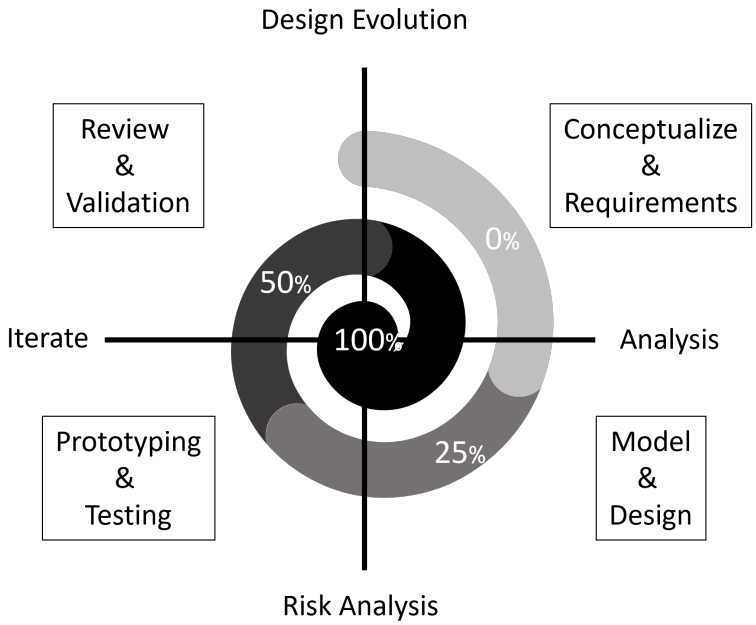

Fig. 3.6: Iterative Spiral Design Flow-Chart.

building it. Thus reducing costly prototyping iterations. MBD methodologies are critical to modern engineering and help reduce the difficulty of engineering complicated interconnected, expensive systems. MBDs need a defined purpose and be focused on a specific set of questions. These can include design verification, optimization, or trade-off decision matrices. MBDs can range in complexity from simple back-of-the-napkin approximations to high intensive numerical CAD simulations. However, a deep and thorough understanding of the physics behind a system is a critical requirement of MBD design, without which the adage "Garbage in Garbage out" becomes painfully accurate. Models are software representations of a system's individual components, environment, and interactions. MBDs help engineers to make good design decisions. Something that is sorely needed in our modern complex design world.

3.3 Traditional Thermal Management Design

The Space Mission Analysis Handbook (SMAD) [60] is often considered the holy bible when discussing the standards of space systems design and NASA's particular brand of

systems engineering. Figure 3.7 below is a flow diagram representing the traditional satellite thermal design process outlined by SMAD. The individual steps are also explained.

1. Establish a mission profile or operational concept. This profile will include estimates of the thermal space environment and predicted thermal limits and variations. Any change in this step will significantly impact the spacecraft thermal design as a whole and may require a full re-design.

2. Define the spacecraft's location and orientation. This step outlines the spacecraft's orbit, trajectory, and attitude.

3. Estimate the internal power profile of the spacecraft. The power absorption and dissipation of the spacecraft. This step will include a breakdown of each active component and its total power/thermal dissipation. The energy density of the spacecraft can be broken down within this step as well.

4. Define the operational and non-operational temperature limits of the spacecraft. This includes maximum/minimum component temperatures, average system temperatures, maximum allowable thermal gradients, and any unique mission requirements.

5. Approximate the spacecraft geometry by simple geometric shapes and bodies. This simplification will help in further Model-Based Design analysis.

6. Simulate the simplified spacecraft within the thermal environment. Move the spacecraft model through the mission profile defined by steps 1 & 2.

   (a) Find the incoming heat flux for each face, shape, or body. Include the maximum—minimum and profile average heat flux with respect to time. Define each spacecraft surface's surface radiation properties: absorptivity & emissivity.

7. Calculate the total input heat flux on the spacecraft from the environmental thermal equations given later in this dissertation or by SMAD 22-21 [60].

8. Compute the spacecraft's thermal IR dissipation capabilities by summing the external surfaces.

9. Compute the spacecraft's steady state and isothermal temperature from the heat balance equation. Include the internal power generation of the spacecraft.

10. Compute the spacecraft's absolute maximum and minimum expected temperatures from the variations in the thermal environment, surface properties, and internal power.

11. Compare these temperatures with the defined requirements and iterate within the set bounds until a closed-form solution is reached.

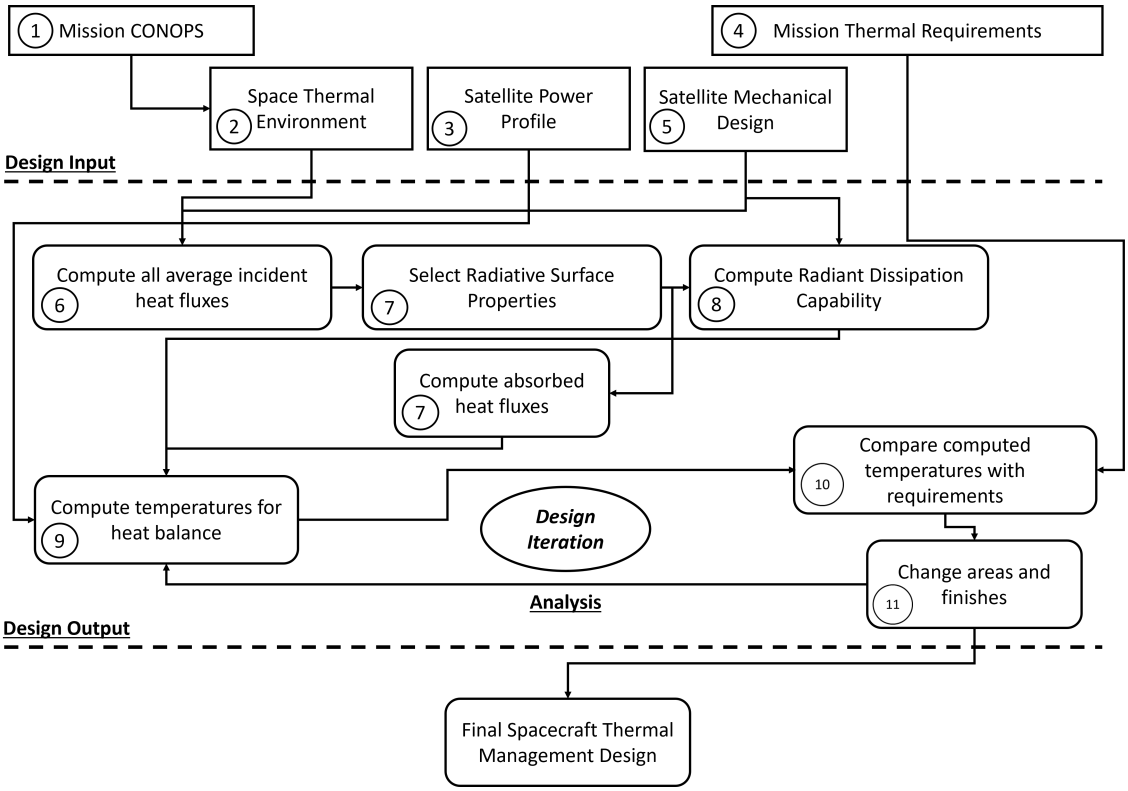

Fig. 3.7: SMAD thermal management design flowchart.

3.4 The Systems Engineering of the Active CryoCubeSat

The Active CryoCubeSat technology is one of the first significant steps toward the ultimate goal of integrated climate control for Small Satellites and CubeSats. It is the first single-phase MPFL heat exchanger system specifically designed for CubeSats and Small

Satellites and represents a novel approach to satellite thermal control and design. The ACCS is a complete system within itself. It integrates and operates within the larger satellite system as an avionics support subsystem, providing thermal feedback control, stable zonal temperature management, and high-thermal energy density rejection for next-generation, high-powered, advanced Small Satellites.

Until now, CubeSat thermal design has relied on passive thermal management techniques, a methodology that has resulted in satellites "surviving" the space environment. Currently, mission CONOPS and objectives are modified or adapted to the thermal space environment. The ACCS technology hopes to change this by disrupting the traditional satellite thermal design and proposing a progressive new approach. The ACCS team hopes to usher in a new era of satellite thermal control where future CubeSats and SmallSats rely on active thermal climate control. These satellites would power through the difficulties of the space environment. A satellite's thermal control system should be able to set and regulate the desired temperatures and gradients within the satellite and maintain those despite the external environment, similar to climate control in a car or house. This strategy will rely upon the adaption of modern engineering technologies and concepts, updated aerospace thermal systems engineering methodologies and procedures, and the latest model-based design tools. In addition, next-generation 3D fabrication techniques will be required to produce and integrate these technologies into the satellite as dedicated multi-functional avionics subsystems. Ultimately, these new technologies will jacket the satellite and control/reject the system's thermal loads as needed. The ACCS technology hopes to rewrite satellite thermal control to be more progressive, innovative, and active. Something that is considered early in the design phase and can be integrated as a COTS part. The ACCS system hopes to introduce the qualities shown in figure 3.8 to the mainstream satellite thermal control community.

The procedure used by the team to develop the ACCS active thermal control technology is outlined below. A support flowchart is given in figure 3.9. The first step was the definition of the technology concept and objectives. These are outlined in the introduction chapter of

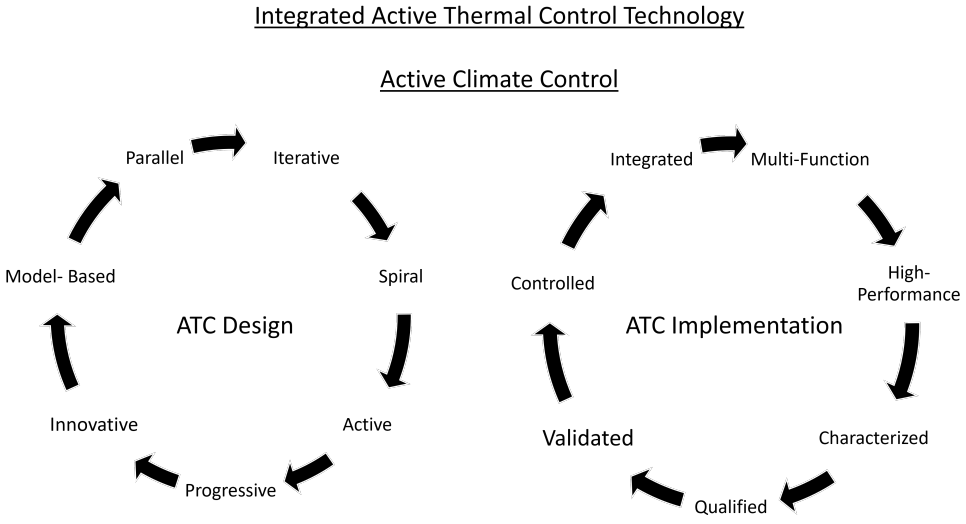

Fig. 3.8: Proposed design methodologies for the next generation of active thermal control technologies.

this work and can be found in the original proposal. From the mission concept, a simplified analytical/numerical model was created. This allowed for the rapid, iterative, model-based design of the ACCS system. This model can then inform "good" design decisions for the mechanical design of the ACCS system. A detailed, high-fidelity, thermal desktop model can be derived from this mechanical design. This creates an iterative loop between the mechanical design, the analytical design tool, and the design verification via thermal desktop. This iterative spiral design will eventually converge to an ideal design for the ACCS system. This design must then be qualified. The first step in this process is component-level testing. Each ACCS component is bench-top tested to demonstrate capability and confirm the quality of the design. Next, the system is fully integrated and qualified in relevant ground-based testing. These tests raised the overall TRL of the ACCS system to $\sim$5. The ACCS system is also characterized in terms of performance and behavior by a series of highly-instrumented ground-based tests. Finally, the characterization data is used to validate the initial analytical and thermal desktop models. This procedure was used to develop the innovative ACCS technology and can be expanded to create similarly active thermal control technologies.

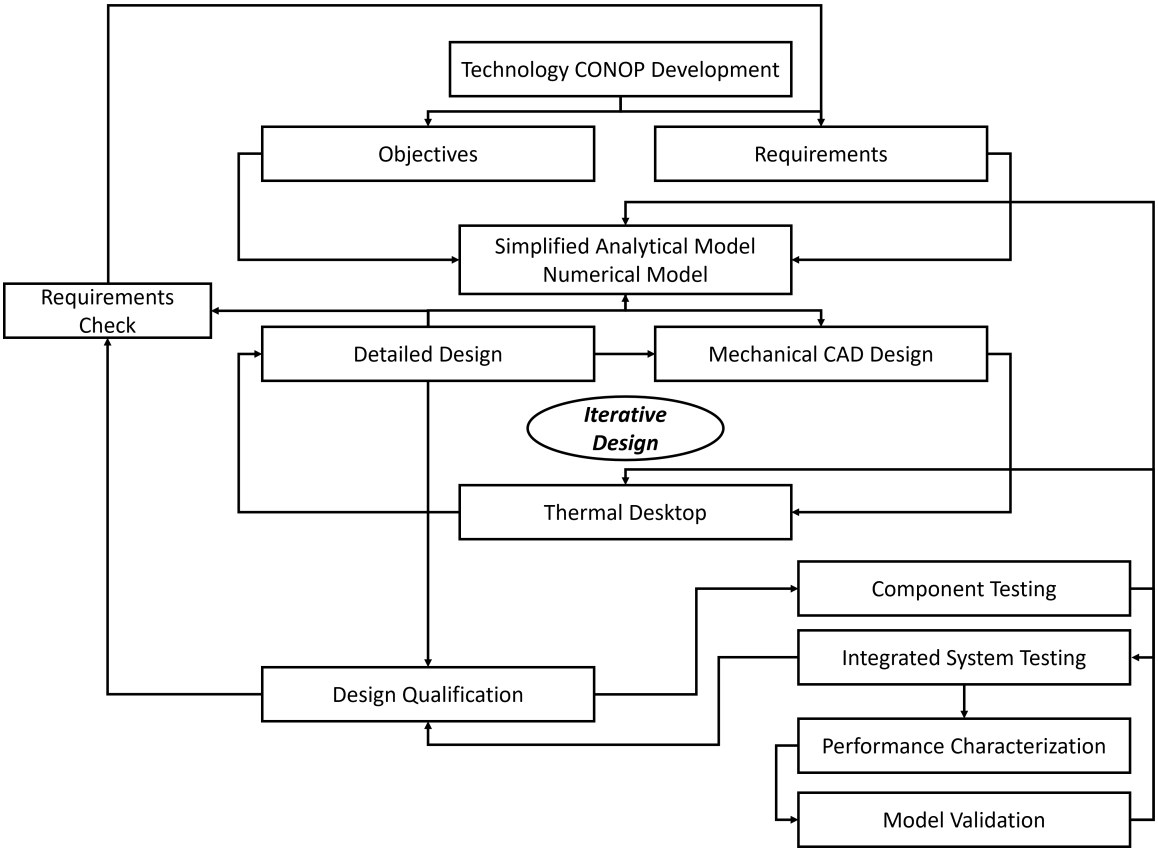

Fig. 3.9: Design procedure for the ACCS technology.

The step-by-step development procedure for a satellite mission utilizing active thermal control technology such as the ACCS is outlined below. Figure 3.10 is the corresponding design flow diagram. This process has been modeled from the NASA SMAD procedure given previously but updated and modified to better aid in the design of single-phase active thermal control technologies for small satellites.

1. Outline the mission profile as a concept of operations (CONOP).
    (a) Define the overall purpose of this mission, the goal, and the why.
    (b) Define high-level mission objectives.
    (c) Create a mission Concept of operations.
    (d) Define the spacecraft orbit and thermal environment, and compute incident heat fluxes.
2. Create system-level thermal requirements.
3. Define the power profile of the satellite.
    (a) Sum all internal active power sources.
    (b) Define efficiencies and thermal waste heat.
    (c) Calculate a thermal power density.
4. Create a deployed radiator concept.
    (a) Calculate the required radiator area.
    (b) Define radiator location, attitude, and actuation capabilities.
    (c) Calculate radiator view factors.
    (d) Set radiator surface properties.
5. Compute the total radiative dissipation capabilities of the satellite.
    (a) Compare the total satellite thermal energy density in step 3 and the impact of the thermal space environment in step 1.

Note, at this point within the procedure; an iterative loop is created wherein the mission thermal requirements, satellite power profile, and radiator design are traded off until a satisfactory high-level design is created.

1. Create a single-phase MPFL heat exchanger design.
   (a) Select a suitable working fluid.
   (b) Design the working fluid flow channels for the heat exchanger, radiator, and transfer lines: Flow channel size, length, and geometry.
   (c) Calculate desired flow rates and pressures.
   (d) Down-select a suitable micro-pump.
2. Compute the absorbed ACCS heat fluxes.
3. Compute the total satellite thermal balance on a nodal basis.
4. Compute the system level and component level zonal temperatures.
5. Compare these temperatures, gradients, and thermal fluxes with the defined requirements fo step 2.

Note, at this point, another iterate loop is formed between step 2 and step 10. The ACCS technology design should be iterated until a closed loop design is found that matches the set requirements. Based on this active thermal control design, the mechanical design of the spacecraft can more easily be informed.

3.5 ACCS Systems Engineering Summary

Elon Musk is quoted as saying, "*Rocket Engineering is not like ditch digging. One hundred people can dig a ditch a hundred times faster. For rockets, you have to solve the problem at a particular level of difficulty; one person who can solve the problem is worth an infinite number of people who can't*". Systems engineering requires knowledge, skill, creativity, and the implementation of techniques, methodologies, and a disciplined approach to

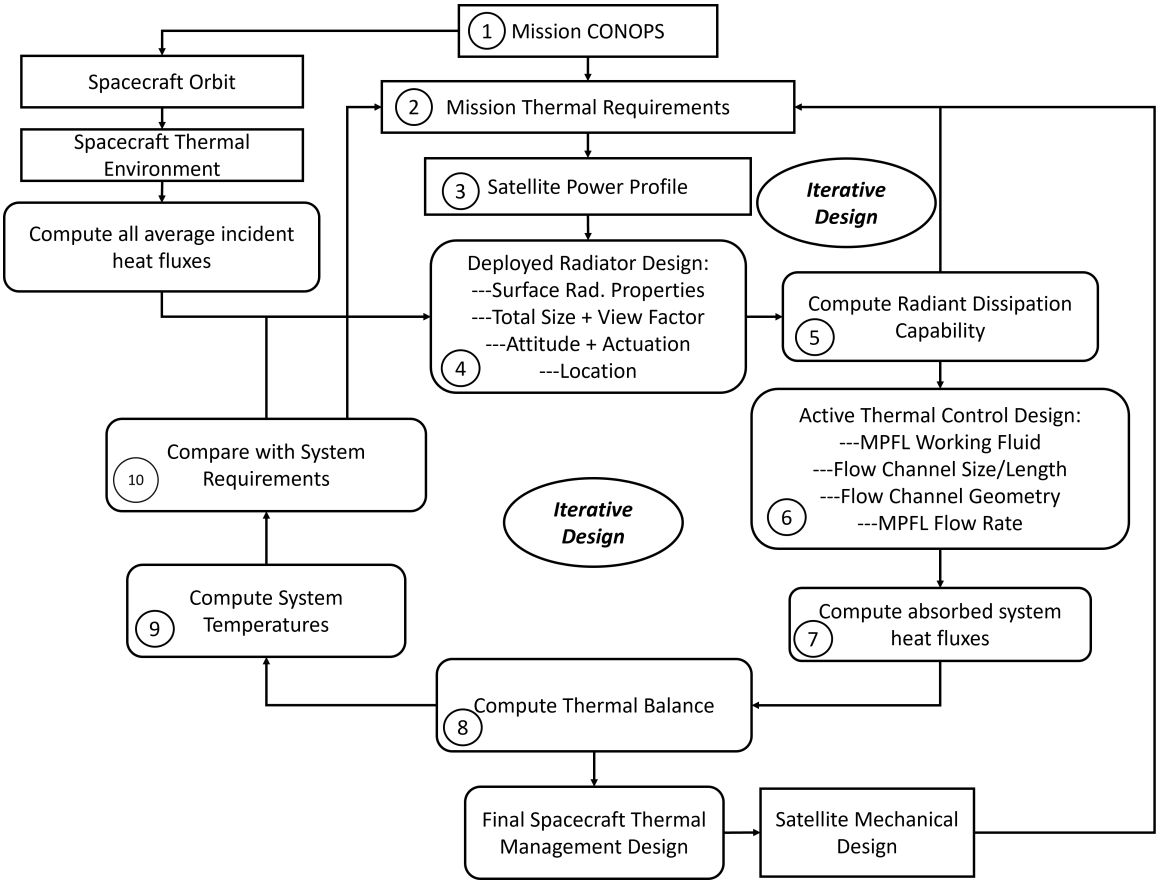

Fig. 3.10: Modified SMAD thermal management design flowchart for the ACCS thermal control technology.

design. This sentiment holds especially true for the development of the ACCS system. The ACCS team developed a novel active thermal control technology through systems engineering based on a single-phase, mechanically pumped fluid heat exchanger design. This technology leveraged state-of-the-art 3D manufacturing techniques to create integrated multifunctional structures. The team was also able to create a set of model-based design tools that, when combined, can rapidly and accurately predict the performance and behavior of systems like the ACCS technology. New and updated systems engineering methodologies, procedures, and flowcharts/state-design diagrams were also created to support the future development of ACCS technologies. Ultimately, this technology was fabricated as a realistic ground-based prototype and validated through extensive, highly-instrumented thermal vacuum tests. Overall, the ACCS system has successfully demonstrated the development of new thermal control technology for CubeSats and Small Satellites. The ultimate goal of the research goes far beyond single-phase thermal control. The ACCS is a stepping stone on the path towards fully integrated active climate control systems for satellites and space vehicles. This dream includes end-to-end control of the various thermal control parameters of radiation, conduction, convection, and mass transfer. Advanced technologies would include active electro-chromatic emissivity control, origami-folding radiators, dual axis tracking radiators, active two-phase heat transfer systems, and the marriage of heat-pipe technology with pumped fluid loops. The ACCS team also hopes that the systems engineering and design methodologies outlined in this chapter will be a starting point for a future renaissance of satellite thermal control development. The team also hopes to inspire future satellite systems designers to approach thermal control from a progressive standpoint and apply active thermal control techniques in their solutions.

CHAPTER 4

ACCS Theoretical Foundation

In Theory There Is No Difference Between Theory and Practice, While In Practice There Is

Benjamin Brewster

4.1 Introduction

The operational theories governing the ACCS technology are derived from the fundamentals of thermodynamics and heat transfer. Specifically, advection through the pumped fluid loop, convection within the heat exchanger, radiation from the dedicated deployable tracking radiator, conduction within the active components, surface contacts, and UAM structures. The topic of heat transfer is vast, complex, and incredibly varied. The governing equations presented in this chapter are a small part of a larger complex whole. However, they more than adequately capture the ACCS system's behavior and form the analytical model's foundation. Many of the formulas below are considered foundational and will be given concisely, without derivation, and without a great deal of background. References can be found below and in the literature review of this chapter.

Heat transfer can occur in a variety of ways. The primary are conduction, convection, radiation, and mass transfer. Thermal heat and heat transfer are merely the transfer of energy or the kinetic vibrations of atoms [35, 44–46, 122–124].

- The transfer of heat within a solid body is known as conduction. Conduction is the transfer of kinetic energy, and therefore heat, by direct contact.
- Convection is the transfer of energy/heat by the movement of fluid. Convection is often considered a unique and singular method of heat transfer. However, in reality,

it is formed by two other heat transfer methods working in tandem: advection or the bulk movement of fluid and conduction within and through that fluid. Once again dictated by kinetic energy and momentum.

- Radiation is the transfer of thermal energy via the electromagnetic spectrum. Radiation can also be considered the transfer of energy as quantized light.

- Mass transfer is the simplest of the heat transfer methods. It consists of moving an object of high thermal energy from one place to another. This can be through bulk fluid transfer, as in the case of ACCS. Or simply moving a hot ingot of metal from the furnace to a bench. The movement is the transfer of energy.

These basic equations of heat transfer are given below and begin with conduction. Q represents the total thermal power in watts transferred from point A to point B. The material conductivity is given by k. Conductivity is a measured, sometimes derived, property that indicates how easily thermal energy can move within a material. A & L represent the physical geometry of the heat transfer. ΔT is the thermal gradient that drives the transfer of energy. By the second law of Thermodynamics, concisely stated by Carnot [125].

"wherever there exists a difference of temperature, motive power can be produced. "

Energy must flow from hot to cold; this temperature difference forms the motive gradient, which drives heat transfer.

$$Q_{Conducted} = \frac{k \cdot A \cdot \Delta T}{L} \tag{4.1}$$

Convection is the transfer of heat into and out of a fluid, not necessarily the transfer within it. Therefore, this transfer always takes place over a surface and is defined by that contact. The term h is the convective coefficient. Convection and the convective coefficient are highly dependent on the situation. Key factors include fluid contact area & type, surface geometry, fluid motion and properties, and the velocity of the fluid. Similar to conduction, a temperature gradient provides the motive force for the energy transfer. At its most fundamental, convective heat transfer is governed by the following equation.

$$Q_{Convected} = h \cdot A \cdot \Delta T \tag{4.2}$$

Radiation is unlike conduction and convection because it does not require a medium to transfer energy. Instead, thermal energy is transferred directly through electromagnetic quanta of energy, as laid out by Planck [126]. The energy transference of radiation is dependent on the frequency & wavelength of the EM spectra, the surface properties of the emitting body, and its temperature. When two bodies radiate to each other, the transfer is governed by the material surface properties of the bodies and their geometric and physical relationship. Once again, thermal energy/temperature forms the motive force driving radiative heat transfer. A material's surface can transmit, absorb, or reflect thermal radiation. The summation of how radiation can interact with a material is shown below in equation 4.3. Radiation is often wavelength-dependent (Specular). From Kirchoff's law, the absorption and emission of a body are identical for a given wavelength. Each value in the following equation, 4.3, can vary between 0 and 1.

$$\alpha(\lambda) + \rho(\lambda) + \tau(\lambda) = 1 \tag{4.3}$$

Radiation is a line of sight transfer and, therefore, highly dependent on the relative view factors of one body to another. Stephan Boltzmann's equation 4.4 gives the overall transfer of power through radiation. σ is the Boltzmann constant, A is the total emitting area. Radiation is related to the temperature of the body to the fourth power, T^4.

$$Q_{Radiated} = \sigma \cdot A \cdot T_{Rad}^4 \tag{4.4}$$

The final method of heat transfer will not be shown here in equation form. Instead, it will be discussed as a logical concept. Thermal energy can be contained within a body, as represented by an elevated temperature (above absolute zero), similar to potential energy. This stored energy can be moved from one location to another and then allowed to transfer heat in more traditional ways. This research will use the concept of bulk fluid motion

to transfer thermal energy from inside the ACCS heat exchanger, and inside the satellite bus, to the externally deployed radiator. By linking this bulk fluid motion, i.e. advection, substantial amounts of thermal power can be transferred over large distances with relatively small thermal gradients. This is ideal for situations where large amounts of power need to be rejected by space-based radiators, which by the laws of physics also need to be large. Each of these fundamental methods of heat transfer is present in the ACCS system. All of the current formulations are considered 1D and steady state. Control volumes for each simplified node of the ACCS are used to simplify and explain the analytical process. Each of the equations used by the ACCS will be discussed in detail, along with concluding remarks in this chapter. The equations shown in this chapter will be directly used in the Analytical design model, and indirectly used in the TVAC characterization analysis code. These basic formulas also form the basis of the Thermal Desktop heat transfer numerical model.

4.2 ACCS: Radiative Heat Transfer

The ACCS radiator relies on wavelength-dependent heat transfer to reject the bulk dissipation of the internal radiator, satellite bus, and payload. This "Gray-Body" radiation i governed by the modified form of Boltzmann's equation.

$$Q_{Radiated} = \eta \cdot \sigma \cdot \epsilon \cdot A \cdot (T_{Rad}^4 - T_{Space}^4) \tag{4.5}$$

This version of Boltzmann's equation has an added efficiency term, η, to account for any linear or constant unknowns, non-idealities, or variations in the ACCS radiator performance. The emissivity, ϵ, of the radiator is a measure of how well its surface can emit EM radiation. The radiator is coated in Aeroglaze Z306 black, a high emissivity paint, with an approximate emissivity value better than 0.9. The T^4 of the radiator is balanced by the T_{Space}^4. This balance refers to Prevost's law of exchanges, which states that all bodies are emitting and absorbing radiation at all wavelengths at all times. Essentially, while the ACCS radiator is emitting energy to space, space is radiating energy back. Figure 4.1 below shows the radiator control volume. Energy is deposited on the radiator by the pumped fluid loop heat

exchanger and then radiated out to deep space by radiation. Additional sources within the radiator control volume include the inputs from the thermal space environment.

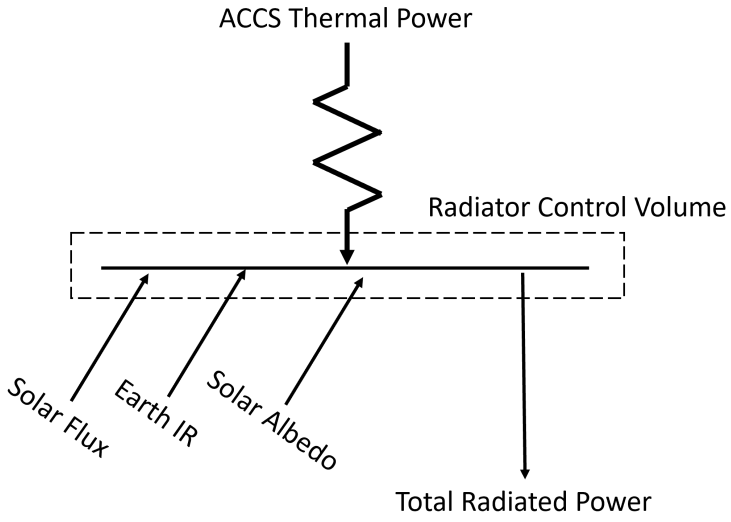

Fig. 4.1: Heat transfer control volume for the ACCS radiator. Thermal inputs and outputs are labeled.

The thermal space environment is often simplified to three key sources—the energy radiated by the sun, which is directly incident to the spacecraft. The reflected solar energy from the Earth's atmosphere, called the albedo, and the infrared thermal energy of the planet earth or "Planet-Shine." The following equations for each are derived from the model of a flat plate in orbit about the earth [1]. This plate interacts with the space environment and is physically oriented with respect to the sun and Earth, as shown in figure 4.1. The solar flux incident on the flat plate is given by the following.

$$Q_{Solar\ Flux} = G_S \cdot A \cdot \alpha_S \cdot \cos(\psi) \tag{4.6}$$

The first term, G_s, is a measure of the intensity of solar energy at 1 AU. This value varies depending on the current solar cycle and the particulars of the sun at any given moment, but for this research, it is averaged to a conservative ∼1420 W/m2. The area term is representative of the total panel area, and the solar absorptivity of the plate's

surface material is given by α_S. The ψ term is the incident angle of the collimated solar rays to the orientation of the flat plate. The radiation emitted by the sun is blackbody in nature, but for this research, the wavelengths are broken down into two broad categories: solar energy and IR energy. For the equation above, all values are indicative of solar energy.

Solar albedo refers to the energy reflected by the Earth's atmosphere, which rebounds and impacts the space vehicle. Often at a different angle and surface than the original solar flux.

$$Q_{Albedo} = G_S \cdot (AF) \cdot A \cdot \alpha_S \cdot F_e \cdot \cos(\theta) \tag{4.7}$$

AF is the albedo factor, a percentage measure of how much of the incoming solar radiation is reflected. This value can vary a great deal, but a simplified estimate can be set to 0.35 or 35% reflection. Fe is the view factor of the flat plate's surface back to the Earth's disk. This term depends on the plate's orientation and orbit altitude. The view factor for a flat plate in orbit can be calculated from a custom VBA code, adapted from [1].

The planet Earth radiates as a black body in the infrared spectrum. This blackbody source is critical to spacecraft thermal design because while the spacecraft is trying to release thermal energy via IR, the Earth radiates back to the spacecraft in the same wavelength. The blackbody temperature of the Earth is approximately ~250 K. The equation for planet-shine IR radiation is given below, 4.8. For this case, the absorptivity of the plate is wavelength (IR) dependent α_{IR}.

$$Q_{Earth\ IR} = \sigma \cdot A \cdot \alpha_{IR} \cdot F_e \cdot T_e^4 \tag{4.8}$$

The various thermal inputs of the space environment can be summed on the ACCS flat plate radiator model, as shown in figure 4.2, along with the heat exchanger dissipation and total radiator output power. Equation 4.9 sums the total radiator inputs to the control volume and, with no energy storage, sets them equal to the output radiation. This forms the fundamental energy balance of the ACCS radiator.

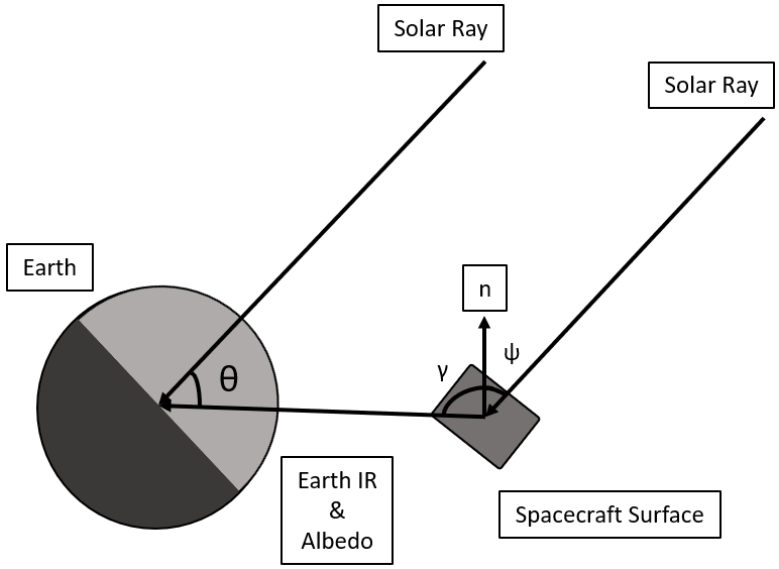

Fig. 4.2: Flat plate space environment model [1].

$$Q_{Out} = Q_{In} = \eta \cdot \sigma \cdot \epsilon \cdot A \cdot (T_{Rad}^4 - T_{Space}^4) = Q_{Solar\ Flux} + Q_{Earth\ IR} + Q_{Albedo} + Q_{Dissipation} \tag{4.9}$$

The ACCS energy balance can be solved for the steady-state working temperature of the radiator at any given thermal load, as shown below in equation 4.10. It should be noted, that the radiator for the ACCS technology forms the coldest point, reference temperature, within the heat exchanger system. This radiator surface temperature will then be extrapolated to every other node within the ACCS system to help derive their temperatures.

$$T_{Rad} = \frac{(Q_{Diss} + G_S \cdot A \cdot \alpha_S \cdot cos(\psi) + \sigma \cdot A \cdot \alpha_{IR} \cdot F_e \cdot T_e^4 + G_s \cdot (AF) \cdot A \cdot \alpha_s \cdot F_e \cdot cos(\theta) + T_{Space}^4)^{\frac{1}{4}}}{\eta \cdot \sigma \cdot \epsilon \cdot A} \tag{4.10}$$

4.3 ACCS: Conductive Heat Transfer

Conductive heat transfer is everywhere within the ACCS system and dictates how the

heat and energy is transferred within the UAM bodies of the heat exchanger and radiator, as well as the active systems of the cryocooler, pump, guard heaters, etc. It even dictates the contact resistance between all the various components. The conductive interactions of the ACCS system are explored in more detail in the analytical modeling chapter and in the excel based thermal transfer/parasitic tools. For this chapter, the only conduction terms discussed are that of the 2D heat transfer between the surface of the UAM heat exchanger/radiator and the embedded flow channels. The heat of the tube, or conversely, that of the surface, will travel both vertically and laterally within the UAM body. 2D conduction is somewhat more complex than 1D conduction and often requires a known analytical solution to Fourier's equation. The 2D conductive geometry of the ACCS is shown below in figure 4.3.

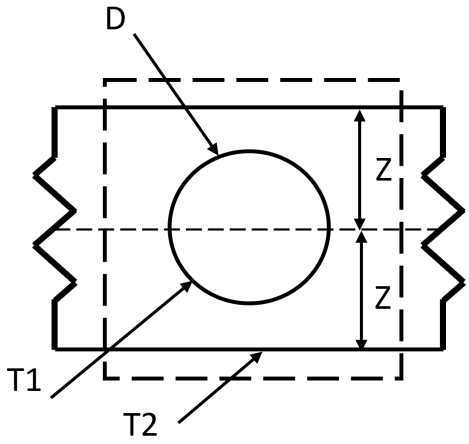

Fig. 4.3: 2D Conduction shape factor control volume.

Geometries such as this are standard, and conductive shape factors are available to allow for an easy analytical solution. Shape factors, given by S, combine the Length and Area term of Fourier's equation, aka the shape of the conduction, into a geometry-specific term. A given shape factor will satisfy a specific geometry and can be derived or looked up in shape factor tables. The basic Fourier conduction equation is modified to include the shape factor term, as given below. Where S is calculated as shown for the geometry given

in figure 4.3.

$$q_{Diss} = k \cdot S \cdot \Delta T \qquad \text{where} \qquad S = \frac{(2 \cdot \pi \cdot L)}{\ln \frac{(8 \cdot z)}{(\pi \cdot D)}} \tag{4.11}$$

The flow channel surface temperature of the radiator and HX can be found by solving for temperature, eq 4.12. More advanced conduction problems were solved as part of the excel-based analytical modeling tools developed for the ACCS research. Those will be discussed in greater detail later.

$$T_{Channel} = \frac{q_{Diss}}{K \cdot S} + T_{Surface} = \frac{q_{Diss}}{k \cdot (\frac{2 \cdot \pi \cdot L}{ln(8z/\pi D)})} + T_{Surface} \tag{4.12}$$

4.4 ACCS: Convective Heat Transfer

Convective heat transfer refers to the transport and exchange of thermal energy through the movement and interactions of fluids. Specifically, it refers to the transfer of heat through fluid contact with a solid instead of mixing between fluids. Convection can be either forced or natural. Forced convection occurs when an external force governs the movement of fluid. Natural convection occurs due to the bulk movement of fluid due to thermal-density forces such as buoyancy, etc. Convection is linked by advection, the bulk transfer of fluid, and conduction within the liquid itself. The ACCS is a forced convection system. Working fluid is transported from the internal heat exchanger to the external radiator by a micro pump and motive pressure gradients. Heat is transferred through the UAM fluid channels to and from the heat exchanger and radiator bodies. This transfer of heat is shown in figure 4.4. The convective control volume encloses the fluid channel. Energy enters the CV as mass (fluid) transfer, and partially exits through convection heat transfer with the channel walls. The remaining thermal energy exits the CV with the fluid as residual heat.

The basic equations for the heat carried by the fluid and the heat transferred to the radiator and HX bodies are given by equations 4.13 & 4.14. Convection occurs over an area and is purely a surface phenomenon.

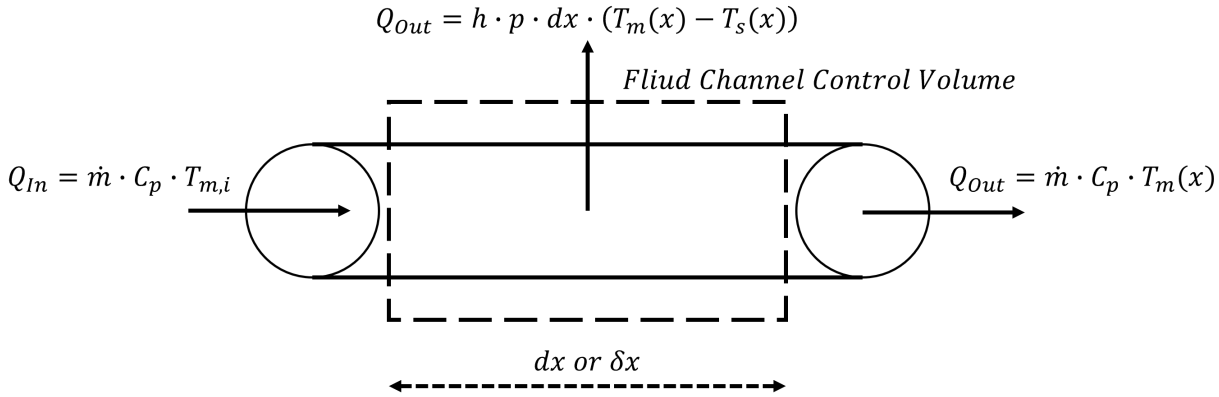

Fig. 4.4: ACCS Convective control volume.

$$Q = h \cdot A \cdot \Delta T \tag{4.13}$$

$$Q = \dot{m} \cdot C_P \cdot \Delta T \tag{4.14}$$

The convective transfer variable h is the proportionality constant that relates the thermal flux within the system and the motive force or temperature difference. *dotm* is the mass flow rate in kg/sec of the fluid, while C_P is the specific heat capacity of the fluid in J/kgK. Heat capacity is essentially a direct measurement of how much thermal energy a given fluid can carry at a given temperature. The thermal gradient referred to by ΔT can be the fluid temperature at the entrance vs. the exit of the control volume or the difference between the fluid and channel wall temperatures. The volume flow rate and relative fluid velocity can be calculated from,

$$\text{Volume Flow Rate} = \frac{\dot{m}}{\rho} \qquad FluidVelocity = \frac{\dot{m}}{\rho A} \tag{4.15}$$

The UAM channels of the ACCS system are not perfectly circular. Instead they are formed by a half U-shaped channel with a height larger than the width. The hydraulic diameter of this non-circular flow channel can be calculated from equation 4.16. The hydraulic diameter is an equivalent diameter for non-circular flow geometries. Defined by the

ratio of the area to the perimeter.

$$D_h = \frac{4 \cdot A}{P} \tag{4.16}$$

An essential aspect of convection analysis is the flow regime. Flow regimes can, broadly, be broken down into three categories: Laminar, Turbulent, and transitional. Laminar flow is characterized by minimal mixing between flow boundary layers. Fluid lines travel in roughly parallel paths and do not necessarily mix unless acted upon by an outside force. Conversely, the turbulent flow regime is quite the opposite. Flow lines and boundary velocity boundary layers mix and tumble continuously, forming a chaotic flow pattern. Transitional flow falls in between laminar and turbulent. The flow can oscillate back and forth and have aspects of either simultaneously. The Reynolds number is a calculated value that relates the dynamics of the fluid, its properties, and the geometry of the flow channel to a dimensionless ratio. This Reynolds ratio can be used to determine the flow regime type. The Reynolds number equation is shown below, where fluid density, velocity, and flow diameter are divided by the fluid's viscosity. Reynolds numbers are experimentally derived and traditionally correspond to each flow regime.

$$Re = \frac{\rho \cdot V \cdot D}{\mu} \tag{4.17}$$

$$\begin{gathered} \textit{Laminar} \longrightarrow \textit{Transitional} \longrightarrow \textit{Turbulent} \\ 0 \leq Re \leq 2300 \quad 2300 \leq Re \leq 4000 \quad Re \geq 4000 \end{gathered} \tag{4.18}$$

Another important flow parameter is that of the Prandtl number. The Prandtl number is the ratio of the thermal boundary layer to the hydrodynamic boundary layer. Essentially, it gives the relative dominance of the thermal boundary to the momentum boundary layer. Or how fast heat transfer takes place with respect to thermal diffusion vs. momentum diffusion. Large Prandtl numbers indicate that the bulk transfer of the fluid is far more dominant than the internal conduction of the fluid. Small Prandtl numbers indicate the

opposite. That internal conduction is critical. Liquid metals are an example of liquids with small Prandtl numbers. The Prandtl number is calculated from,

$$P_R = \frac{(C_P \cdot \mu)}{k} \tag{4.19}$$

The convection coefficient is the ratio of the fluid thermal flux to the temperature gradient. This is defined by the flow geometry, conductivity of the working fluid, and the Nusselt number, as shown. The Nusselt number is the ratio of convective to conductive heat transfer.

$$h_{avg} = \frac{\ddot{q}}{\Delta T} = \frac{Nu_{Dh} \cdot D_h}{k} \tag{4.20}$$

Many different correlations exist for Nusselt number [127]. However, each equation differs regarding appropriate convection analysis (Forced vs. Free), flow geometry, and the specific flow regime. The Reynolds and Prandtl numbers for the ACCS system are given below: two-primary Nusselt numbers were used, the classic Dittus Boelter correlation and the more specialized Gnielinski Correlation. For the ACCS, the Gnilinsky Nusselt correlation was primarily used. Both are given below in equation 4.22 & 4.23. For basic laminar flow, the Nusselt number is greatly simplified to a constant value.

Laminar Flow Regime

$$Nu = 3.66 \quad \text{for constant temperature} \quad \text{and} \quad Nu = 4.36 \quad \text{for constant heat flux} \tag{4.21}$$

Dittus Boelter Correlation

$$Nu_{Dh} = 0.023 \cdot Re_{Dh}^{0.8} \cdot Pr^{0.4} \quad for \quad 0.6 \leq Pr \leq 160 \quad \& \quad Re_{Dh} \geq 10000 \tag{4.22}$$

Gilinsky Correlation

$$Nu_{Dh} = \frac{(f/8)\cdot(Re_{Dh}-1000)\cdot Pr}{1+12.7\cdot(f/8)^{\frac{1}{2}}\cdot(Pr^{2/3}-1)} \quad for \quad 0.5 \leq Pr \leq 2000 \quad \& \quad 3000 \leq Re_{Dh} \leq 5\cdot 10^6 \tag{4.23}$$

Both Nusselt calculations require the friction factor. The Darcy-Weisbach friction factor, derived from the Moody diagram, relates the pressure loss for an enclosed incompressible flow to the relative velocity of that flow. The friction factor below is the Petukhov correlation, eq 4.24. Selected due to the particulars of the ACCS system. When combined, these terms can derive the convection coefficient for the ACCS flow.

$$f = (0.79 \cdot ln(Re) - 1.64)^2 \tag{4.24}$$

The energy balance across the ACCS convection control volume, shown in figure 4.4, is given below by equating the total thermal input to the total output. Thermal input is provided by fluid advection, while output is convective heat transfer through the channel walls and advection of the exiting fluid. This thermal balance is:

$$Q_{In} = Q_{Out} = \dot{m} \cdot C_P \cdot T_{m,i}(x) + h \cdot p \cdot dx \cdot (T_m(x) - T_s(x)) \tag{4.25}$$

The fluid inlet temperature is given by $T_{m,i}$ (initial temperature) and the control volume is on a per unit length bases (dx). Therefore, the total convective area is the perimeter multiplied by the finite or total channel length. The outlet temperature of the fluid is given by $T_m(x)$, while the channel surface temperature is $T_s(x)$. The total rejected heat can be quantified as the dissipated heat and calculated by summing the heat loss per unit length of the channel.

$$\Delta q = q_{Diss} = \dot{m} \cdot C_P \cdot (T_{m,i} - T_m(x)) = \int_0^x h \cdot p \cdot (T_m(x) - T_s(x))dx \tag{4.26}$$

This term can be integrated over the total length of the channel to derive an equation for the fluid temperature at any longitudinal point with respect to the inlet temperature, channel surface temperature, and fluid properties. The integrated solution to this equation is given below for the assumption of constant internal flow channel surface temperatures. Equation 4.27 can be simplified and solved for $T_m(x)$ [128].

$$q_{Diss} = \dot{m} \cdot C_P \cdot (T_{m,i} - T_m(x)) = h \cdot p \cdot \frac{\dot{m} \cdot C_P \cdot (T_s - T_{m,i}) \cdot (1 - e^{\frac{-h \cdot p \cdot x}{\dot{m} \cdot C_P}})}{h \cdot p} \tag{4.27}$$

$$T_m(x) = T_s - (T_s - T_{m,i}) \cdot (e^{\frac{-h \cdot p \cdot x}{\dot{m} \cdot C_P}}) \tag{4.28}$$

$$T_m(x) = T_{m,i} + (T_s - T_{m,i}) \cdot (1 - e^{\frac{-h \cdot p \cdot x}{\dot{m} \cdot C_P}}) \tag{4.29}$$

The constant surface temperature of the body (flow channel surface temperature) can be determined by back calculating the thermal flux. As shown in 4.30. The fluid temperature as a function of length can also be considered the initial inlet temperature of the body.

$$T_s(x) = T_m x + \frac{q_{Diss}}{\dot{m} \cdot C_P \cdot (1 - e^{\frac{-h \cdot p \cdot x}{\dot{m} \cdot C_P}})} \tag{4.30}$$

For the assumption of constant surface flux, $T_m(x)$ can be solved, eq 4.31, while the variation in surface temperature is calculated from equation 4.32.

$$T_m(x) = T_{m,i} + \frac{q_s'' \cdot p \cdot x}{\dot{m} \cdot C_P} \tag{4.31}$$

$$T_s(x) = T_{m,i} + \frac{q_s'' \cdot p \cdot x}{\dot{m} \cdot C_P} + \frac{q_s''}{h} \tag{4.32}$$

Two final performance equations were used in the analysis of the ACCS system. These

are the log mean temperature difference and number-of-transfer-units. The logarithmic temperature difference (LMTD) is a measure of the temperature-driving force of a heat exchanger system. It is the logarithmic average of the extreme differences in temperature within the system. For the ACCS, this is the difference between the constant surface temperature of the channel walls and the inlet/outlet temperatures of the working fluid. LMTD is essential because, unlike a straight average, it gives a more accurate representation of the differences between the temperature extremes within a system. The LMTD for the ACCS is calculated from,

$$LMTD = \frac{(T_s - T_m(x)) - (T_s - T_{m,i})}{ln\left((T_s - T_m(x))/ln(T_s - T_{m,i})\right)} \tag{4.33}$$

The Number of Thermal Transfer Units, equation 4.34 is a relative measure of efficiency. It is the unitless ratio of heat transferred to a working fluid by convection to the maximum ability of that fluid to transfer that heat. As the ratio approaches one, the overall efficiency of the heat exchanger approaches 100%. Meaning that all of the heat transferred to the fluid is successfully transferred by the fluid out of the control volume. If the number is greater than one, the convective heat transfer is greater than the total capacity of the fluid at a given temperature gradient. An NTU greater than one is not physical, instead, a given fluid would undergo a phase change [129].

$$NTU = \frac{h_{avg} \cdot A}{\dot{m} \cdot C_P} \tag{4.34}$$

4.5 Conclusions

The heat transfer and thermodynamic analytical equations given in this chapter form the theoretical framework for the ACCS technology and can be modified as necessary to describe the various thermal resistance networks within the ACCS system. While basic, these equations are incredibly adaptable to complex situations and model the performance and behavior of the ACCS system well. These equations also provide a deeper understanding of the ACCS heat transfer systems. The theories laid out in this chapter are primarily used

in the excel based analytical model. Future models will expand this basic theory to feature more complex and specialized 2D & 3D transient solutions with more realistic boundary conditions.

CHAPTER 5

Active CryoCubeSat Design

Every Great Design Begins With An Even Better Story

Lorinda Mamo

5.1 Introduction

The story of the ACCS design began with the problem every engineer wants to have. That of success and progress. CubeSats began with very humble origins. Considered an early effort in standardization, CubeSats started out as learning tools for universities and small companies. CubeSats were not considered useful scientific testbeds by the greater community until many years later. In fact, CubeSats were often referred to as space debris in the early days. However, as time passed and modern technology and engineering were integrated with CubeSat design, those opinions quickly changed. Within just a few short years, CubeSats had proven their worth as cost-effective scientific instruments and engineering tools. Overall, CubeSats have had a meteoric success story and now feature prominently in the space community. In fact, CubeSats and other classes of small satellites might dominate space someday.

It is this success that begins the current design story. CubeSats are becoming more successful, more popular, and more advanced. Engineers are leveraging modern technology to push the boundaries of CubeSat even further to accomplish more complex mission objectives. This push is for science and technology payloads, CubeSat buses, and subsystems. An important example of this technology growth is power generation and energy storage. Modern CubeSats are more than capable of generating over 100 W of peak power. This level of onboard energy, in turn, allows for more complex and high-powered payloads,

buses, and missions to be developed. However, because CubeSats are inherently small, this increase in overall power has naturally led to an increase in the relative power density of Small Satellites. When a satellite is scaled to the size of a shoebox, placed in orbit with the thermal space environment, and the various heat transfer methods reduced to radiation, a thermal management problem quickly becomes apparent. Naturally, a thermal bottleneck has developed in CubeSat payload and mission design. To help solve this thermal problem, new, advanced thermal control technologies are required. The ACCS is one of these technologies.

The ACCS is an active thermal control technology based on a two-stage design. The first stage is formed by a mechanically pumped fluid loop (MPFL) heat exchanger and single-phase heat transfer. A low viscosity working fluid is circulated in a closed loop between an internal HX and an externally deployed radiator. An integrated miniature cryocooler forms the second stage and provides cryogenic cooling for advanced electro-optical IR payloads for Earth science and heliophysics. The ACCS active thermal control system provides bus-wide thermal management, temperature control, and payload-targeted thermal support. Modern advanced COTS parts and Additive manufacturing/3D printing enables this technology. Overall, the critical design considerations for the ACCS project include UAM fabrication techniques for the heat exchanger & radiator, The Ricor K508N cryocooler, the TCS M510 micro-pump, and the Novec 7000 working fluid. Figure 5.1 below shows assembled CAD of the ACCS heat exchanger system. Featured are the UAM HX panel, working HTF channels, Ricor K508N cryocooler, and TCS M510 micro-pump.

The ACCS system is an in-lab technology demonstration and proof of concept for single-phase active thermal control on CubeSats and Small Satellites. The specific design requirements and objectives for this project are given in detail in the introduction chapter. However, for the current discussion, a few key objectives are to actively control the thermal load of an advanced payload with an active system of less than 1U and raise the TRL of MPFLs, and UAM manufacturing to at least a $\sim$5 (TBR).

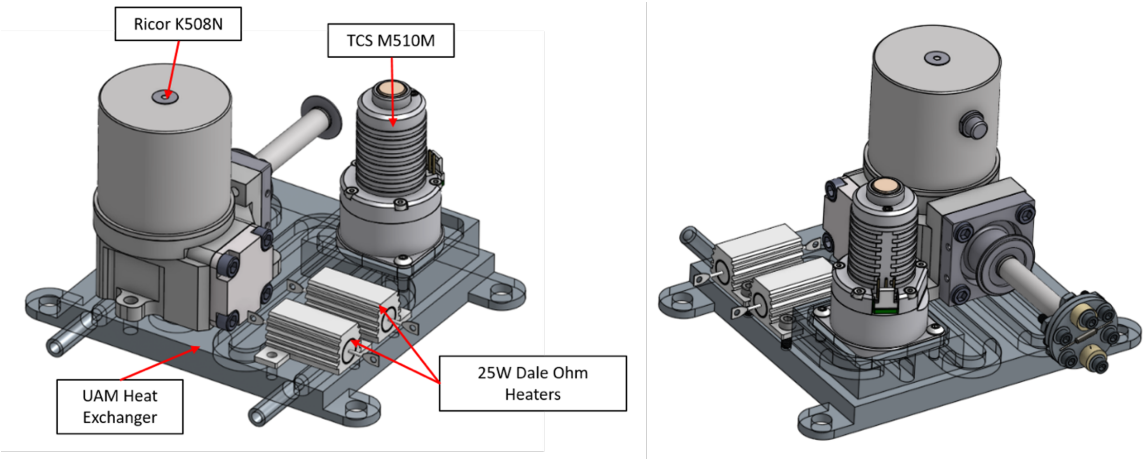

Fig. 5.1: Assembled CAD of the ACCS heat exchanger assembly featuring the TCS M510 micro-pump, Ricor K508N cryocooler, and UAM HX.

5.2 Advanced 3D Fabrication: Ultrasonic Additive Manufacturing

Ultrasonic Additive Manufacturing (UAM) is a metal deposition hybrid 3D printing process in which the advantages of additive and subtractive fabrication are combined into a single machining process. This hybrid process combines both benefits and allows for complex 3D shapes, voids, and internal passageways to be created with high dimensional accuracy and smooth surface finishing. UAM fabrication is based on Ultrasonic cold welding or cold solid-state atomic bonding. An ultrasonic weld head or "Sonotrode" applies downward force/pressure along with a lateral ultrasonic scrubbing force to weld thin metal foils, sheets, or tapes locally to a base metal, figure 5.2, [2]. The ultrasonic frequency vibrations (20-30 kHz) are generated by dual, tuned ultrasonic transducers and transferred to the welding horn. On a micro-scale, the ultrasonic vibrations combined with the downward force of the weld head break up surface oxides and cause local asperities to yield and collapse, resulting in minimal heating of the surface material ($< 250^\circ$ F) and plastic deformation of the metal surfaces. UAM welding promotes material diffusion and recrystallization at the material substrate, forming a true metallurgical bond. Bulk UAM 3D fabrication is accomplished by building up these thin metal layers. Periodic subtractive machining adds detailed features and finishes the process. An advantage of UAM is that it can be performed by a custom three-axis mill and does not require any unique environment. Print sizes of up to 6 x 6 x 3

ft are possible at a print rate of greater then 30 cubic inches. UAM fabrication is unique in that different materials can be bonded to form composite structures. Aluminum 6000 & 7000 series are standard, along with copper, stainless steel, and hybrids. Post-processing of UAM materials often includes Hot Isothermal pressing (HIP).

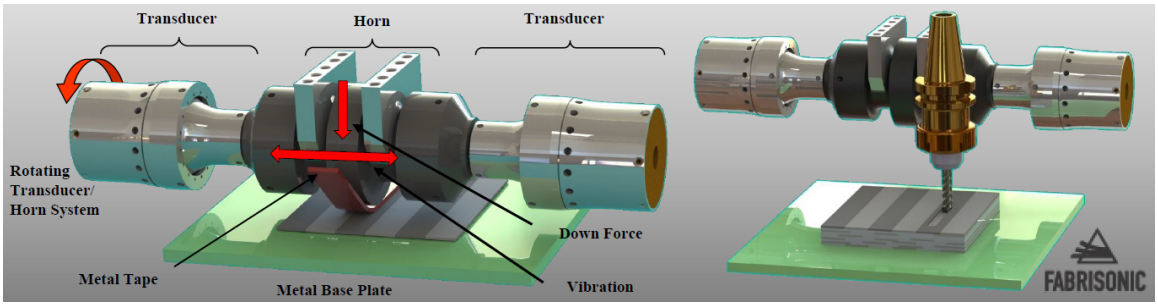

Fig. 5.2: Fabrisonics UAM cold ultrasonic weld head [2].

3D UAM fabrication was a critical technology for the success of the ACCS system. Ultimately, it allowed the USU/JPL teams to create a thermal control system with heat transfer structures and interfaces integrated directly with and into the heat exchanger, radiator, and CubeSat structure, something that would normally be impossible with traditional manufacturing techniques. By leveraging UAM techniques, the ACCS fluid channel network could be integrated, miniaturized, and simplified. The advantages of UAM as a fabrication technique for single-phase active thermal control systems cannot be overstated. By utilizing UAM, the ACCS team was able to create multi-function CubeSat structures with significantly improved thermal conductances over traditional epoxy bonded or welded tubing systems. Material laminates and mixed composites can also be leveraged to combine the mechanical and thermal advantages of different materials. A final but crucial aspect of 3D printing and UAM manufacturing is rapid design iteration and minimal turnaround time/effort. Traditional MPFL systems require skilled technician labor to fabricate and are very tedious and time consuming, requiring multiple steps and checks. UAM and 3D fabrication enable engineers to rapidly iterate designs and create integrated mechanical structures without further assembly.

5.3 ACCS Heat Exchanger Design

The ACCS heat exchanger collects concentrated thermal energy from the CubeSat payload or bus and transfers it via the working fluid/MPFL to the radiator. The heat exchanger operates as a distinct and often isolated thermal zone within the satellite. Components requiring high power dissipation or setpoint temperature control can be directly mounted to the HX. These thermal loads are transferred through the solid Aluminum (or copper composite) UAM body to the embedded fluid channels by conduction. Lateral 2D conduction spreads the thermal load across the HX and into the working fluid channels. Ideally, the ACCS heat exchanger operates as near to isothermal as possible. Heat exchanger efficiency is an area of ongoing research for the ACCS team. An ISO CAD view of the ACCS heat exchanger as a finalized design is shown in figure 5.3.

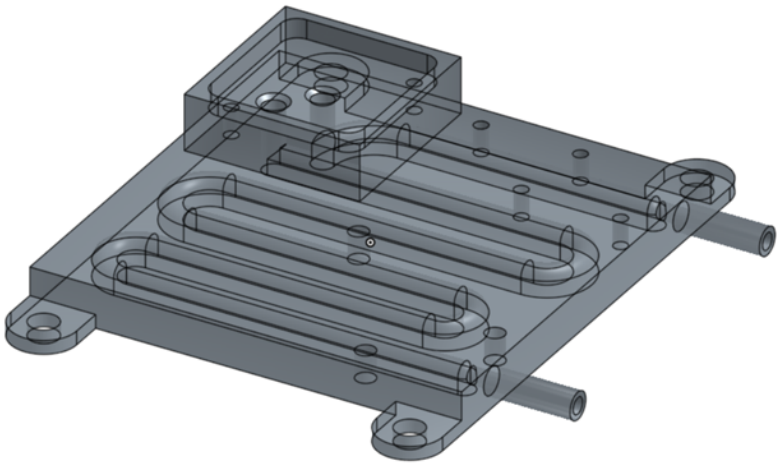

Fig. 5.3: Finalized ACCS heat exchanger design. Cooling channels are shown along with various mounting points and the working fluid inlet/outlet.

An original requirement for the ACCS system was to limit the internal volume requirements of the heat exchanger assembly to less than 1U. Therefore, the ACCS HX is sized at 10 X 10 cm (1U) and only 1 cm thick. See figure 5.5 below. As a proof of concept, the ACCS needed to represent not only a miniaturized MPFL system but one appropriate for CubeSats. The ACCS HX is a six-pass heat exchanger with approximate tube spacing of 1 cm and lengths of 9 cm. The HX cooling channels are designed with a gradual 180^o

bend radius (1 cm) to minimize flow pressure losses. The flow pattern concentrates the embedded tubes under the cryocooler mounting point with four passes, improving the rate of heat transfer and decreasing transient gradients. The ACCS design optimizes the overall thermal removal of the cryocooler waste heat. The number and shape of the working fluid channels are directly related to the isothermality and efficiency of the heat exchanger. Due to the nature of UAM 3D printing, as both a subtractive and additive process, flow channels must be designed with a flat UAM foil side. This means that circular flow channels are not possible with UAM fabrication. Instead, rectangular or U-shaped channels are required. The U-shaped channels for the ACCS are designed with a hydraulic diameter of ∼0.25 inches to maintain hydraulic similarity with the rest of the fluid network and the standard stainless steel tubing used by the ACCS test cube. Channel dimensions are shown below in figure 5.4.

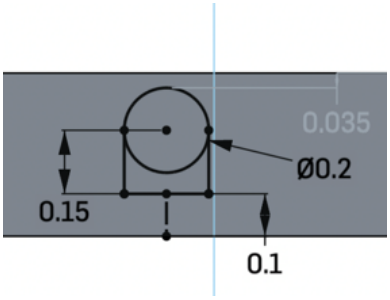

Fig. 5.4: UAM flow channel profile for the ACCS heat exchanger and radiator. Units are in inches.

The ACCS heat exchanger inlet and outlet are terminated with standard, machined, quarter-inch tube studs. Tube studs are not, generally, a practical design for CubeSat applications. However, they are ideal for ground-based testing and interfacing with the test cube Swagelok compression fittings used throughout the rest of the design. The TCS M510 micropump is mounted on the square pump pedestal, shown in the upper right of figure 5.5. This pump pedestal includes the manifold mounting points for the micropump and the vertical inlet and outlet for the fluid channels. These channels are drilled directly into the bisected fluid paths shown below. The raised HX pedestal serves several purposes:

the M510 comes standard with 8 mm ports. These need to be gradually narrowed down to 6.35 mm (0.25"). Elevating the pump pedestal allowed more room for machining these inlet/outlet gradual contractions. In addition, at the time of design, the leak rate of the M510 flat surface seals was unknown. The lip of the pump pedestal provided a convenient area to apply a backup single-use gasket material, such as silicone RTV.

Mounting holes in each corner of the HX stick out past the 1U footprint and provide convenient attachment points for Teflon mounting bolts. These studs provide thermal isolation and mechanical suspension of the ACCS HX within the test cube. The HX is coated with a gold chemfilm to preserve the aluminum surface's thermal contact resistance and prevent surface oxidation. The bottom of the HX is black anodized to control the emissivity value and provide an ideal surface to view with the instrumented FLIR IR cameras. Mounting points for the TCS M510 micro-pump, Ricor K508 cryocooler, and Dhale-Ohm guard heaters are shown below in figure 5.5, along with a fabrication photo of the ACCS heat exchanger.

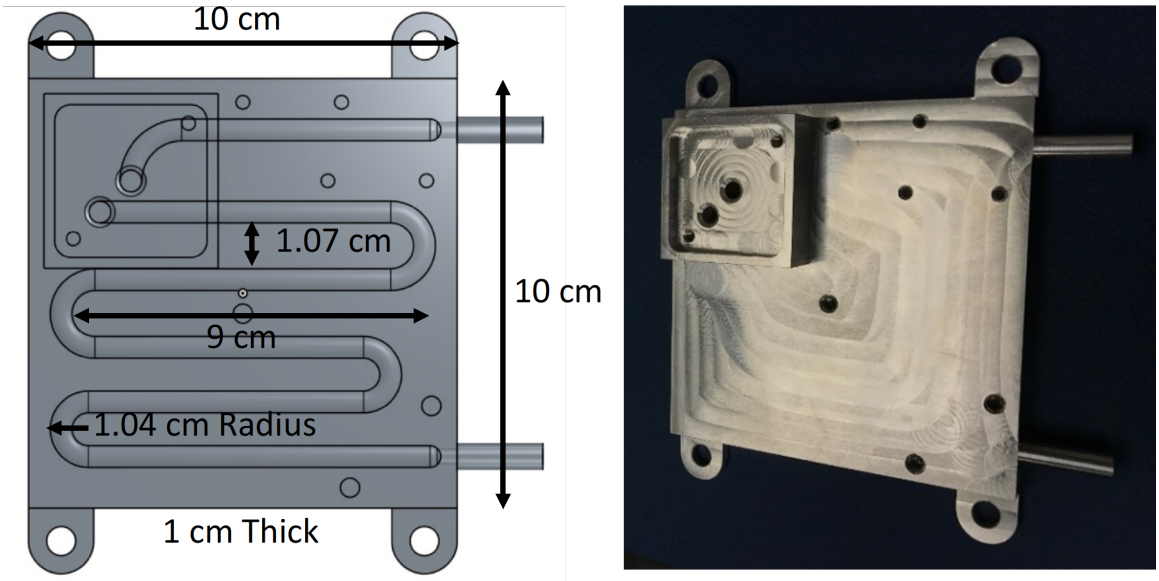

Fig. 5.5: ACCS heat exchanger design. Flow channel layout and finished part.

The ACCS heat exchanger was designed to accommodate the integrated K508N cryocooler, the M510 micro-pump, and parallel guard heaters. Each of these required a flat mounting surface. However, if requirements were different, other designs would be preferred. Initially, the Lockheed Martin Pulse Tube Cryocooler was considered for the ACCS project. The LM PTC operates with a split tube design. The LM cryocooler would have required that the compressor and cold finger expander be mounted separately. The expander would need to be mounted by the collar, penetrating through the heat exchanger plate. With UAM, the heat exchanger could interface with various active components in 3D, improving the overall heat transfer tremendously. Ultimately, the ACCS heat exchanger described above is a simple yet effective design. More advanced, efficient, and practical designs are possible and should be explored in future research.

5.4 ACCS Radiator Design

Radiators are the key to thermal control for space applications and allow for consistent, practical heat transfer. The ACCS system features a large, dedicated radiator appropriate for 6U and 12U CubeSats. The radiator is fabricated from UAM from 6061 equivalent aluminum and finished with traditional machining techniques. It features embedded flow channels with a ~0.25" hydraulic diameter in a four-pass design with soft 180^o bends. Like the UAM Heat Exchanger, the radiator requires U-shaped channels with a UAM layered roof. The total tubing length of the radiator is 124.5 cm. Figure 5.6 below shows an ISO view of the original radiator design CAD. Dimensions are also shown, including overall size, tubing length, and spacing. The ACCS radiator was envisioned as an idealized radiator for a CubeSat or Small Satellite and was designed for simplified, easy-to-model thermal performance.

Standard CubeSat sizes, as proscribed by NASA, dictate the overall dimensions of a CubeSat. Specifically, 6U CubeSats (12 x 24 x 36 cm) and 12U (23 x 24 x 36 cm). The ACCS radiator was sized to match the dimensions of a 6U or 12U CubeSat, nominally 22 x 36 cm. However, due to the size restrictions of the CSE TVAC chamber, the equivalent area was redistributed as a slightly wider and shorter radiator, see figure 5.6. This change in

shape helped to fit the ACCS radiator in the available footprint of the test cube. Mounting holes were included along the edges of the radiator and near the center. Similar to the HX, the radiator inlet and outlet are machined quarter-inch tube studs. Swagelok compression fittings with Teflon farrels were used to couple the radiator to the tubing network.

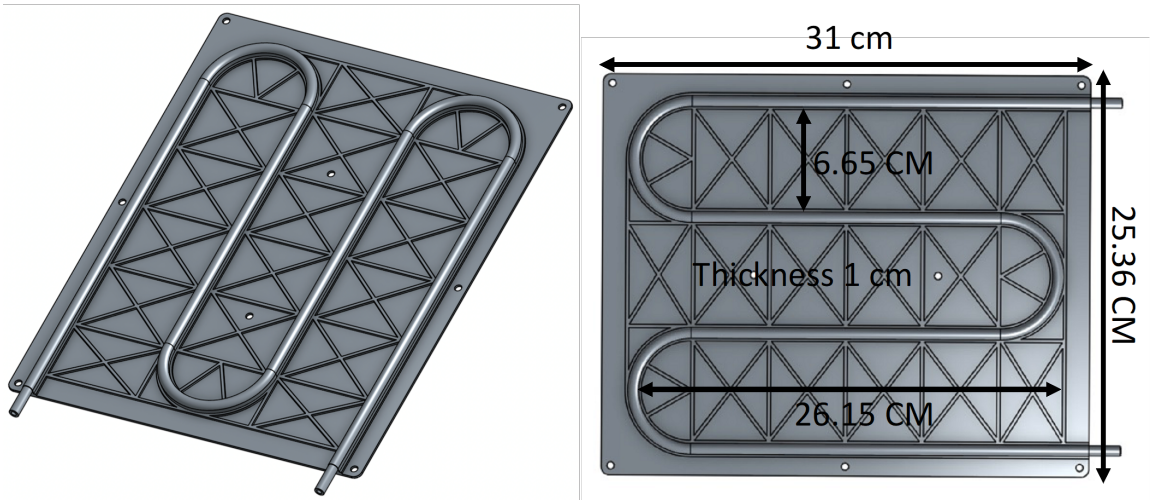

Fig. 5.6: Accs radiator design. 6U cross-hatched panel with embedded flow channels.

JPL consultants modeled the four-pass design in Thermal Desktop to optimize the radiator's thermal gradients (isothermality) and minimize the total fluid channel length. The design shown maximized the tubing spacing for a given desired radiator efficiency. Overall, the radiator flow channels for each pass were approximately 26 cm long and spaced by 6.65 cm. A gap of nearly ∼0.5" was left around the circumference of the radiator. Fabrisonics recommends that hermetic seals or UAM voids should not be placed closer to an edge. The ACCS radiator is 1 cm thick (the fluid channels being the thickest point) and requires light-weighting. The fluid channels were machined into circular domed channels for light-weighting. Most of the remaining radiator area was machined to a panel only 1.5 mm thick, significantly reducing the weight. This thin plating would only be supported by the structure of the tubing and could tend to bend or buckle. Therefore, stiffening structures, aka ridges, were added through cross-hatching. These cross-ribbed patterns were precision machined directly into the finished UAM panel. Figure 5.7 below shows the ACCS radiator

at a variety of steps. On the far left, the ACCS radiator is newly fabricated; in the middle, the radiator has been surface treated and black anodized; and on the far right, the radiator has been painted with Aeroglaze Z306 high emissivity black paint.

Fig. 5.7: ACCS UAM Radiator. Left: as machined, middle: black anodized, right: painted with Z306 black paint.

Fabrisonics recommended that for hermetic UAM channels, there should be a minimum leak path of 0.1 inches. The ACCS radiator U-shaped channels were formed into a platform design to increase the minimum thickness of the panel to accommodate this requirement. Additional material was included on the flat UAM side of the channel, and the outer wall of the channel was machined down to a 0.125-inch ledge. This design ensured that at no point was a UAM layered leak path closer than 0.1 inches to the pressurized flow conduits. This platform design and U-shape of the channel are shown below in figure 5.8 as a section cut view, left, and CAD design right.

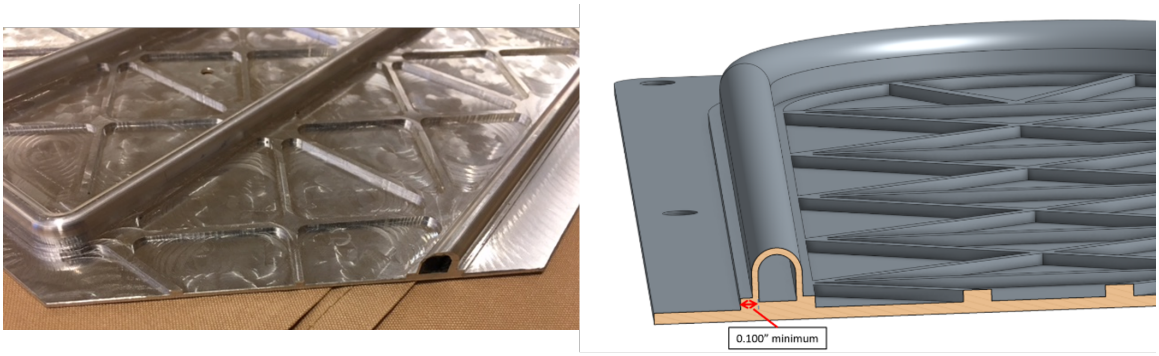

Fig. 5.8: Cutaway view of the ACCS radiator embedded flow channel.

The ACCS radiator was designed for high efficiency and to maximize thermal rejection from a 6U or larger CubeSat. The radiator design was based on heat transfer principles and best practice mechanical design with expertise in UAM design from Fabrisonics and JPL's previous radiator design experience. Overall, the ACCS radiator performed as predicted and can be modified in the future to be even better

5.5 ACCS Cryocooler: The Ricor K508N

The ACCS system is an active thermal control technology aimed at CubeSat thermal power management and temperature control. A specific technology target for the ACCS was the thermal accommodation of miniature high-powered cryocoolers for cryogenic electro-optical IR instrumentation. The cryocooler selected for the ACCS system is the Israeli-made Ricor K508N tactical cryocooler. The K508N is a Stirling cycle cryocooler featuring an integrated rotary compressor design. The K508N is a long-life, high-reliability variant of the standard K508 model. The K508 and the K508N have a long-flight heritage, with the K508N serving on the Mars Curiosity rover. The K508N is rated to over $+20,000$ hours of 24/7 service lifetime and features an improved ambient temperature to input power ratio. When combined with the motor and driver's real-world efficiencies, the K508N thermodynamic Stirling cycle has an overall efficiency of approximately $\sim 7.3\%$, which is about 20% of the ideal Carnot efficiency. Like other cryocoolers, the K508N operates via thermodynamic transfer of oscillating compressed helium gas. For the K508N, this internal helium gas is sealed with advanced C-ring seals. These seals are ideal for high ambient temperature environments and long leak-free operation. Figure 5.9 shows the ACCS K508N. The cold tip extends to the right, with the motor housing and rotor crankshaft housing clearly visible.

The K508N features a ruggedized design with advanced steel materials, surface plating, and a laser-welded cold finger assembly. Ricor has optimized the K508N to include the latest mechanical design improvements, including optimized bearings, preloaded internal parts/arrangements, dynamic mechanical greases, and advanced seals. As a rotary Stirling cycle, the K508N does generate vibration and jitter; however, with the robust structure and careful internal design mentioned above, the natural frequency of the cryocooler has been

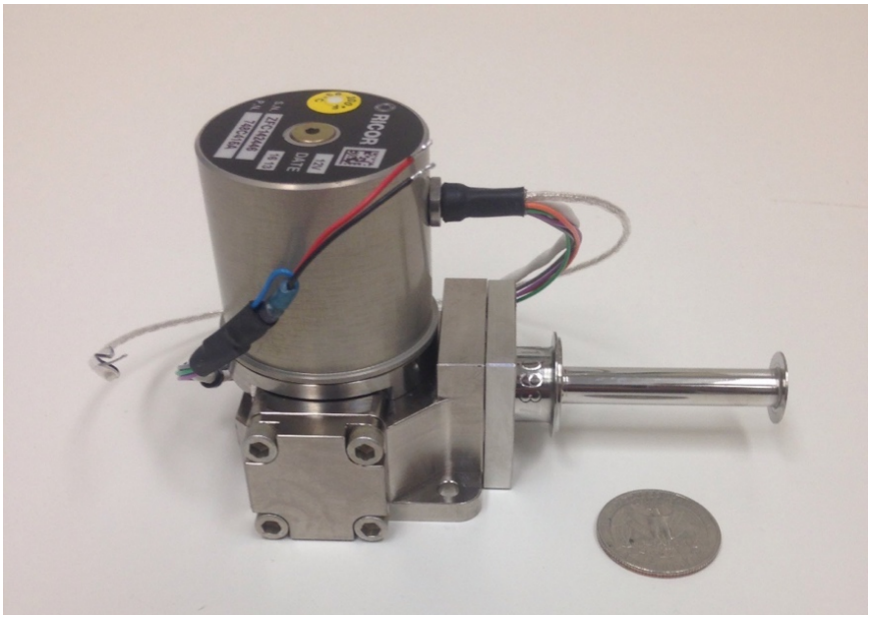

Fig. 5.9: ACCS Ricor K508N cryocooler with integrated HyB18N controller compared to a quarter.

increased compared to the K508 mode. The performance characteristics of the K508N are listed in Table 5.1 below. The K508N features an improved integrated analog controller based on the time-tested Hyb18N logic board. This single PCB integrates the cold-tip temperature setpoint controller and motor controller/driver. The Hyb18N is enclosed within the top motor casing of the integrated K508N cryocooler.

Ricor K508N	
Size & Weight	71 x 58 x 115.5 mm & 475 grams
Power	5.5 to 20 W
Cooling Capacity	900 mW @ 110 K with 71 C ambient 550 mW @ 77 K with 71 C ambient
Cold Tip Temperature	65 to 150 K
Operational Temperature	-40 to +85 C
MTTF	>28,000 hours
Service Life	15 Years

Table 5.1: Ricor K508N performance metrics.

The K508N is an ideal cryocooler for the ACCS system and CubeSat platforms/missions. It is cost-effective, miniature, reliable, and powerful—more than capable of support-

ing advanced payloads and ensuring mission success. The ACCS K508N is a 12-24 V model with a charged pressure of 35 atm. The K508N is directly mounted to the ACCS heat exchanger with an indium soft metal thermal interface patch. This thermal interface helps to reduce the contact resistance between the cryocooler and HX. The total thermal load of the cryocooler is transferred by the mechanical structure and rejected to the mounting base HX and the embedded fluid channels. The ACCS cold tip copper mount is clamped to the K508N cold expander. This copper mount is instrumented for temperature and thermal load control of the cryocooler. Figure 5.10 below shows CAD modeling of the Ricor K508N with various views.

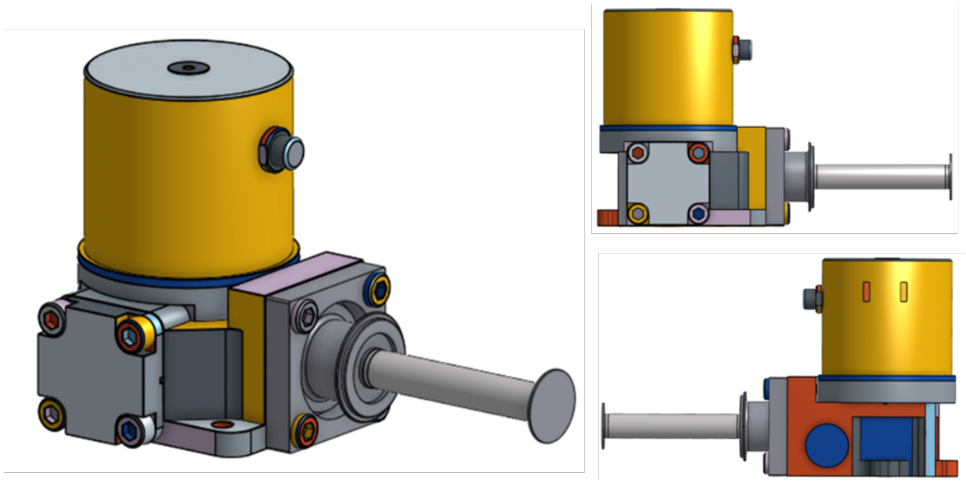

Fig. 5.10: CAD views of the Ricor K508N Stirling cryoccoler.

The ACCS system originally proposed to integrate the Lockheed Martin micro-pulse tube cryocooler, recently tested to a TRL of 6 by LM. This advanced cryocooler is based on a pulse-tube design and features a low mass, low volume form factor with minimal exported vibrations. In addition, the LM cryocooler has essentially no moving parts, allowing for high reliability and a projected lifetime of +100,000 hours. LM initially agreed to loan a porotype of the micro-pulse tube cryocooler to USU for integration and testing with the ACCS system. However, due to unforeseen flight requirements and scheduling conflicts, the USU and ACCS team pivoted to the Ricor K508N as a COTS replacement. Figure 5.11

shows the LM micro-pulse tube cryocooler and the original heat exchanger assembly design. Note that the compressor body and cold head are directly integrated with the UAM panel and fluid channels. Future heat exchanger designs could include advanced UAM cryocooler mounting structures. These improved designs could interface the working fluid channels directly with a given cryocooler's various critical thermal zones. Thermal channels could wrap around thermal zones or be directly integrated with the cryocooler body for both integrated and split cryocooler designs. Ultimately, advanced active cooling will help to enable future generations of high-efficiency, low-power cryocoolers for space applications.

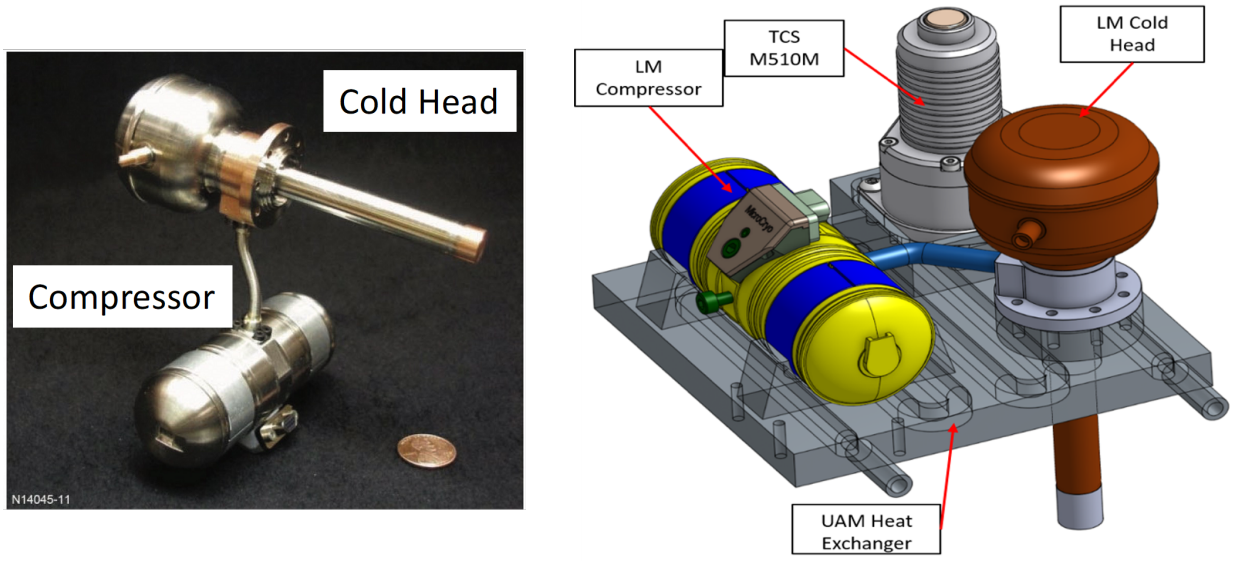

Fig. 5.11: Lockheed Martin Pulse Tube Cryocooler, [3]. Right: Concept design for the integration of the LM cryocooler with the ACCS heat exchanger.

5.6 ACCS Micro-Pump: The TCS M510 Centrifugal Pump

As a pumped fluid loop, the heart of the ACCS system is the TCS M510 centrifugal micro-pump. At the beginning of the ACCS research, a full trade study was performed to down-select the ideal micro-pump for the ACCS application. Project defined requirements included: miniaturized size, low power, high-pressure differential, and variable flow up to 1000 mL/min. Ultimately, the M510 was selected and has proven to be an ideal pump for

applications like the ACCS.

The M510 is a miniature high-power centrifugal micro-pump driven by a powerful brushless DC motor, which can generate low-vibration, pulseless flow up to 10 liters/minute. Table 5.2 gives the characteristics and operational performance of the M510. The M510 utilizes an external motor driver; the EQI-M control board regulates input power and drives the pump's closed-loop speed/power control. The voltage input for the EQI-M ranges from 12-24 V, while pump speed control is governed by either an onboard potentiometer or a 0-5 V analog control signal. Pump RPM can be read as a frequency-based square output wave from the controller. The M510 is machined from solid aluminum alloys with a stainless-steel impeller volute. A critical design feature of the M510, which makes it particularly appealing for space applications and the ACCS system, is that the M510 is a "Canned" pump design. The impeller, drive shaft, and rotor are enclosed within a PEEK plastic case. The M510 canned pump does not have any dynamic seals. No shaft seal exists, and the working fluid is allowed to permeate the rotor assembly. The entire pump is filled with the working fluid and enclosed by a single static collar seal. The BLDC electromagnets drive the rotor through this PEEK case with a plain bearing guiding the drive shaft. The pump's dynamic motion is entirely submerged with the working fluid. A canned pump design improves performance and lifetime by reducing/eliminating many common failure modes associated with dynamic shaft seals. The M510 comes in various mounting styles, however, for integration with the UAM heat exchanger of the ACCS, a manifold mount version was selected and is shown below in figures 5.12 & 5.13. The pump inlet and outlet are sealed by static O-rings and mounted directly (flush) to the UAM heat exchanger.

TCS M510 Micro-Pump	
Size	63 x 32 x 31 mm
Weight	170 grams
Power	2.5 W typical (43 W max)
Maximum Free Flow	>8 L/min
Max Differential Pressure	700 mbar (1.5 bar Intermittant)
Max Static Pressure	+100 bar
Operating Temp	-20 to +80 C
Operating Life	20,000 hours typical (special variants >100,000 hours)

Table 5.2: Specifications and performance data for the TCS M510.

As a centrifugal pump, the M510 obeys the pump affinity laws, which state that for a similar pump (size & power, etc.), the flow rate, developed pressure, and required power can be related by the pump's RPM. This principle is explained in detail in later chapters of this dissertation. Because of this similarity law, the M510 can be characterized in terms of flow, pressure, and power by lab testing and that data can be extrapolated and fitted to predict the operational performance of the pump. The M510 has an open impeller design with an overall diameter of 22 mm and individual impeller blade lengths of 7 mm. The M510 is vacuum compatible with hermetically sealed options available. The M510 is shown below in figure 5.12 as a CAD model with the impeller design shown in a cross-sectional view. The M510 comes standard with 3/8ths flow ports, which need to be stepped down to a quarter inch for the ACCS system. This is accomplished by machining a gradual flow constriction/expansion directly into the UAM heat exchanger pump mount. Another advantage of the TCS line of centrifugal pumps and the M510 especially is that because of the rotor's precision balancing; the pump outputs minimal vibrations, jitter, and acoustic noise.

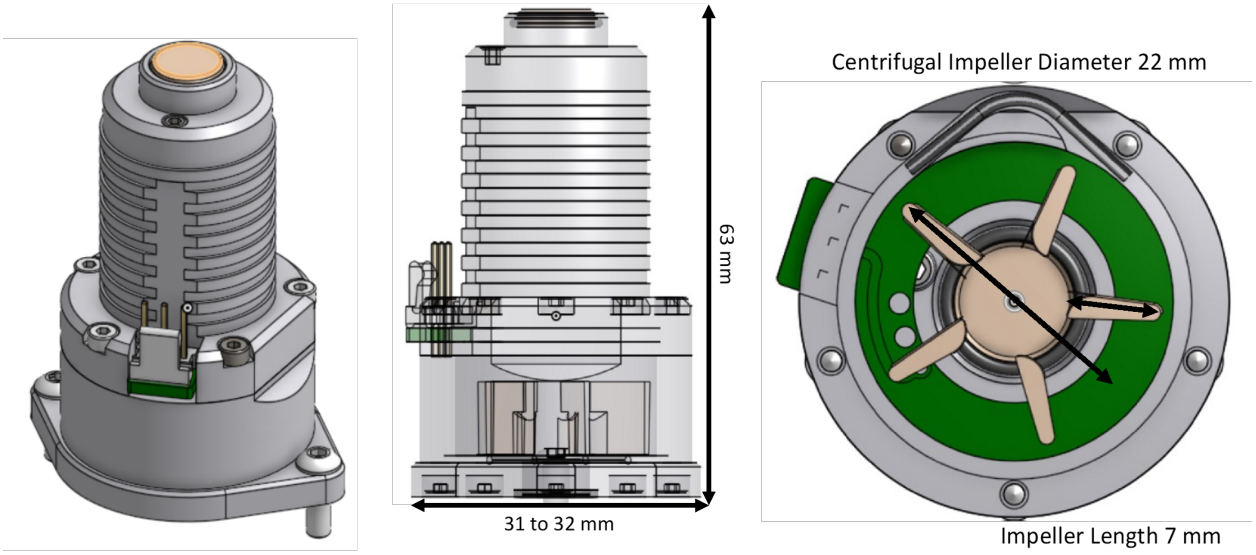

Fig. 5.12: Various views of the TCS M510 centrifugal micro-pump.

TCS offers a wide variety of pumps for many different applications. The M400 and

M410 (long life) pumps are smaller lower power variants. These pumps would be ideal for a small MPFL application in a 3U CubeSat or as a dedicated payload support ACCS system. Perhaps even a better option would be the mid-sized M450. The M450 centrifugal pump is nearly identical to the M510 and has many of the same features and benefits. However, it is significantly smaller, requires less power, and offers less flow/pressure. It also comes standard with quarter-inch flow ports. The M450 has an integrated pump controller, although external controllers are available. TCS also offers micro-geared pumps for higher viscosity applications. These are not appropriate for Novec 7000 as a working fluid but could be helpful for specific designs. Figure 5.13 below shows the M510 (left), the EQI-M controller (center), and M400 (right) pumps compared to a quarter. The small size of the M510 micro-pump, its low power requirements, high flow rates, and long life make it ideal for space and CubeSat applications like the ACCS system.

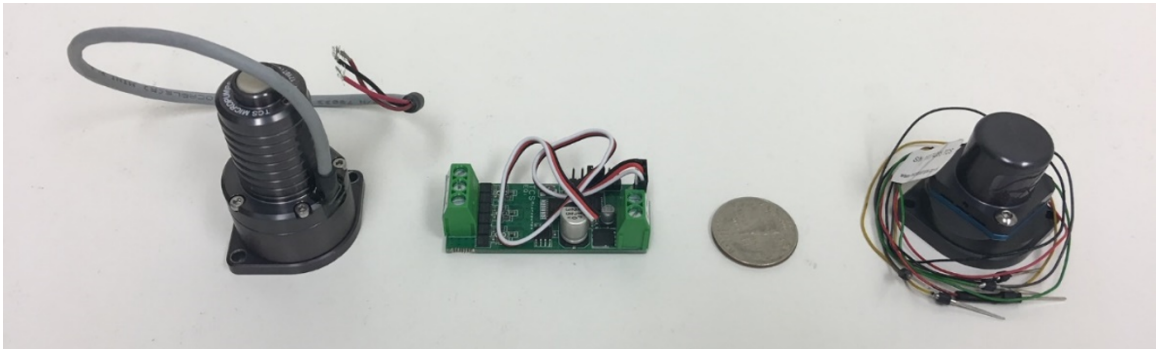

Fig. 5.13: TCS M510 & M400 micro-pumps.

5.7 ACCS Thermal Heat Transfer Fluid: Novec 7000

As an active pumped fluid loop system, the ACCS requires an advanced heat transfer fluid (HTF). Common working fluids such as water or antifreeze were not appropriate due to the operating environment of satellites and the nature of the ACCS application. Specifically, the ACCS working fluid had to perform well as an HTF, have a low viscosity and a low pour point (freeze point), and be safe to handle in student-run labs. An ideal thermal working fluid will have high thermal conductivity, high specific heat, medium density, high

vapor pressure, and low viscosity. These characteristics improve the convective heat transfer capabilities of the fluid while reducing the pumping requirements.

The key requirements for the ACCS working fluid were:

- Density
- Low viscosity
- A high thermal conductivity
- Specific Heat
- Liquid Vapor Pressure
- Safety
- Ease of Use
- Cost & Availability

The working fluids trade study for the ACCS project included Galden HTF's, Dynaline fluids, the Novec line of Hydrofluorocarbons, silicone oils, and Paratherm CR. The complete list of considered HTF's is given below in Table 5.3.

Galden HTF's	Fluorinert HTF's	Silicone Oils	Novec Hydrofluorocarbons	Dynaline
Galden HT55	FC-72	Slytherm XLT	Novec 7000	Dyn HC-50
Galden HT70	FC-87		Novec 7200	Dyn HF-LO
Galden HT80			Novec 7500	Dyn Lo-170
				Dyn-MV

Table 5.3: Working fluids considered for the ACCS system.

Based on this research's analytical heat transfer and pressure drop modeling and a set of strict flow-down requirements. The HTF selection was narrowed down to Paratherm CR, Novec 7000, Galden HT-80, and FC-72. The physical properties of each fluid are compared below in figures 5.14. A decision matrix is given in Table 5.4, which explains the final HTF selection.

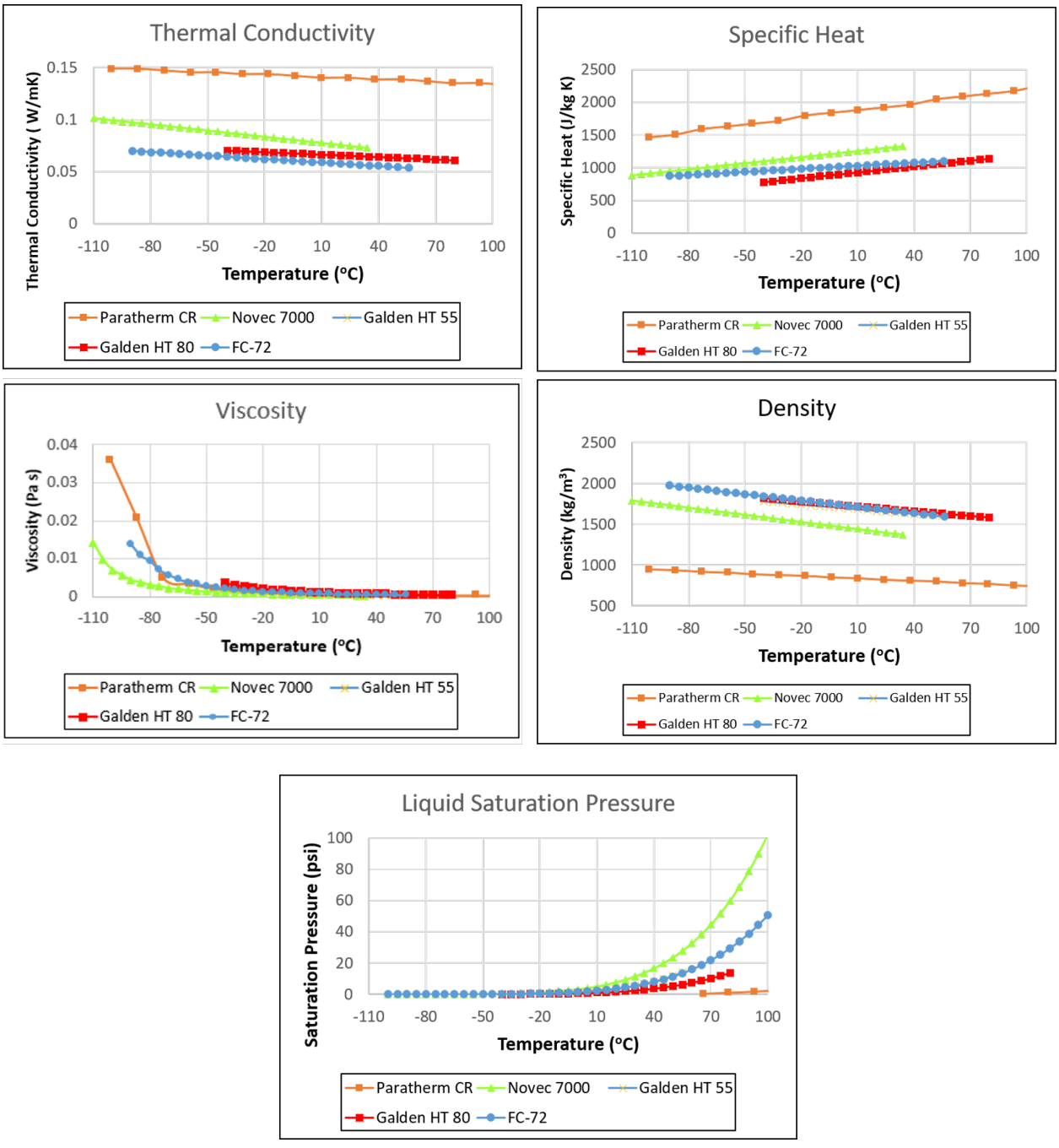

Fig. 5.14: Fluid properties for the various working fluids considered for the ACCS project.

Working Fluid Trade Study Decision Matrix						
Parameter	Thermal Conductivity	Specific Heat	Dynamic Viscosity	Density	Vapor Pressure	Pour Point
	W/mK	J/kgK	mPa sec	Kg/m^3	psi	°C
Effect	Thermal Transfer	Thermal Transfer	Decreases Pressure Drop	Reynolds #	Cavitation	Low Temp.
Fluid Req: -20 °C	>0.1	>1000	<1.00	Approx. 1000	>0.34	<-100
Ranking						
	Best 1st	Good 2nd	Acceptable 3rd	OK 4th	Worst 5th	
Working Fluid Ranking						
Paratherm CR	1	1	2	5	1	-110
Novec 7000	2	2	1	4	5	-122
Galden HT 55	3	4	4	3	3	-115
Galden HT 80	3	4	5	2	2	-110
FC-72	5	3	3	1	4	-90
Hydrofluorocarbons: Novec 7000 & Silicone Oil: Paratherm CR @ -20 C						
Novec 7000	0.0797	1225.56	0.77	1530.2	1.129	-122
Paratherm CR	0.144	1787.17	1.35	871.43	NA	-110

Table 5.4: Summary of the ACCS heat transfer fluid tradestudy.

Paratherm CR is, in many ways, an ideal HTF for the ACCS system. However, it is slightly toxic. Therefore, it was decided early on that because students would be handling these chemicals, only non-toxic, non-dangerous fluids would be down-selected despite any other advantages those fluids might have. Future systems developed by other researchers, companies, NASA, or JPL could very easily down-select an even more appropriate HTF for active thermal control systems like the ACCS. Ultimately, Novec 7000 was selected as the ACCS's HTF.

Novec 7000 (N7000) is a colorless, odorless hydrofluorocarbon heat transfer fluid. As a high resistivity dielectric, it is commonly used as an emersion cooling liquid for electronics, a mild solvent, and a direct expansion refrigerant for two-phase heat transfer systems. It requires little maintenance and can remain in closed-loop service for years. It is a Hydrofluoroether (HFE) with the physical chemistry of 1-methoxyheptafluoropropane (C3F7OCH3). HFEs were created as a complex organic alternative to ozone-depleting chemicals such as CFC's, HFC's, HCFC's, and PFC's. In fact, N7000 has almost no Ozone Depletion Poten-

tial (ODP), and a high molecular weight ensures that the N7000 molecule remains in the atmosphere for only a few weeks. Furthermore N7000 has a minimal Global Warming Potential (GWP) of only 530, and a non-volatile residue of only 25.0 ppm. These features make it an attractive working fluid for aerospace heat transfer systems. The ACCS research has proven that N7000 is a useful low-temperature HTF for single-phase heat transfer systems. The material properties of Novec 7000 are given below in Table 5.5.

Novec 7000 Properties (@ 25 °C)	
Critical Temperatures	Boiling point 34 °C, Freezing point -122 °C, Critical 165 °C
Molecular Weight	200 g/mol
Critical Pressures	Vapor pressure 65 kpa, Critical 2.48 Mpa
Latent Heat of Vaporization	142 kJ/kg
Liquid Density	1400 Kg/m^3
Coefficient of Expansion	0.0022 k^{-1}
Viscosity	Kinematic Viscosity 0.32, Absolute viscosity 0.45 cp
Specific Heat	1300 J/kgK
Thermal Conductivity	0.075 W/mK
Dielectrics	Volume Resistivity 10^8 Ohm-cm, Dielectric Strength >25 kV

Table 5.5: 3M Novec 7000 fluid properties.

5.8 Conclusions

The ACCS active thermal control system is an advanced custom MPFL solution for CubeSats and Small Satellites. Each component of the ACCS required careful selection and design. The heat exchanger and radiator designs are based on idealized thermal heat transfer modeling, the expert advice of Fabrisonics, and the extensive knowledge of JPL. After careful study, the TCS M510 micro-pump, Ricor K508N cryocooler, and 3M Novec 7000 working fluid were down-selected as COTS components. Each of these components works together and forms the heart of the ACCS system.

CHAPTER 6

Active CryoCubeSat Test Cube: Experimental Design

The Test of All Knowledge is Experimentation

Richard Feynman

6.1 Introduction

The primary objective of the ACCS project was to design, develop, and demonstrate the engineering model of the integrated ACCS technology in a relevant ground-based environment and to raise the NASA technology readiness level to ∼5. A complementary secondary objective was to characterize the behavior and performance of the ACCS technology, to better inform future designs and flight-like prototypes. The performance data generated by the characterization was also used to validate the ACCS analytical and Thermal Desktop numerical models. The ACCS engineering unit was fabricated into a highly instrumented test bed with each of the primary systems represented. Individual components could operate independently and as part of the larger active thermal control system. This experimental setup was dubbed the "Test Cube." The ACCS test cube was not a flight-like design; it was an in-laboratory operational test bed with idealized behavior and maximum instrumentation. The choice to build an engineering unit vs. a flight prototype was an early phase decision and is consistent with the research objectives and requirements of the original ACCS proposal.

The ACCS test cube was designed to characterize the thermal energy transfer from the heat exchanger to the deployed radiator through the single-phase mechanically pumped fluid loop. The ACCS test cube was also intended to characterize the micro-pumps working performance and demonstrate the integration and thermal accommodation of the Ricor

K508N cryocooler. The cryocooler performance was measured by the cold tip's thermal rejection capability and temperature stability. The ACCS test bed also demonstrated the use of Ultrasonic Additive Manufacturing (UAM) panels for the heat exchanger and radiator. The ACCS TVAC test required the characterization and technology demonstration to take place in a relevant ground-based environment. Therefore, the test cube was built for a mid-to-high vacuum chamber. Liquid nitrogen shrouds provided a cold-radiation rejection background for the UAM radiator. MLI, G10, UHMW, and kevlar thermal isolators were used to isolate the system and minimize thermal parasitics. The entire ACCS test cube was designed to minimize thermal losses or external gains to idealize the modeling and simplify the analysis. ACCS testing requirements included exercising each of the active components throughout their entire range to determine the impact of each on the integrated system. The mechanically pumped fluid loop was deeply investigated for the effect of flow rate and the control of heat exchanger rejection temperatures through duty cycling and throttling the flow rate between laminar and turbulent flow regimes. The accommodation of the cryocooler was studied, along with the impact of rejection temperature on overall performance. The stability of the cold tip was of paramount concern as that directly affects payload and mission success. Ultimately, the performance of the ACCS system was characterized by three different thermal vacuum tests. Each test had a different objective and test plan. Figure 6.1 shows the ACCS test cube and CSE TVAC chamber.

6.2 USU & JPL TVAC Lab Facilities

The Center for Space Engineering (CSE) facilities at Utah State University were used to develop and thermal vacuum test the ACCS technology. Other facilities included the USU student machine shop, 3D design lab, Thermal Management Technologies lab, and JPL thermal fluids lab. The ACCS team included USU undergraduate and graduate students, staff, and faculty. JPL backing was provided along with expertise, design, and modeling. On two separate occasions, JPL staff traveled out to USU and provided in-person support for the initial setup and testing of the ACCS test cube and the second TVAC characterization test.

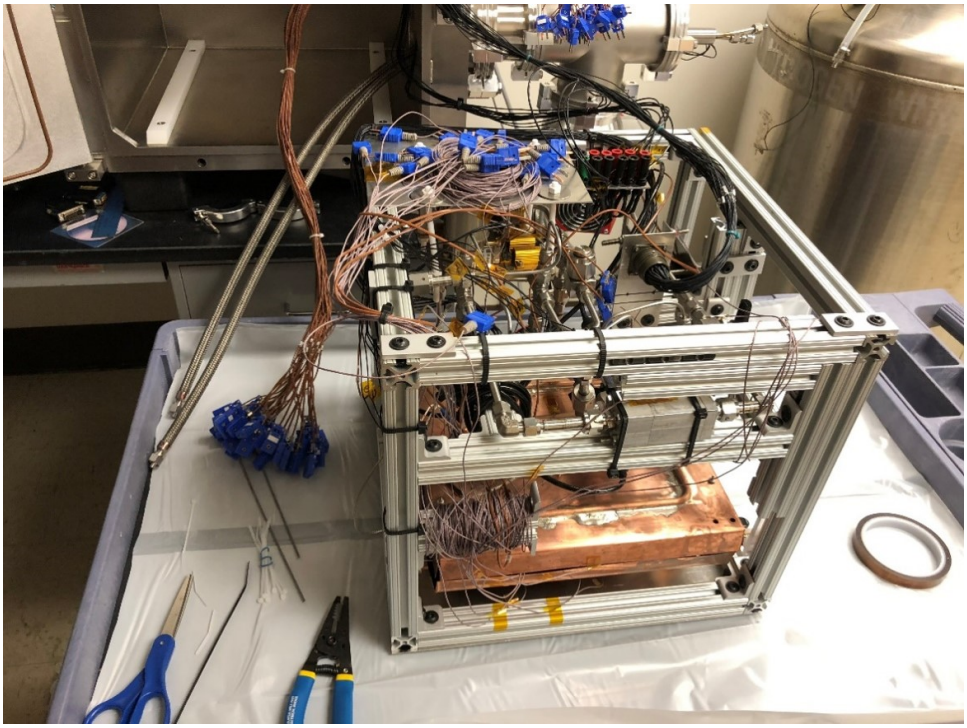

Fig. 6.1: ACCS Test Cube (without MLI) foreground, CSE TVAC chamber background.

The CSE was not initially set up for this type of research. Early support from USU's Mechanical and Electrical engineering departments and the Multiscale Thermophysics Lab (MTL) at USU helped to furbish the CSE with the required test equipment. The CSE TVAC lab includes a 16-inch (per side, cubic internal) Kurt J. Lesker vacuum chamber with an attached Pfeiffer HiPace 300 turbopump (controlled via a TC 400), a Pfeiffer DCU, and a 2015 Adixen Pascal rotary vane rough pump. A 250-liter liquid nitrogen tank provides LN2 cryogenic cooling to the chamber. An Omega PID temperature feedback controller controls the cooling temperature and rate. The KJL TVAC chamber features custom Douglas KF electrical feedthroughs. Chamber telemetry includes signal voltage, power, and thermocouples. Quarter-inch Swagelok LN2 feedthroughs and high current power transfer feedthroughs are included separately. A Pfeiffer cold cathode sensor monitors chamber vacuum pressure. USU's electrical shop provided power supplies, multi-meters, oscilloscopes etc., for power and instrumentation. Figure 6.2 below shows the USU TVAC chamber and workstation for the ACCS research. The CSE TVAC chamber is considered

a dirty chamber because numerous materials, epoxies, and silicon are allowed. Due to outgassing and contamination concerns, many of these materials would not be appropriate in high vacuum or flight-certified chambers. However, the CSE TVAC chamber is a general use, non-sensitive, mid-vac chamber capable of handling numerous materials and test articles.

Fig. 6.2: Top left & right: KJL 16 cubic inch TVAC chamber with attached high vacuum pumps. Bottom left: ACCS research computer and electronic setup.

6.3 Test Cube Design

The ATA test bed was designed as a 16-inch on-a-side cube to fit within and maximize the available space of the CSE KJL vacuum chamber. Electrical, fluid, and gas feedthroughs were only available on the right-hand side of the chamber. Other designs would have been considered if the chamber had been larger or smaller with different feedthrough configurations. The primary ACCS test cube components that had to be included were the heat

exchanger assembly, radiator, LN2 shrouds, fluid network, purge & fill valves, and instrumentation. Internal space within the CSE chamber was at a premium. Therefore, it was critical to design the test cube to be as compact and space efficient as possible.

An early decision was to utilize the entirety of the available chamber volume by forming the test bed into a matching cubic form factor. Hence, the ACCS test cube. Framing would be required to provide mechanical support and thermal isolation to the various test cube components and to form a structure that could be wrapped in external MLI. This framework was constructed from standard 1-inch 8020 T-slot framings. Because of its ubiquity in engineering design and its lego-like ability to conform to any simple design, 8020 framing is ideal for test bed construction. The ACCS test cube T-Slot frame was built from standard 1010 segments. The outer shell formed the cube, while internal components such as the accumulator, pressure transducers, and heat exchanger were supported by additional short lengths of T-slot, framing internal to the cube. A thin sheet of aluminum was used as the floor of the test cube. This floor plate included mounting points and insulation for the LN2 shrouds.

The first test cube design decision came with the location and orientation of the radiator. As the largest single component, its location had to be decided on first. Based on its size and the fact that it would need to be entirely enclosed by LN2 cooling shrouds, the radiator and LN2 stack up should form the base of the test cube. This had the added benefit of isolating the test cube's cold, thermally controlled region from any sensitive instrumentation, the fluid accumulator, valves, etc. The LN2 shrouds were separated from the baseplate by long threaded stainless steel rods capped by G10 sleeves and washers, which helped to isolate the shrouds from the rest of the CubeSat and chamber. It should be noted that the threaded SS rods did not contact the LN2 plates directly. Instead, they provided a clamping force for the G10 sleeves and rigidity to the shroud stack-up. A 20-layer MLI blanket was custom fitted to the LN2 shroud assembly (top & bottom). The MLI helped to minimize thermal radiation transfer from the rest of the system to the shroud assembly and vice versa. LN2 was pumped to the shrouds from the external MVE pressurized tank (less than

20 psi). Three-feet braided flex lines were attached to the chamber's liquid feedthroughs and threaded below the shroud stack up to connect to the shrouds inlet/outlet. These LN2 connection ports can be seen in figure 6.1 and figure 6.24. Incorporating LN2 flex lines into the design was critical for accessing the shroud ports after the test cube was inserted into the vacuum chamber. The LN2 tubes flexibility allowed the feedthroughs to be ported to an easily accessible area; this also helped to maximize the size of the test cube. Otherwise, additional space would have had to be left open for wrench access. The LN2 flex lines were insulated from the test cube by resting on thick UHMW standoffs.

The ACCS heat exchanger assembly was suspended from the roof of the test cube, see below in figure 6.3, by a thin aluminum plate and Teflon threaded rods, washers, and bolts. The exact positioning and stability of the heat exchanger were crucial to the allignment of the fluid network and radiator. The HX assembly consisted of the Ricor K508N cryocooler, cold tip and mounting interface, TCS M510 micro-pump, and guard heaters. Due to its size and weight, the parker diaphragm accumulator was mounted separately. Similarly, the Venturi flow meter and differential pressure transducers were directly supported by the 8020 frame and plumbed separately. Figure 6.3 below shows the original CAD design of the ACCS test cube. Great care was taken to ensure that the heat exchanger assembly, flow path, and radiator were thermally isolated from the rest of the system. Thermal isolation helped to ensure that only the heat generated by the ACCS system was transported to and rejected by the radiator. This was important from a modeling and validation perspective. Ensuring that the test cube was thermally ideal and simplified as much as possible. Thermal parasitics did exist and are naturally an intrinsic part of a real-world experimental setup; therefore, strategically located TCs were used to help quantify these thermal parasitics for later correction, post analysis and subtraction (as a bias) from data sets.

Figure 6.4 shows various views of the ACCS system as CAD, with critical components labeled and called out. Including all of the major flow path components, the radiator/LN2 stack up, the heat exchanger assembly, and various instrumentation. Some features were removed from these CAD models to highlight other areas, including the LN2 side wings, MLI

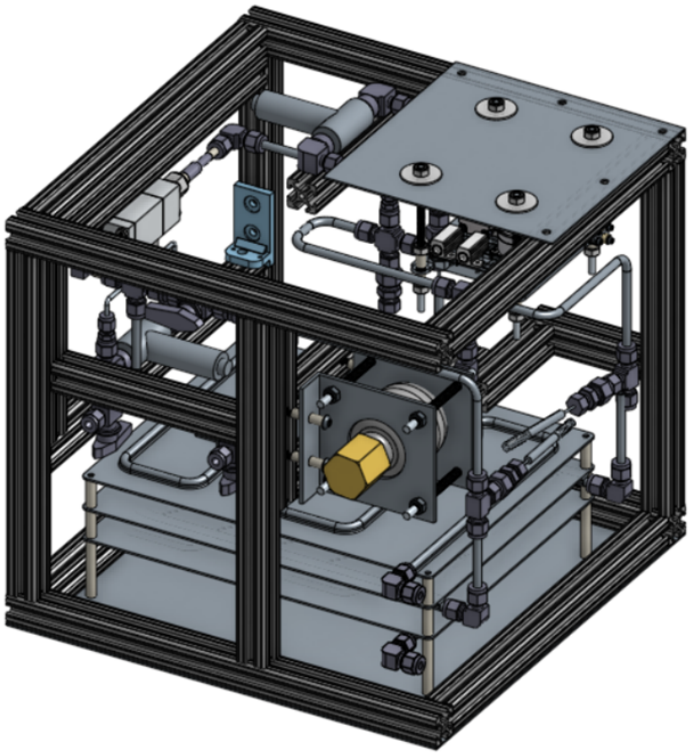

Fig. 6.3: Original CAD design for the ACCS test cube.

wraps, and electrical connection points. Both the radiator and heat exchanger assemblies included crossed Swagelok flanges on the inlet and outlet for direct measurement of pressure (drop/gradients for the heat exchanger & radiator) and temperature. Of particular interest are the general design of the ACCS test cube, the flow paths, and the locations of the heat exchanger assembly, radiator, and LN2 shrouds. Some instrumentation is also shown.

6.4 Flow Path Design & Geometry

Designed as a simple closed-loop circuit, the ACCS flow path minimizes the system's major and minor losses and subsequent internal pressure drops. The flow path required internal routing from the suspended heat exchanger to the radiator, accommodating instrumentation, the Venturi flow meter, the purge & fill valves, flow particulate filters, and the accumulator junction. Figure 6.5 shows a block diagram of the ACCS fluid network with key components labeled. Quarter inch stainless steel tubing was used for the flow paths, while swagelok compression fittings were used for the majority of the fittings, junctions

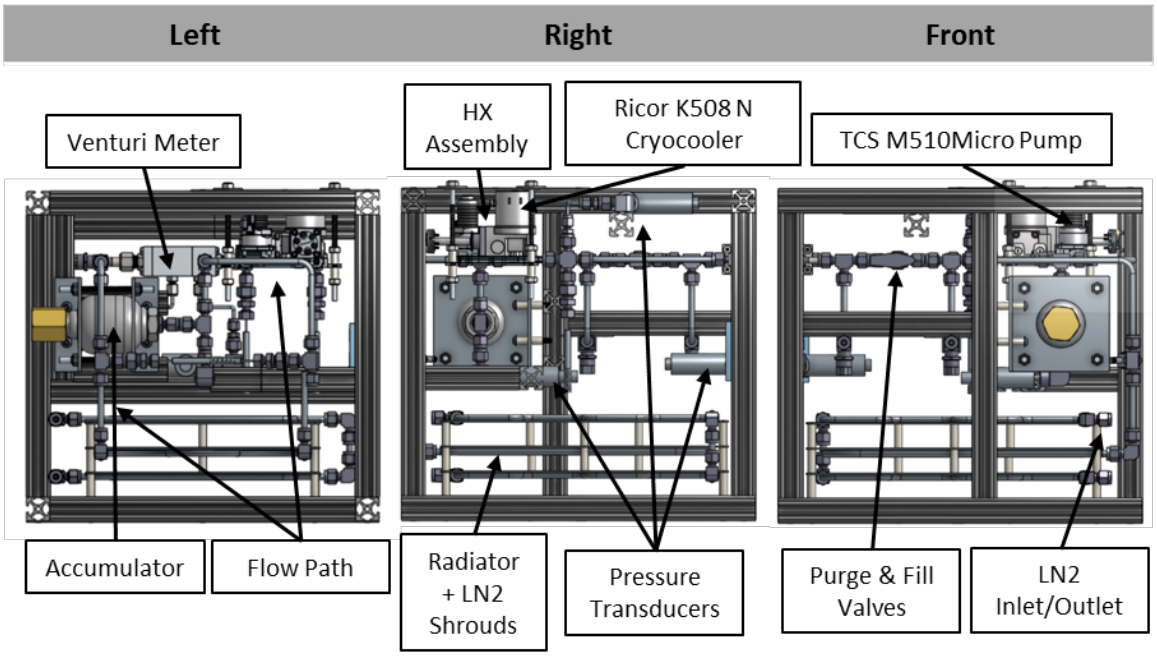

Fig. 6.4: Labeled test cube CAD design, various views.

and valves. The pressure gauges came standard with NPT fittings which were adapted to swagelok. In some special cases, soft metal VCR fittings were used when a specific fluid joint required repetitive replacement or movement. The entire ACCS test cube was characterized for leak rate at Thermal Management Technologies (TMT) using an Adixen SM-18 helium leak detector by TMT staff. The ACCS fluid loop was qaulified as leak tight with measured spot leak rates below e^{-7} Torr L/sec.

The ACCS fluid path begins at the ACCS heat exchanger. Flow is generated by the TCS M510 micro-pump, internal to the UAM HX channels. This flow, upon exit, is immediately measured for temperature and absolute pressure by a Honeywell FP2000 differential pressure transducer and dual type-T Omega immersion probe temperature sensors. The fluid then enters the Venturi meter, which determines the flow velocity as a function of the constricted pressure drop. Next, the liquid is pumped past the P&F valve assembly and the loop isolation valve, capable of breaking the closed fluid loop. The flow path is teed off at this point, leading to the system's accumulator and static pressure transducer. Finally, the working fluid enters the horizontally mounted radiator. At this point, another

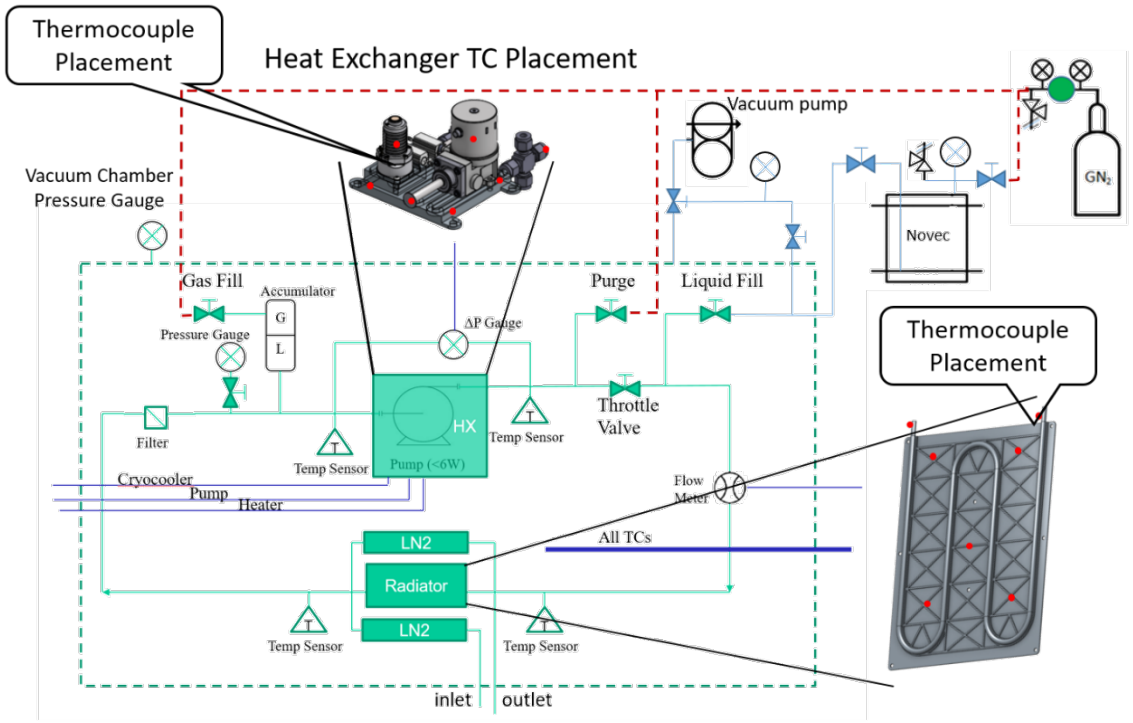

Fig. 6.5: Conceptual diagram, with labels, of the ACCS flow path and major components.

set of immersion probes monitors the fluid's average inlet and outlet temperature. The temperature difference between the heat exchanger's outlet and the radiator's inlet (and conversely) indicates the thermal energy lost or gained by the working fluid from the test cube structure itself. Essentially, it is a measure of how adiabatic (thermally isolated) the ACCS system is and can be used to correct for parasitic losses and gains in the post-analysis of the TVAC characterization data. Upon exiting the radiator, the fluid is forced vertically back to the level of the heat exchanger and through a Swagelok particulate filter. Finally, the N7000 reenters the heat exchanger. Overall, it should be noted that because the ACCS fluid network is a closed loop and the fluid returns to the heat exchanger at the same vertical level as it left, the net change in pressure loss due to gravitational losses is zero. Figure 6.6 Shows simplified CAD modeling of the ACCS fluid network, heat exchanger, and radiator, without any support structures or equipment.

Purge and fill valves are intrinsic to closed-loop fluid systems and are critical to the operation of the ACCS. The ACCS P&F valve assembly is composed of three distinct ball

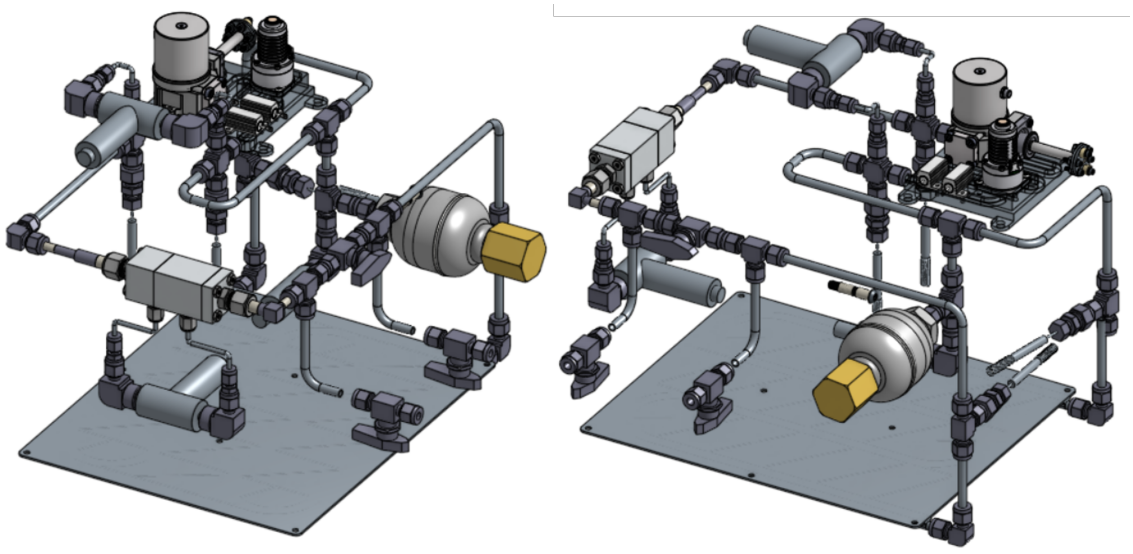

Fig. 6.6: Skelatonized CAD design of the prototype ACCS technology.

valves to minimize the impact on the pressure drop. Two external valves allow the working fluid to be injected into the ACCS system and blown back out of the system. The flow path can be isolated or broken by a third valve mounted perpendicular to the flow path (directly in line with the primary flow) to the first two inlet/outlet P&F valves. The P&F operation of the ACCS begins with filling and pressurizing the external N7000 fill tank, see figure 6.8, to the desired static working pressure of the ACCS system. At this point, the P&F tank outlet valve is closed, as are both the ACCS inlet and outlet valves. Next, a rough HVAC pump is connected to the P&F tank and the ACCS system through a T-junction. The ACCS inlet valve is opened, and the entire system, including the tubing leading to the filled and pressurized N7000 P&F tank, is evacuated. This step is critical; the P&F tank could force pressurized working fluid, N7000, into the ACCS system and compress the existing internal atmosphere, creating a partially dissolved gas/fluid mix or trapping internal bubbles and gas pockets within the closed fluid loop. Once the ACCS static pressure transducer confirms that all internal gases have been evacuated, the vacuum pump is sealed off with a separate valve, and the P&F outlet valve is opened. This forces, under pressure, the working fluid into the ACCS system. Filling is complete when the internal ACCS pressure reading matches the external P&F pre-charge pressure. The ACCS

inlet valve can then be closed, the flow isolation valve opened, and the external P&F tank removed. The ACCS system fill operation is then complete. To purge the ACCS system, a GN2 nitrogen tank is attached to the inlet port of the ACCS system, the flow isolation valve is closed, and the ACCS outlet valve is opened. The GN2 tank applies a slight gas pressure to blow the N7000 working fluid out of the fluid network into a recovery vessel. Because the ACCS is a clean closed loop system, the working fluid can be recycled and used again. This operation is shown as a block diagram in figure 6.5. The ACCS P&F valve network is shown above, figure 6.6, in CAD form, and below, figure 6.7, implemented as part of the ACCS test cube.

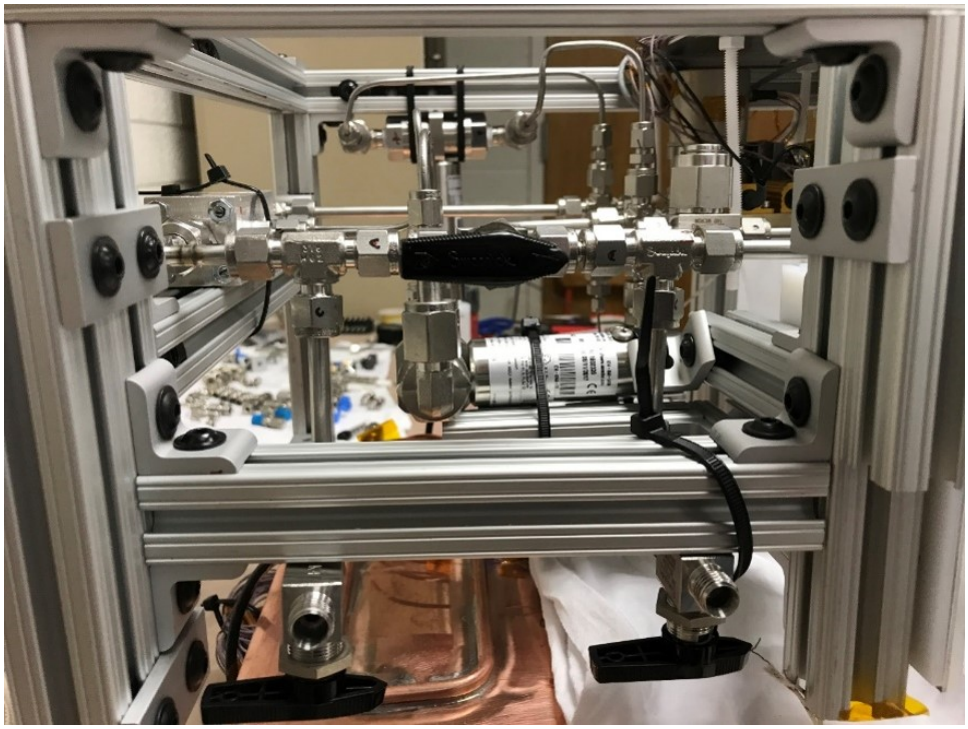

Fig. 6.7: ACCS purge and fill valves

Figure 6.8 shows the external P&F system for the ACCS test cube. The bottom tank holds the Novec 7000 and is capable of both positive and negative (vacuum) internal pressures. An emergency release valve is attached to the tank to ensure that the maximum rated pressure of the tank cannot be exceeded. The fill line allows the liquid-gas interface of

the N7000 to be pressurized to the selected pre-charge value. The attached pressure gauge indicates the relative (gauge) pressure of the tank. The fluid outlet line extends as a stem below the surface of the N7000 nearly to the base of the fluid chamber. Shut off valves along the fluid outlet line, allow separation and isolation of the pressurized N7000 from the ACCS system and vacuum pump. The final section of the outlet line is a wire braided flex line to allow for less rigid connections to the ACCS P&F valves.

Fig. 6.8: External fill system for the ACCS test cube. Components include: tank, fill stem with valves, vacuum line, gas line, relief valve, and pressure gauge.

The ACCS test cube is composed of several subcategories. The first is the actual ACCS thermal control system. Mechanically, including the cryocooler, micro-pump, heat exchanger assembly, fluid network, accumulator, and radiator. The second is electronics and instrumentation. Finally, the third category is all of the support equipment. This last

category includes the ACCS test cube frame, LN2 shrouds, support structure, thermal isolation, and many others. An experimental test setup such as the ACCS test cube requires a significant amount of mechanical and electrical support equipment. Figure 6.9 shows the test cube at an early stage of development. Much of the internal electronics and instrumentation are missing. Instead, this is a simplified representation of just the ACCS technology, including the visible fluid path and the mechanical support features of the ACCS test cube. The entire structure is wrapped in a custom-designed MLI shield, as shown below. The internal LN2 shroud assembly also features MLI, figure 6.9 right. UHMW insulation standoffs were bolted or strapped to the outer test cube structure at various points to prevent direct contact between the LN2 cooled section and the rest of the assembly. Primarily to mitigate any contact between the internal LN2 MLI and the outer MLI or vacuum chamber walls.

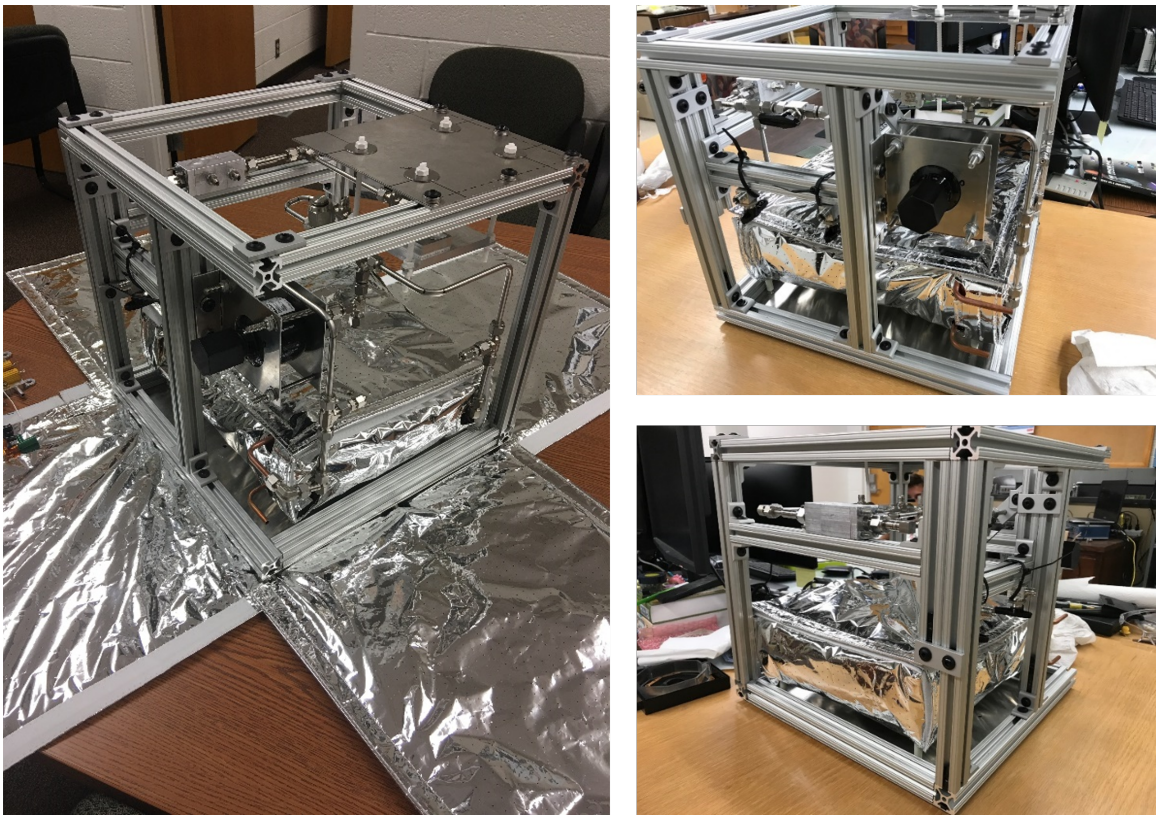

Fig. 6.9: Completed ACCS test cube without power or instrumentation.

6.5 Heat Exchanger Design

The ACCS heat exchanger was designed in the previous chapter as a simplified 1U test bed for the MPFL and cryocooler. The ACCS K508N cryocooler is directly mounted to the UAM heat exchanger with Indium foil as a thermal interface to reduce resistance between the cryocooler compressor body and the HX. Two double-backed flow channels lay directly below the cryocooler; see Design chapter. The TCS M510 pump is mounted on a custom pedestal machined directly into the UAM heat exchanger. This pedestal allows for the use of a single-use RTV gasket if necessary. Dual 20 Ohm Dhale heaters are wired in parallel (10 Ohm total resistance) and mounted near the fluid inlet of the ACCS system. These heaters can provide up to 30 Watts additional thermal load to the ACCS system. These Dhale ohm resistors serve as guard heaters, providing minimum heating levels during low power or shutdown periods. In addition, they allow the total thermal load to vary and the ACCS system to be exercised throughout its thermal range. It should be noted that neither the cryocooler nor the micro-pump can change their thermal loads without affecting performance/operation. Instead, the K508N power depends on its feedback loop, while the M510 thermal load is simply a by-product of the generated flow for the MPFL.

The heat exchanger surface was coated with gold Chem-film to prevent surface oxidation and to preserve and improve the surface thermal contact resistance. The bottom of the heat exchanger was black anodized to provide a high emissivity surface for the IR cameras to view. Dual FLIR Lepton (V2.5-radiometric & 3.0-high resolution) IR cameras are mounted to observe the heat exchanger temperature distribution. One was mounted directly underneath the heat exchanger looking at the flat, black bottom surface. This camera was focused on observing the isothermality of the heat exchanger and the possible thermal variations within the working fluid channels, and the various mounting points for the active ACCS components. The second camera looked directly at the heat exchanger assembly from a side view. This camera observed the variations in the cryocooler, pump, and heater temperatures compared to the heat exchanger UAM body. Both of these cameras are discussed in more detail in the various instrumentation discussions of this dissertation.

The heat exchanger is suspended vertically from the ceiling (upper right quadrant) of the ACCS test cube. Quarter-inch mounting points on all four corners. Insulating Teflon (PTFE) threaded rods with matching washers and nuts were used to isolate the heat exchanger from the test cube frame thermally. Crossed Swagelok fittings on the inlet and outlet of the heat exchanger permitted teed-off measurement of the differential pressure generated across the heat exchanger by the M510 Micro-Pump and direct measurement of the working fluid inlet/outlet temperature via emersion probe TC's. The ACCS heat exchanger is shown below in figure 6.10 at various levels of assembly. The Ricor K508N, with a sub-cooled (chilled/frosted) tip, is shown along with the TCS M510 micro-pump, Dhale Ohm heaters, in gold.

The Ricor K508N is an integrated cryocooler where the motor compressor and cold finger are combined into a single working unit. For the K508N, the cold finger and compressor assemblies are modular and can be independently mixed and matched. For the ACCS project, the cold finger assembly featured a blank mounting tip. Therefore, to mount instrumentation or load heaters, a custom copper mounting block was fabricated and integrated, clamped to the cold tip. This mounting block was a solid copper disk, machined to match the blank disk of the K508N cold finger, with six mounting bolt holes. The disk was made from copper to improve the thermal conductance and response of the cold tip. Half circle back plates clamp the front copper disk to the cold tip, and an indium spacer provides thermal contact. Two bolts mount Lakeshore Silicone DT-670 temperature diodes to the tip for cryogenic temperature measurement. A 2 W resistor is mounted directly to the front of the cold tip black via cryogenic Stycast epoxy. This resistor will provide an analog thermal load to the cold tip and cryocooler to simulate the working power and parasitics of a real detector, focal plane, and IR instrument. Figure 6.11 shows the rough design of the cold tip mounting block and the mounting locations of the temperature diodes and resistor.

In total, three silicone DT-670 diodes were mounted to the cryocooler cold tip. Two provided cryogenic temperature monitoring (averaged); see figure 6.11 above. The third diode was wired directly into the Ricor K508N HyB-18 controller. This diode acted like a

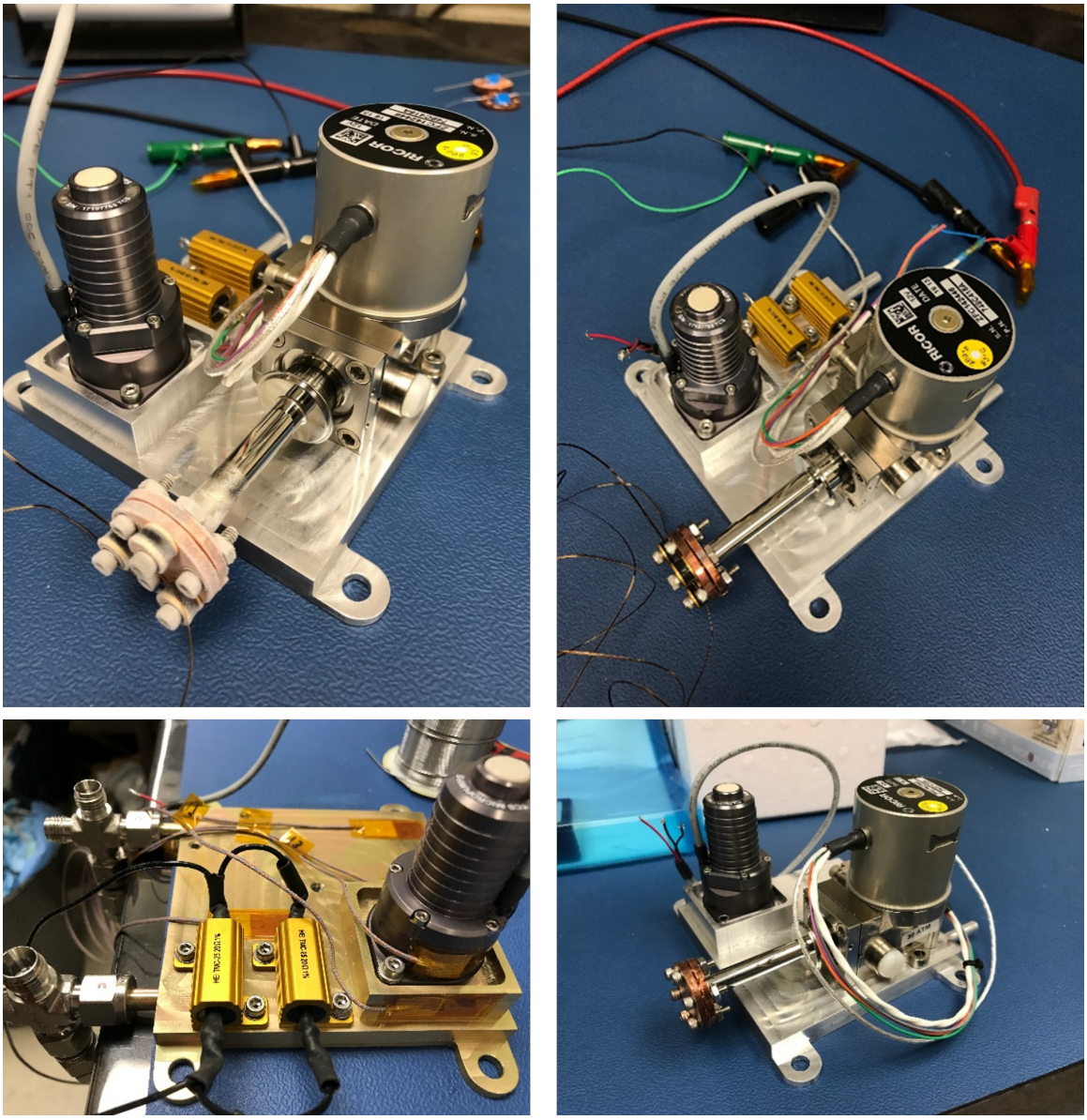

Fig. 6.10: ACCS heat exchanger assembly. K508N cryocooler, M510 micro-pump, and gaurd heaters.

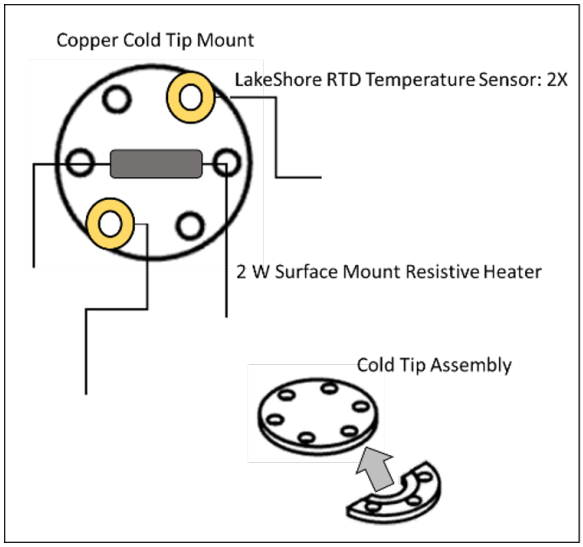

Fig. 6.11: Design & labeled parts for the Ricor K508N cold finger mounting block.

temperature-dependent variable resistor and provided direct setpoint feedback and control of the cryocooler cold tip temperature. The thin (32 gauge) phosphor bronze diode wires of all three DT607s were wrapped loosely around the cryocooler cold finger and spiraled back to the mounting interface. This wrapping helped to prevent parasitic thermal loads from directly impacting the cold finger, which is susceptible to thermal runaway. A crinkled layer of MLI was loosely wrapped (minimize. direct conduction losses) around the cold tip and cold finger and secured by Kapton tape. This MLI wrap protected the cold finger assembly from radiation parasitics. Figure 6.12 below shows the copper cold finger assembly mounted to the cold finger with the attached heater and temperature diodes being wire wrapped in preparation for MLI.

6.6 Radiator Experimental Setup

The ACCS radiator is a maximized 6U design (31 X 25.4 cm), lightweight, with stiffening ribs and elevated flow paths. The total effective area of the ACCS radiator is approximately 0.16 m2, see design chapter. The radiator is a four-pass design and relies on thin plate conduction between fluid channels. Dual parallel wired patch heaters are surface mounted to the flat side of the radiator to provide additional thermal input and to simulate

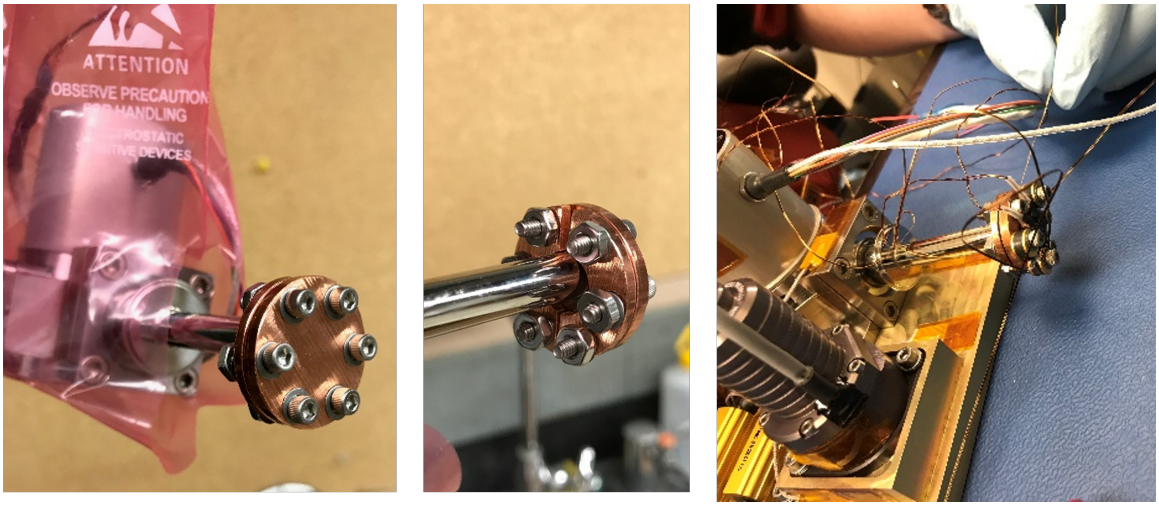

Fig. 6.12: Instrumented ACCS Copper cold tip clamped to the cold finger of the Ricor K508N.

the variation of the thermal space environment. The fluid inlet and outlet are quarter-inch machined tube studs. Teflon-coupled Swagelok connectors are used to convert the radiator/HX fluid studs to standard tubing and connectors. Mounting holes are included along the edge and near the center of the radiator. Figure 6.13 shows the size of the radiator for scaled reference.

To simulate the thermal environment of LEO satellite/radiator to deep space, a series of cryogenic LN2 thermal shrouds were designed and built for the ACCS system. These shrouds were made of thick gauge copper plate, cut and molded to fit directly over and around (top, bottom, & sides) the ACCS radiator. Quarter-inch copper bent tubing criss-cross the shrouds. These tubes are hand brazed onto the copper plates to allow for the free flow of LN2 through the system. The top and bottom shroud tubing are connected through liquid LN2 ports on the primary vacuum chamber feedthrough flange. The flow of LN2 from the 250 Liter external low-pressure tank is controlled by an Omega PID setpoint controller and a high voltage, normally closed, solenoid valve. A bolt-on type K thermocouple, mounted to the middle of the top shroud, provides feedback to the PID controller. The PID loop controls setpoint temperatures of the shroud down to ~90 K. Figure 6.14 below shows, in the top right and left, the ACCS top and bottom shrouds with folded edges and quarter-inch

Fig. 6.13: ACCS 6U Radiator. Black anodized.

tubing inlet/outlet. The inner walls and sides of the shrouds were painted high emissivity black, as will be discussed later.

To correctly and accurately characterize the thermal performance of the ACCS radiator, it was essential to ensure that radiation was the dominant form of heat transfer and that parasitic conductive losses were minimized. The ACCS radiator was suspended between the LN2 shrouds by tensioned Kevlar cables to accomplish this. Aside from the mechanical Swagelok connections of the fluid inlet and outlet, the radiator was entirely isolated with no conductive connection to the test cube or shrouds. Kevlar is a high strength, high stiffness, low conductivity material ideal for thermal isolation applications. High strength Kevlar cord (∼200 lb) was looped through connection points at each corner of the radiator and individually tensioned by wrapping around a machine tuner worm gear. These worm gears featured a 20:1 gear ratio and were mounted to the 8020 framing by custom 3D printed (Resin for low outgassing) L-brackets. Each individual machine screw allowed for the horizontal tensioning and positioning of the radiator. Kevlar suspension is an incredibly

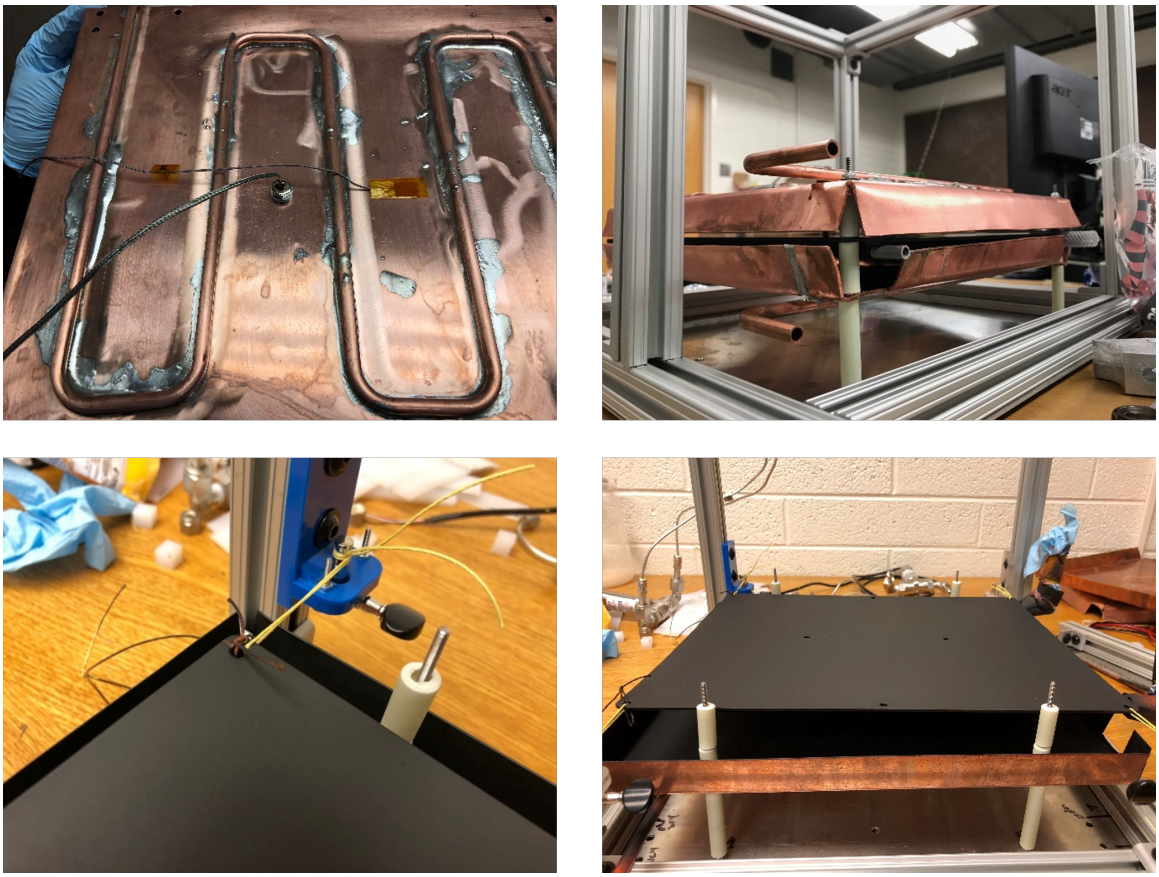

Fig. 6.14: Suspended and thermall isolated ACCS radiator with LN2 shroud stack.

strong, stiff, supportive, and variable mounting technique. Kevlar thread is nearly ideal for thermal isolation; it ensures the only physical contact with a structure is through long, thin, highly insulative conduction paths. Not only are the conduction paths minimized with Kevlar isolation, but the thermal parasitics are simplified and easy to calculate from Fourier's 1D conduction law. TC's mounted on the radiator and machine screw brackets provide the thermal gradients for the kevlar suspension, usually on the order of several hundred degrees. Figure 6.14 above shows the suspended radiator along with the kevlar thread, worm gear tensioner, and 3D printed mounting bracket. The LN2 shrouds are supported by long stainless steel threaded rods and stacked G10 spacers. G10 is known as a thermal isolator, and these supports provide a sturdy platform for the LN2 and internal MLI warp. The top shroud was stacked internally with G10 spacers to the bottom shroud, figure 6.14.

6.7 ACCS Electronics Box: E-Box

The ACCS TVAC characterization required a dedicated electronics box for data acquisition, instrumentation, and power control for each active system. Data acquisition (DAQ) for the ACCS system was accomplished by a National Instruments NI- NI-CDAQ 9178 module. The CDAQ is a universal DAQ chassis and supports various measurement cards. For the ACCS system, a single NI-9205 voltage card coupled with dual NI-9213 thermocouple cards was used. System voltages were either directly logged or dropped to measurable ranges by voltage dividers. Precise current measurements were made by using Linear Technologies LT6105CMS8 current sense amplifiers to convert current signals to voltage signals. Figure 6.15 below shows the ACCS electronics box with the inputs orientated on the left side (power supplies & computer) and outputs (TVAC chamber) on the right. The upper left quadrant is reserved for the pump control electronics. These include the EQI-M V2.0 pump controller and a current sense amplifier. Pump power is three-phase dependent and approximated by measuring the input voltage and current to the controller. BLDC controllers are usually highly efficient, so this is a reasonable approximation. The upper right quadrant monitors the system's various control heaters. These include the HX Dhale ohm

resistors, the radiator patch heaters, and the cold tip resistor. Once again, these signals were monitored via voltage dividers and current converters. The lower right section of the ACCS E-box monitors the three Honeywell FP2000 pressure transducers. Each sensor is wired to a constant 24 V power supply. A returned 4-20 mA signal linearly relates to the pressure. This current sense line is converted to a 0-5 V signal for the NI-CDAQ. The cryocooler was monitored and controlled in the lower left quadrant of the E-box. A constant voltage was applied to the Hyb-18 controller, and the current draw to the cryocooler was observed. As mentioned previously, the Ricor K508N Hyb-18 controller was wired to a DT-670 temperature diode connected to the cryocooler cold tip mount. This control/feedback diode was wired in series, with a variable resistance potentiometer inside the E-box. By changing the potentiometer's resistance, the cryocooler's setpoint control could be dynamically changed from outside the chamber. The LabVIEW CDAQ was mounted at the bottom of the E-box, figure 6.15. Banana cables and jacks connected the E-box to power and support from the CSE's lab power supplies and computers. The data output and signal lines were combined into a single cable and fed to the chamber's electrical feedthroughs and the test cube. The ACCS E-box and electrical equipment all shared a common ground defined by the CSE lab ground, a deeply grounded copper pipe connected to the lab. The internal IR cameras and miscellaneous signal wires were all collected onto screw terminals for processing. External to the chamber, a visible webcam continuously recorded the CSE lab during TVAC testing. NI LabVIEW software, coded by USU, converted all CDAQ data and displayed/recorded real-time data to the lab computers and USU staff. The ACCS E-box was critical to the success of the ACCS TVAC test campaign and provided dedicated data acquisition and control. It also allowed for real-time, in-depth analysis, troubleshooting, and post-processing of the data.

The ACCS test cube is highly instrumented, featuring numerous temperature sensors, a flow rate sensor, pressure transducers, pump RPM readouts, and power monitoring. All of which are critical parameters when characterizing a pumped fluid thermal system. The ACCS features the following instrumentation, table 6.1:

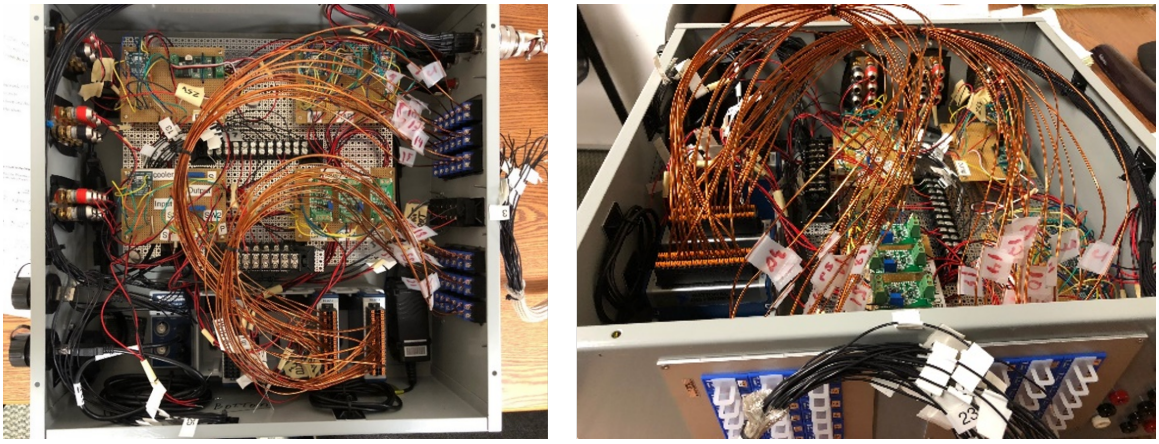

Fig. 6.15: ACCS E-Box. Provided power, instrumentation, and telemetry to the ACCS system during TVAC testing.

ACCS Test Cube Instrumentation		
Measurement Type	#	Notes
System Temperature	30+	Omega type T thermocouples. Surface mount Kapton backed with silicone adhesive
Fluid Temperature	4	Immersion style type T thermocouples
Cryogenic Temperature	3	Lakeshore DT-670 silicone diode temperature sensors
System Differential Pressure	2	Honeywell FP2000 configurable pressure transducer
System Static Pressure	1	Honeywell FP2000 configurable pressure transducer
Pump Flow Rate	1	Custom Venturi flow meter
Pump RPM	1	0-900 Hz RPM signal sampled at 10kHz/sec (Nyquist)
Cameras	3	Two Flir Lepton IR cameras, one visible webcam
Power	N/A	Multiple voltage & current sources

Table 6.1: Summary of the ACCS Test-Cube instrumentation.

System-wide temperature measurement is provided through small gauge surface mount type T thermocouples. These thermocouples provide accurate, rapid monitoring of temperatures and thermal gradients within the ACCS mechanical structure. The majority of these thermocouples were located on the radiator and heat exchanger assembly to accurately determine the absolute temperatures and variations within those key structures. The UAM heat exchanger temperature was monitored by five thermocouples distributed on either side of the plate, see figure 6.16 top right. These thermocouples measure the temperature/thermal distribution within the UAM heat exchanger panel and can be averaged to give an overall temperature. The pump casing temperature is monitored by two thermocouples surface mount TC's. The first is on the pump brushless DC motor, and the second was attached to the rotary vain fluid casing (volute). The cryocooler temperature is similarly monitored via three thermocouples attached to the motor housing, compressor head, and cold finger junction. The heat exchanger guard heaters (Dhale Ohm resistor) temperatures are also measured by a single thermocouple. Immersion TC probes are Tee'd in at the inlet and outlet of both the radiator and the heat exchanger. These immersion probes give highly accurate and fast fluid temperature values, critical for the MPFL thermal analysis. The radiator surface temperature is monitored by eight distributed TC's. However, it should be noted that three TC's failed during testing. Therefore, only the remaining five are considered for this discussion. The radiator TC's provide an indication of the relative isothermality of the radiator, or its thermal distribution and, therefore, its effectiveness. These are critical parameters to consider for future radiator designs. These gradients can also be used to determine the 2D conductive resistance of the thin plate UAM radiator and locate hot/cold spots. These TC's also measure the temperature gradient from the inlet to the outlet of the radiator. The temperature of the LN2 shrouds is also monitored by TC's. However, only a single TC is placed at each plate's center for both the top and bottom shrouds. The remaining thermocouples are distributed throughout the system and monitor the test cube temperature. These include the Venturi meter, accumulator, 8020 framing, Kevlar isolation worm gear mounts, G10 standoff supports, and fluid line tempera-

tures. These general test cube system temperatures are used to calculate parasitic thermal losses/gains within the ACCS system and to monitor the various changes and states of temperature within the test cube itself. The locations of the TC's for the HX and radiator assemblies shown below in figure 6.16 & figure 6.17.

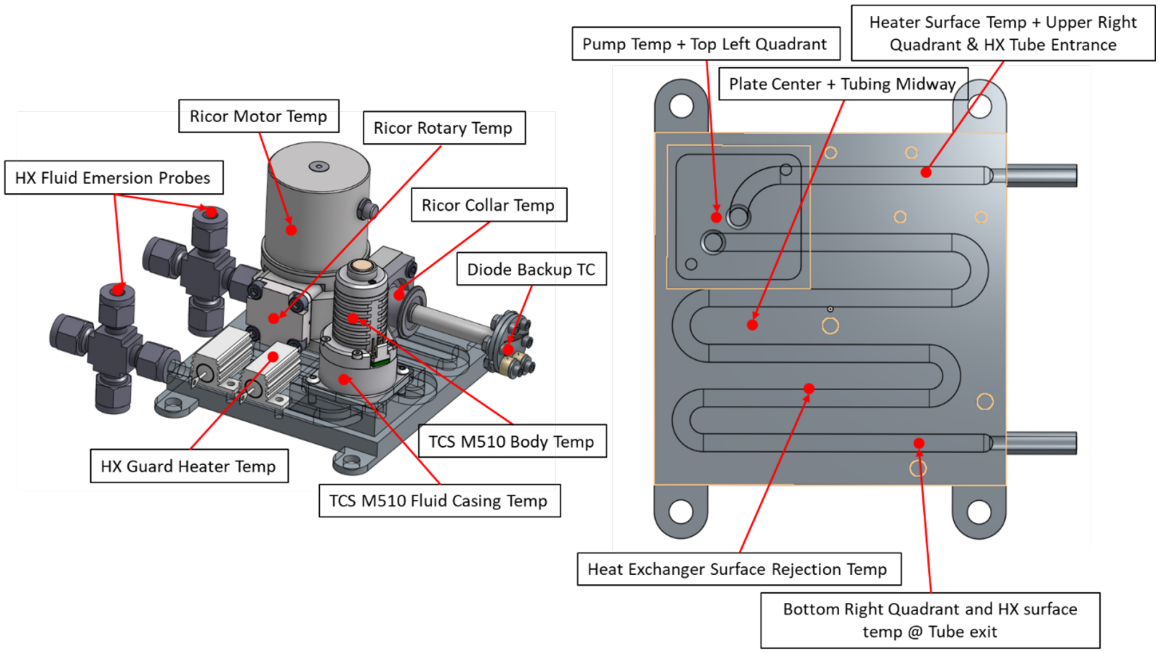

Fig. 6.16: ACCS heat excchanger assembly TC placement.

The differential pressure generated by the Micro-Pump, the Venturi meter and the absolute static pressure of the system is all monitored by dedicated pressure transducers. Each of which is specifically coupled to the fluid network by VCR and Swagelok fittings. The various pressure transducers are located throughout the test cube and are mounted to the 8020 framing due to their weight. The custom venturi meter is located on the cube's left side, near the fluid outlet of the heat exchanger and Micro-Pump. Screw terminals and miniature TC connectors are used to interconnect and route all the various wiring into and out of the test cube. Figure 6.18 below shows the ACCS radiator instrumented with thermocouples and patch heaters suspended by kevlar isolation within the copper LN2 shrouds. The far left shows a Flir camera board observing the heat exchanger assembly.

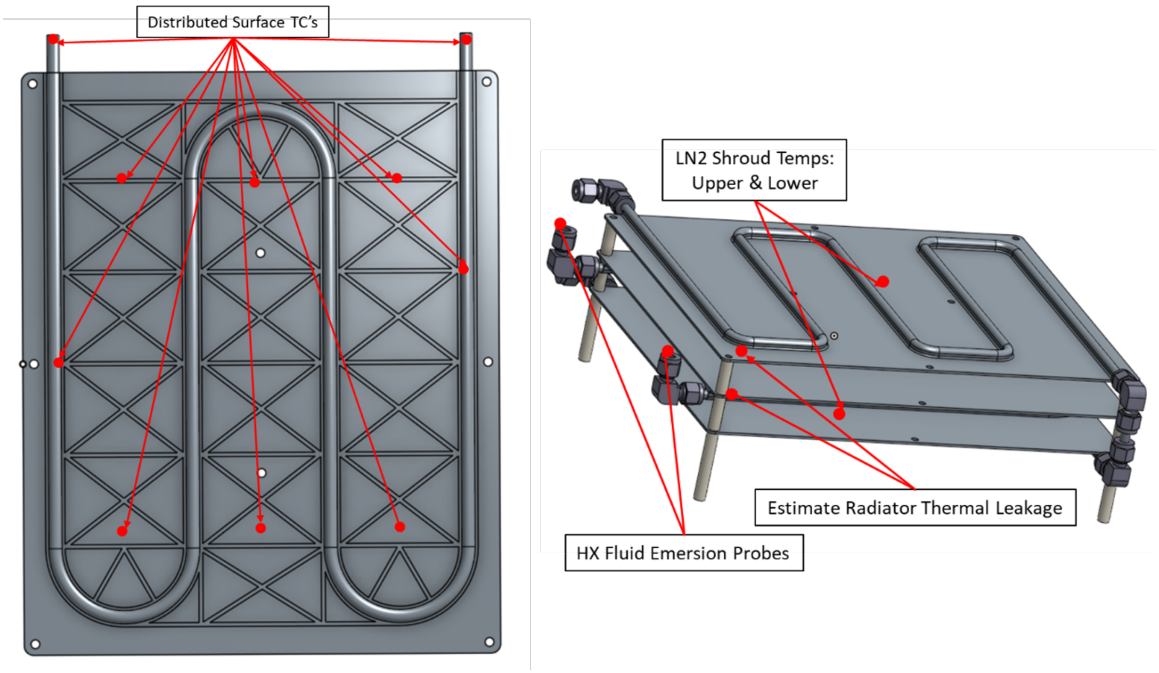

Fig. 6.17: ACCS radiator stack TC placement.

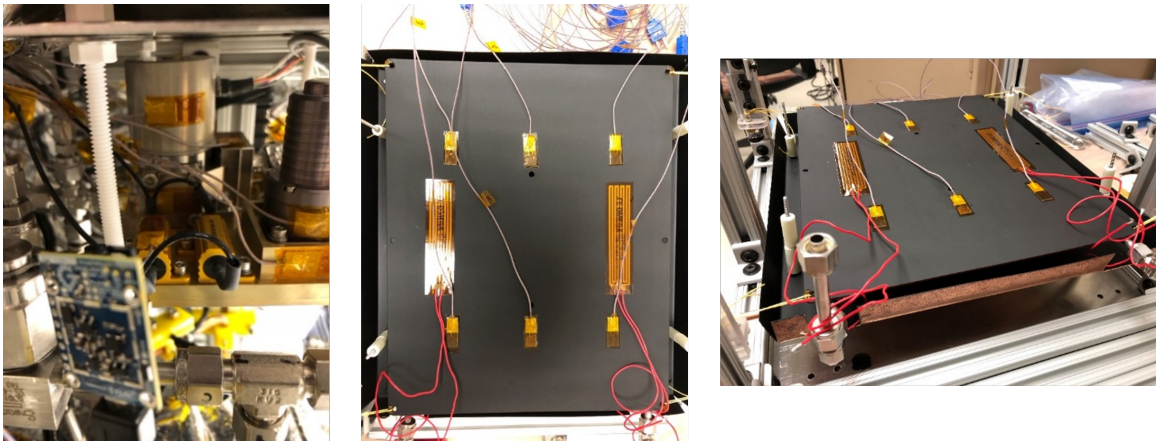

Fig. 6.18: ACCS radiator assembly TC placement.

6.8 ACCS Venturi Flow Meter Design

The ACCS fluid loop required a dedicated flow meter. However, commercially available flow meters either did not cover the entire flow regime required by the ACCS test, injected too much pressure drop within the system, or were not compatible with the Novec 7000 working fluid or vacuum environment. Therefore, a custom venturi meter was designed and fabricated for the ACCS test cube. Venturi meters operate via the modified Bernoulli principle. The modified Bernoulli equation is shown below, where each variable refers to pressure, velocity, and density at a specific point before and after a change in the flow diameter.

$$P_1 - P_2 = \frac{\rho}{2}({\nu_2}^2 - {\nu_1}^2) \tag{6.1}$$

For a Venturi meter, the flow channel is gradually narrowed. In response, the fluid velocity increases to maintain the system's mass flow rate. A decrease in the working pressure counterbalances this increase in velocity. Essentially, velocity and pressure are exchanged. The flow rate of a Venturi meter can be calculated by measuring the change in pressure across the Venturi's throat (constriction), as shown below, where ρ is the working fluid density, and each of the differential parameters are defined by the simplified Venturi flow diagram given in figure 6.19.

$$Q = A_1\sqrt{\frac{2}{\rho}\cdot\frac{(P_1 - P_2)}{(\frac{A_1}{A_2})^2 - 1}} \qquad or \qquad Q = A_2\sqrt{\frac{2}{\rho}\cdot\frac{(P_1 - P_2)}{1 - (\frac{A_2}{A_1})^2}} \tag{6.2}$$

A Venturi meter can be customized (sized) based on the expected flow rate, fluid properties, and measurable pressure range. The ACCS Venturi was sized for Novec 7000, operating between 100 and 1200 mL/min. It should be noted that the ACCS Venturi throat contraction was not sized appropriately for the relative sensitivity of the Honeywell differential pressure transducer. At very low flow rates, less than ~250 mL/min, the differential pressure developed across the Venturi's throat was too low to be easily measured. The signal was lost within the sensitivity noise of that particular pressure transducer. To remedy this,

the Venturi throat should have been narrowed more, or a pressure transducer with higher sensitivity should have been selected for the ACCS test cube. The USU team developed an excel based Venturi meter sizing tool that allows for the rapid design and fabrication of custom flow meters like the one used here. An advantage of Venturi flow meters is that by gradually narrowing the flow orifice and then widening back slowly, the overall permanent pressure drop across the meter is minimal [130].

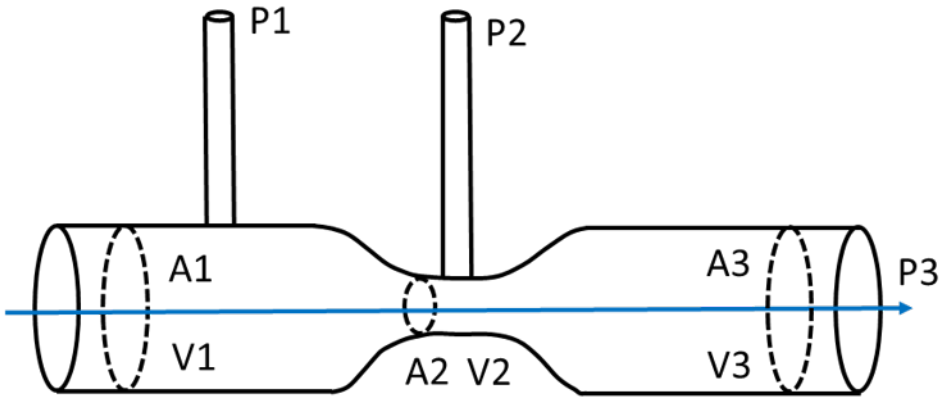

Fig. 6.19: Simplified diagram of the working principle for a Venturi flow meter.

The ACCS Venturi meter was designed as a three-piece structure for easy fabrication. The first block, shown below as a CAD cross-section 6.20, included the fluid inlet and nominal pressure flow port. The second, or middle, section featured the Venturi throat contraction, the low-side pressure port, and the gradual re-expansion of the flow channel. Finally, the last block includes the fluid exit. Overall, the ACCS Venturi meter proved to be accurate for nominal and high flow rates and was a successful addition to the ACCS test cube. Future designs might leverage the capabilities of UAM 3D printing to embed a custom Venturi meter directly into the working panels of the ACCS system. This would allow for on-orbit monitoring of the system's flow rate without a dedicated external flow meter. Future designs will also ensure that a differential pressure transducer with sufficient sensitivity is used to capture low flow rates accurately.

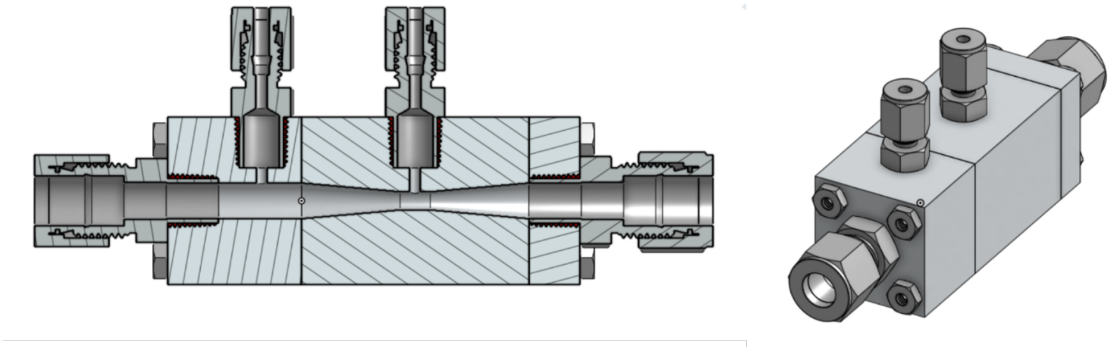

Fig. 6.20: CAD design of the ACCS Venturi meter. Left: cross-section showing the Venturi's throat. Right Isometric view of the three-piece design and pressure ports.

6.9 MPFL Fluid Accumulator

As a pumped fluid loop, the ACCS system requires a fluid accumulator to balance and maintain the static working pressure of the system. Fluid accumulators serve many purposes. However, for a system like the ACCS, they are thermal expansion/contraction pressure balancing and leakage compensation. As the ACCS system changes temperature, the incompressible working fluid expands and contracts at a given rate defined by the fluid properties of Novec 7000 (0.0022 k^{-1}). Given enough heat, this expansion could quickly overpressurize the fluid lines and seals of the ACCS system and cause a rupture or catastrophic failure. On the other hand, if the fluid began to cool, the system's internal pressure would fall and quickly lead to localized vaporization. Most likely to appear as cavitation within the micro-pump. The ACCS is a sealed system designed to last several years in orbit. However, all pressurized systems leak. Therefore, it is critical to characterize the leak rate and have a working fluid reservoir to compensate. The ACCS team performed a trade study on available COTS accumulators and down-selected the Parker 4.6 cubic inch (75 mL) diaphragm accumulator. In a diaphragm accumulator, a rubber membrane separates the fluid and gas. The size (working volume) of the ACCS accumulator was entirely based on the thermal expansion/contraction of N7000, and was calculated from the internal fluid volume of the ACCS, Novec 7000's thermal expansion coefficient, the pre-charge and initial static pressure of the ACCS MPFL. The sizing equations for accumulators are not given here but are based on the temperature-dependent behavior of fluids and the

ideal gas law. Figure 6.21 below shows the Parker accumulator used by the ACCS system. The fluid side was connected via an NPT fitting, while the gas side featured a stem valve with a secondary static seal cap.

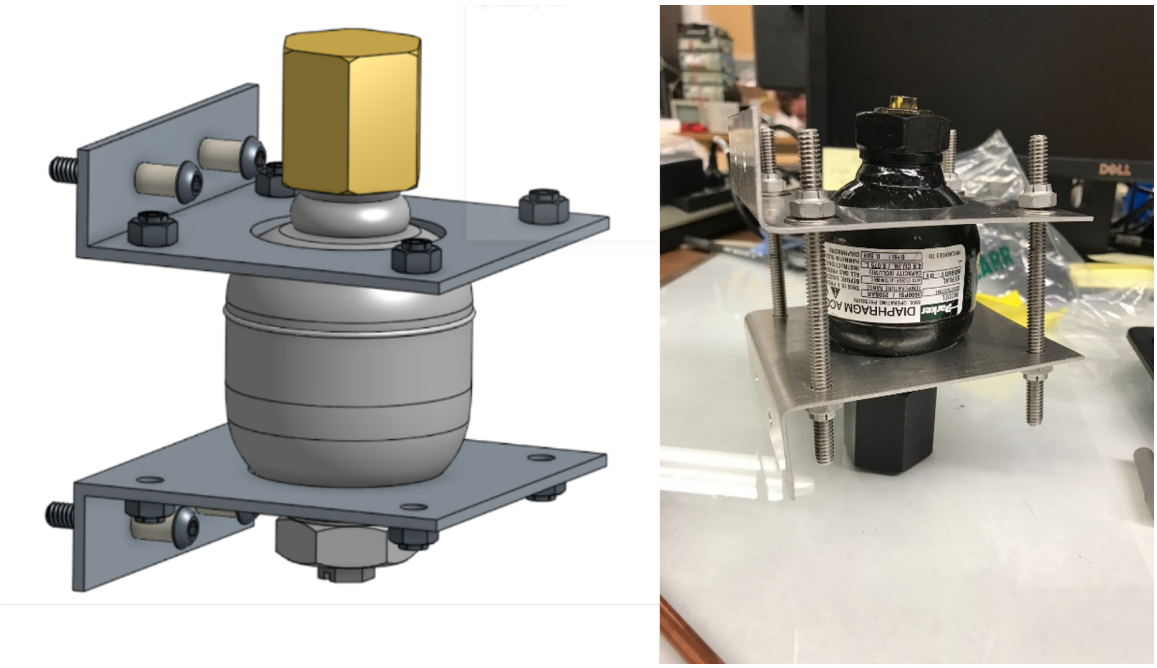

Fig. 6.21: Left: CAD design of the ACCS fluid accumulator. Right: Parker (COTS) diaphgram accumulator.

6.10 Radiator Surface Coating

The ACCS radiator is solid 3D UAM printed 6061 Aluminum. Originally anodized black for radiative surface properties and wear resistance. However, during the manufacturing process, the newly 3D printed UAM parts were heat treated through Hot Isostatic Pressing (HIP) process. Generally this process improves the overall performance of the part by reducing the porosity of the metal and improving the layer-to-layer bonding of the UAM. However, during this process, the ACCS radiator was removed from the non-oxidizing Argon gas environment prematurely and at a relatively high temperature, causing the surface to oxidize aggressively. Later, during the anodizing process, these high oxide regions did not take the black dye as readily and created a patchwork variation in the anodized surface coloring.

This variation in color can be seen below in figure 6.22 as lighter regions. Discoloration is a cause for concern because the radiator's emissivity, reflectivity, and absorptivity are critical and a direct function of the surface properties. A radiative black paint was added as a topcoat to ensure that the radiator was operating at its best efficiency. Aeroglaze Z306 was chosen for the paint due to its superior properties, high relative emissivity, and space flight heritage. Z306 Aeroglaze is a flat black, low outgassing polyurethane coating. Commonly, a white radiator surface is chosen to maximize IR emissivity while limiting solar absorption. However, for ground testing, a high emissivity/absorptivity black was preferred. The Z306 emissivity is commonly reported in the literature. However, it was also experimentally measured via a Gier Dunkel radiometer (JPL). Test coupons were sprayed simultaneously with the radiator and shrouds and sent to JPL for testing. This is discussed in more detail in the calibration chapter of this dissertation.

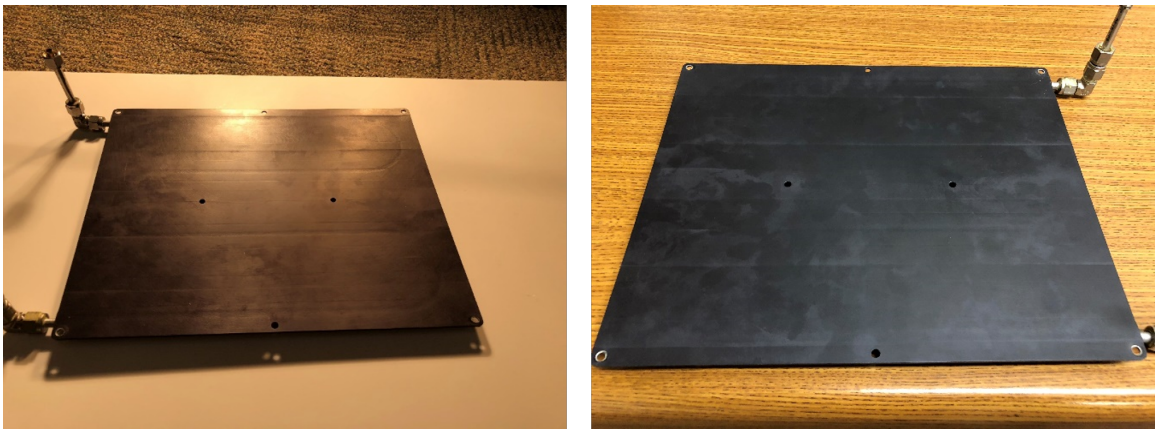

Fig. 6.22: Black Anodized radiator showing discoloration (splotches) from HIP process.

For the ACCS system, both the radiator and internal copper shrouds required Z306 paint. Z306 is ideally applied with a spray gun in multiple layers with a primer coating as the first layer. USU labs were set up with a painting booth for this procedure. The Z306 was prepared as specified by the manufacturer's guidelines [131, 132]. Z306 cures in relatively high humidity ($> 50\%$) over several days. Because Utah is a dry ($< 15\%$ humidity) environment, special humidity boxes were built with saturated salt water baths

as moisture sources. A relative temperature and humidity sensor monitored the relative climate of these humidifiers. The USU spray painting setup and final black Z306 coated radiator and shrouds are shown below in figure 6.23.

Fig. 6.23: Z306 painting booth at USU.

6.11 ACCS Test Cube Conclusions

The ACCS test cube was designed for the characterization and TRL advancement of the ACCS technology. As such, it was highly successful. Over several weeks in a thermal vacuum, spanning three separate tests, the ACCS test cube successfully characterized the performance and behavior of the ACCS active thermal control system and raised the technology TRL to ∼5. One of the primary objectives of the ACCS research was to design a

thermal control system that could accommodate the high-power requirements of a miniature tactical cryocooler on a CubeSat platform. The ACCS test cube successfully demonstrated the accommodation of the Ricor K508N cryocooler as an active component of the ACCS system.

As a highly instrumented test bed, the ACCS cube was able to characterize the performance of the TCS M510 micro-pump and fit its behavior to the Centrifugal affinity laws. Thus, fully describing the M510 behavior in analytical form for future systems. The inclusion of so many temperature sensors enabled detailed post-processing of the flow of thermal energy within the system. The ACCS TVAC characterization also successfully demonstrated UAM technology as a thermal control technology and an ideal platform for integrated fluid networks. Ultimately, the characterization test data collected by the ACCS test cube will aid in the future design and refinement of the ACCS system as well as similar technologies. Figure 6.24 below shows the completed ACCS test cube on the left and the test cube integrated with the TVAC chamber on the right.

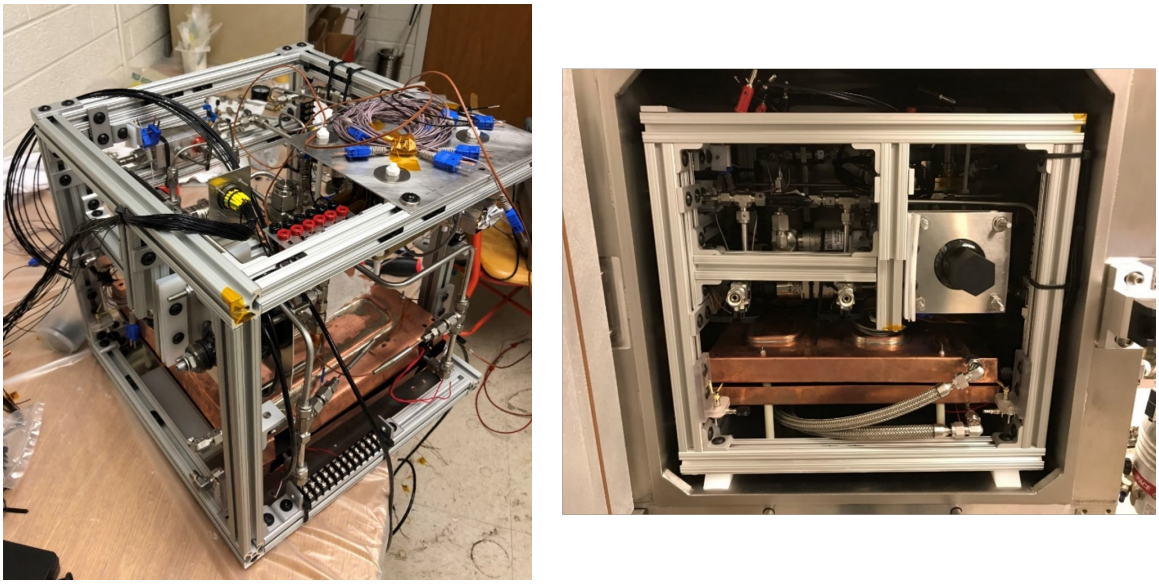

Fig. 6.24: The completed ACCS test cube on the bench (left), and integrated with the USU (CSE) TVAC chamber.

CHAPTER 7

ACCS Experimental Uncertainty & Calibration

Exploring the Unknown Requires
Tolerating Uncertainty

Brian Greene

7.1 Introduction

Experimental engineering is entirely dependent on good testing, and a test is only as good as the measurement it's based on.

Metrology is the science of measurement and all of its applications. Instrument accuracy, precision, uncertainty, and error are all critical considerations in the design of an experimental test and can often be overlooked. Minor errors in measurement or key uncertainties in sensitive data can easily cascade throughout a test and result in erroneous data, ballooning uncertainties, missed trends, or errors that simply result in the wrong conclusions. Calibration can help by comparing key measurements to known standards, confirming the accuracy and precision of an instrument while reducing uncertainty and error. Overall, calibration improves the confidence of a given measurement and validates the test as a whole. The ACCS TVAC tests are not only a technology demonstration but also a characterization of the performance and behavior of the system. The results of which will help to inform future designs and research. This chapter will cover the accuracy and uncertainty of the ACCS TVAC instrumentation and measurement, as well as the prior calibration done by the project. A summary of the total quantitative uncertainty for each instrument is given in Table 7.2.

7.2 ACCS Error Sources

The ACCS TVAC cube is a highly instrumented test bed for the characterization and

demonstration of the ACCS technology. A sensor and measurement list includes power regulators, current sensors, thermocouples, temperature diodes, pressure transducers, a flow meter, and IR/visible cameras. Table 7.1 below summarizes the various instruments included in the ACCS TVAC characterization.

ACCS Test Bed Instrumentation		
System-Wide Temperature	**30X**	30x Omega Type-T Thermocouples
Cryocooler Cold Tip	**3X**	Cryogenic Lakeshore DT-670 Silicone Diodes
System/Pump Flow Rate	**1X**	Custom Venturi Flow Meter
Pump Differential Pressure	**1X**	Honeywell FP2000 15 psid Transducer
Venturi Differential Pressure	**1X**	Honeywell FP2000 5 psid Transducer
Static System Pressure (Absolute)	**1X**	Honeywell FP2000 150 psia Transducer
RPM	**1X**	TCS EQI-M Controller RPM Output
IR Cameras	**2X**	Flir Lepton Radiometric Cameras
Active Component Power	**7x**	Power regulators, voltage & current sensors

Table 7.1: ACCS Test Bed "Cube" Instrumentation.

The ACCS test bed consists of a variety of COTS and custom instruments. All of which are directly controlled by the ACCS electronics box, the design of which is detailed earlier in this dissertation. A National Instruments Data Acquisition system monitors and captures each measurement in real-time. The NI-CDAQ 9178 module. A single NI-9205 voltage card measures the pump RPM, various voltages, currents, and powers with 16-bit Precision, while two dedicated NI-9213 24-bit TC modules directly measure thermocouples. Linear Technologies LT6105CMS8 current sense amplifiers are used to convert 4-20 mA and raw current values to voltages. A connected PC logs all of the data and captures video from the two integrated IR cameras as well as the test monitor webcam.

7.3 Metrology & Calibration

The ACCS instrumentation was calibrated prior to integration with the test cube. This calibration helped validate the given sensors and measurements and determine the overall uncertainties, random errors, and measurement biases present in the test results and data. The ACCS calibration campaign includes temperature sensors, pressure transducers, the

Venturi flow meter, pump RPM frequency, and radiator gray-body emissivity.

The ACCS is, at its heart, a thermal control system and is, therefore, highly instrumented for temperature. The ACCS features 30 type T thermocouples calibrated by submersion in a temperature-controlled bath with De-Ionized water. The bath thermometer and a standalone DT-670 diode were used as reference "true" temperatures. The calibration profile was to warm the water from room temperature to 50 oC and hold that for a sustained period. The water was cooled to 0 ^{o}C before rapidly heating to elevated temperatures. This profile was intended to mirror the test profiles planned for the TVAC characterization as well as determine how accurately the various temperature sensors would respond to rapid temperature swings. The temperature profile for all 30 TCs is shown below in figure 7.1. Slight variations exist between each sensor. However, in general, all TCs agree quite well with each other. The average standard deviation for each grouping of 15 (0-14 & 15-30) was around 0.06, figure 7.2. This relatively tight tolerance around the mean temperature indicates that the batch-produced TCs are precise when calibrated against each other.

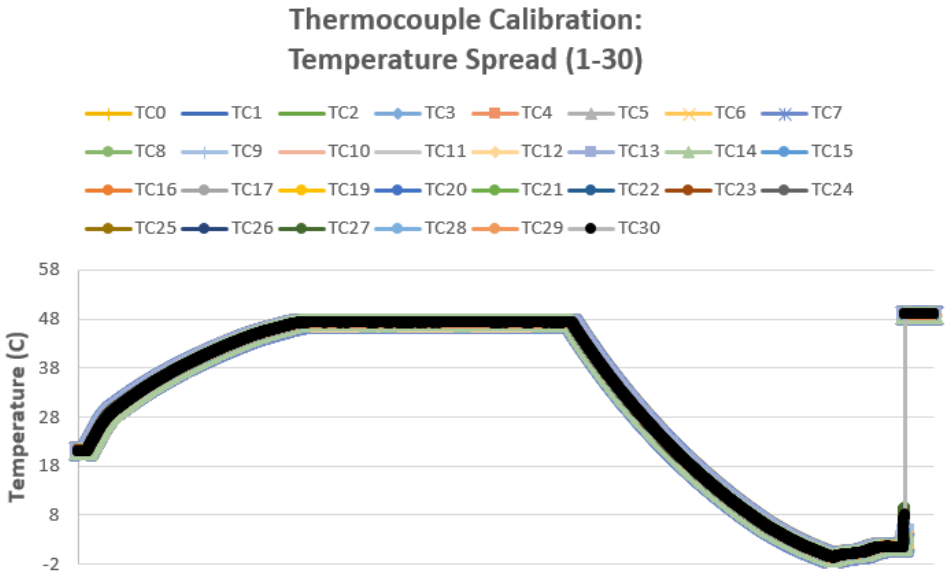

Fig. 7.1: ACCS test cube thermocouple calibration data.

The average temperature profile for each (grouped) batch of 15 is shown below in figure

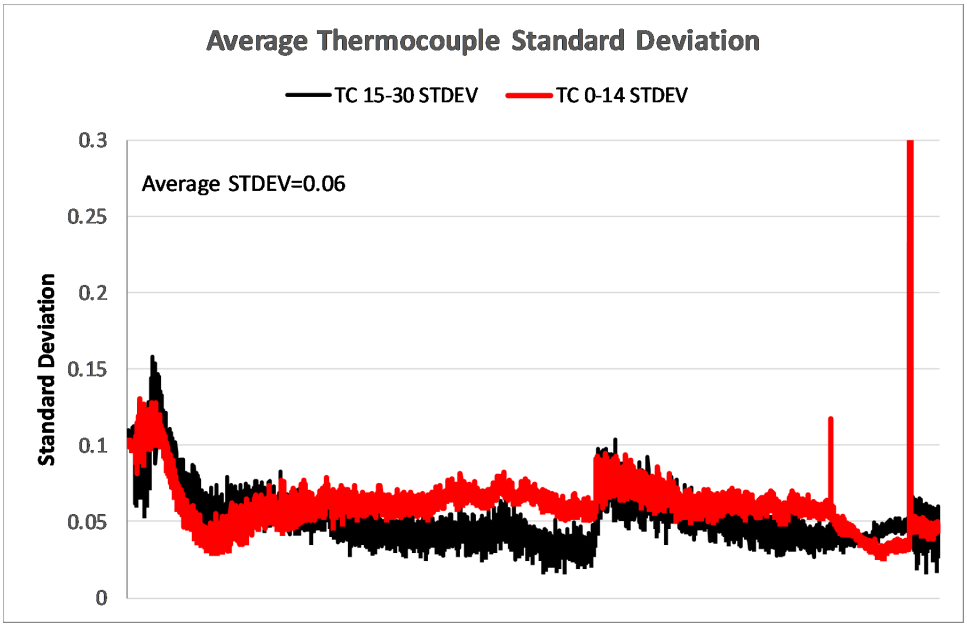

Fig. 7.2: Thermocouple standard batch deviation. Batch #1 0-14, Batch #2 15-30

7.3 along with the temperature profile of the DT-670 reference diode. As can be seen, in figure 7.4, a slight negative bias exists for all of the thermocouple readings. This low reading bias of ∼1.77 ^{o}C was used to adjust all TC readings for the ACCS TVAC characterization.

The Lakeshore DT-670 silicone diode is an industry standard for cryogenic temperature measurement of cryocooler cold tips. Based on the principle of variations in voltage across a well known Silicon PN diode junction with a constant current. DT-670 diodes feature tight tolerances, and accuracies and often do not require individual calibration within batches. Although, calibration is available upon request. Three DT-670 diodes (coupled with a 121 constant current source) from the same batch were used to monitor the ACCS Ricor K508N cold tip. Two diodes were compared and averaged as cold tip temperature, while the third was fed back to the cryocooler HyB-18 controller for set-point control. DT-670 diodes follow a tight calibration curve from 1.5 K to 450 K. Figure 7.5 below shows the calibration curve used by the ACCS research along with a linearized curve fit for direct translation of voltage to temperature within the LabVIEW test code. For this research, it was assumed that the averaged cold tip values were accurate and could be used as a reference within the ACCS system.

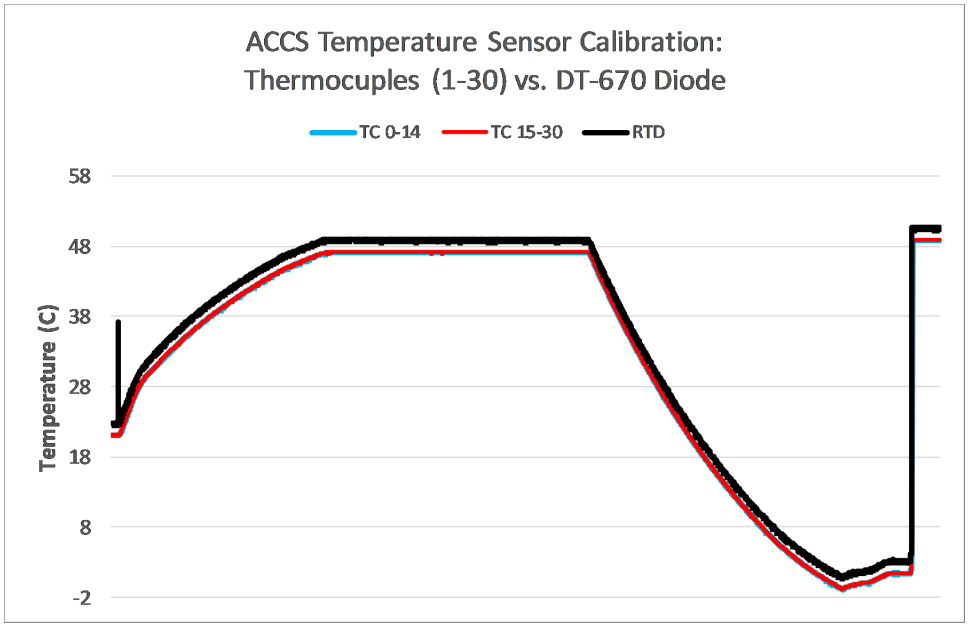

Fig. 7.3: Average thermocouple temperature response. Referenced to a factory calibrated LakeShore DT-670 diode.

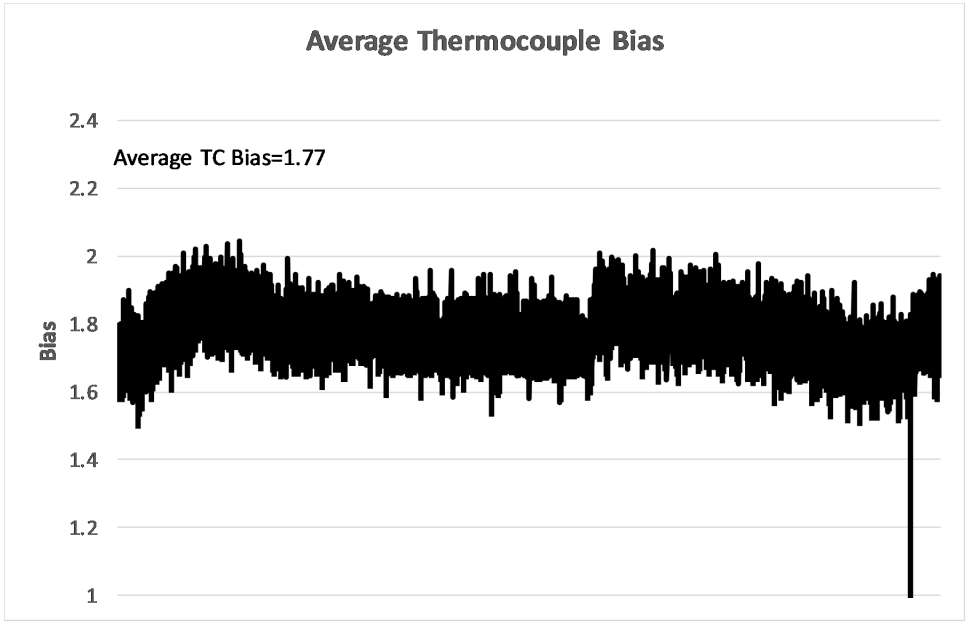

Fig. 7.4: ACCS thermocouple average bias.

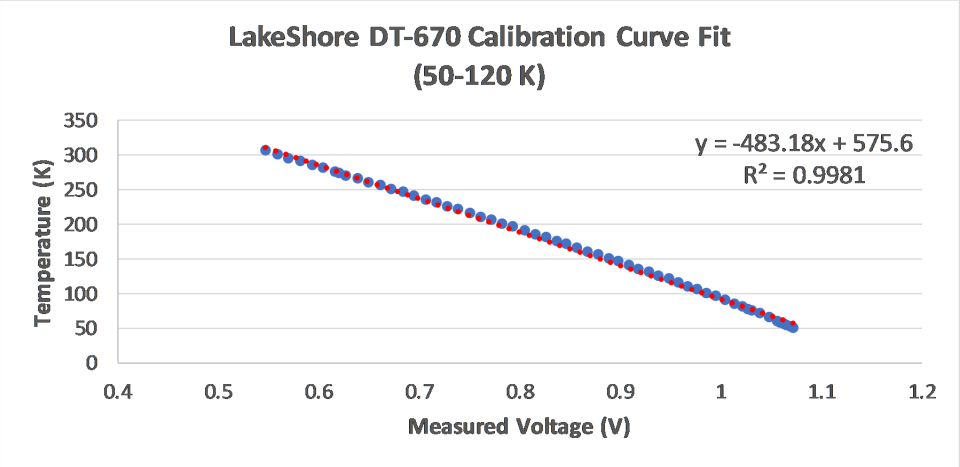

Fig. 7.5: Calibrated temperature vs. voltage response curve for the DT-670 diode.

Honeywell FP2000 series pressure transducers were used for monitoring the differential pressure drop across the M510 pump, the absolute static pressure of the pumped fluid loop, and the flow rate (DeltaP) across the Venturi flow meter. These FP2000 series pressure transducers come pre-calibrated with calibration certificates and linear data points for pressure vs. output. Each FP2000 transducer is rated to 0.25% of measurement (1% of full scale). Each transducer is tuned to a different range based on expected values. The linear calibration curves for all three of the ACCS transducers are given below in figure 7.6.

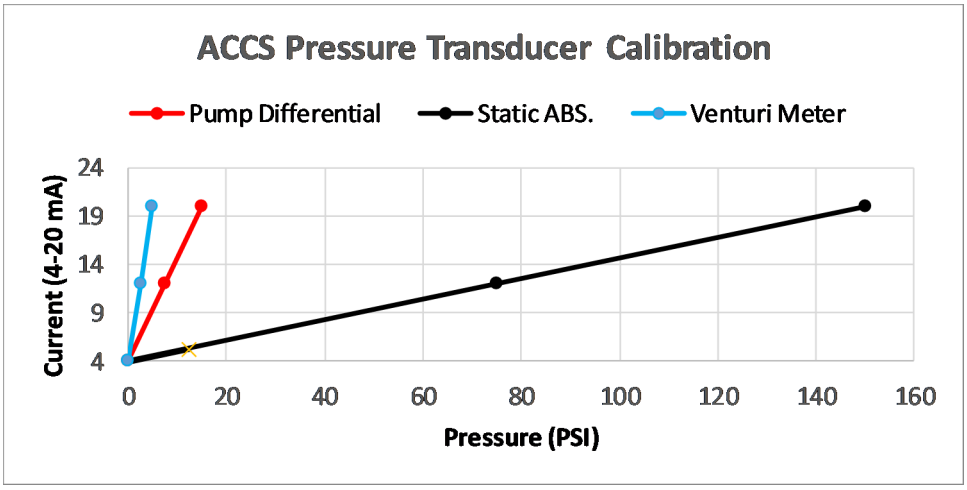

Fig. 7.6: Calibration curves for the ACCS HoneyWell FP2000 pressure transducers.

For several reasons, a custom Venturi flow meter was down-selected for the ACCS test cube. The first was the flow rate range. Many COTS flow meters are limited to specific flow rates, which do not cover the wide range required by the ACCS system (∼100 to ∼1200 mL/min). Another critical feature of Venturi meters is that they impose relatively low permanent pressure drops within the system. The gradual compression/expansion of the fluid results in only a few tenths of a PSI drop. Finally, a custom Venturi meter could be sized for the ACCS system and designed to be vacuum compatible. The design and governing equations of the ACCS Venturi meter are given in the experimental setup chapter of this dissertation.

Venturi flow rate calculations depend on fluid properties, the geometry of the flow meter, and the pressure drop across the compression zone [130]. This pressure drop is directly translatable to the flow rate. Therefore, the accuracy of the pressure transducer can be converted to flow accuracy. However, this was unnecessary because the Venturi flow meter was calibrated before use by a beaker flow rate test. Fluid was pushed through the meter at various flow rates and collected in graduated cylinders. The fill time for each given beaker was recorded to calculate an analog flow rate. The output of the Venturi meter was simultaneously monitored. The flow profile of this test is shown below in figure 7.7.

Each of the flat, steady-state flow peaks above is averaged as single data points and plotted below, 7.8, against the corresponding beaker flow rate data. The error is also calculated and plotted on the second Y-axis. As seen below, overall the custom Venturi flow meter is accurate across most of the ACCS flow range. Relatively high errors exist at the extremes of both low and high flow. The overall calibrated error is 14.85%. Excluding the first and last data points, the error is reduced to ∼0.67% across the majority of the flow range. These errors are included in all future calculations of flow rate as relative error bars.

A final important aspect of the pump flow rate is the pump RPM. The TCS M510 dedicated EQI-M controller outputs the pump RPM as a 0-5 V square wave signal. The square wave frequency is directly related to the pump RPM by a multiplicity factor of ten. This RPM frequency signal is clear and highly repeatable with distinct frequency peaks.

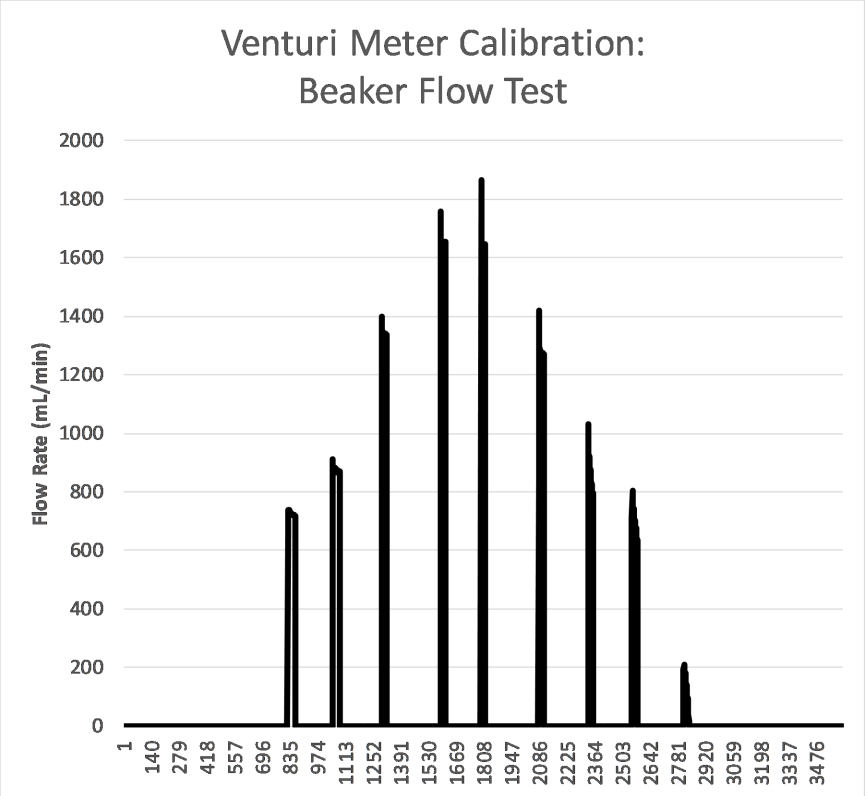

Fig. 7.7: Digitized flow data from the ACCS venturi meter. Various flow rates (peaks) are produced by forced flow through the venturi meter.

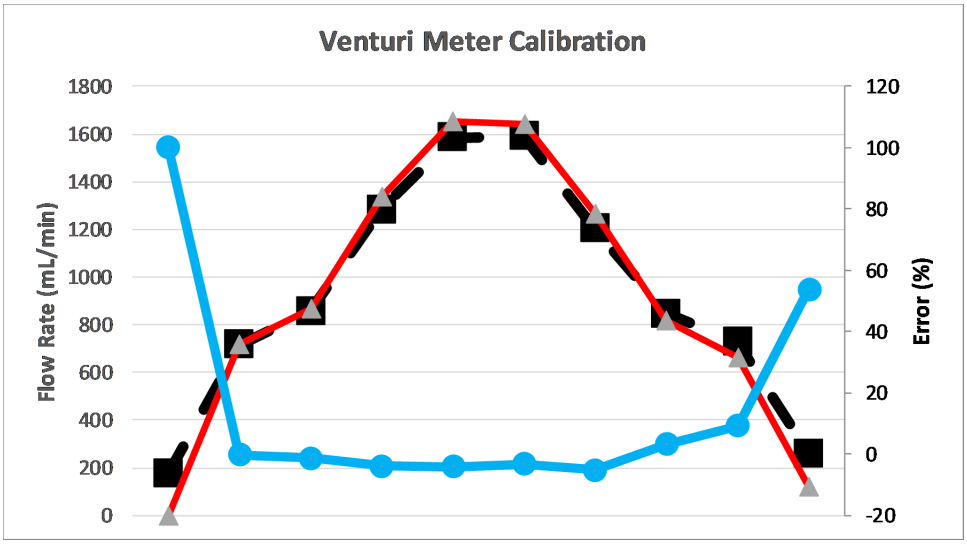

Fig. 7.8: Calibrted flow response curve of the ACCS venturi flow meter. Note, at low flow rates, the venturi meter is relatively inaccurate.

An example of the LabVIEW NI-DAQ measured RPM signal is shown below transformed (Through Fourier DFT) to a frequency in figure 7.9. The x-axis represents the Fourier frequency bin. This value can be converted to frequency and RPM from the following equation.

$$PumpRPM = 10 \cdot \text{Fourier Frequency at Peak} = Freq_{Bin\#} \cdot \frac{SampleRate}{Num(DFT_{Points})} \tag{7.1}$$

The sample rate was set to 10kHz, and the number of discrete Fourier Samples was 4000. This ensured that the square wave was captured and that the DAQ Sample rates were set high enough to accurately reproduce the square wave signal and corresponding frequency via Nyquist sampling. Notice the clear signal peak of the RPM as well as much smaller harmonics. The RPM signal, Fourier frequency, and corresponding RPM number were all captured real-time by the NI-DAQ and recorded in the text output.

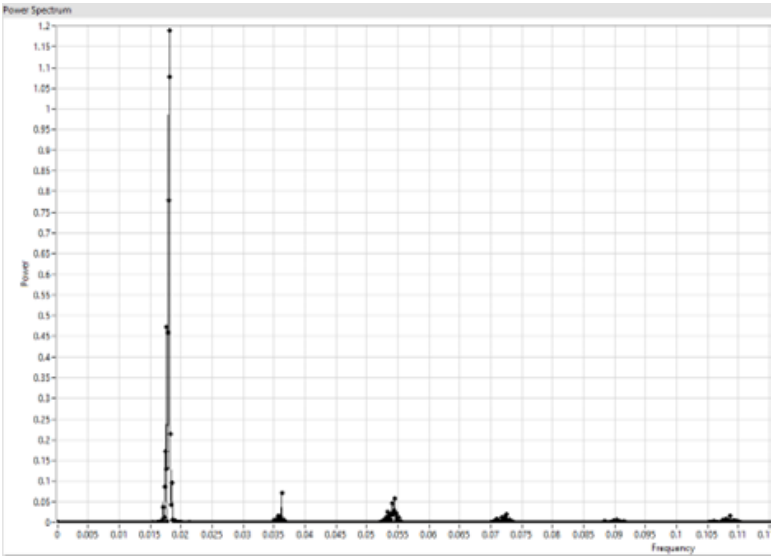

Fig. 7.9: RPM frequency signal of the TCS M510 micro-pump. The x-axis represents teh Fourier frequency bin

The RPM signal is highly linear with respect to control voltage for the Pump EQI-M V2.0 controller. This relationship is shown below, 7.10, along with a trendline equation

which can be used to relate control voltage to RPM back to flow rate, pressure drop, and power performance for the TCS M510 micro-pump.

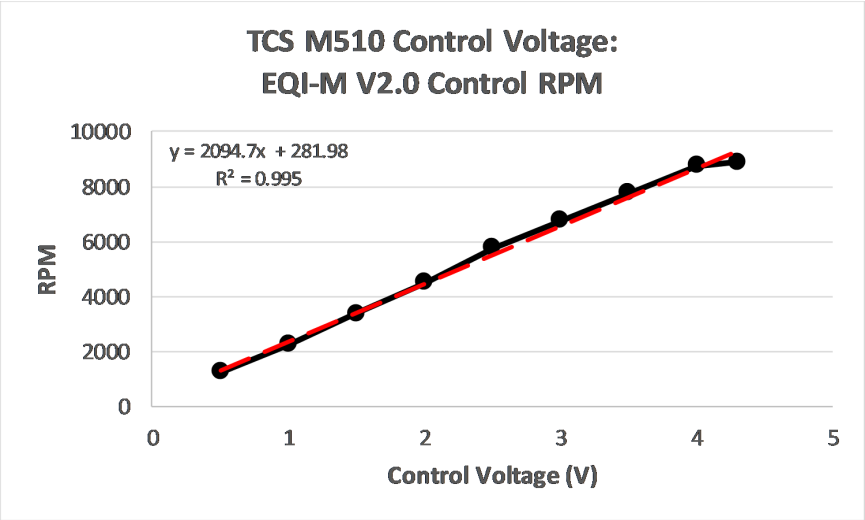

Fig. 7.10: TCS M510 input "Control-Voltage" vs. pump RPM's.

Because the Venturi flow meter was not accurate across the entire flow range of the pump, it was essential to create a flow curve and set of equations to calculate the calibrated/corrected flow rate of the ACCS test cube system. Centrifugal pumps obey the basic Affinity/Similarity laws that state for geometrically similar pumps, aka the impeller diameter/shape are constant, the flow rate, pressure drop, and power can be directly related to the pump RPM's. These equations are very useful because they allow flow rate calibrations of the pump to be extended to the TVAC characterization. Essentially, these affinity laws can translate a calibration curve over a specific flow range to extend across the entire flow rate range of the ACCS TVAC characterization. The affinity laws state that the change in flow rate is linearly related to the RPM, that pressure drop is related to the square of the RPM, and power to the cube. The three affinity laws are given below in equations 7.2 to 7.4. The flow rate is given by q, while dp is the pressure drop and P is the pump power.

$$\text{1st Affinity Law} \quad \frac{q_1}{q_2} = \frac{RPM_1}{RPM_2} \tag{7.2}$$

$$\text{2nd Affinity Law} \quad \frac{dp_1}{dp_2} = \frac{RPM_1^2}{RPM_2^2} \tag{7.3}$$

$$\text{3rd Affinity Law} \quad \frac{P_1}{P_2} = \frac{RPM_1^3}{RPM_2^3} \tag{7.4}$$

The ACCS flow rate/Venturi calibration data is plotted below, in figures 7.11 through 7.13. Each fitted curve represents the affinity laws as they pertain to the ACCS centrifugal pump. Each equation can then be used to predict similar flow rate, pressure drop, and power performance for the TCS M510 pump across the entire ACCS TVAC characterization range. The equations shown have a high degree of fit as can be seen by the R2 residual value exceeding 0.99 for each.

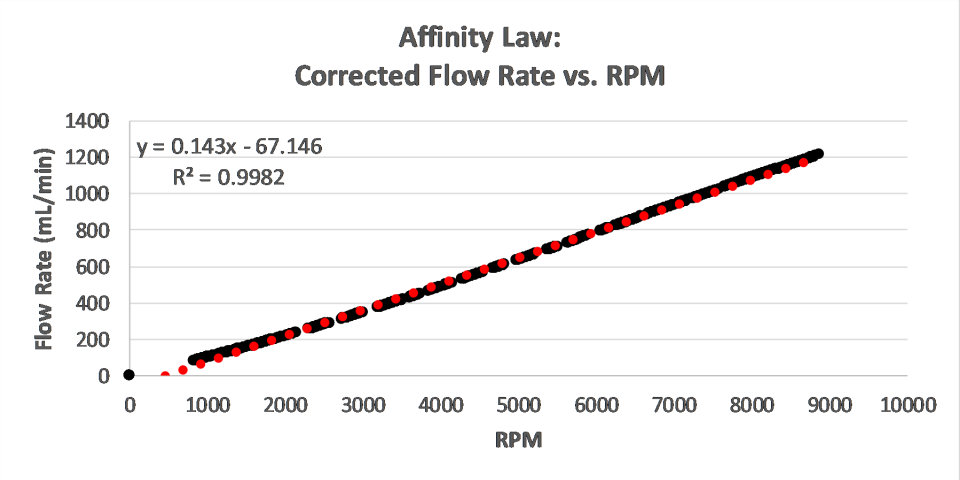

Fig. 7.11: ACCS TCS M510 pump affinity law #1. Linear response of flow rate to RPM.

These affinity laws were combined to create a set of corrected flow rate equations that directly relate the ACCS system flow rate to the measured RPM. The ACCS custom Venturi flow meter was inaccurate at flow rates below ~450 to 600 mL/min. To compensate for this, the more accurate region of higher flow was calibrated and correlated to RPM. Then, because centrifugal pumps follow the affinity laws given above, the linear relationship between flow rate and RPM could be extrapolated backward to the lower flow rate regimes.

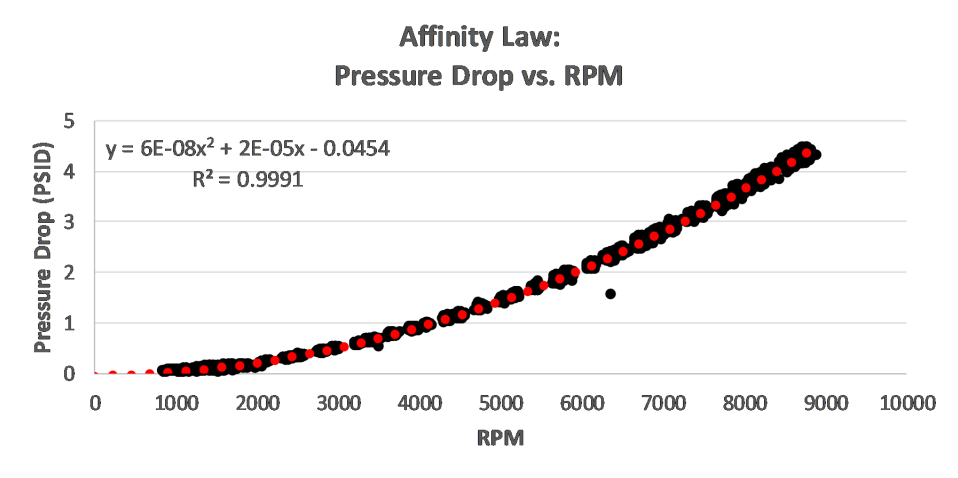

Fig. 7.12: ACCS TCS M510 pump affinity law #2. Quadratic response of pressure drop to RPM.

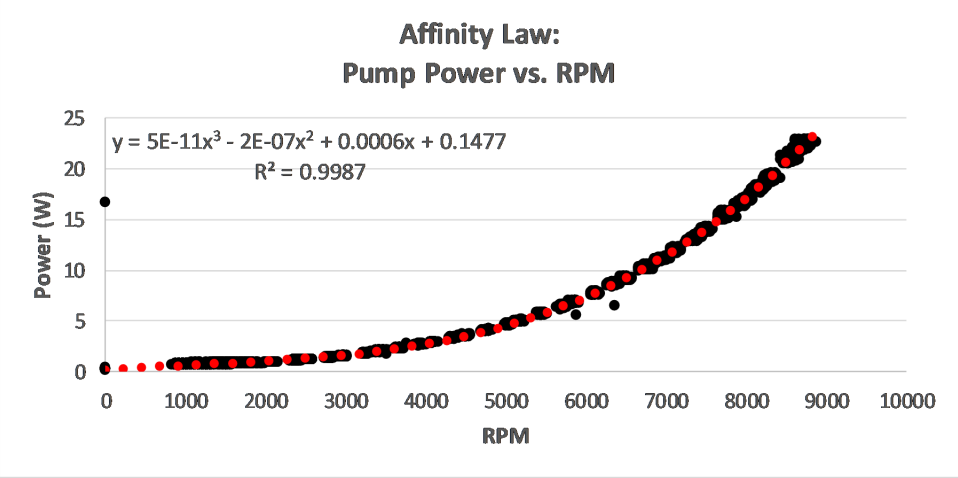

Fig. 7.13: ACCS TCS M510 pump affinity law #3. cubic response of power to RPM.

This is not ideal but compensates for the shortcomings of the Venturi meter, which are discussed in more detail within the experimental design chapter. It should be noted that, overall, this approach has proven to be highly accurate and corresponds quite well with analytical and numerical modeling. Corrected and calibrated flow rate data was plotted, and curve fitted as a ratio of flow rate to RPM. Figure 7.14 summarizes this data along with a 2nd-order polynomial curve fit. This equation directly relates the flow rate to RPM by replacing x with RPM. This equation covers the flow rates deemed accurate from figure 7.8. i.e. ∼450 to 1200 mL/min. The entire flow regime is given in the appendix. A more targeted curve fit for the ∼800 mL/min to ∼1200 mL/min flows considered most accurate is given in figure 7.15. These equations are used in the MatLAB data processing code to correlate flow and RPM. In fact, in post-processing, the Venturi signal flow rate is recorded but only used as an accuracy check for these plots and equations.

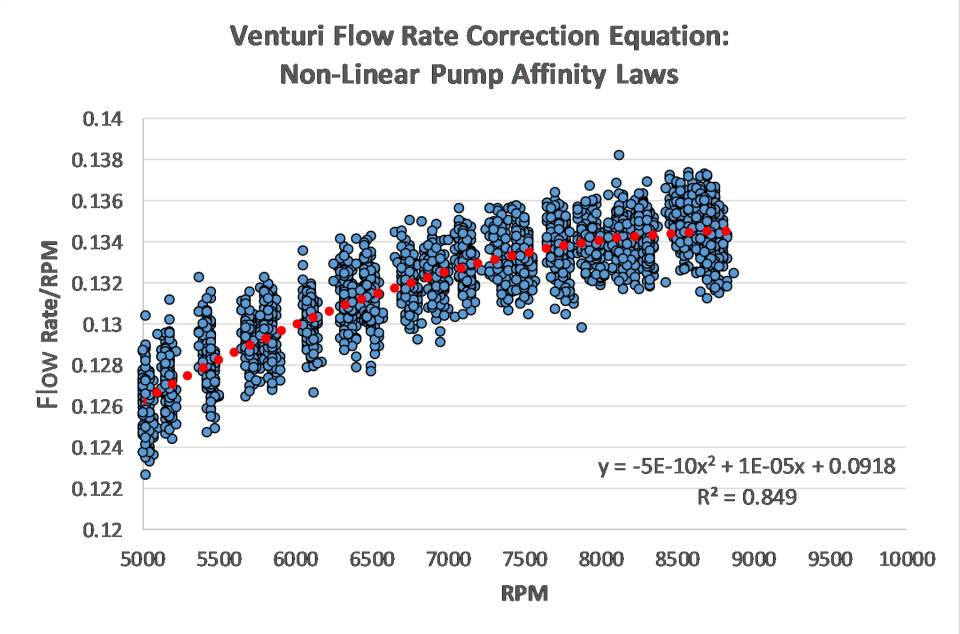

Fig. 7.14: Venturi meter flow rate curve & fitted equation used for the Analysis of the ACCS data.

The plots above relate the ratio of flow rate to RPM. The direct linear correlation of flow rate to RPM for the calibrated and validated higher flow regimes is given below in

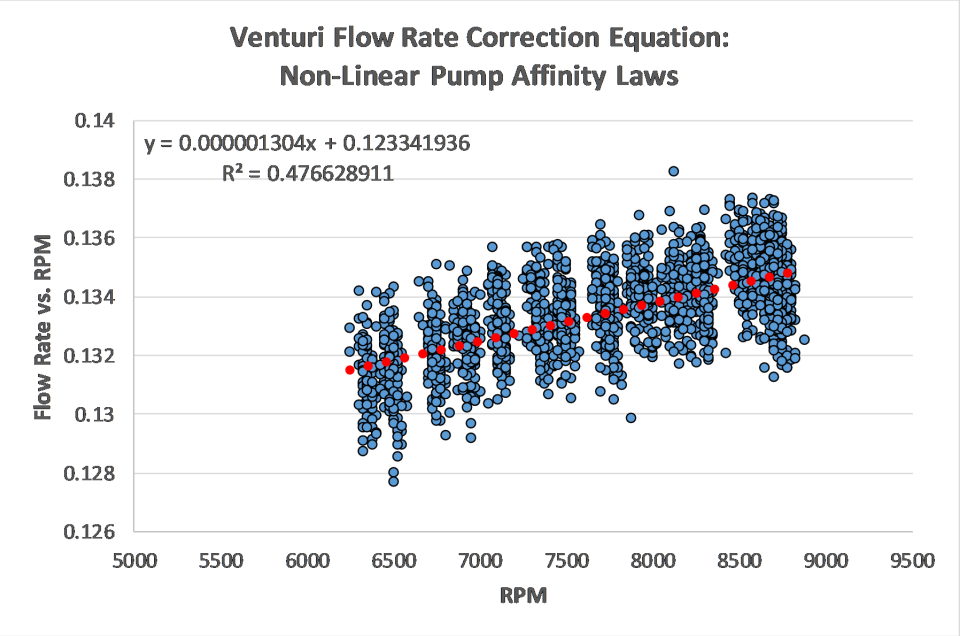

Fig. 7.15: Linearized flow rate curve for the ACCS venturi meter with curve fitted equation.

figure 7.16. This curve-fitted equation can be considered an experimentally derived first affinity law for the TCS M510 over the calibrated flow rate range shown in figure 7.8. The now corrected flow rate can be used to compare the recorded pump differential pressure as a direct measurement vs. as a calibrated flow figures 7.17 & 7.18. The relative error is once again shown on the second vertical Y-axis in figure 7.18.

The exact emissivity of the ACCS radiator is essential to determine how much thermal energy is radiated at a given temperature and power. Essentially, the efficiency of the radiator. The emissivity is also critical to the analytical and numerical models because it has a linear effect on the rejected power as a function of temperature to the fourth. The ACCS radiator was painted with Aeroglaze Z306 black high emissivity paint. Reported emissivity values of between 0.94 and 0.97 are reported. However, because this is a critical aspect of the ACCS design, the actual emissivity of the radiator was determined by direct calibration. Emissivity testing was done at JPL via test coupons painted in an identical procedure to the radiator. A TESA 2000 emissivity/reflectivity meter was used to make these measurements. The results are shown below as direct spot measurements of emissivity

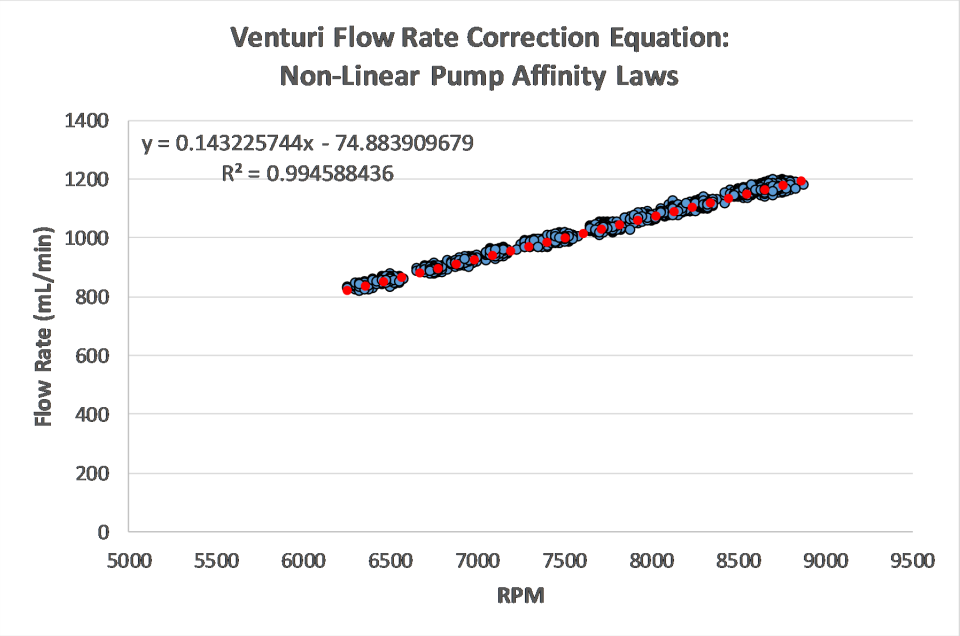

Fig. 7.16: Experimentally derived linear affinity law for the ACCS system. The curve fitted equation can be used to predict the flow rate of the ACCS as a function of RPM.

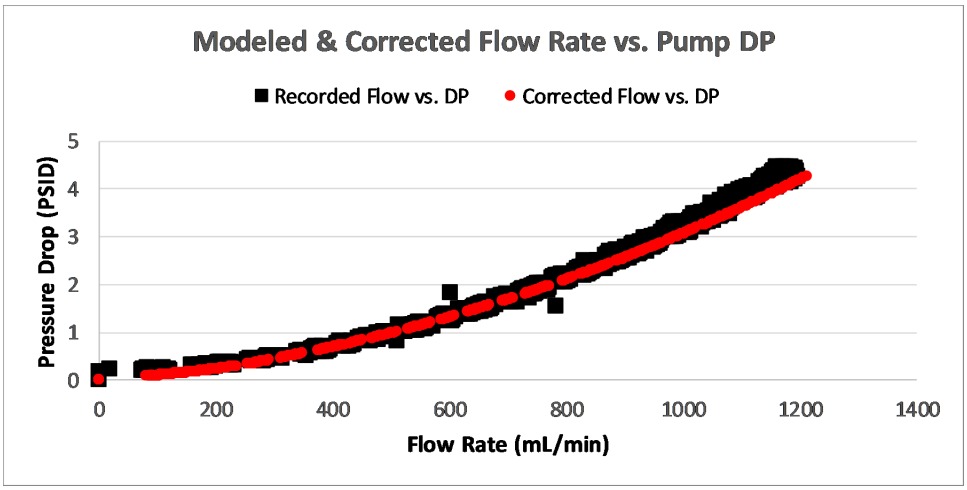

Fig. 7.17: ACCS pressure drop (Measured vs. modeled) with corrected flow rates.

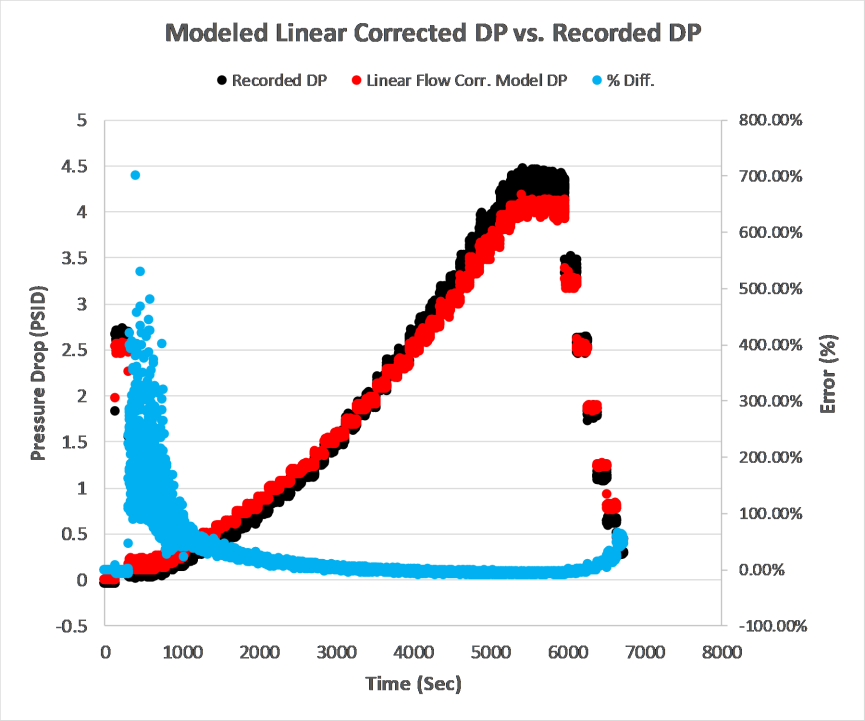

Fig. 7.18: ACCS pressure drop comparison & relative model error.

for two of the four test coupons sampled. From the results, an average value ∼0.9 was determined for the ACCS radiator gray-body emissivity.

7.4 ACCS Uncertainty

Each of the sensors and instruments used in the ACCS test cube for TVAC characterization have a set of random error or uncertainty values. These are tabulated below 7.2 for quick reference.

A note on the flow rate uncertainty: The calibration beaker test determined that the Venturi meter monitored by NI-DAQ and LabVIEW tended to underread at low flow rate values and resulted in an error of between ∼0.7 and ∼15%. This was confirmed by further testing. Subsequently, the derived flow rate equations "corrected" the flow rate values. This correction resulted in differences of, on average, 21.14%. The difference exceeded 111.1% at low flow rates, while higher flow rates only changed by roughly 3.4%. Assuming that the adjusted flow rate is correct. This would mean that the Venturi meter had an average error

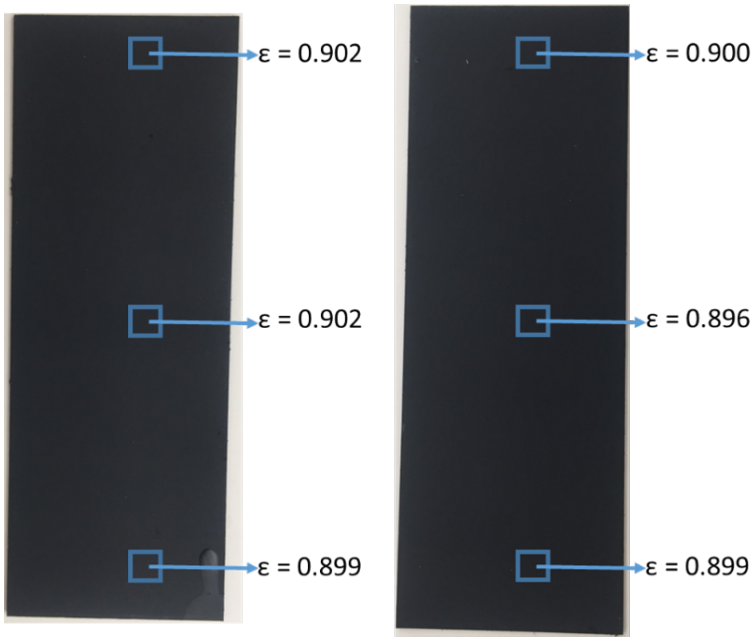

Fig. 7.19: Emissivity measurements of the Aeroglaze Z306 black paint used as a high emissivity surface coating for the ACCS radiator. Two sample coupons were measured by JPL with a TESA 2000 emissiometer/reflectometer instrument.

ACCS Measurement and Instrument Uncertainty	
Type T Thermocopules	±1 °C or ±0.75% whichever is larger +1.77 °C Constant Bias
Lakeshore DT-670 cryogenic diodes	12 to 32 mK
HoneyWell FP2000 pressure Transducers	0.25% (1% of full scale)
Venturi Flow Meter	0.67% to 14.85%
Corrected Flow Rate	Corrected Flow Difference by up to 21.14%
Power, Voltage, Current, & RPM	16-bit Precision
FLIR Lepton IR Camera	±5 °C

Table 7.2: Metrology summary for the ACCS test-cube. Random uncertainties and biases are listed for each of the major sensor within the system.

of nearly 16.13%. Because of this, the linearized and extrapolated flow vs. RPM equations were derived. Essentially, capturing the highly accurate flow regime of the Venturi meter and linearly extrapolating that profile backward, via the first pump affinity law, to the lower flow rate ranges.

7.5 Conclusions

The ACCS active thermal control system has been implemented into a highly instrumented test bed. Every effort has been taken to ensure the accuracy and Precision of the various test measurements made during TVAC characterization. The various known uncertainties of the COTS sensors have been reported here and as error bars in the results chapter. In addition, numerous metrology efforts have been made to calibrate the various sensors and provide experimental validation to all measurements. This has, ultimately, provided a high level of accuracy and Precision to the ACCS testing. Overall measurement uncertainties are well below 5% and, in most cases, are almost negligible with respect to the measurement range itself. Likewise, errors have been reduced wherever possible and cataloged as necessary. Therefore, it can be concluded that the various results given in this dissertation can be taken as accurate within the scope of this chapter.

CHAPTER 8

Systems Engineering Analytical Model

Design adds value faster than cost

Joel Spolsky

8.1 Introduction

One of the most critical aspects of engineering design is a thorough understanding of the fundamental physics involved. From this basic theory, creativity and good design can follow.

A simplified analytical model is a critical tool for the early phase design of space systems. Especially a rapid analytical model that can provide a more fundamental understanding of the basic physics of the system. This chapter details the creation of such an analytical design model for the ACCS system. A simplified analytical tool for the rapid iterative design and performance prediction of the ACCS active thermal control system. Based on a steady-state, simplified 1D nodal analysis and the working principles laid out in this dissertations theory chapter, this analytical model is an essential tool and is based on the principles of systems engineering, including principles 3 & 5 from the NASA SE principles list [133]. During subsequent design phases, more detailed broader models and analytics will take over, such as numerical Thermal Desktop models and flow simulations. However, in the early stages of development, a simple analytical modeling tool allows the systems engineers to make rapid design decisions, forecast behavior trends, understand the impact of components on the whole and gain an appreciation of the overall capabilities and limitations of the system.

The development of the various ACCS analytical models was a fundamental objective of this research/dissertation and is a central part of the systems engineering methodologies

outlined in this work. This chapter will detail the node-by-node derivation of the ACCS excel based analytical rapid design tool. The results of the model are compared to experimental TVAC characterization data points. Furthermore, the ACCS analytical model was also used to predict the impact of each aspect of the MPFL heat exchanger on overall system temperatures. This predicted behavior is shown below for each node. Secondary pressure drop models based on major and minor flow losses and the more advanced 2k method were also developed and are described below. Finally, a basic radiation and conduction heat transfer tool was developed that helps to predict two-node, 1D heat transfer, and system parasitics commonly encountered in satellite design. Basic theory can be referenced in Chapter 4, while supplementary material, including model interface screenshots and code snippets, can be found in online ACCS repositories. Excel and VBA coding were used for the ACCS analytical model due to Excel's widespread use, GUI interface, data analysis capabilities, visual basic coding/macros, and the fact that it is already a very common systems engineering tool. The ACCS analytical model focuses on steady-state solutions, as opposed to transient, because, generally, the system response is much faster than the orbital period experienced by most spacecraft. However, transient analysis is essential and features more heavily in the control algorithm (PID) modeling and numerical Thermal Desktop simulations discussed later in this work.

The basic thermal model of the ACCS system is shown below in figure 8.1. Heat transfer begins with a conduction interface at the heat exchanger. Thermal loads from the cryocooler, guard heaters, and pump are transferred to the working fluid, which is then circulated to the radiator. This energy transfer is nearly isothermal, depending on the integration with the mechanical structure and isolation design. The process is reversed at the radiator, and radiation releases thermal energy to the space environment

8.2 Model Objectives

The analytical model objectives are broadly categorized into capability, accuracy, ease of use, and systems engineering utility. They are listed below:

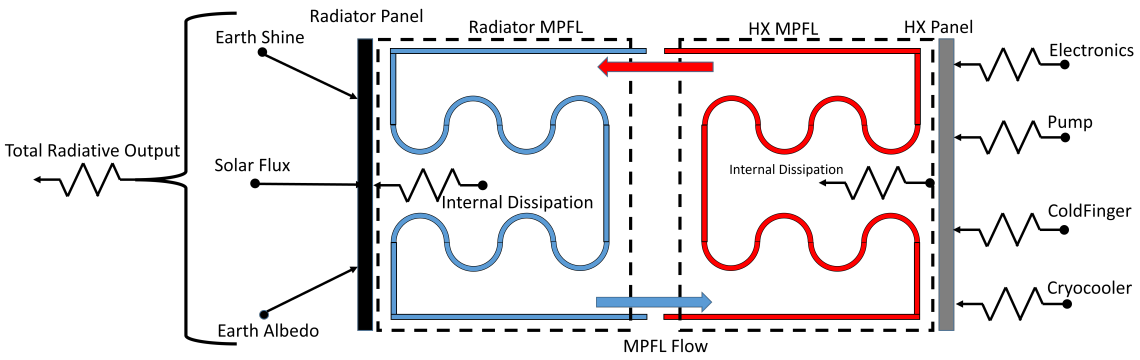

Fig. 8.1: Basic conceptual block diagram of the ACCS analytical model.

- Provide a deeper understanding of the ACCS system through basic theory and logic. Including behavior, component-to-system impact, overall capabilities, and limitations
- Serve as an aid to systems engineering design methodologies
  - Pre-Phase A & Phase A tool
  - Parallel design tool
  - Rapid design iteration
  - Back of the napkin modeling tool for Q&A
- Predict the overall performance and behavior of the ACCS system
  - Node Temperature prediction accuracy within $< 5\%$ of experimental results
- Create high-fidelity performance/impact curves for each aspect or parameter of the design
- MPFL system pressure drop and flow regime predictions
- Basic conduction/convection/radiation heat transfer and parasitic analysis

8.3 Analytical Model CONOP & Details

The ACCS analytical model is broken down in figure 8.1, into a block diagram showing the various nodes, the flow of thermal energy, and analysis types. Thermal energy flows

from the heat exchanger to the radiator. However, the radiator forms the model's base and starting point. This model relies on a closed-loop solution and, therefore, needs a point at which the thermal energy can be summed. Essentially, a point at which to start the analysis. Without the space thermal environment, the model would be entirely symmetric, and the analysis could be started from either end. However, the space environment serves as an additional input/output to the radiator, not the heat exchanger. Therefore, the radiator must serve as the first node. Once a thermal balance on the radiator has been established, the flow of heat through the radiator and into the fluid can be determined. At this point, subsequent energy balances can be summed and conserved at each system node. The thermal connection between the radiator and HX nodes is fluid advection and convective heat transfer. The working fluid is circulated between the heat exchanger and radiator through an optional control valve, which controls the fluid mixing between the HX and the radiator. Figure 8.2 below shows a state diagram of the ACCS analytical model with each node labeled and the heat transfer analysis describing that node. Key assumptions for the ACCS model include the following:

- Nodal heat transfer analysis
  - Nodes are well insulatedl
  - Nodes are well insulated
  - Isothermal nodes
  - Energy is conserved within a node
- 1D heat transfer between nodes
- Steady-state thermal analysis
  - Transient analysis is optional and can be added

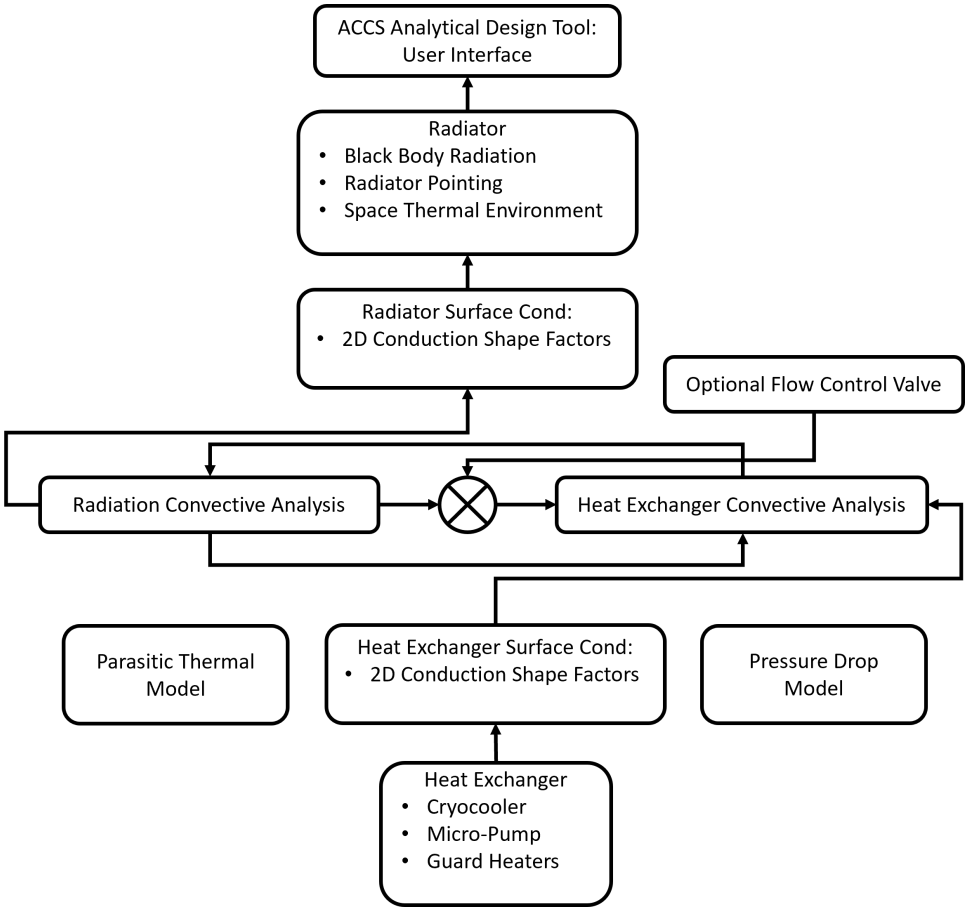

Fig. 8.2: ACCS analytical model block diagram. Showing node interactions and interconnections.

8.3.1 Node 1: Radiation and the Space Environment

The ACCS radiator is modeled as a gray body, subject to the basic (modified) Stephan Boltzmann equations (Chapter 4). The radiator is the first node of the analysis because it's a point at which all of the thermal energy within the ACCS system can be summed. This summation includes the internal energy transferred by the pumped fluid loop and heat exchanger, the environmental thermal load, and the total radiated power. This energy balance sets the baseline temperature for the whole ACCS system. Fundamentally, no point within the ideal ACCS model can be colder than the radiator without reversing the energy flow direction. Node 1 serves as the interface between the ACCS system and the space environment, where the physical parameters of the ACCS radiator, spectral emissivity, total area, and view factor are defined along with the orbital specifics (altitude, orientation, etc.), and the space thermal environment. From this node, an isothermal surface temperature approximation for the radiator can be derived.

Modeling begins with setting the basic parameters for Boltzmann's equations. The emissivity of the ACCS radiator is variable, considered uniform and temporally constant, but can be defined by the user. For this study, the emissivity was set to 0.9 (black anodized and painted with Z306 black, IR absorptivity matches at 0.39) to match the calibrated values; see the previous chapter. Solar absorptivity is the converse of this at approximately 0.1. A variable efficiency term is included to account for non-ideal, linear variations within the radiator. However, for this analysis, it was not needed and remained set at 1. The rejection temperature of deep, black space is either an idealized 4 K or a more realistic 75-90 K for TVAC shroud LN2 rejection temperatures. The solar flux, earth black body temperature, and albedo factor are all user-set and remain at conventional values of 1420 W/m2, 255 K, and 35%. The total radiative area of the ACCS radiator is fundamental to its performance and was carefully determined. The total surface area was found from CAD modeling, while the various view factors were calculated by importing the CAD directly into Thermal Desktop and performing a high-fidelity mesh. TD's built-in Monte Carlo ray tracing algorithm was used to determine the radiator's self-view factor. This factor was then

used to correct the radiator area for the analytical model. The total effective area of the ACCS radiator was found to be 0.1608 m2. This is slightly larger than a flat double-sided 6U surface.

The radiator can be modeled as a flat plate in orbit [1], which is somewhat of a simplification and does not take into account the view factor or thermal impact from the satellite itself but is sufficient for this level of modeling. The basic equation for solar flux at earth orbit is given below in equation 8.1, where G_S is the solar constant, α_s is the solar absorptivity of the radiator, and ψ is the incident angle. When multiplied by the area of the radiator, 8.1 gives the total absorbed solar power of the radiator. For this calculation, the radiator area is divided by two because the incident solar energy can only impact one side of the radiator at a time.

$$q_S = G_S \cdot \alpha_S \cdot cos(\psi) \tag{8.1}$$

Solar albedo is calculated from AF the variable albedo factor, F_e the view factor of the panel to the earth disk and θ which is the angle between the direct solar rays and the radiator orbital position.

$$q_a = G_S \cdot (AF) \cdot \alpha_S \cdot F_e \cdot cos(\theta) \tag{8.2}$$

The impact of earth IR on the satellite thermal system is significant and, unlike solar and albedo, roughly constant throughout an orbit. Earth IR or planet shine does not depend on eclipse and is given below.

$$q_e = \sigma \cdot T_e^4 \cdot \alpha_{IR} \cdot F_e \tag{8.3}$$

T_e is the blackbody temperature of the earth. Once again, total incident power can be calculated by including the area of the radiator corrected for orientation and view factor. Figure 8.3 below shows how the above equations relate to a flat plate in a standard circular LEO orbit. The view factor of the radiator to the earth disk, Fe, is calculated from a more

complex geometrical analysis given by Belle et al. [1]. This analysis is implemented (VBA Code) as an excel function.

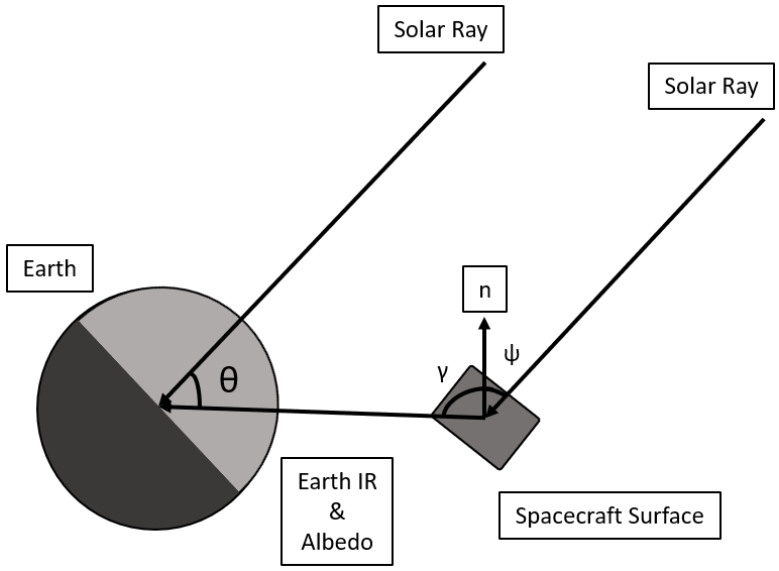

Fig. 8.3: A surface on a spacecraft in orbit is exposed to direct solar, direct Earth IR, and reflected solar (albedo) radiation [1].

An excel "what-if" VBA code was written as a GUI function to explore the impact of individual variables on the system. This analysis helps the design engineer explore each variable's impact on the whole system. What-if analyses were used to model the magnitude of the various space environmental sources and their impact on the system as a function of variation in orientation and orbital angle for the ACCS radiator at a 45 W rejection and a medium flow rate (∼450 mL/min), is given in figure 8.4 Below.

As can be seen, the thermal input of the space environment can vary widely, with solar input reaching nearly 30 W under the right conditions for a radiator the size of the ACCS. This additional thermal load can have a considerable impact on the performance of a thermal control system. Therefore, it is critical to control the overall view factor of the radiator to the space environment. This is why a deployable tracking radiator is an advantage to the ACCS system. Dashed curves in figure 8.4 indicate the relative thermal input of the various environmental loads on the ACCS system, in addition to the set 45 W.

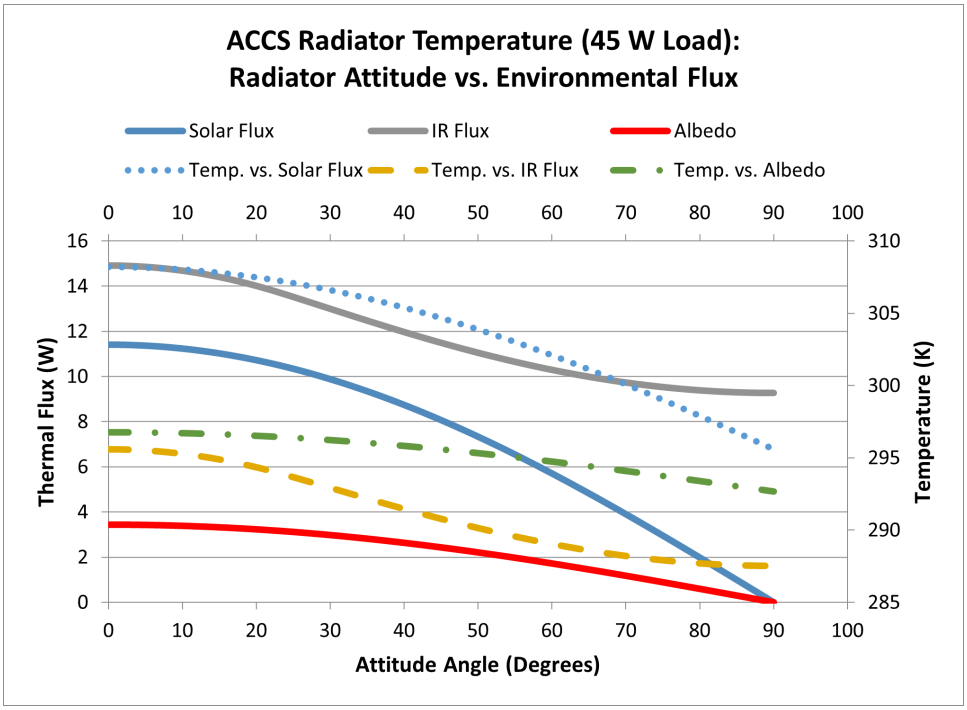

Fig. 8.4: ACCS analytical prediction of the impinging solar flux on a 6U radiator as a function of solar attitude angle.

The size and surface area of the radiator are fundamental to how much power can be rejected at a given temperature. A larger radiator can dump more power at colder temperatures, while the inverse is also true. Figure 8.5 below shows the impact of the area on radiator performance. The solid curves represent standard power loads, while the red dashed lines represent standard radiator sizes. This figure is useful because it answers the fundamental question of how big a single-phase heat transfer system/radiator, like the ACCS, must be to reject a certain amount of power at any given temperature. The ACCS analytical model includes the impact of the space environment, however figure 8.5 represents only the dissipated thermal load of the spacecraft as a function of radiator area.

As the thermal load on the system goes up, the radiator temperature rises as a function of T^4. ACCS temperature control/feedback will set this value to some extent through control of the radiator view factor and the thermal load on the heat exchanger system, but in general, this baseline cold temperature will be dictated by physics. The ACCS can, however, throttle the working fluid flow rate to move the heat exchanger temperature closer

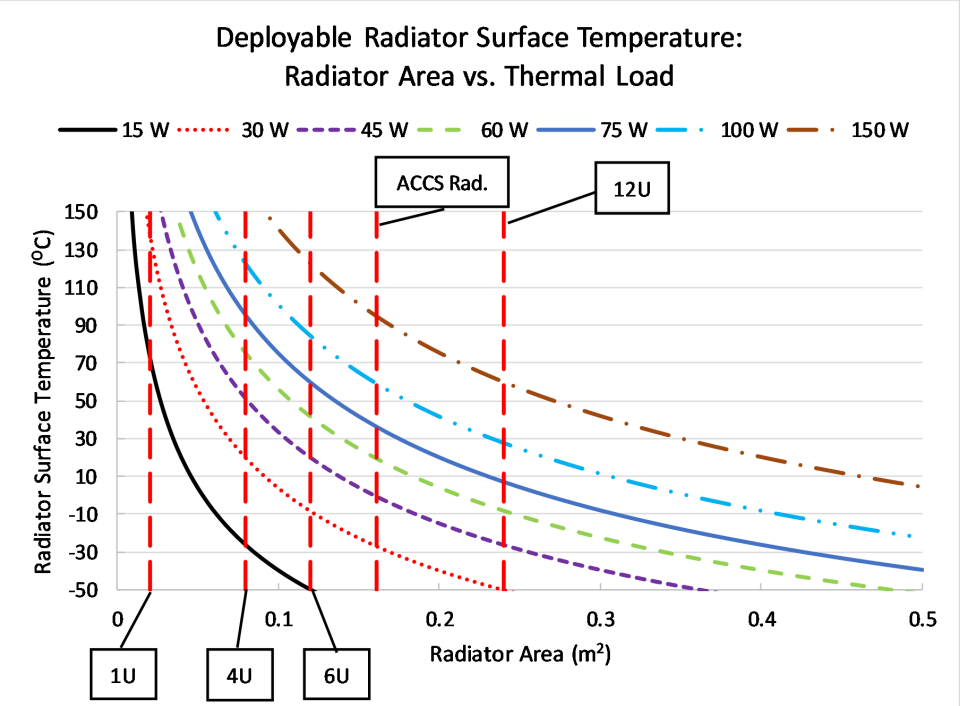

Fig. 8.5: ACCS 6U radiator area vs temperature for assorted thermal loads. Note, the impact of the space environment has been neglected.

or further away from the radiator value. Essentially, the ACCS system can change the gradient between the radiator and the heat exchanger through the working fluid's flow rate (advection/convection link). The radiator temperature will set the starting temperature for the next node within the ACCS model. Based on this fundamental behavior, it is important to hot bias the design and size of the ACCS radiator. By planning for and designing to the worst-case thermal loads, the system can more easily be tuned down in temperature as the thermal profile varies. Figure 8.6 below shows how the ACCS rejection radiator temperature changes as a function of the total power.

8.3.2 Node 2 & 6: Radiator conduction, 2D Shape Factors

Both the heat exchanger and radiator have embedded flow channels. The resistive path between any one embedded flow channel and the surface is inherently more complicated than the simplified 1D conduction analysis and isothermal body behavior assumed throughout the rest of the model. Therefore, 2D conduction shape factors were used. Shape factors are used

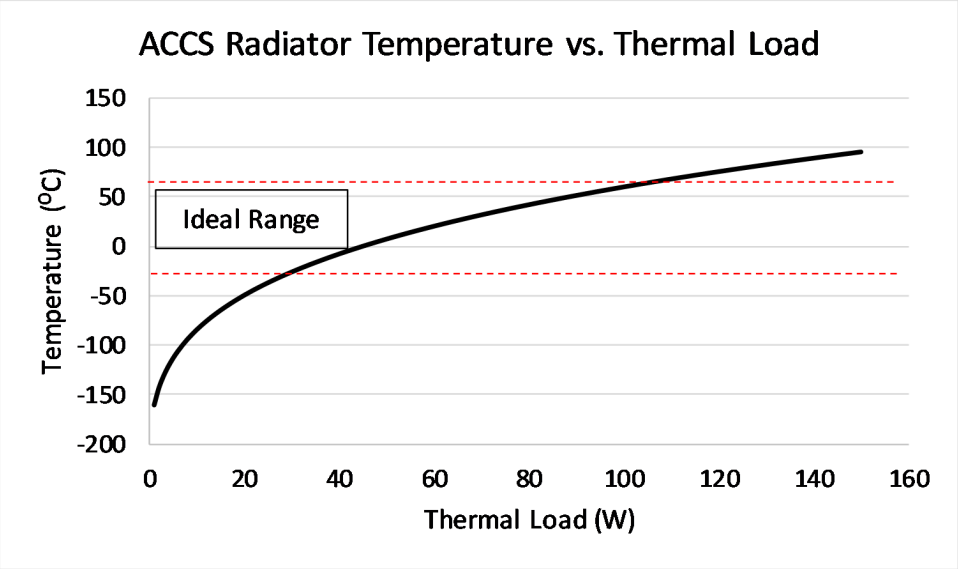

Fig. 8.6: The ACCS radiator (0.1608 m^2) rejection temperature as a function of total thermal power.

to solve analytical heat transfer problems between complex 2D & 3D geometries. A resistive network is drawn between the ACCS-embedded fluid channel and the corresponding surface. The standard 1D Fourier equation is used, where the area and length terms are replaced with an equivalent, derived, shape factor term S. The various shape factor terms, [35], used for the ACCS analysis are given in the Appendix. Figure 8.7 below shows an embedded flow channel with conductive, resistive paths extending beyond the simple 1D analysis. For shape factor analysis, the depth of the tube is considered infinite. The Excel tool allows the user to select which shape factor to use, material conductivity, tube diameter, length, and tube-tube separation.

It should be noted that because both the radiator and heat exchanger are fabricated from AL 6061, and the depth of the fluid channel walls is quite small, on the order of less than 0.1 inches, the temperature gradient through the material is often negligible.

8.3.3 Node 3 & 5: Radiator Convective Heat Transfer

Nodes 3 and 5 focus on the convective heat transfer to and from the heat exchanger and radiator. The physical flow parameters are defined in the general input/output of the excel

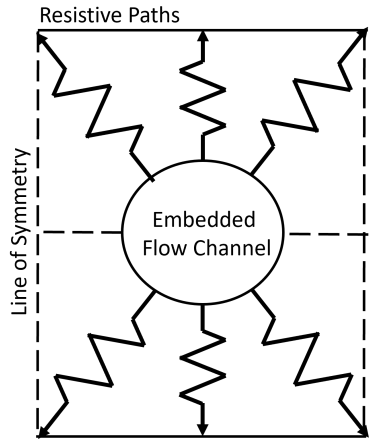

Fig. 8.7: Resistive network for the ACCS embedded flow channels based on standard 2D conductive shape factors.

tool, but are transferred to these nodes. Flow channel length, hydraulic diameter (UAM channels are not entirely circular), and flow rate. The system's mass flow rate and velocity are calculated for each node and can vary depending on the design. The working fluid can be selected from a drop-menu GUI within the individual node worksheet. A separate sheet contains temperature-dependent values for each fluid, including viscosity, density, fluid conductivity, specific heat, and Prandtl number. Working fluid options include Novec 7000, Paratherm CR, Galden, IPA, and water etc. Next, the Reynolds, Prandtl, and Nusselt numbers are calculated along with the friction factor and convection coefficients. The exact formulation for the transport equation is user-specified, but the Gilinsky correlation seems to be the most accurate for this application and is considered the default. The theory chapter of this work details the various equations and correlations used by these nodes. The actual fluid temperature is calculated as either a constant surface temperature or constant surface flux heat transfer within the fluid channels. Either simplification is appropriate. However, in general, the assumption is isothermal for the model. Therefore, a constant surface temperature is a better approximation. It should be noted that these assumptions and simplifications are not physical and do not take into account the thermal gradients throughout the UAM heat exchanger and radiator.

The heat exchanger and radiator are directly (physically) tied by the fluid loop, and

therefore, the outlet of one must be the inlet of the other. Thus, the two nodes must correlate and match initial conditions. To accurately model this boundary condition, the radiator outlet and heat exchanger inlet fluid temperatures are automatically set with an excel "What-If" analysis coded directly into VBA as a function. It relates the total required thermal dissipation of both nodes to their initial temperatures and iterates until a closed solution is found. That minimum temperature forms the connecting link between the two nodes. As a starting point for the heat exchanger, the total dissipated energy can be summed and used to calculate an exit temperature, aka an inlet temperature for the radiator. Without this connecting What-If code, the two nodes could not correlate, the energy would not sum, and the fluid loop would be incomplete. Both of these nodes rely heavily on excel VBA codes and functions. The fluid temperature varies as it progresses along the length of the flow channels and is used to calculate the surface temperature of the UAM channels and the thermal gradients between the fluid and the channel walls. Different temperature profiles are calculated, including the Log-Mean temperature difference and the total number of thermal transfer units (NTU), which helps to determine the effectiveness/efficiency of the ACCS convective system. Finally, the equivalent flow resistivity is calculated for both nodes, which can be used to compare the ACCS system to more traditional conductive heat transfer methods. An interesting feature of the flow within the UAM heat exchanger is that the Reynolds numbers are not the same as in the radiator. The physical parameters of each do not have to be the same and often would not be in a real physical system. However, the differences in the current ACCS system arise from the pump's localized turbulence. The TCS M510 is a centrifugal pump with 11 mm impeller blades. This results in a 22 mm total impeller diameter. As the pump rotates, the localized fluid within ten working diameters is more turbulent. This exit length turbulence increases the localized Reynolds number and is determined by the specific pump impeller Reynolds number. The pump impeller Reynolds number is given below,

$$R_{ei} = \frac{N_i \cdot D_i^2 \cdot \rho}{\mu} \tag{8.4}$$

$$N_i = \frac{RPM \cdot 2 \cdot \pi}{60} \tag{8.5}$$

Where, N_i is the impeller tip speed and D_i is the total impeller diameter, approximately 22 mm for the TCS M510. However, because each of the individual vanes are roughly 7 mm long, an equivalent diameter of 14 mm was used. See figure 8.8 below for the M510 impeller design. x_L is the total heat exchanger UAM fluid channel length.

$$Re_{eq} = \frac{(10 \cdot D_h) \cdot Re_i \cdot Re \cdot (x_L - 10 \cdot D_h)}{x_L} \tag{8.6}$$

The heat exchanger Reynolds number is essentially a weighted average of the impeller Reynolds coupled with the regular UAM flow channel Reynolds, weighted by the total heat exchanger flow path length and the turbulent exit region of the pump. This difference between the heat exchanger and radiator Reynolds numbers means that the convective heat transfer is not the same, nor are the thermal gradients within each node symmetric. This results in the working average temperatures of the fluid and heat exchanger varying quite a bit and sometimes unexpectedly with respect to flow rate, temperature, and total system power.

The ACCS system is somewhat oversized in terms of flow channel diameter and pump power. This means that to enter a truly laminar flow regime, the flow rate must be only, on average, below ~200 mL/min. The transition from laminar to turbulent flow was not tested thoroughly enough due to the low-end sensitivity of the custom Venturi flow meter. The ACCS model, however, is more than capable of exploring the various flow transition regimes and can be used for future designs to optimize the physical flow parameters as well as the pump power and flow rate to create ideal thermal gradients. The following graphs represent the modeling and predictive capability of the ACCS analytical model. By using custom "What-If" functions, the various flow parameters can be explored. Figure 8.9 below shows the ACCS system heat exchanger temperature vs. thermal power and flow rate, with given design parameters. The HX temperature for both the 100 and 400 mL/min flow

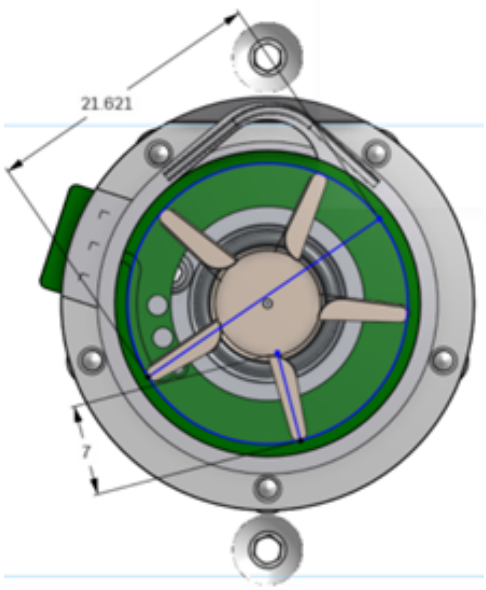

Fig. 8.8: TCS M510 impeller size & design.

rates drop in temperature after approximately 30 W. This is because the fluid temperature increases enough to lower the working viscosity to such an extent the fluid begins to tumble and becomes turbulent. This transition can be seen in Figure 8.10. For ∼400 mL/min of flow, when the HX and fluid temperatures drop and the thermal power approaches 30 W. The radiator temperature does not vary like this but instead continues to rise as $T^{1/4}$. The 800 mL/min flow rate does not follow this trend because the fluid velocity is sufficient to maintain turbulence at even low fluid temperatures. This temperature dependence on the Reynolds number is an interesting aspect of the ACCS system. It adds another design variable to the system, which must be accounted for.

The heat exchanger temperature with respect to flow rate and power is a critical aspect of the ACCS system and forms the heart of the PID feedback and control algorithm. From figure 8.11 below, the flow rate dictates at what heat exchanger temperature a given thermal load will achieve. For instance, the model predicts that if the flow rate is scaled between ∼150 mL/min and 450 mL/min the temperature variations for 30 to 60 W can be on the order of more than 50 °C. The 30 W curve shows a double-step function. This is because both the heat exchanger and the radiator transition to turbulence, but not at the same flow

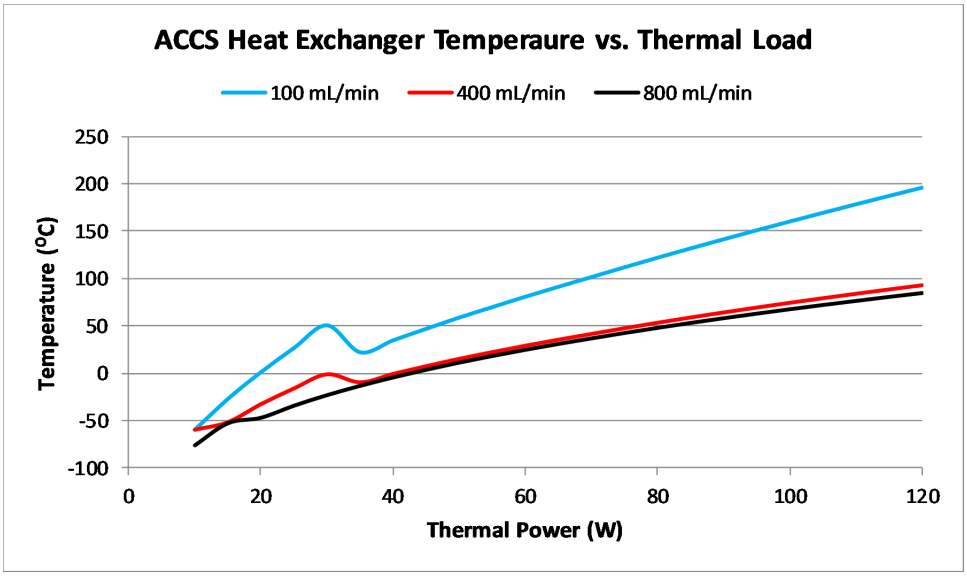

Fig. 8.9: ACCS average heat exchanger temperature as a function of flow rate and power.

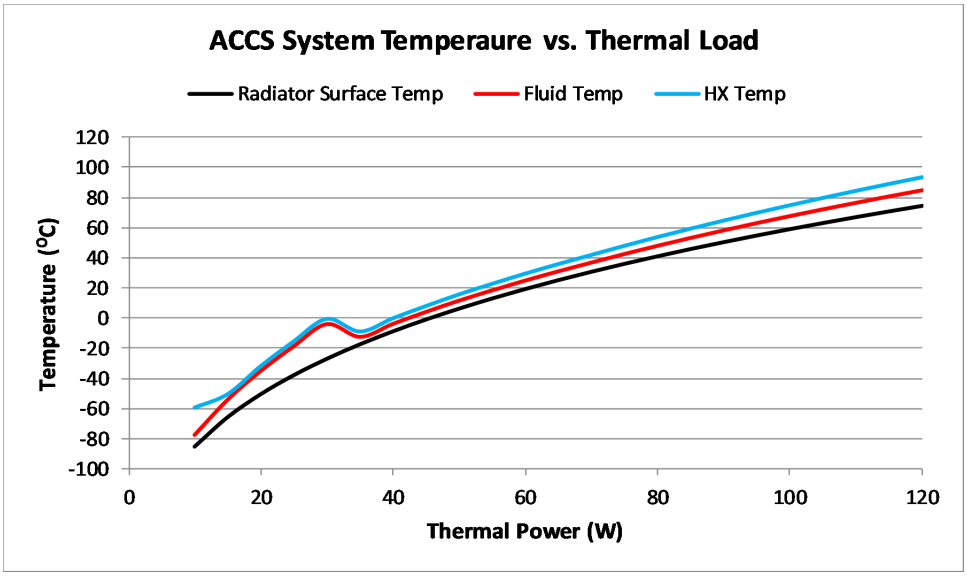

Fig. 8.10: ACCS system temperatures as a function of thermal power. Flow rate = 400 mL/min.

rate.

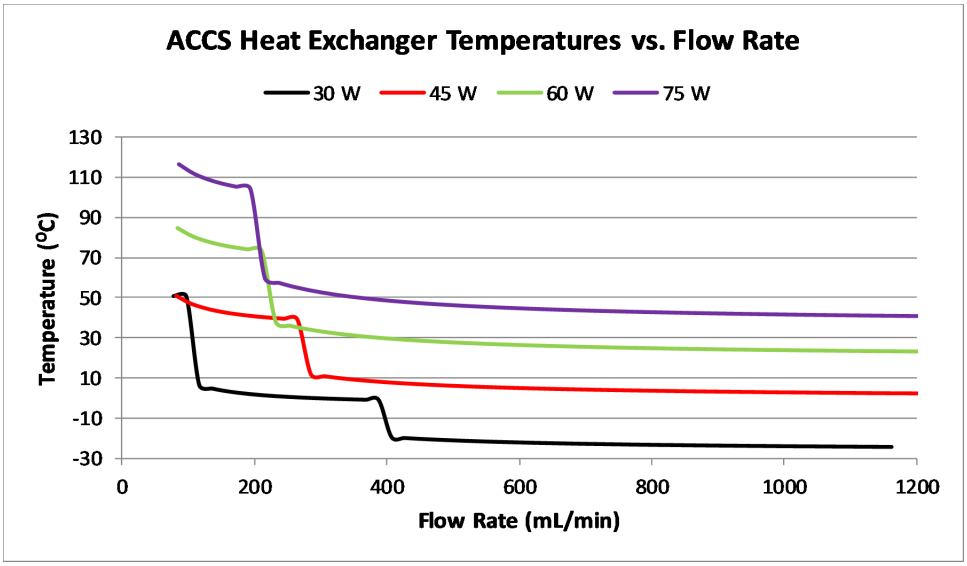

Fig. 8.11: Predicted temperature of the ACCS heat exchanger as a function of flow rate. Notice the curvature and transitional steps from laminar to turbulent flow regimes.

The thermal gradients between the ACCS heat exchanger and radiator are shown below in figure 8.12. As can be seen, the transitional flow regimes for most of the powers occur around ∼200 mL/min for the given ACCS system and physical parameters of the test Cube. The higher power curves transition sooner than the low power due to the temperature dependency of the fluid viscosity. The thermal gradients begin to flatten out after ∼500 mL/min. This indicates that flow rates above this are not contributing to the total system thermal gradients and are essentially a waste of pump power. The M510 micro-pump begins to stall below ∼100 mL/min for the given flow channels. Therefore, it can be assumed that the ideal range of the pump is between ∼100 and ∼500 mL/min.

The question of ideal physical flow parameters is important to design. Therefore, the effect of flow channel diameter is explored in figure 8.13. The ACCS flow channels use UAM fabrication techniques that result in a non-circular flow conduit diameter. Therefore, the hydraulic diameter is used to approximate. As the hydraulic diameter increases, two parameters work counter to each other to affect the Reynolds number and flow regime for

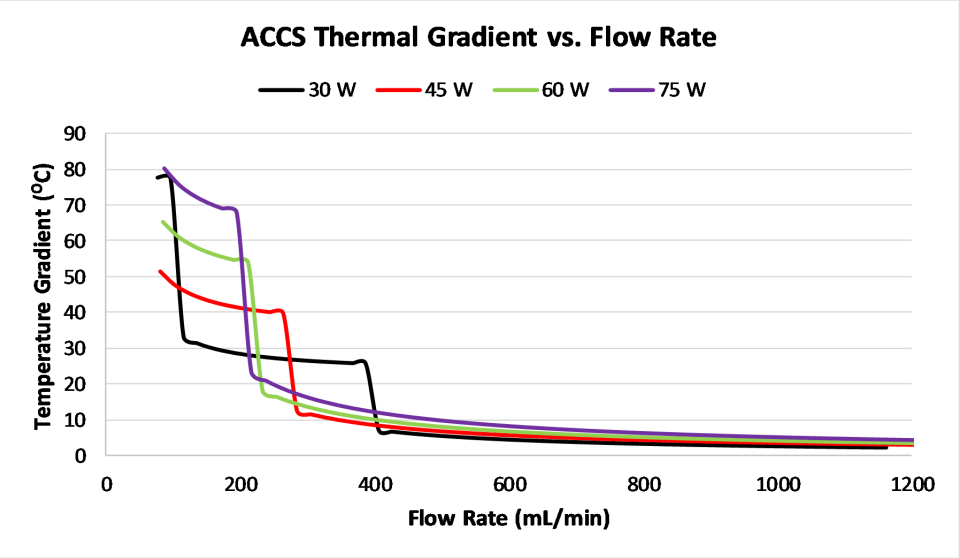

Fig. 8.12: Predicted gradients of the ACCS system as a function of flow rate. Notice the curvature and transitional steps from laminar to turbulent flow regimes.

the heat exchanger and radiator. As the flow diameter increases, the Reynolds number does too. The fluid has more room to begin tumbling, and turbulence can increase. However, the relative fluid velocity decreases if the flow rate is held constant. This lowers the Reynolds number faster than the diameter increases it. Therefore, an increase in the diameter for the radiator will cause an overall decrease in the Reynolds number. This is not the case for the heat exchanger; however, because the micro-pump creates an equivalent Reynolds number for the HX and the turbulence caused by the pump extends to 10 working diameters (current model approximate), the overall Reynolds number is amplified by the change increase in working diameter. This can be seen in figure 8.13 below. For the 30 W, ∼100 mL/min black curve, both the HX and radiator are laminar until the hydraulic diameter increases above 0.2 inches. At this point, the HX Reynolds crosses the threshold into the transitional/turbulent regime. The corresponding HX temperature drops because now the convective transfer between the HX and the fluid is much more efficient. Conversely, the HX is fully turbulent for the 45 W ∼400 mL/min red curve due to flow rate and overall fluid temperature. As the hydraulic diameter increases, the radiator flow velocity decreases. This results in the radiator subsiding to laminar flow. The heat transfer from the fluid to the radiator drops, the

resistivity increases, and the efficiency drops. Therefore, the overall system temperatures rise. The sharp nature of these changes is not entirely physical and is simply an artifact of the modeling transition cutoffs used in the model. The actual temperature changes would be much more gradual. In fact, this whole phenomenon should be explored with dedicated numerical flow modeling and further experimental testing.

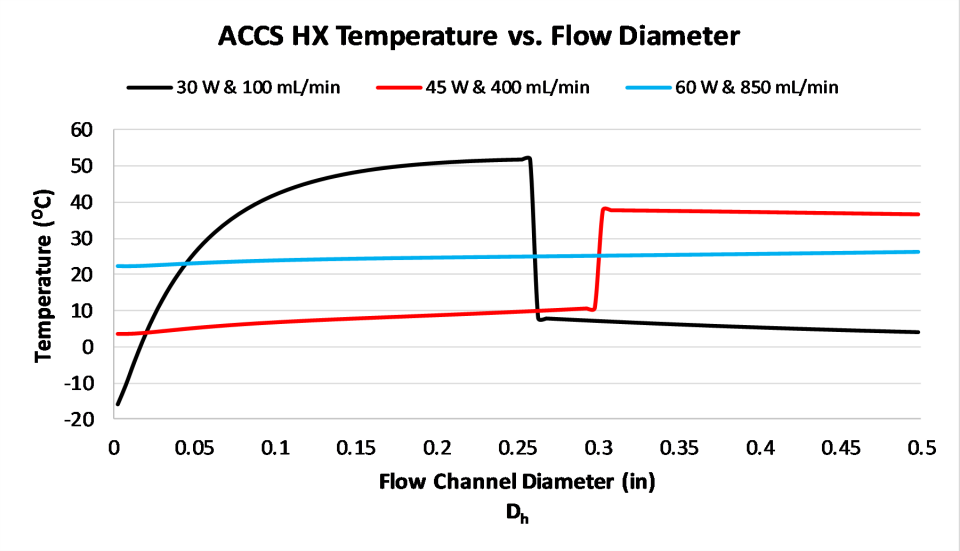

Fig. 8.13: Effect of UAM flow channel hydraulic diameter on heat exchanger rejection temperature.

The question of flow path length is entirely dependent on what assumptions are made during modeling. For a constant surface temperature model, the overall temperatures of either the HX or radiator are reduced as the flow path is lengthened. This trend exists because the relative difference in temperature between the surface of the channel and the working fluid, for a given thermal power load, can be lower for longer tubing. Basically, the thermal flux of the system is distributed over a larger area. For the ACCS system, the overall tube lengths for the HX and radiator are design parameters that also need to take into account the pump pressure drop, the head losses of the system, and the lateral distance between channels. This last design parameter effects the isothermal average temperature of the body, and the desired gradients between the heat exchanger, working fluid, and radiator.

From figure 8.14, for ~400 mL/min and 50 W of thermal load, the overall temperatures do not change much for flow path lengths greater than 100 cm. Therefore, it could be argued that anything beyond this value is not required for the given flow parameters.

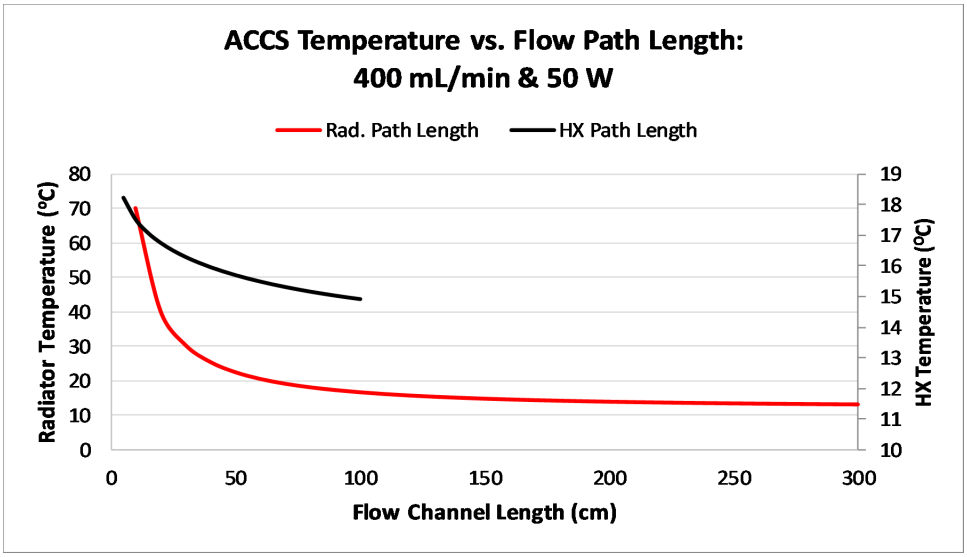

Fig. 8.14: Predicted "average" temperature of the ACCS radiator as a function of flow channel length.

The convection coefficient is essentially a measure of the MPFL thermal conductivity. It determines how much power can be transferred to the working fluid over a specific temperature gradient and working area. For the ACCS system, this is shown along with HX/radiator Reynolds numbers as a function of flow rate and system thermal load. From figure 8.15, it can be seen that once again, for the current system, a flow rate over ~500 mL/min increases the convection coefficient linearly. However, it is already well above the required value to transfer the given thermal load of 50 W. Therefore, it is once again a waste of pump power to exceed this flow rate. Figure 8.16 indicates that for the given flow rate of 400 mL/min the system parameters become constant after 60 W. This is due to the extrapolation features and range of the fluid properties within the ACCS model.

The Log-Mean temperature difference directly indicates how much heat is transferred (relative) within a heat exchanger. It is a logarithmic ratio of the hot and cold extremes

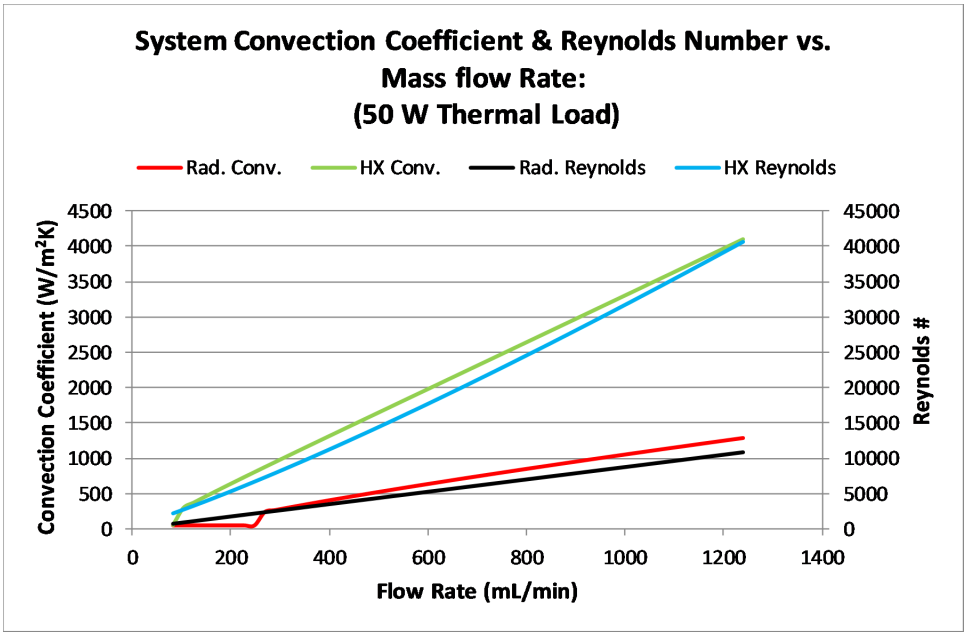

Fig. 8.15: Predicted behavior of the relative convection coefficient & Reynolds numbers for the ACCS system as a functino of flow rate for the heat exchanger & radiator.

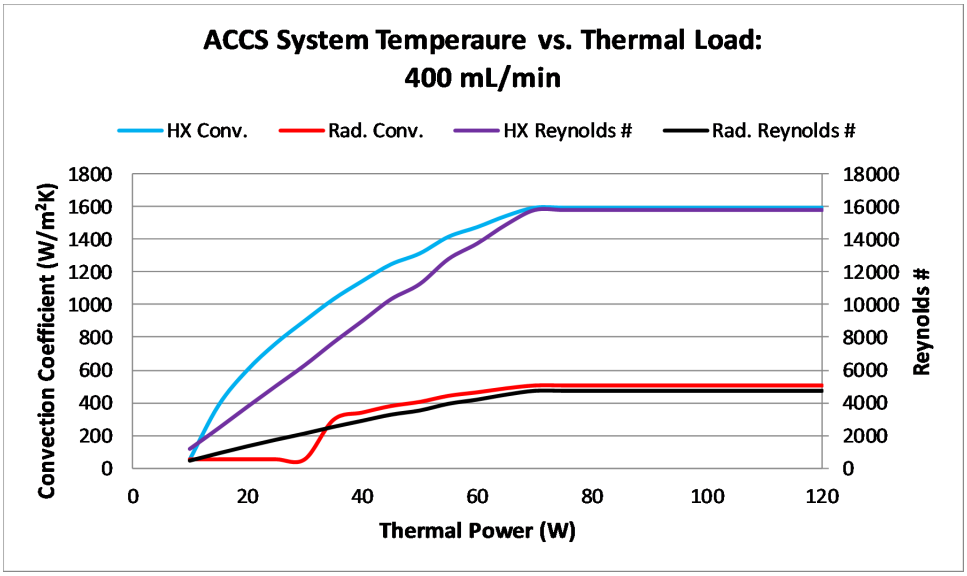

Fig. 8.16: Predicted behavior of the relative convection coefficient & Reynolds numbers for the ACCS system as a functino of thermal power load for the heat exchanger & radiator.

within both the heat exchanger and radiator. Larger LMTD values correspond to larger heat transfers. The node resistivity is also given in figure 8.17, which indicates the resistive difficulty of the thermal transfer within each node. For the ACCS system, the LMTD follows similar patterns to the previous parameters. At 50 W the heat exchanger is entirely turbulent due to the influence of the pump, while the radiator transitions after ∼200 mL/min. The resistivity and LMTD flatline after ∼500 mL/min, once again indicating that this should be the upper limit of flow rate for the given system.

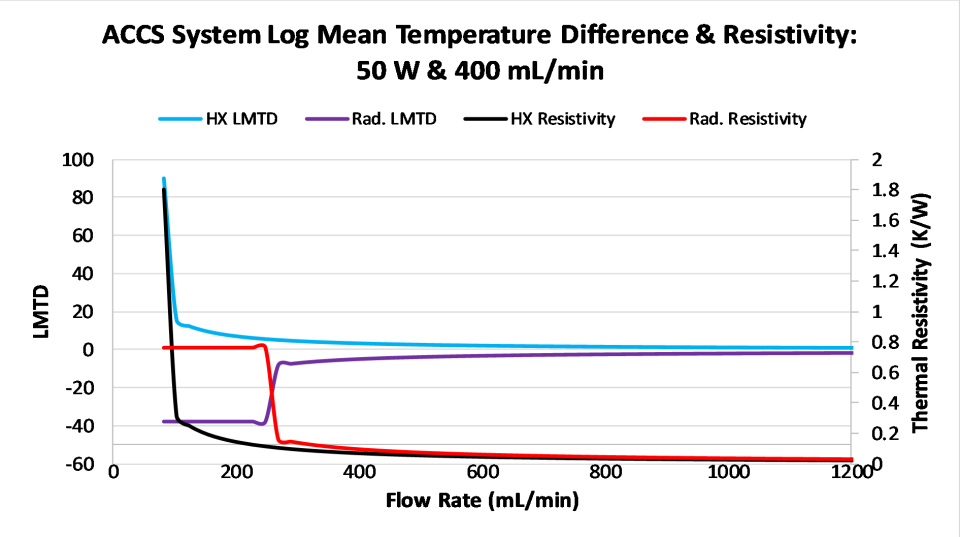

Fig. 8.17: ACCS LMTD & resistivity for the heat exchanger and radiator nodes.

The Number of thermal Transfer Units (NTU) is a dimensionless ratio of the overall convective heat transfer to thermal momentum transfer for a heat exchanger system. It is a measure of flow area, heat capacity, and fluid flow rate. This single NTU function becomes a monotone value to compare the overall effectiveness of a heat exchanger system. Physical and flow-specific parameters can be compared with the NTU method. The NTU method is also an indication of how effectively the fluid is transferring heat. The NTU equation is given by:

$$NTU = \frac{h_{avg} \cdot A}{\dot{\vec{m}} \cdot C_p} \tag{8.7}$$

Where h_{avg} is the average convection coefficient, A is the total fluid-to-surface contact area, $\dot{\vec{m}}$ is the fluid mass flow rate, and C_p is the specific heat of the working fluid. The maximum thermal power a given fluid can transfer is given by equation 8.8, which forms the base of the NTU equation.

$$q_{max} = \dot{\vec{m}} \cdot C_p \cdot (T_{hot} - T_{cold}) \tag{8.8}$$

This equation indicates that any value greater than 1 is not-physical in the sense that the convective heat transfer is capable of transferring more energy to the fluid than the fluid can actually carry. Essentially, a thermal designer would want a heat exchanger to operate with a high NTU of less than one. Figure 8.18 & 8.19 below show the NTU function for the ACCS system at 50 W and ~400 mL/min. As can be seen, the heat exchanger NTU is greater than one, which simply indicates that the turbulence caused by the pump increases the convective heat transfer of the heat exchanger to a point beyond which the working fluid can accommodate. A similar phenomenon is shown in figure 8.19. As the thermal power increases, the fluid viscosity decreases, and the convection coefficient increases. This results in a NTU ratio greater than one.

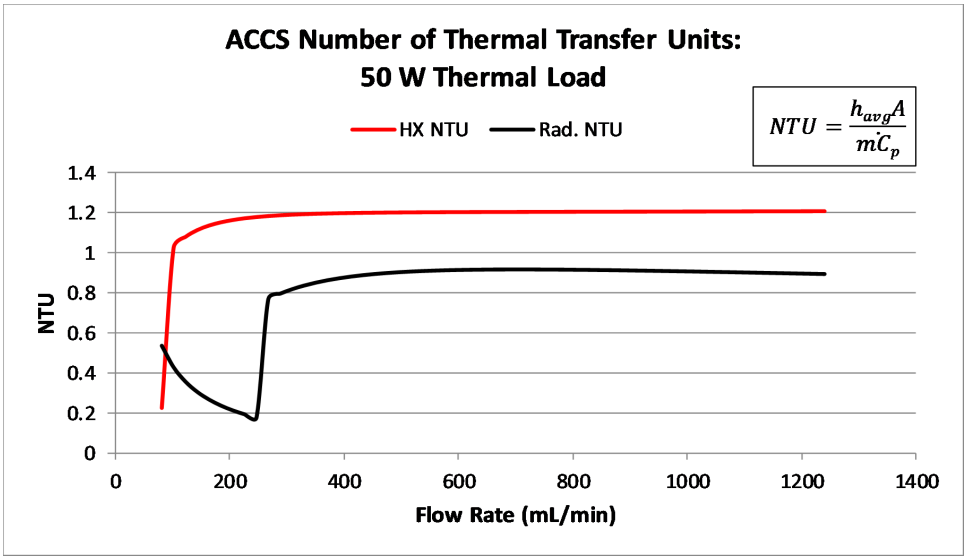

Fig. 8.18: ACCS NTU effectiveness ratio as a function of flow rate.

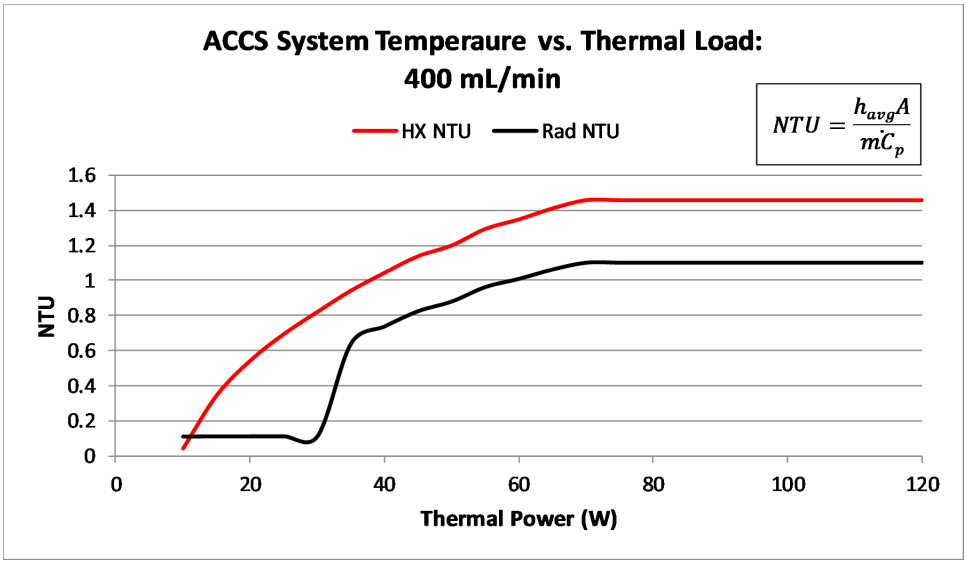

Fig. 8.19: NTU effectiveness ratio as a function of system thermal power.

8.3.4 Node 4: Optional Flow Diversion Valve

An early design concept for the ACCS technology included a diverter valve. A three-way valve that could funnel the majority of the working fluid back into the heat exchanger and by-pass the radiator entirely. This would be desirable in the extreme case of a low-power shutdown of the whole satellite. If the power on the ACCS system fell below a certain value, the radiator would continue to cool down and the working fluid could become very cold. Novec 7000 is a low-temperature heat transfer fluid and has a pour point of nearly -122 °C. It is unlikely that real-world temperatures would ever get that cold. However, if the working fluid fell too far below -20 °C. The pump could begin to fail. Soft O-ring seals would fail between -30 °C and -60 °C, and eventually, the cryocooler would fail at ∼-55 °C. Basically, a diverter valve included within the ACCS system could fold the majority of the working fluid back into the heat exchanger and allow the internal heat of the satellite to keep the working fluid warm. The pump could operate in a reduced state, and the cold radiator fluid and internal heat exchanger fluid could mix slowly to keep temperatures at a minimum value.

However, it was decided early on that an appropriate miniature COTS valve was not

available and would significantly increase the complexity of the ACCS system. Therefore, it was left out, and the analytical model code, which would have taken this flow characteristic into account, was set to a null value. The concept of a diverter valve is still a good one, and the reasons for it are valid. Therefore, future designs should consider its inclusion if an appropriate valve could be found.

8.3.5 Node 7: Basic Conduction with Cryocooler and Micro-Pump

A final step for the analytical model is to attempt to calculate the temperature distribution through the Micro-pump and cryocooler. Similar to the numerical model (Chapter 9) the analytical model simply assumes conduction through a solid stainless steel body. This is not a terribly accurate assumption, but the heat exchanger rejection temperature is the most important for the model. Based on that rejection (accommodation) temperature, Ross-like diagrams can be used to estimate the temperature and performance of the cryocooler. The micro-pump body temperature is very similar to that of the working fluid due to immersion.

8.3.6 Pressure Drop Analysis

The pressure drop within a pumped fluid loop can be estimated in a number of ways. The first method utilized by the ACCS is a traditional head loss analysis. Known as the k-method, the physical mechanics of the MPFL are broken down into two major categories, major and minor losses. Major losses are those caused by friction between the moving fluid and the flow channel walls. Minor losses are categorized as any disturbance in the flow that results in a pressure drop, including fittings, valves, expansions/contractions, and any number of other flow parameters. The ACCS model uses the head loss to create a rapid analysis tool for estimating the pressure drop within the TVAC characterization test cube. These excel tools and others are available online in various ACCS data repositories. The head-loss method is fast, easy to implement, and relatively accurate. However, a more detailed and accurate model is desirable for the analysis of the ACCS system. A pressure drop model based on the 2k method, which takes into account the effects of Reynolds number

on minor losses, was implemented in Matlab. This 2k method was initially developed with support from the JPL thermal analysis team. Figure 8.20 below shows the measured pressure drop across the M510 pump as a function of the corrected flow rate. The modeled pressure drop from the 2k analysis is superimposed. As can be seen, the model accurately predicts the pressure drop of the ACCS test cube.

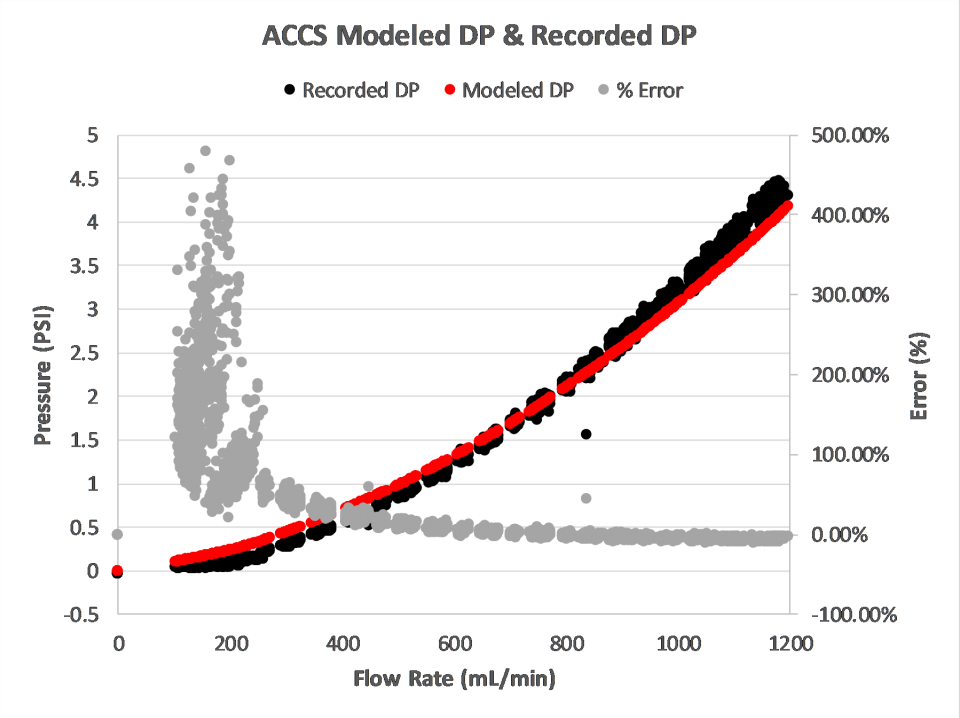

Fig. 8.20: Comparison of the 2k predicted pressure drop of the ACCS system vs. the experimentally measured values.

The 2k method shown above has an overall accuracy of better than 22.6% and an accuracy of 7.5% from ~250 mL/min to 1200 mL/min. At lower flow rates, the custom-built Venturi meter used in the ACCS test cube loses accuracy. Therefore, below ~250 mL/min, the overall model error increases to ~124.1%. Based on this analysis, the 2k method is more than accurate enough for the ACCS technology.

8.4 Comparison with Experimental Data

The ACCS analytical model was validated by direct comparison with experimental,

steady-state data collected during the ACCS TVAC characterization. Data from January and September are included in this analysis. Figure 8.21 shows the analytical model data overlaid with the experimental. System power is equal to total radiated power. Error bars on the measured temperature are included, however, they are not readily visible due to the relatively high accuracy of the calibrated thermocouples. Temperature is averaged across all relevant heat exchanger TC's. Two different curves are shown below, both turbulent but differing in flow rate significantly. The temperature varies to one-fourth as expected from Boltzmann's equations. Overall, model accuracy is high. Better than 0.5% on all data points. Point-by-point model error is given in figure 8.22. From this comparison, it can be concluded that the ACCS analytical model is more than capable of accurately predicting the behavior of the ACCS system. A model like this is an ideal rapid iteration design tool for the spacecraft thermal systems engineer. Each of the data points shown below is broken down by flow rate in the appendix.

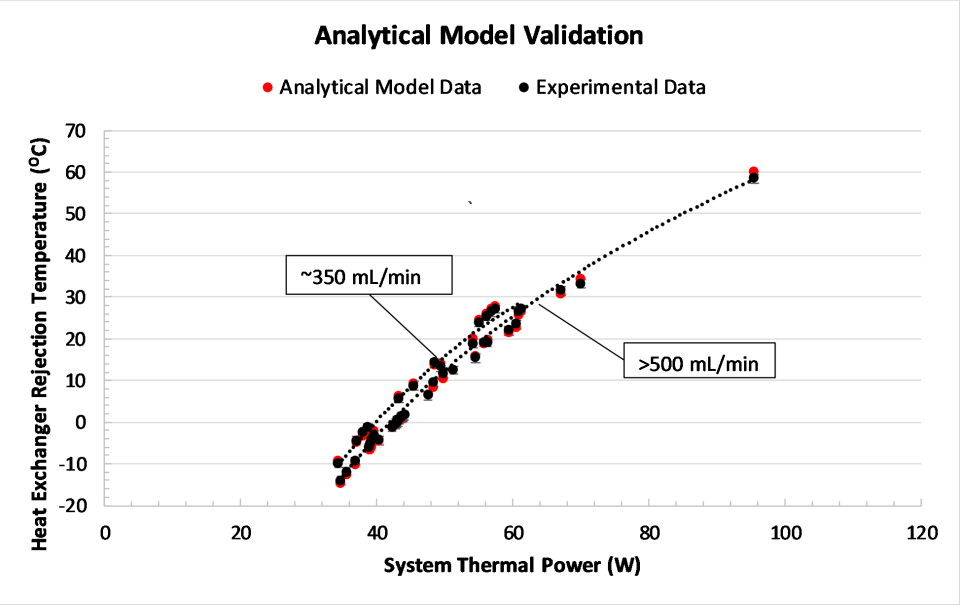

Fig. 8.21: Direct comparison of temperature vs. thermal power for the ACCS analytical model and experimentally derived data.

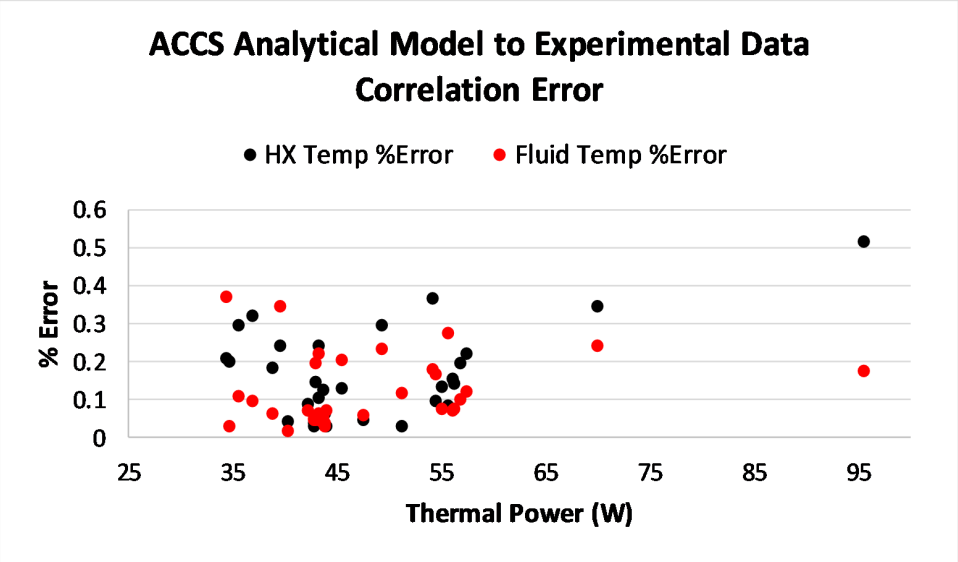

Fig. 8.22: ACCS analytical model accuracy vs. measured data as a function of thermal power.

8.5 Cold Tip Parasitic Load Approximation

The thermal load of the detector is one of the factors directly responsible for the overall cold tip temperature. The Ricor K508N is capable of rejecting 1 W of thermal power. However, ideal cold tip thermal loads should be kept below ~250 mW. The majority of this power will stem from the detector and focal plane assemblies. Therefore, a great deal of care must be taken to limit the overall thermal parasitic's on the cold tip. The following diagram, figure 8.23, shows the ACCS CONOP for isolating the IR instrument detector through progressive cold shields. Resistive networks, radiation and conduction are shown between layers. For the cold tip parasitic model, the spacecraft structure is considered to be at approximately 300 K, while the ACCS isolation frame is held at roughly 250 K (-20 °C). A cold stop instrument shield separately cooled to less than 180 K will form another barrier for thermal leaks. Finally, the cooled FPA is exposed to the environment through radiation and mounting conduction from the cold shield and the estimated internal generation of the detector. The overall load on the cold tip is approximately ~150 mW, which is overall lower than the required ~250 mW. The various thermal loads shown in figure 8.23 are approximated and were derived from the ACCS excel thermal parasitic heat transfer tool.

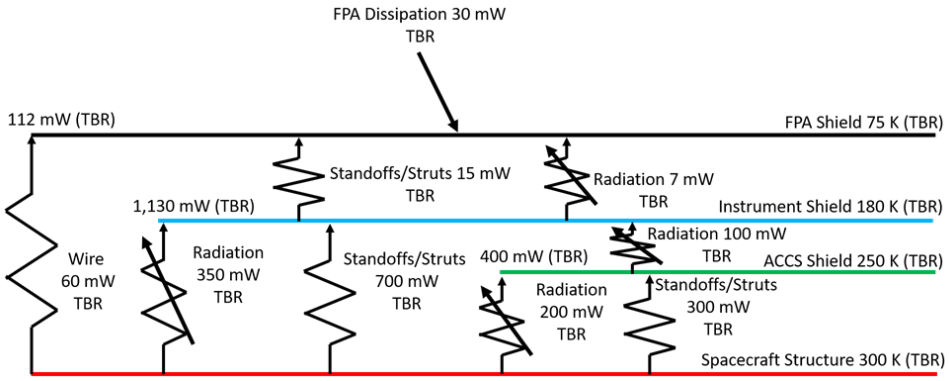

Fig. 8.23: Block flow diagram of the ACCS cold tip parasitic model. The assumed resistive network and approximate temperatures and thermal parasitics are shown.

8.6 Conclusions

The ACCS analytical model is an ideal rapid iteration design tool for the early-stage development of active thermal control technologies like the ACCS system. It is a powerful tool and resource when coupled with systems engineering design methodologies. This model also demonstrates that when thermal and temperature design is treated as a priority in satellite development and taken into account early in the design process satellite, thermal control can significantly help operations and overall mission success. This analytical model is highly accurate and has been extensively validated by comparison to experimentally determined performance data. The ACCS model is more than capable of predicting the performance and behavior of the ACCS system. In addition, it can be used as a design tool to see how each of the control variables and mechanical design aspects of the ACCS impact the integrated system. This information allows idealized design criteria to be determined early and prioritized in phase-A design. The ACCS analytical model is an invaluable resource for systems engineering and pre phase-A and phase-A development of spacecraft single-phase MPFL active thermal control systems.

8.7 Future Analytical Modeling Work

The next iteration of the ACCS analytical model will feature a more detailed 2D conduction analysis for the heat exchanger and radiator panels. Transient solutions will also be

included along with a basic geometrical radiator to spacecraft view factor analysis. Orbital space thermal environment analysis will include transient behavior and time variable environment power input. More detailed flow characterization will also be included. Featuring in-depth thermal and momentum boundary layer and flow regime prediction. A full characterization of the pump will be used to create discretized pump curves and equations to fully predict the TCS micro-pumps' flow, pressure, and power. This data can be incorporated directly into the analytical model and improve the modeling of the pump. The 2k pressure drop model will be integrated with the thermal model. This will improve the accuracy and reporting of both models. The ACCS analytical model can be incorporated with STK and thermal desktop to form even better on-orbit predictions. Conduction gradients between radiator UAM tubing will be analyzed to find the ideal hydraulic diameter, length, and flow channel spacing for each design.

Future versions of the ACCS model will be developed and used by Systems engineers to accurately and quickly predict the performance of active thermal control systems like the ACCS. These models will be offered as preliminary design tools during the early stages of mission formulation and design. When coupled with Systems engineering design methodologies and the concept of tackling spacecraft thermal control in a parallel fashion to the payload, bus, and mission development, the difficult space environment can be used as a tool for mission success.

CHAPTER 9

Thermal Desktop: ACCS Numerical Simulation

Simulations aren't as good as the real thing, but they're a close second

---

9.1 Introduction

Modeling and simulation are critical aspects of engineering design. They allow for detailed performance and behavior predictions, especially in diverse conditions. A well-validated model enables the engineer to develop confidence and a deeper understanding of design without the often-prohibitive expanse of real-world prototypes and testing. Thermal Desktop (TD by CRTech) is an end-to-end PC thermal modeling tool that combines CAD design with integrated finite-difference, finite-element, and lumped-capacitance objects that can be combined with thermal-specific parameters such as contactors, conductors, insulation, and heat loads. Thermal Desktop works seamlessly with RadCAD, a radiation simulation software that utilizes Monte-Carlo ray tracing to calculate form and view factors, radiative conductors, and environmental heating rates. CRTech also offers fluid flow analysis through FloCAD and many others [47]. The ACCS thermal desktop model was developed by USU students with the help and guidance of the Jet Propulsions Laboratory.

Thermal Desktop is useful for the ACCS system because it allows a more detailed finite element numerical model of the system to be created. This is especially important because it provides a deeper, high-fidelity insight into the structure's thermal gradients, especially across the heat exchanger and radiator. It also helps to pinpoint aspects of thermal interest within the system, such as resistive points and hot/cold points. Thermal Desktop is also ideal for in-depth analysis, complex radiation-to-conduction interactions, and orbital/environmental modeling. Without TD our understanding of the ACCS would

be limited to the existing prototypes and environmental characterization tests. However, it should be noted that TD models are complex and time-consuming to create. They also require a not-insignificant run time. Therefore, they are not appropriate for rapid design iterations like the analytical modeling tool developed by this research. They are, however, ideal for in-depth modeling and post-design analysis of the ACCS system.

TD was used to model the entirety of the ACCS system. Including the pumped fluid loop, internal conduction, and radiative exchanges. Once fully built and validated, the ACCS TD model was used to run a select few steady-state cases. Then directly compared to existing TVAC data. The results of this comparison are given in this chapter. The existing TD model could also have been used to predict the transient response of the ACCS system. These numerical results are essential to this research because they validate the existing analytical rapid design tool, complement the existing TVAC characterization data and provide a deeper understanding of the ACCS system as an integrated whole. In addition, by developing a numerical model of the current ACCS system, future designs can easily modify and adapt TD to benefit their own analysis. Figure 9.1 below shows an overview of the ACCS TD model in wire frame. The heat exchanger is floating above the enclosed radiator, wrapped in MLI and LN2 shrouds. The Ricor K508N cryocooler and TCS M510 micro-pump are mounted on top of the heat exchanger. Red arrows indicate thermal loads into the system.

9.2 Simulation Objectives & Testing Plan

The original objective of the ACCS project was to develop a series of systems engineering design methodologies and tools to aid in the development of active thermal control systems. A detailed numerical finite element model is a critical tool in this process. The stated objectives of the TD model are:

- Compliment and expand the existing analytical design tool and TVAC characterization data
- Provide a deeper, high-fidelity transient analysis of the ACCS system

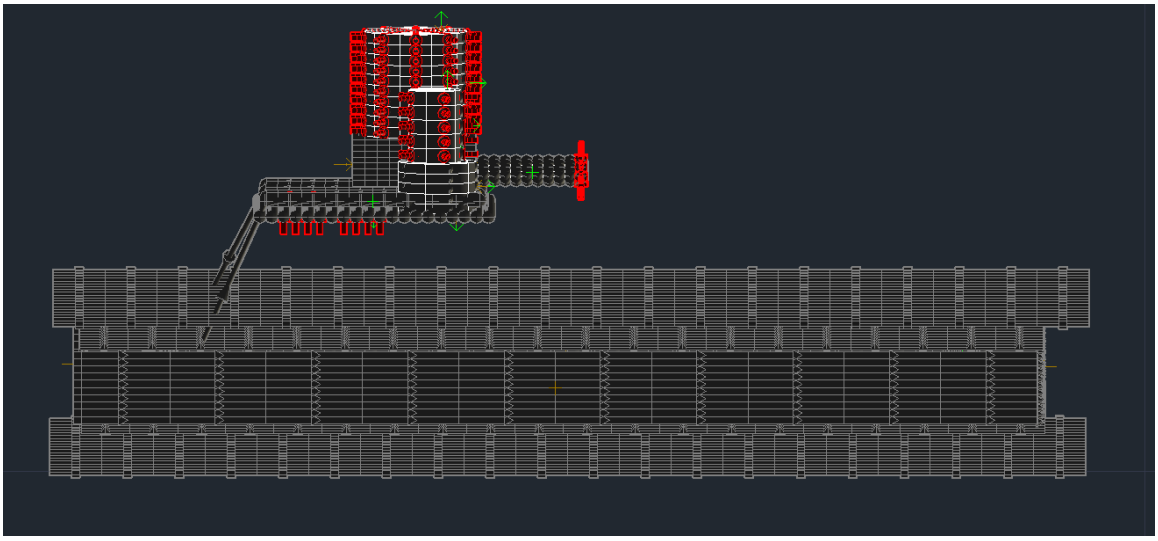

Fig. 9.1: Numerical Thermal Desktop model of the ACCS system.

  - Pre-Phase A & Phase A tool
  - Detail thermal gradients and points of interest within the system
  - Detail the flow of thermal energy within the system
  - Characterize the radiative performance/design of the ACCS system
  - Provide complex radiation view factor analysis
  - Provide orbital simulation of the ACCS system in a complex radiation environment

- Provide system validation and expand the ACCS analysis to more diverse conditions and environments than are possible with TVAC characterization
- Create a numerical model that can be adapted and used as an advanced predictive tool for the ACCS system and others like it

The ACCS TD model was developed in stages as simple 2D and 3D geometric nodal shapes connected by one-dimensional heat flow conductors and basic radiation view factors. Due to the difficulty in setting up each simulation case and the required run times, only 11 cases were selected for direct comparison to the experimental data. These 11 data cases and

their analysis is discussed in this chapter, with a single representative case used to demonstrate the colormap temperature distribution modeling of Thermal Desktop. Additional data and colormaps are given in the Appendix.

9.3 ACCS Model Design

The ACCS TD model consists of four primary sub-models: The heat exchanger assembly, radiator plate, flow advection simulators, and shrouds/MLI. The HX assembly includes the cryocooler, pump, cold tip, and guard heaters connected to the radiator by flow conductors. The radiator plate is free-floating, modeled as ideally isolated from the rest of the system. LN2 shrouds completely enclose the radiator top, bottom, and sides, serving as a cold stop boundary condition for the RadCAD heat transfer model. MLI insulation on the top and bottom of the LN2 separates the radiator and heat exchanger assemblies from radiation transfer. A final outer shield of MLI encloses the entire model in a shielded box, not shown in the model below. This outer MLI encloses the entire model and forms a radiative boundary for the system. The heat exchanger and radiator are tied by one-way conductors simulating the convective heat transfer of the pumped fluid loop.

The ACCS TD model is shown in figure 9.2 below. The heat exchanger is floating above the radiator. Block models of the cryocooler and pump are contact mounted to the heat exchanger, while tubing mimics the embedded flow channels of the UAM HX. The heat exchanger and the radiator are both formed from TD surface objects. Essentially, 2D shapes with zero thickness. Material properties and equivalent conductive thickness/capacitive mass are assigned as working properties for each object. Surface thermal loads (nodal point loads) are applied to various zones to match the real-world ACCS prototype. In this case, the motors of both the pump and cryocooler, as well as the cold tip and surface mount heaters. Each TD surface is a simplified block version of the real ACCS part. Nodes are distributed across each surface and form the finite element/difference model. TD radiative transport is active for the ACCS model, so relative positioning and line of sight are important. Therefore, relative positions, distances, and view factors are all approximately equal to the test cube prototype. LN2 shields and MLI blankets (Not shown) interact with the radiator to form

the basic heat transfer mechanisms of the system. The heat exchanger assembly is highly simplified. Radiative transfer is not considered for the active parts and features of the HX. Instead, the heat exchanger forms an almost exclusively conductive model. Figure 9.3 below shows an up-close detailed view of the TD heat exchanger. While TD is capable of meshing realistic CAD models, this analysis is far slower and resource-intensive than with primitive objects such as surfaces, solids, and nodes. To maintain the simplicity and speed of this first-order simplified numerical model, only basic shapes were used to approximate the real-world ACCS system.

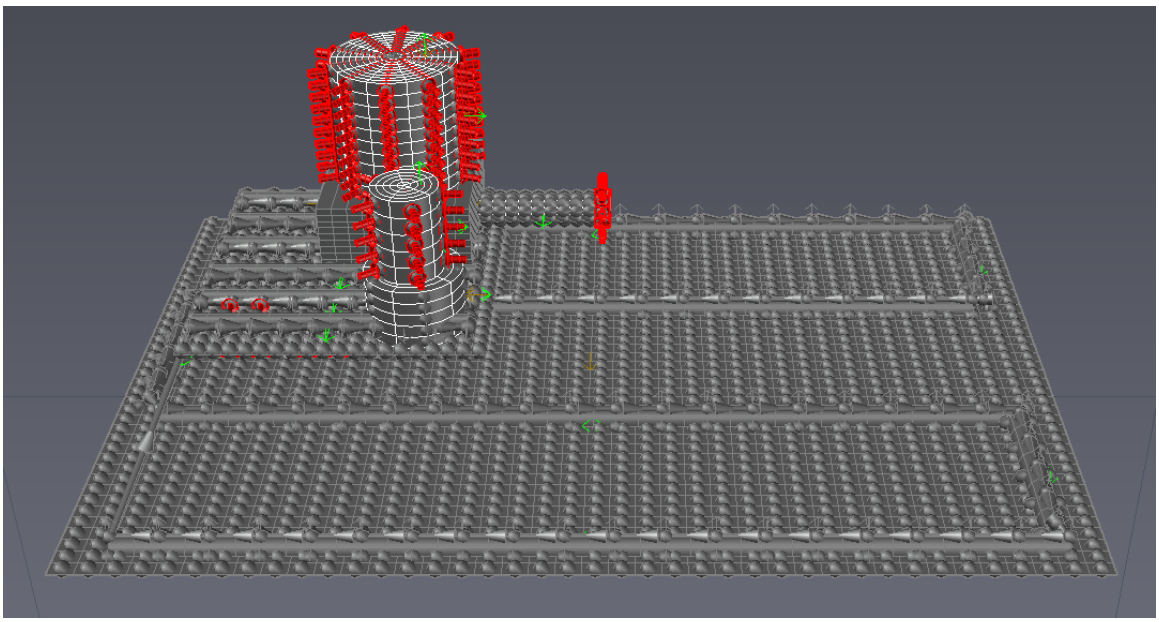

Fig. 9.2: ACCS radiator and heat exchanger assemblies shown as nodal objects.

The ACCS radiator is critical and very likely the most important component in terms of overall impact on the analysis. The overall area was critical to match to the actual ACCS 6U UAM radiator prototype. Because the real radiator is light weighted with UAM flow channel and ribbing features, the area is not as simple as a double-sided flat plate of 20 X 30 cm. Instead, the actual CAD of the ACCS radiator was imported into Thermal Desktop and meshed. A Monte Carlo ray tracing program was then used to determine not only the exact surface area of the ACCS radiator but the view factor of the radiator

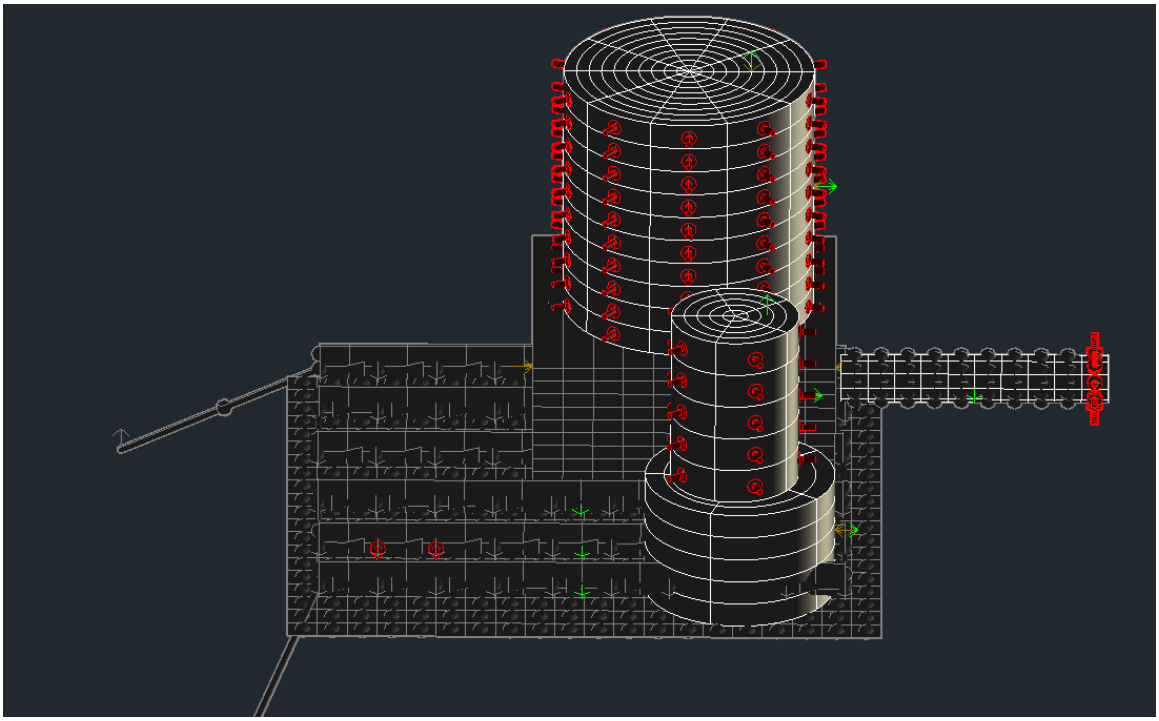

Fig. 9.3: The ACCS heat exchanger assembly formed from TD primmitive shapes.

to the enclosing LN2 shrouds and the view factor of the radiator to itself. This ratio was then used along with the exact area to calculate an equivalent flat plate radiator. The TD radiator tubing's view factor (ray blocking) was also considered and subtracted from this equivalent area. Therefore, it can be determined that the TD ACCS radiator is of a shape and size that do not match either the real-world prototype or the analytical design tool. However, mathematically, its represented area matches perfectly. The ACCS TD radiator flat plate thickness is set to be the same as the actual radiator base plate (UAM) thickness. The TD radiator/HX material is approximated as pure Aluminum 6061. The flow tubing is modeled as half-circle primitive tubes floating just above the radiator's surface. These tubes are conductive along their length and circumference and are connected to the radiator via surface contactors. Square tubing corners and bends are used to represent the smooth 180-degree bends of the real-world UAM radiator. This was done for simplicity and because of the inherent limitations of TD primitive shape modeling. Surface power loads (not shown below) are connected directly to the radiator, offset on each side from the center of the

plate, to simulate the thermal input of the radiator surface heaters. In TD all material and optical properties, as well as conductance and contact resistance values, are user specified. The radiator plate, flow-tubing, and one-way flow conductors are shown below in figure 9.4.

A critical aspect of the ACCS radiator plate design is the level of isothermality, radiator temperature and thermal gradients, and overall heat transfer efficiency. All of which are complex and difficult to model with closed analytical methods. Thermal Desktop, however, as a CAD-based FE & FD tool, is ideal for this kind of analysis. The relative resolution of the thermal model and thermal gradients within the system can easily be increased by simply increasing the number of nodes. The number and type of nodes represented by the ACCS TD model were a compromise of model resolution and resource allocation/simulation time requirements.

Fig. 9.4: The ACCS UAM radiator assembly formed from TD primmitive shapes. One-way conductors, nodes, and tubing channels are shown.

An interesting aspect of thermal Desktop is that while fluid flow analysis is available via the FloCAD tool add-on, another, more straightforward option is to simulate heat transfer

via convection and fluid flow as a one-way conduction path. Thermal Desktop allows the normally bi-directional thermal contact between any two nodes to be changed to a heat flow path with a single direction, not unlike a fluid advection. The value of this conduction path is equivalent to the heat capacitive flow value of the working fluid. i.e., the mass flow rate multiplied by the heat capacity of the fluid. This simplified one-way conductor can model simplified convective heat transfer for both the laminar and turbulent flow regimes with reasonable accuracy and speed. This method is lacking compared to traditional CFD methods but is sufficient for this model. Figure 9.5 shows the simplified geometry of the radiator with one-way conductors along the top of the fluid channels. These conductors transfer the bulk fluid heat transfer of the working fluid along the length of the channels, while normal conduction transfers the heat around the tube's circumference. In TD one-way conductors are marked by an arrow showing the direction of heat transfer. See the highlighted sections below.

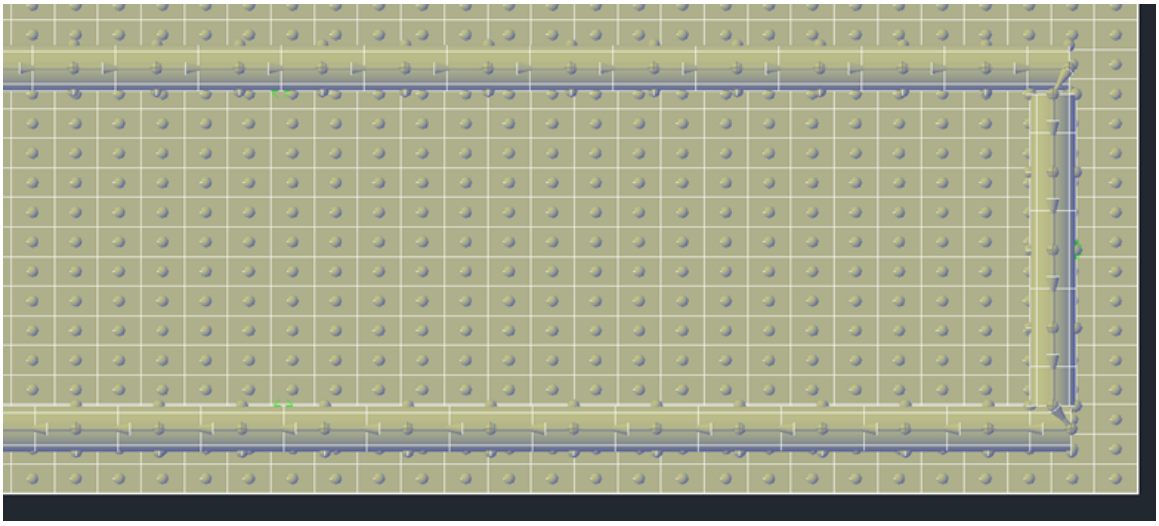

Fig. 9.5: One way conductors, shown as directional arrows, can simulate basic fluid flow advection & convection in Thermal Desktop.

9.3.1 Thermal Desktop Contactors

Surfaces, volumes, and nodes within thermal Desktop can be connected via nodal or

surface contactors. There are several types of contactors, but the most common form is contact resistance. Contactors are highly geometry-dependent and must be user specified. Therefore, it is critical that the modeled geometry accurately represent the physical system in terms of size, shape, and relative position. The value of the contactor is entirely dependent on the situation and requires an in-depth knowledge of thermal heat transfer, common contactor types, values, materials, and mechanical connection. Numerous references within the literature discuss contact resistance and provide either experimentally look-up tables with pre-determined values or guidance on calculating contact resistance. An example of the contactors used in the ACCS TD model is shown below in figure 9.6. The yellow lines represent a node-to-surface contact between the heat exchanger and the flow channels.

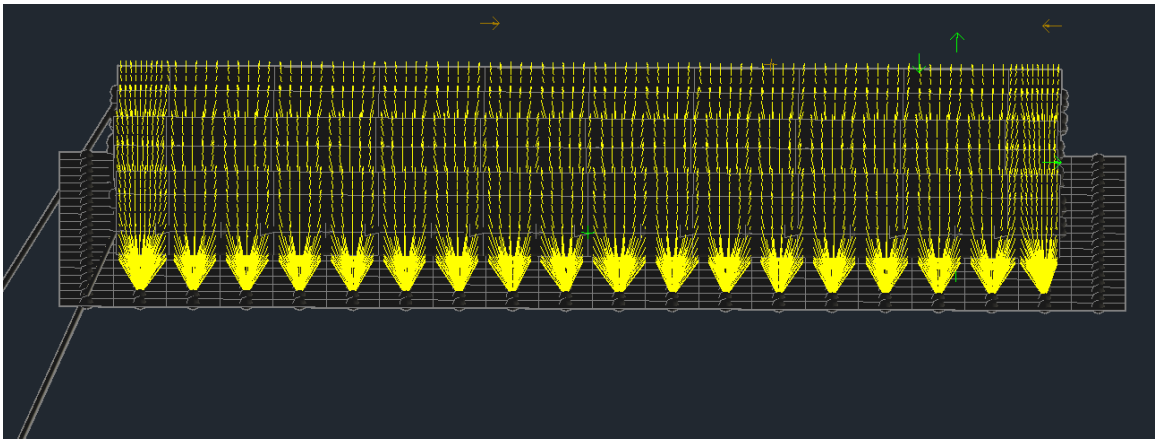

Fig. 9.6: Node-surface contactors for thermally connecting the flow channels to the heat exchanger.

9.3.2 TD Design for the ACCS Pump & Cryocooler

The Ricor K508N and TCS M510 are modeled as representative volumes and shapes in the most basic sense. Both the cryocooler and pump are simplified to a much greater extent than the heat exchange or radiator. The cryocooler is modeled by a series of stainless steel blocks, cylinders, and cubes mounted with high-conductivity interfaces to represent a continuous material. The ACCS team did not attempt to model the internal structure or

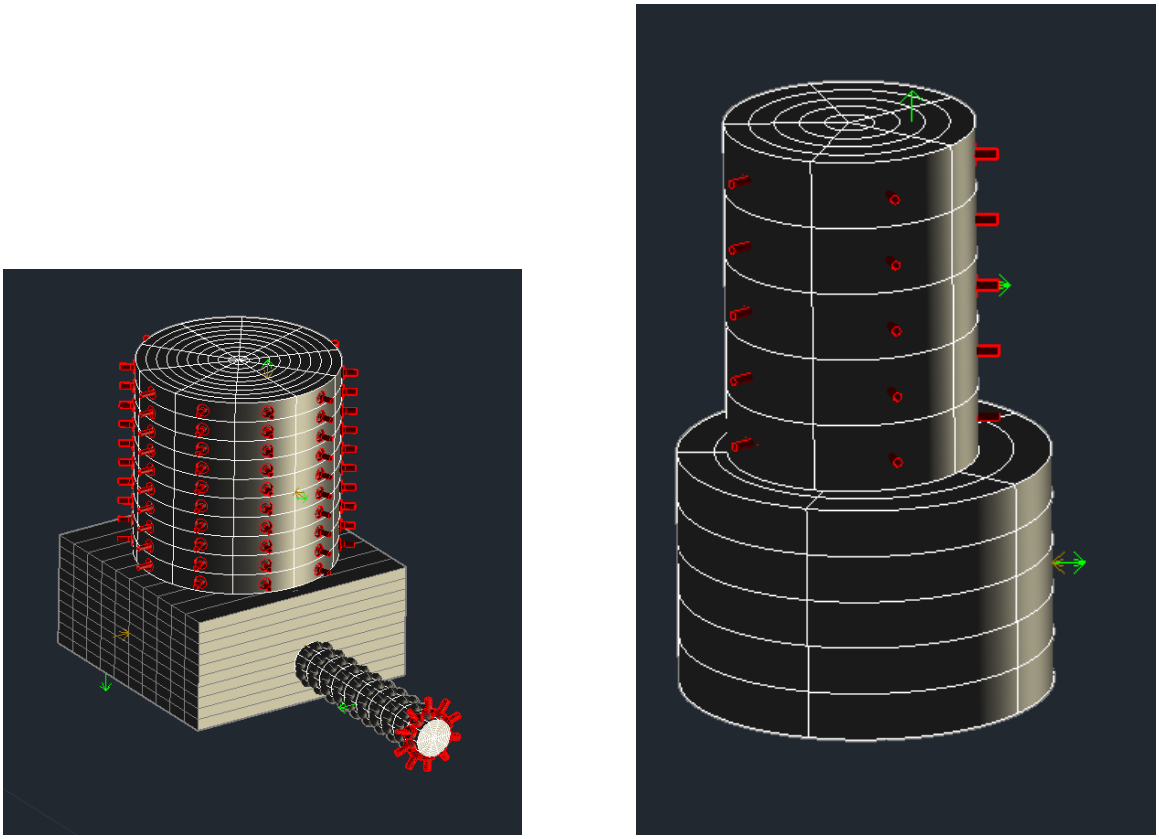

Fig. 9.7: ACCS simplified Ricor K508N cryocooler and TCS M510 micro-pump.

mechanisms of the cryocooler or cold tip. TD models of typical or specific cryocoolers do exist, but they are far too complex for the current analysis. The pump is modeled in a very similar fashion. With solid TD objects representing the motor and impeller housing. The cryocooler is mounted to the heat exchanger via contactors set to simulate a semi-rough stainless steel to aluminum interface with an indium spacer. Because the pump directly interacts with the fluid, the contact with the heat exchanger is set to be artificially high. Both the cryocooler and the pump are accurate in terms of size, weight, location, and approximate material/density. Figure 9.7 below shows the simplified TD models for the Ricor K508N and TCS M510. Thermal loads are distributed, shown as red arrows, on the motor housing for each and on the cold tip of the cryocooler.

9.4 Results & Model Validation

The ACCS thermal desktop model was compared to several experimental data points collected by the ACCS team during TVAC characterization. These steady-state data points were used as experimental validation for the ACCS model. Only eleven data points were chosen due to the time required to run each analysis. These eleven data points were selected as good representations of the experimental data collected. The eleven cases were varied as much as possible in terms of input parameters such as flow rate and total thermal load, with high and low power cases and high and low flow rates being considered. Another parameter that was studied was whether the radiator heater was activated or not. It should be noted that the cryocooler and pump were modeled; however, the cryogenic behavior of the cold tip was not. The TD model inputs include the component power for each of the active systems, the flow rate, and the convective "one-way conductor" values for the fluid channels. The average heat exchanger and radiator temperatures and max/min values were extracted from the model and compared to the experimental data. Table 9.1 (continued in 9.2) below details the results of the thermal desktop model. Radiated power was used for the TD model validation shown in this chapter. The total "corrected" power was also modeled. This data is shown in the Appendix. Similar to the analytical model, the temperatures vary by a greater degree, but the overall error is, on average, still within 5%.

The results show that the simplified ACCS TD model is very accurate. With average temperature errors on the order of less than 0.5%. Maximum and minimum values for the heat exchanger and radiator were also quite accurate and consistent with experimental TC values in terms of location. Generally, only varying by a few degrees. This is remarkable because the TD model is highly simplified, and the number of thermocouple instrumentation on the radiator prototype is limited. The radiator surface topology is also quite complex. These results indicated that the UAM prototype radiator is behaving nominally and that the TD model is more than capable of predicting the highly linear behavior of the ACCS system.

A temperature analysis/validation of the cryocooler and pump is shown in Table 9.3

Case # + Notes		Heat Exchanger Rejection Temperature (°C)				Radiator Surface Temperature (°C)			
		TD Model		Exp. Data		TD Model		Exp. Data	
1	Thermal Power (W) 35.52	Average				Average			
		-12.61		-12.00		-15.9		-16.14	
	Fluid Flow Rate (mL/min) 890.05	Min	Max	Min	Max	Min	Max	Min	Max
		-13.52	-11.66	-13.12	-10.99	-16.83	-14.71	-16.95	-15.73
		Error: 0.23%				**Error: 0.0936**			
2	Thermal Power (W) 43.0	Average				Average			
		0.5		0.52		-3.47		-3.64	
	Fluid Flow Rate mL/min 890.55	Min	Max	Min	Max	Min	Max	Min	Max
		-0.56	1.56	-1.32	1.92	-4.59	-2.03	-4.64	-3.09
		Error: 0.0065%				**Error: 0.064%**			
3	Thermal Power (W) 43.23	Average				Average			
		3.84		5.62		-3.15		-3.29	
	Fluid Flow Rate (mL/min) 354.66	Min	Max	Min	Max	Min	Max	Min	Max
		2.74	6.28	2.75	8.03	-4.91	-0.62	-4.75	-2.48
		Error: 0.64%				**Error: 0.055%**			
4	Thermal Power (W) 56.9	Average				Average			
		25.05		26.42		15.85		15.76	
	Fluid Flow Rate (mL/min) 352.67	Min	Max	Min	Max	Min	Max	Min	Max
		23.57	28.69	22.17	30.14	13.54	19.16	13.89	16.98
		Error: 0.46%				**Error: 0.028%**			
5	Thermal Power (W) 95.46	Average				Average			
		60.52		58.41		55.57		55.51	
	Fluid Flow Rate (mL/min) 868.43	Min	Max	Min	Max	Min	Max	Min	Max
		59.22	62.3	50.85	62.98	52.1	63.61	53.21	59.77
		Error: 0.64%				**Error: 0.019%**			

Table 9.1: Numerical HX & Radiator "Thermal Desktop" model data compared to ACCS experimentally characterized data for select cases.

Case # + Notes		Heat Exchanger Rejection Temperature (ºC)				Radiator Surface Temperature (ºC)			
		TD Model		Exp. Data		TD Model		Exp. Data	
6	Thermal Power (W) 36.89 Fluid Flow Rate (mL/min) 890.94	Average				Average			
		-10.08		-9.42		-13.50		-13.70	
		Min	Max	Min	Max	Min	Max	Min	Max
		-11.02	-9.06	-10.73	-8.48	-14.46	-12.26	-14.66	-13.07
		Error: 0.25%				**Error: 0.078%**			
7	Thermal Power (W) 39.51 Fluid Flow Rate mL/min 355.94	Average				Average			
		-4.29		-2.98		-9.04		-9.26	
		Min	Max	Min	Max	Min	Max	Min	Max
		-5.05	-2.8	-4.24	-1.73	-10.68	-6.41	-10.73	-7.25
		Error: 0.482%				**Error: 0.085%**			
8	Thermal Power (W) 54.5 Fluid Flow Rate (mL/min) 1099.73	Average				Average			
		16.93		15.38		12.85		12.65	
		Min	Max	Min	Max	Min	Max	Min	Max
		15.61	19.36	12.81	16.89	11.3	15.09	11.36	14.21
		Error: 0.537%				**Error: 0.068%**			
9	Thermal Power (W) 43.74 Fluid Flow Rate (mL/min) 729.39	Average				Average			
		0.81		1.40		-2.33		-2.51	
		Min	Max	Min	Max	Min	Max	Min	Max
		0.05	1.75	0.44	2.46	-3.72	-0.05	-3.74	-0.83
		Error: 0.215%				**Error: 0.066%**			
10	Thermal Power (W) 43.19 Fluid Flow Rate (mL/min) 729.14	Average				Average			
		-0.04		0.45		-3.14		-3.59	
		Min	Max	Min	Max	Min	Max	Min	Max
		-0.8	0.92	-0.66	1.52	-4.52	-0.86	-4.58	-1.66
		Error: 0.179%				**Error: 0.081%**			
11	Thermal Power (W) 38.89 Fluid Flow Rate (mL/min) 743.88	Average				Average			
		-6.9		-6.12		-10.08		-10.29	
		Min	Max	Min	Max	Min	Max	Min	Max
		-7.69	-5.87	-7.20	-5.26	-11.24	-8.72	-11.37	-9.14
		Error: 0.288%				**Error: 0.083%**			

Table 9.2: Numerical HX & Radiator "Thermal Desktop" model data compared to ACCS experimentally characterized data for select cases.

for an even finer selection of cases. Once again, the accuracy is remarkable. Especially considering that the cryocooler and pump are highly simplified. Only consisting of solid blocks with internal conduction, it would be quite easy to assume that their internal mechanisms and complexity would not easily lend themselves to modeling, much less accuracy. However, TD predicted temperatures match experimental values within 5% on average. Max, min temperatures vary by 5 to 10 °C. However, this is still quite accurate, considering that these active systems were not directly modeled.

Case # + Notes		Ricor K508N Cryocooler Body Temperature (ºC)				TCS M510 MicroPump Body Temperature (ºC)			
		TD Model		Exp. Data		TD Model		Exp. Data	
1	Thermal Power (W) 35.52	Average				Average			
		1.67		4.46		-7.98		-11.84	
	Fluid Flow Rate (mL/min) 890.05	Min	Max	Min	Max	Min	Max	Min	Max
		-12.4	19.78	-1.51	16.64	-10.63	-5.05	-13.42	-10.27
		Error: 1.01%				**Error: 1.47%**			
5	Thermal Power (W) 95.46	Average				Average			
		73.69		72.43		66.26		56.45	
	Fluid Flow Rate (mL/min) 868.43	Min	Max	Min	Max	Min	Max	Min	Max
		60.78	82.89	64.87	79.12	61.95	66.75	54.32	58.57
		Error: 0.37%				**Error: 2.97%**			
8	Thermal Power (W) 54.5	Average				Average			
		30.01		29.69		26.39		15.34	
	Fluid Flow Rate (mL/min) 1099.73	Min	Max	Min	Max	Min	Max	Min	Max
		16.82	47.75	25.27	37.95	21.2	31.95	15.06	15.62
		Error: 0.11%				**Error: 3.82%**			
10	Thermal Power (W) 43.19	Average				Average			
		12.2		14.04		2.53		0.26	
	Fluid Flow Rate (mL/min) 729.14	Min	Max	Min	Max	Min	Max	Min	Max
		0.08	30.9	8.96	23.73	0.94	4.24	-0.93	1.45
		Error: 0.64%				**Error: 0.83%**			

Table 9.3: Numerical Ricor K508N cryocooler & TCS M510 micro-pump "Thermal Desktop" model data compared to ACCS experimentally characterized data for select cases.

Plots of the ACCS experimental performance data vs. Thermal Desktop model are shown below in figure 9.8. The semi-linear nature of the temperature vs. power curves

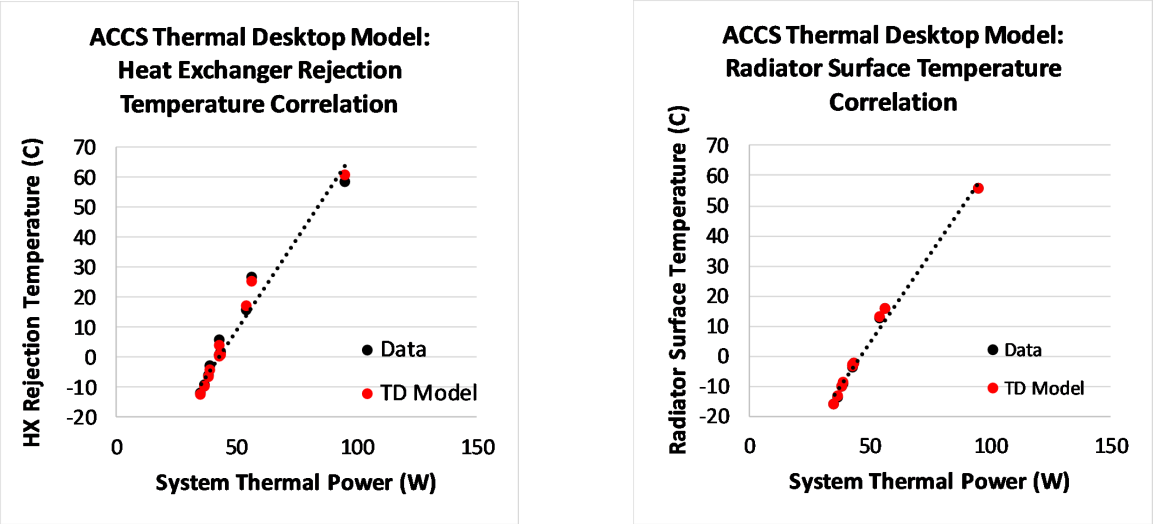

Fig. 9.8: Comparison of the average heat exchanger and radiator surface temperatures of the ACCS Thermal Desktop model to experimentally collected performance data of the test cube.

is demonstrated by the predictive line. A plot of the error vs. thermal power is given in figure 9.9. Generally, the TD model error increases with power and seems slightly higher for low flow rates. Figure 9.10 shows the errors as a function of case number for comparison to the data tables. Plots of the TD model with corrected total power are given in the Appendix. Figure 9.11 compares the experimental and numerical data, point for point, to the analytical design tool results. As can be seen, all three closely agree. This indicates the predictive accuracy of the TD model and confirms that it has been validated.

9.5 Thermal Desktop Temperature Color Maps

As mentioned previously, an aspect of thermal Desktop that makes it an incredibly valuable modeling tool is that of colormaps. TD can help engineers visualize the thermal gradients and flow of thermal energy within a system through colormaps. These maps help to determine where the heat is propagating within the system and pinpoints temperature zones of interest. A general view of the ACCS system as a colormap is given below in figure 9.12. Temperatures along the Y-axis of the colormap are given in Kelvin. Figures 9.13 through 9.15 show the colormaps for the HX assembly, HX plate, and radiator. All of the

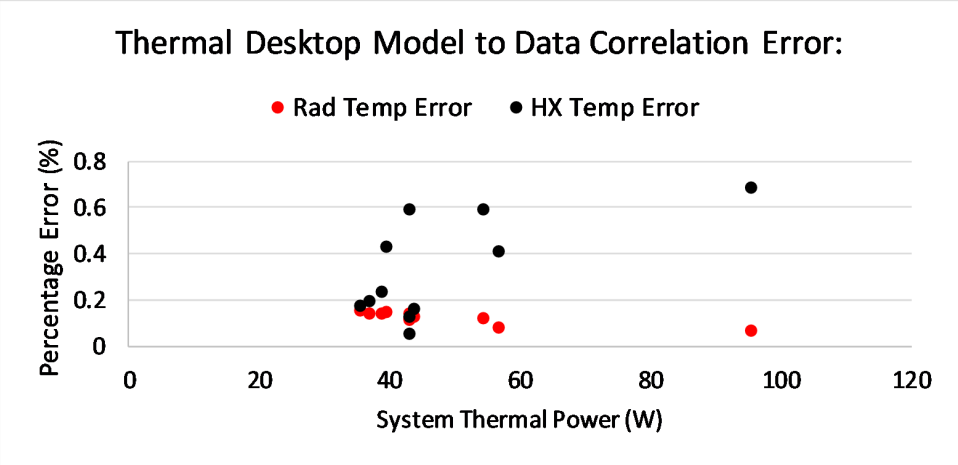

Fig. 9.9: ACCS Thermal Desktop error vs. radiated thermal power.

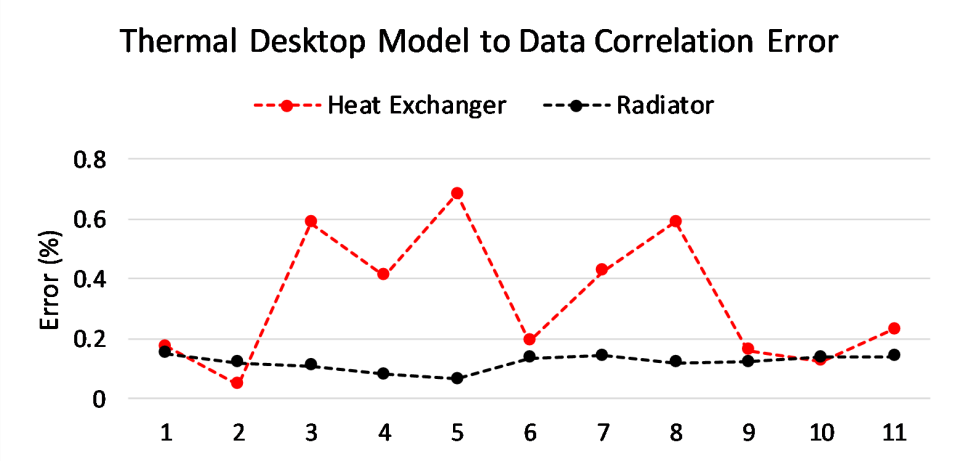

Fig. 9.10: ACCS Thermal Desktop error as a function of case number.

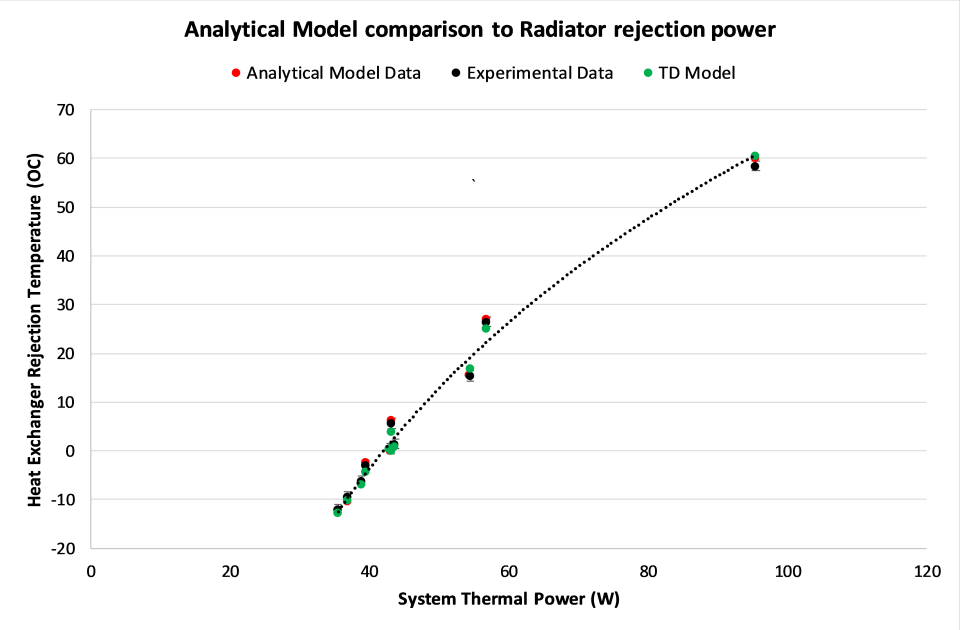

Fig. 9.11: Final ACCS model comparison. TD vs. Analytical vs. Experimental.

colormaps shown below are from case #8. The total input power for that case is 54.5 W radiated (60.37 W total), with a flow rate of ∼1100 mL/min, and a combined flow heat capacity of ∼33.25 W/°C. The cryocooler and pump both exhibit higher temperatures at their motor interfaces. The heat exchanger's thermal zones are shown in figure 9.15. The hottest location, the bottom left, corresponds to the pump interface. This is consistent with reality, as can be seen in Table 9.2. Because of the high flow rate represented by the selected case, the M510 pump, ∼1100 mL/min, is outputting nearly 20 to 25 W of thermal power. The coldest location on the Heat Exchanger is in the opposite corner at the fluid outlet. This is once again consistent with experimental data for this case, considering that all of the temperatures considered are surface TC values, which are greatly affected by the high thermal load represented by the selected case. The working fluid temperature would be at a minimum at the fluid inlet and a maximum at the outlet.

The radiator colormap is of particular interest. Hot thermal zones exist at the radiator inlet and under the inlet patch heater. The flow channel tubing remains consistently hotter than the surrounding radiator surfaces. The coldest points are in the middle of the radiator, away from the central flow channels. This gradient is only a degree or two but could

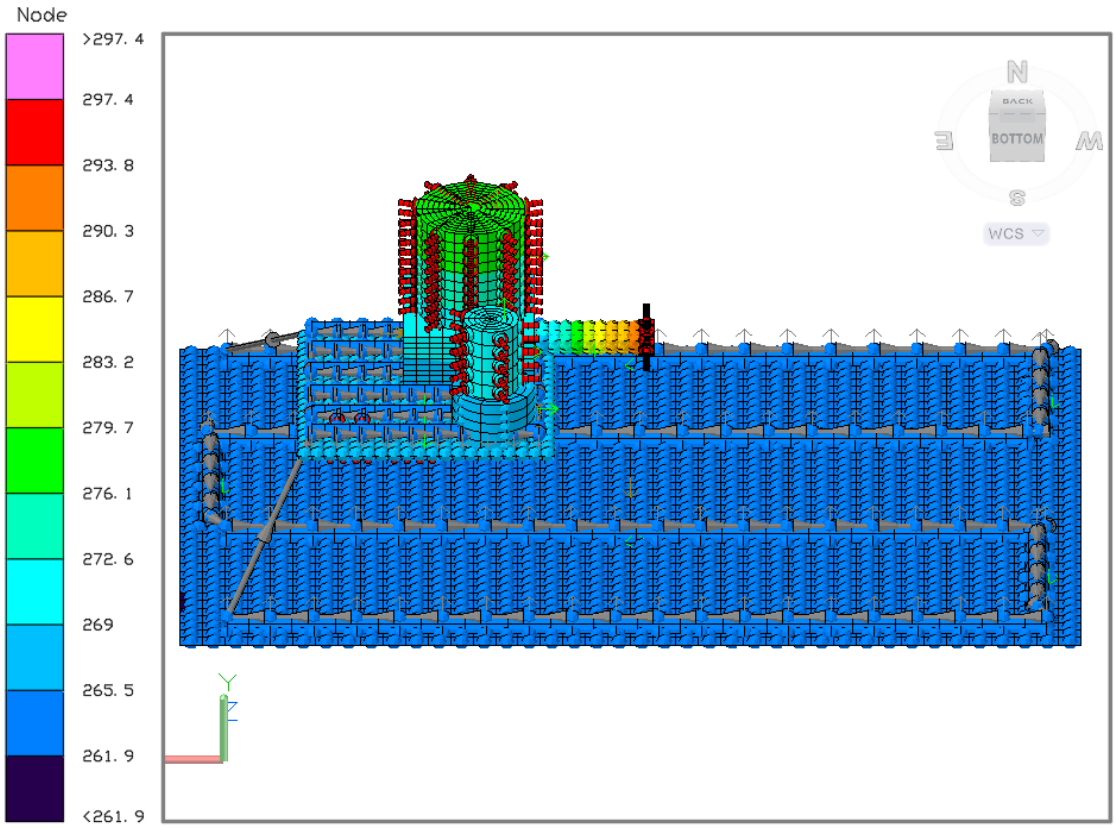

Fig. 9.12: Temperature color map of the ACCS system for Case #8.

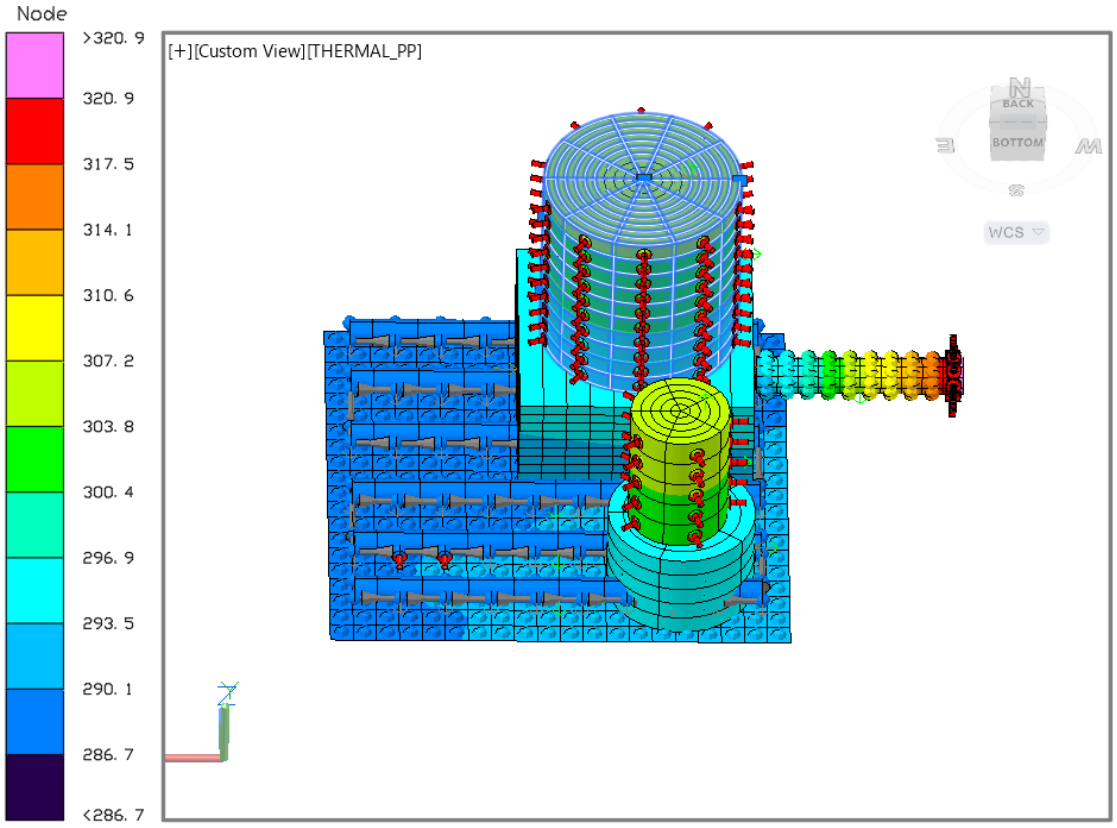

Fig. 9.13: Colormap of the ACCS heat exchanger assembly (Case #8). Shown with cryocooler, cold tip, and pump assemblies.

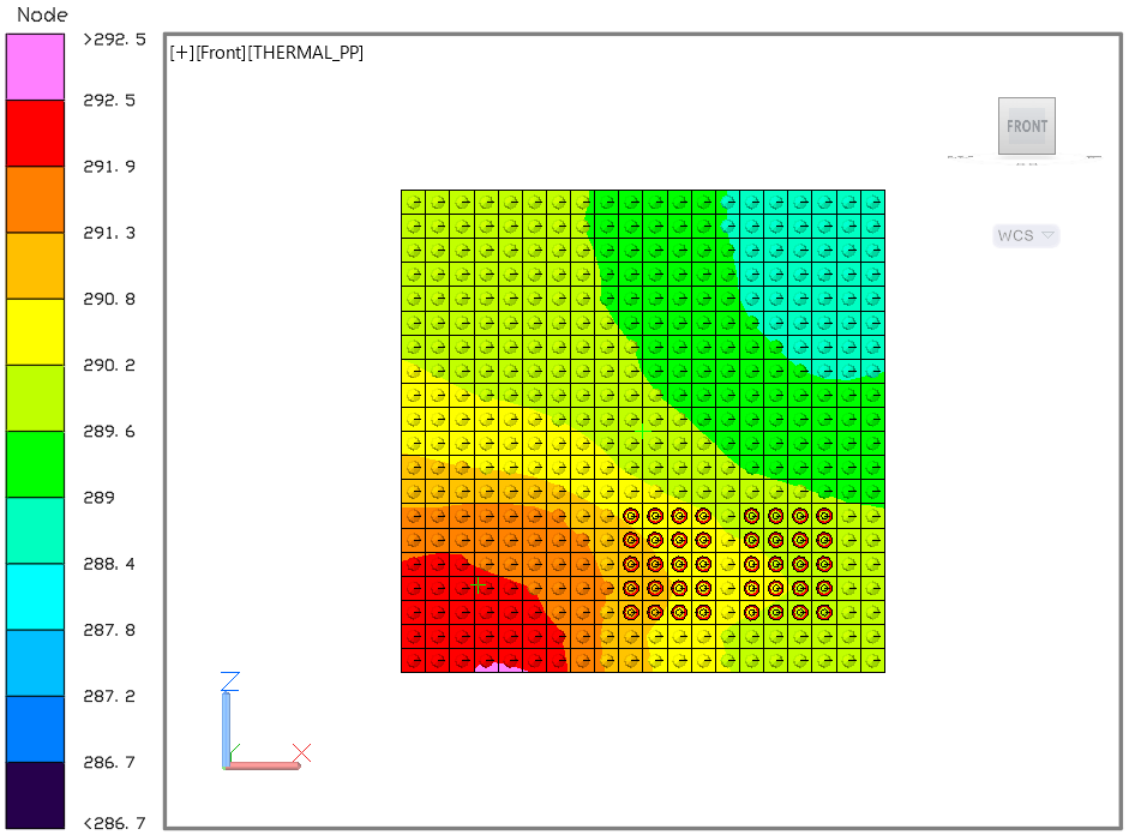

Fig. 9.14: Colormap of the ACCS heat exchanger plate (Case #8). The hot thermal zone represented shown in the bottom left represents the significant thermal load imparted by the pump at high-flow rates.

potentially indicate non-isothermal behavior in this region. Future radiator designs might want to have flow channels closer together or a UAM composite material that includes a high conductivity layer to even out temperatures and improve efficiency.

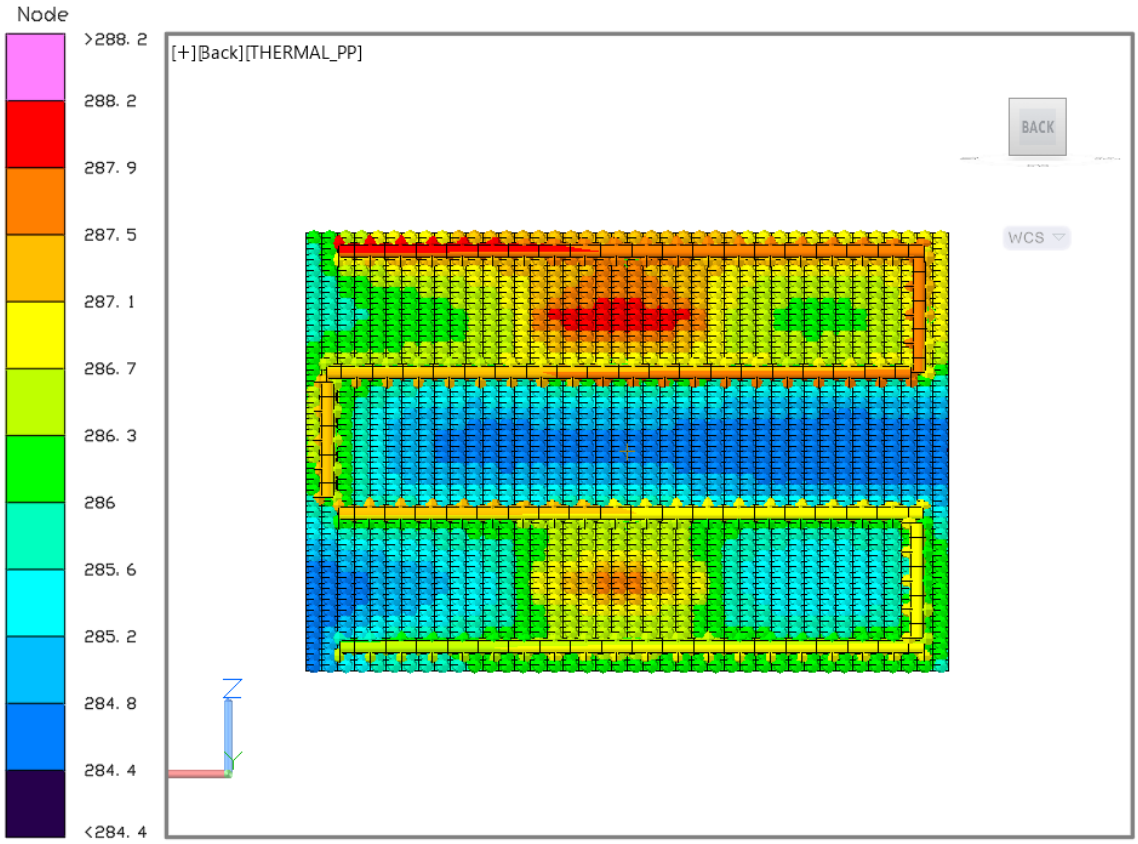

Fig. 9.15: Colormap of the ACCS radiator (Case #8).

9.6 Future Thermal Desktop Modeling

The ACCS TD model is a simplified first-generation model. Only suitable for simple view factor radiation analysis and understanding the basic thermal gradients and temperature zones within the ACCS system. More advanced models would have significantly more capability and utility and could be used to design future ACCS systems, whole satellite structures, and CubeSat missions. The next generation of ACCS TD models should feature meshed (high node count) CAD models with improved realism. Complex contac-

tors, for improved accuracy and detailed orbital radiation analysis. The pumped fluid loop should also be modeled with the full thermohydraulic capabilities of FloCAD in the next version. FloCAD analysis would enable modeling of the changes in the flow regime, flow velocity/thermal boundary layer analysis, and much more. Accurate models of the cryocooler, cold tip, and pump could be created to match their real-world counterparts better. Temperature-dependent properties could be encoded along with dynamic control of the heat loads and flow rates. Transient analysis of the heat flow within the heat exchanger, flow path, and radiator are critical and should be explored in more detail. The current ACCS TD model is not appropriate for orbital analysis. However, future models will feature flight-like designs and include satellite structures. This transient orbital analysis will be critical for future missions. One final aspect of the ACCS system that should be explored in future versions is the PID control and feedback algorithm. Modeling the PID algorithm in TD would help the team to understand its behavior and performance better and greatly aid its development.

Future ACCS models should be broken up into two major categories and focus on two key aspects of simulation design. Simplified (but realistic) fast predictive models and hyper-realistic in-depth analysis models. The simplified fast models can still include realism but should use standard block geometry, basic CubeSat structures, and pseudo thermal connections to speed up analysis. Hyper-realistic models should mesh geometry and focus on in-depth transient and steady-state analysis with highly realistic radiation analysis, flow simulation, and mechanical conduction. Between these two distinct model types, future versions of the ACCS technology can be rapidly and easily developed and integrated into advanced next-generation CubeSat science and technology missions. Ultimately, the current project did not have sufficient funding or time to create all of these detailed Thermal desktop models; however, future projects can and will develop them.

9.7 Conclusions

The ACCS Thermal Desktop is a relatively simple but highly effective model of the ACCS system. Validation with experimental results has shown that it can predict behavior,

performance, and temperatures to within 1%. Thermal Desktop has allowed the ACCS system to be explored at a much deeper level with component-by-component and node-by-node accuracy. In addition, the TD model has allowed for complex radiation and transient 3D temperature analysis of the ACCS system. Future projects will continue the numerical analysis started by this research and use Thermal Desktop to model hyper-realistic active thermal control systems like the ACCS for advanced Small Satellite missions.

CHAPTER 10

Results: Thermal Vacuum Performance Characterization

Research is creating new knowledge

Neil Armstrong

10.1 Introduction

The final objective of the original ACCS proposal was to characterize the Active CryoCubeSat thermal control system in a relevant ground-based environment, aka a thermal vacuum environment. To accomplish this, a highly instrumented testbed ("Cube"), figure 10.1 below, was built to demonstrate the thermal performance of the ACCS system. This characterization focused on the ACCS system on a component level as well as an integrated whole. Characterization included temperature stability and control, heat exchanger thermal transfer (convective analysis), and thermal radiative balance. Ultimately, the final performance criteria for the ACCS system was its ability to maintain an ideal thermal environment for the integrated Ricor K508N cryocooler and, by extension, the cold tip to detector thermal balance/temperature. Testing was performed at Utah State University in the Center for Space Engineering TVAC lab facilities. The Jet Propulsions Laboratory provided support. ACCS TVAC characterization and performance results are described in detail in this chapter. Supplementary material and additional results are included in the Appendix.

10.2 Test Overview & Objectives

The overall objective of the ACCS TVAC testing can be summarized as:

- Characterize the thermal performance (Performance Envelope) & behavior of the ACCS system

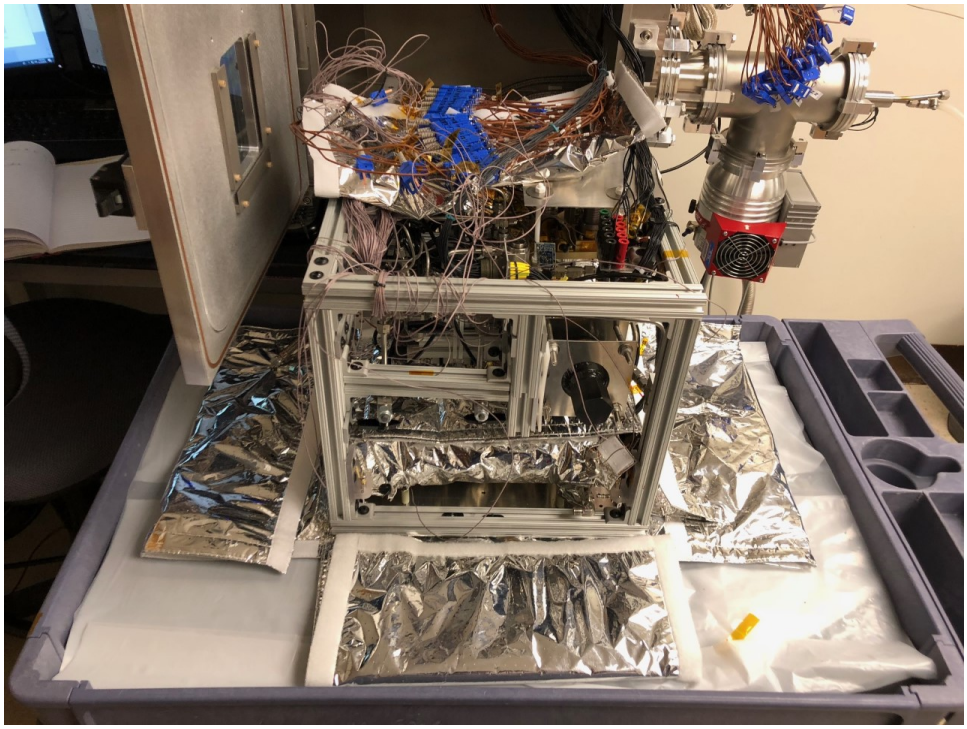

Fig. 10.1: ACCS Test cube: An instrumented test bed for the TVAC characterization of the ACCS thermal control system.

- Demonstrate the ACCS system in a relevant TVAC environment
  - Raise the Technology Readiness Level (TRL) of the ACCS system to 5 (TBR)
- Demonstrate thermal accommodation of the integrated cryocooler
  - Maintain a stable cold tip temperature with thermal loading
- Satisfy the performance requirements and goals of the ACCS proposal
- Demonstrate the ACCS in a pseudo-thermal orbital environment
- Characterize the ACCS system's response curves for control and feedback

The original ACCS proposal requirements are given below in Table 10.1. Performance metrics listed in green were met, yellow were approximately satisfied with some caveats (see table notes), and red were not met. It should be noted that all performance requirements were satisified as well as most goals.

Development Objective	Performance Required	Performance Goal
A miniature mechanically pumped fluid loop thermal control system for a CubeSat	*Thermal Load*: > 30 W *Interface*: 20-30°C *Power:* < 4 W *Mass*: < 2 kg *Volume*: < 1U (1000 cm^3)	*Thermal Load*: > 60 W *Interface*: 10-30°C *Power:* < 0.3 W *Mass*: < 0.5 kg *Volume*: < 0.3U (<0.5U)
A cryogenic cooling system for a CubeSat	*Temperature:* < *100K* *Thermal Load*: > 50 mW *Power:* < 15 W *Mass*: < 1 kg *Volume*: < 1U (1000 cm^3)	*Temperature:* < *75K Thermal Load*: > 250 mW @ >80 K *Power:* < 5 W (CC Steady State) *Mass*: < 0.2 kg *Volume*: < 0.3U

Table 10.1: Original ACCS performance requirements.

Two separate TVAC test campaigns captured the majority of ACCS TVAC characterization. The first was primarily focused on the performance averages and extremes of the ACCS system. Pushing the system to both hot and cold thermal limits. Varying the single-phase working fluid flow rate from ∼350 to 1100 mL/min maximum flow. This defined the performance envelope of the ACCS system and allowed for the derivation of thermal balance, flow rate, and temperature stability curves which describe the behavior of the ACCS system. The first TVAC test also featured several orbital simulations, in which the ACCS system was cycled through pseudo ∼90-minute orbits. The typical orbit variation in the thermal space environment was modeled by varying the thermal loads on the radiator. The cryocooler's cold tip temperature stability and thermal environment were carefully monitored

The second TVAC test focused entirely on deriving the control response curves of the ACCS system. These response profiles were used, by USU students, to develop a feedback and control algorithm to regulate the ACCS heat exchanger temperature by flow rate as the total system power was varied. The details of this control algorithm can be found in Mattos & Anderson et al [26]. The ACCS system was broken down by control input type. System inputs were varied ("Impulse" set points) between 50%, 25%, and 75% of max range. These impulse responses were then used to define the ACCS systems response and tune a PID control algorithm to control the various set point temperatures throughout the

system. A block diagram of how the ACCS active thermal control system operates and can be controlled is shown below in Figure 10.2. Note that the Heat exchanger and radiator setpoints are controlled by the system's pump power, flow rate, and various guard heaters, as well as the pointing of the deployable radiator. System disturbances include the thermal space environment (orbit), the power requirements of the satellite bus, and the thermal specifics of the payload. The operational concept in figure 10.2 also shows how the ACCS results can be analyzed and used to predict behavior. Ultimately, the inputs of the system are thermal power and flow rate, with the output being system temperature.

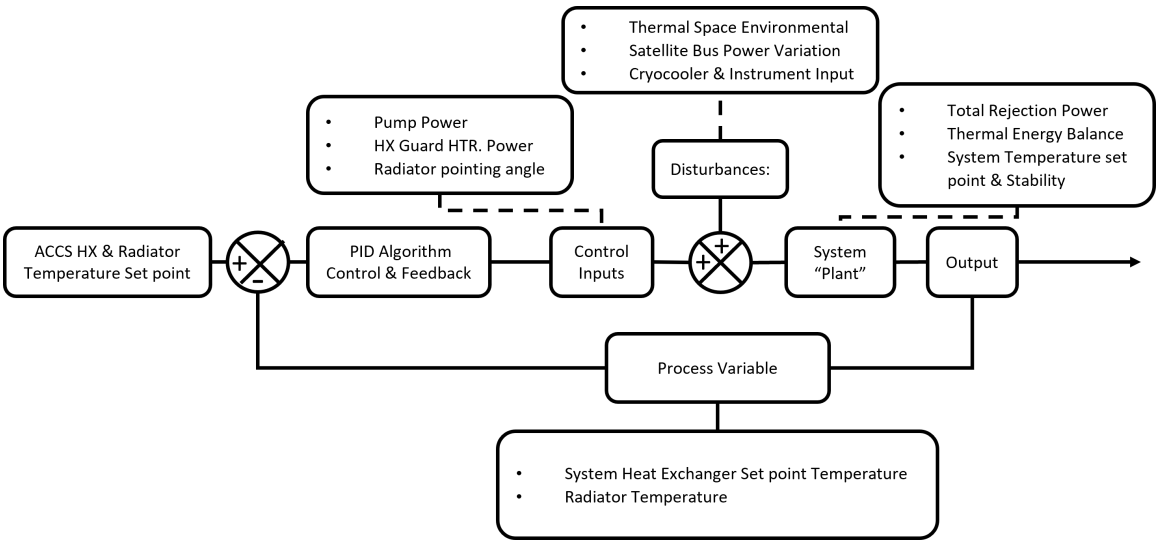

Fig. 10.2: Basic Design for the ACCS Feedback and control algorithm.

The ACCS system is instrumented for temperature, pumped fluid flow rate, pressure (static & differential), and power. Thermocouples measure non-cryogenic temperatures and gradients within the system, while dual cryogenic silicone diodes monitor the cryocooler's cold tip temperature. A custom-designed Venturi Flow meter, see experimental design chapter, measures the system flow rate with differential pressure transducers monitoring the pressure produced by the pump, the venturi meter, and an absolute static gauge for overall system pressure. The input power of each active system is continuously monitored. These individual powers are added to determine the summed total thermal power of the

system. The ACCS test cube is well insulated with G10 standoffs, Kevlar thread isolation of the radiator, UHMW plastic insulators, and MLI. The total power is "corrected" for parasitic's within the Matlab data analysis code. The capacitive energy balance of the working fluid is determined for the heat exchanger, radiator, and for the connecting tubing. The temperature distribution across the surface of the radiator was used to calculate a radiative power loss for the system. This radiative thermal power is often used as total power because it more accurately describes the system and includes any unknown losses within the system. A CONOPS diagram of the ACCS system is given below in figure 10.3. The accuracy of the test bed instrumentation is shown as error bars in the following data. However, due to the relatively high accuracy of the various sensors used in the ACCS characterization, the error bars are often indistinguishable from the data points. A more detailed explanation of the error analysis for the ACCS characterization is given in the experimental uncertainty chapter of this dissertation. Thermocouple placement and descriptions are shown in figure 10.4. It should be noted that radiator TC's #3, 5, and 6 did not read correctly after installation. Therefore, their data was not used in the analysis of the ACCS system. The performance results of the ACCS system are highly dependent on radiator size. Future ACCS mission design can reference the current results for a similar 6U deployed radiator system. If a different radiator design is required, then the excel based analytical modeling tool, along with the Thermal Desktop numerical model, should be used to predict the behavior.

The TVAC characterization tests are broken down by date, case #, power profile, and heat exchanger Temperature in Tables 10.2 & 10.3 below. Each case number represents a steady-state data point for the ACCS system. While the dynamic nature of the ACCS is important and is included in the orbital simulation and analysis, the steady-state performance will dictate behavior. Therefore, the allowable steady-state variation in temperature was set to no more than a quarter of a degree per hour. The September 2018 TVAC test took nearly 200 hours (continuous), while the January 2019 test lasted just under 100. System absolute pressure was pre-charged to 60 PSIa and varied between ~40 PSIa and

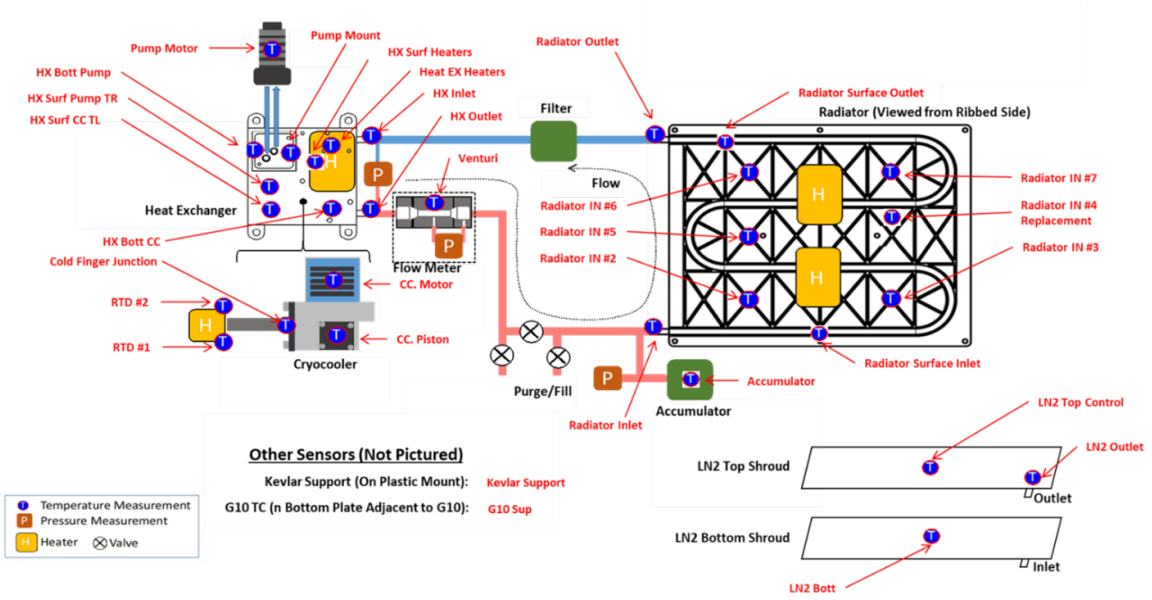

Fig. 10.3: ACCS Test concept of operations (CONOPS) & instrumentation layout.

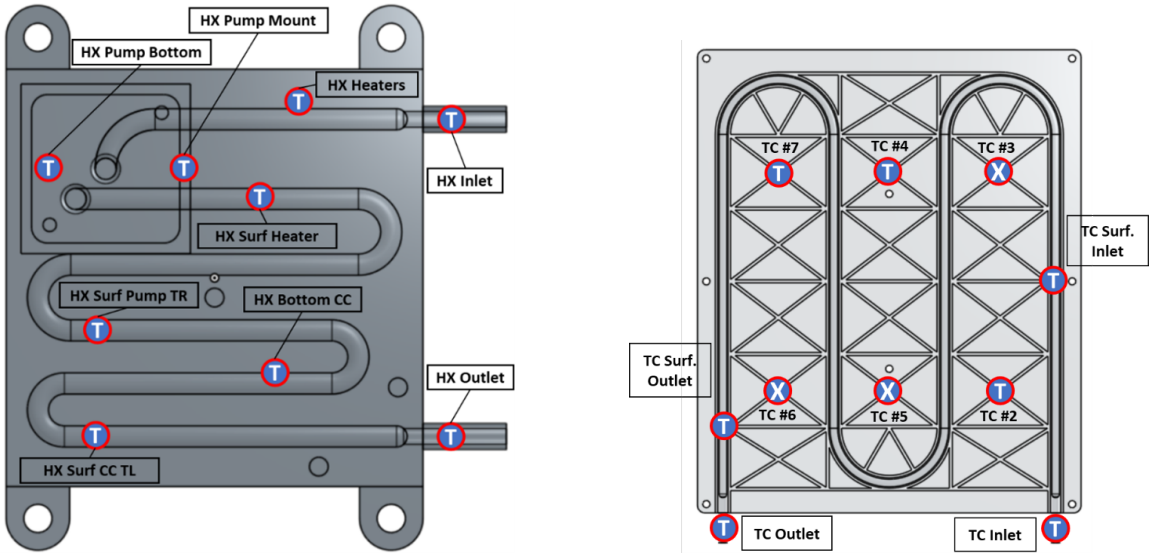

Fig. 10.4: ACCS heat exchanger & radiator thermocouple placement and description.

∼70 PSIa. Figures showing the variation and trends of system pressure are given in the Appendix. TVAC chamber pressure was maintained below $e^{-}6$ mbar and the LN2 shrouds were held between 100 K and 150 K. The variation in shroud temperature for the top and bottom shroud as a function of case number, aka time is shown in the appendix. The Ricor K508N cold tip setpoint was ∼85 K for the September 2018 characterization and ∼115 K for the January 2019 test. The processed data for each TVAC test is shown in figures 10.5 & 10.6. Total corrected power, along with system pressure, is shown on top, followed by a power breakdown for each active component of the ACCS system. The variations described in Tables 10.2 & 10.3 can be seen graphically here. The third sub-figure shows average HX, fluid, and radiator temperatures on the left scale and cold tip temperatures on the right. Finally, the system's dynamic energy balance is shown in the bottom figure. The total corrected power and radiated power are fairly similar. Further analysis is given in the energy balance section. Test case numbers are used to distinguish various steady-state data points and to help in comparison.

ACCS TVAC Characterization: Performance Envelope Derivation (September 2018)				
Case #	Total Power (W)	Heat Exchanger (^{O}C)	Cold Tip Temp (K)	Notes & Objectives
3	31.5	-12.0	85.6 (0.512 W)	Cold Case---Flow Rate ~890 mL/min
4	31.8	-9.9	85.1 (0.512 W)	Cold Case--- Flow Rate ~350 mL/min
5	42.5	0.52	86.5 (0.512 W)	Mid Power--- Flow Rate ~890 mL/min
6	42.3	5.6	86.1 (0.512 W)	Mid Power--- Flow Rate ~350 mL/min
7	58.2	19.0	88.5 (0.512 W)	High Power--- Flow Rate ~890 mL/min
8	57.7	26.4	74.6 (0.288 W)	High Power--- Flow Rate ~350 mL/min
9	57.6	27.1	53.6 (0.0 W)	Cryocooler Performance: Zero Load
10	57.1	25.5	90.24 (0.5 W)	Cryocooler Performance: Expected Load
11	56.3	24.0	130.8 (1.0)	Cryocooler Performance: High Parasitic's
12	N/A	N/A	N/A	Orbital Variation---High & Low Flow Rate
13	111.1	58.4	83.2	Hot Case---Maximum Power Rejection
14	41.7	8.7	N/A (CC Off)	Space Env. Low Thermal Input (6 W)
15	48.3	13.2	N/A (CC Off)	Space Env. Mid. Thermal Input (12 W)
16	54.5	18.9	N/A (CC Off)	Space Env. High Thermal Input (18 W)
17	56.7	19.8	N/A (CC Off)	Pump Flow Rate ~580 mL/min
18	76.4	33.2	N/A (CC Off)	Max Pump Flow Rate ~1163 mL/min
19	N/A	N/A	N/A	Orbital Variation stability via pump throttling
20	N/A	N/A	N/A	Orbital Variation stability via pump throttling

Table 10.2: ACCS TVAC Characterization: Performance envelope .

ACCS TVAC Characterization: Response Curve January (September 2019)				
Case #	Total Power (W)	Heat Exchanger (^{O}C)	Cold Tip Temp (K)	Notes & Objectives
1	31.9	-9.4	116.4	September Comparison Case
2	41.3	1.3	120.6	Nominal Case
3	36.4	2.9	121.1	Flow Rate Variation: Low ~350 mL/min
4	41.6	1.3	122.5	Flow Rate Variation: Nom. ~730 mL/min
5	56.7	15.4	123.2	Flow Rate Variation: High ~1100 mL/min
6	41.3	1.4	124.5	Nominal Case
7	30.2	-14.1	123.2	HX HTR: Low 25%
8	41.8	0.03	119.5	HX HTR: Nominal 50%
9	52.7	12.5	120.0	HX HTR: High 75%
10	41.5	0.45	118.2	Nominal Case
11	36.2	-6.1	121.2	Radiator HTR: Low 25%
12	41.8	-1.2	121.3	Radiator HTR: Nominal 50%
13	46.9	6.4	107.3	Radiator HTR: High 75%
14	41.6	1.0	128.7	Nominal Case
15	37.9	-4.4	110.4	Cold Tip HTR: Low 25%
16	42.0	-0.45	110.3	Cold Tip HTR: Nominal 50%
17	44.0	1.63	115.9	Cold Tip HTR: High 75%
18	42.0	-0.32	110.2	Nominal Case

Table 10.3: ACCS TVAC characterization: System response profiles.

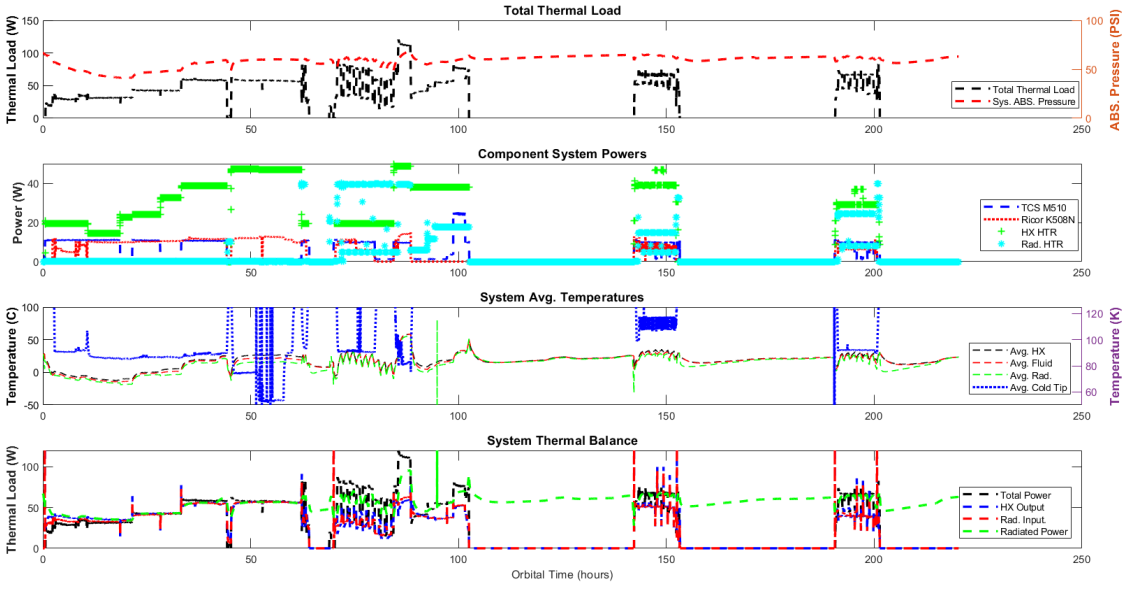

Fig. 10.5: ACCS TVAC characterization performance results. September 2019 TVAC data

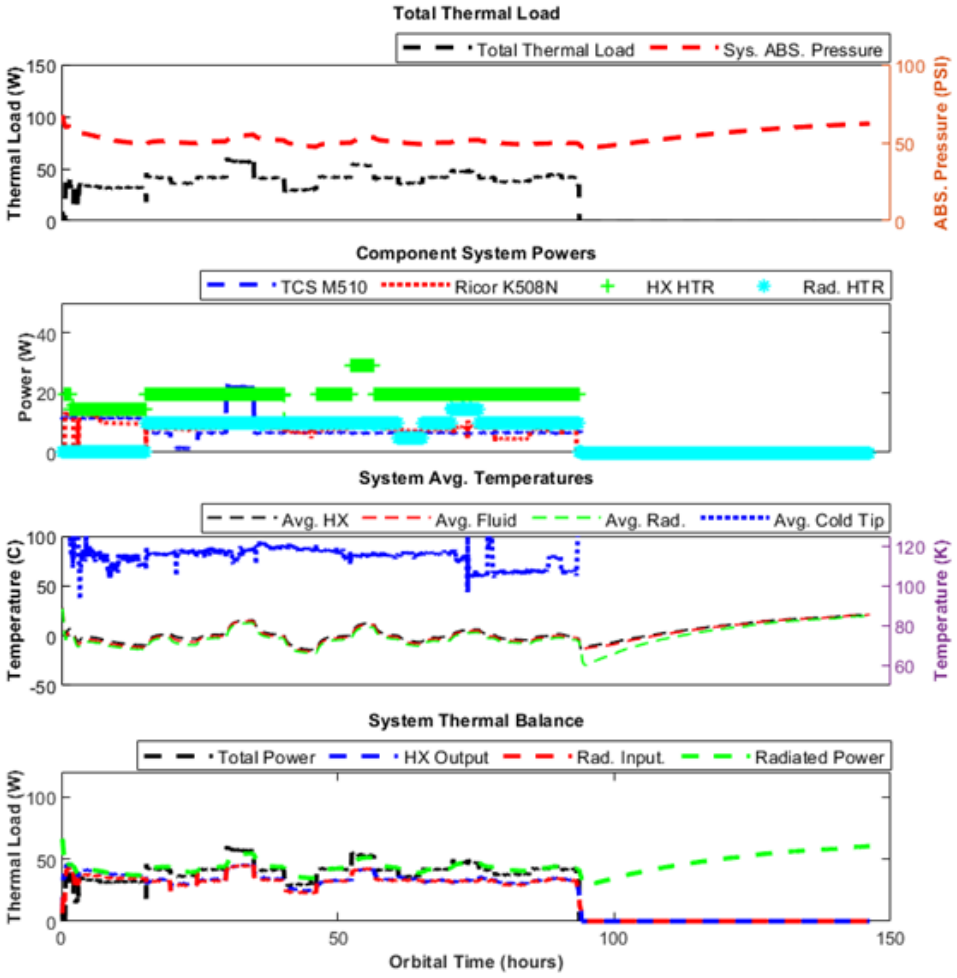

Fig. 10.6: ACCS TVAC characterization response profile. January 2020 TVAC data.

The following results of the ACCS experimental data will start with a discussion on the thermal energy balance within the ACCS system, followed by an overview of the various steady-state temperatures of the heat exchanger, working fluid, and radiator, along with their relative temperature gradients. A full review of the transient orbital simulation will be given with the response/performance curves (performance envelope) of the ACCS system as a series of experimentally derived design charts for future ACCS technologies. The performance of the TCS M510 micro-pump will be shown as flow vs. developed head vs. power curves and derived pump affinity laws. The Ricor K508N cryocooler will be given as a 3D performance chart. Finally, the overall power vs. temperature of the ACCS system will be given as a singular performance curve and compared to the analytical and Thermal Desktop models. This final diagram is the culmination of the ACCS experimental work and demonstrates the overall behavior of the ACCS active thermal control technology as well as the validity of the developed design models.

10.2.1 Results: ACCS First Stage Temperature and Thermal Balance

The thermal balance of the ACCS system is a key aspect of the performance envelope. It indicates roughly what steady state temperature the system will reach for a given thermal load. Figure 10.7 below shows the ACCS thermal balance as a function of heat exchanger rejection temperature. The total power is corrected for the test cube's wire-line losses and thermal parasitics. The radiative power is calculated by taking the average surface temperature of the radiator and using Stephan Boltzmann's law to estimate power. The HX and radiator energy balances are found by using the heat capacity of the working fluid, Novec 7000, the flow rate of the fluid, and the temperature difference between the inlet and outlet of each to calculate the energy caried by the fluid out of the HX and into the radiator. The total power of the system matches quite well with the radiated power at lower temperatures and thermal loads. However, past 60 W they begin to diverge. This is most likely due to unaccounted-for thermal leaks within the system. These could include high-temperature radiative leaks from the HX, variations in the efficiency of the micro-pump, simplification of the electrical to thermal power assumption, and many others. It

was determined from analysis of the predictive analytical and numerical models, the energy balance between the HX and radiator, and the overall linearity of the system that the radiated power is most likely the most accurate of the two. Therefore, unless otherwise stated, the radiated power is referred to from here on out.

The fluid's capacitive energy balance indicates how much energy is absorbed internally to the heat exchanger and how much is deposited to the radiator or HX. These two values are nearly identical, only differing by a slight parasitic loss in the connecting fluid lines, see appendix. The HX and radiator energy balances do not always match that of the total power or radiated power. This is because when the radiator heater is active to simulate the space environment or add additional thermal load to the system, it only raises the radiator's temperature. It does not inject additional thermal power back into the ACCS system. If the radiator heater power was added to the HX and radiator energy balance, they would match that of the radiated power.

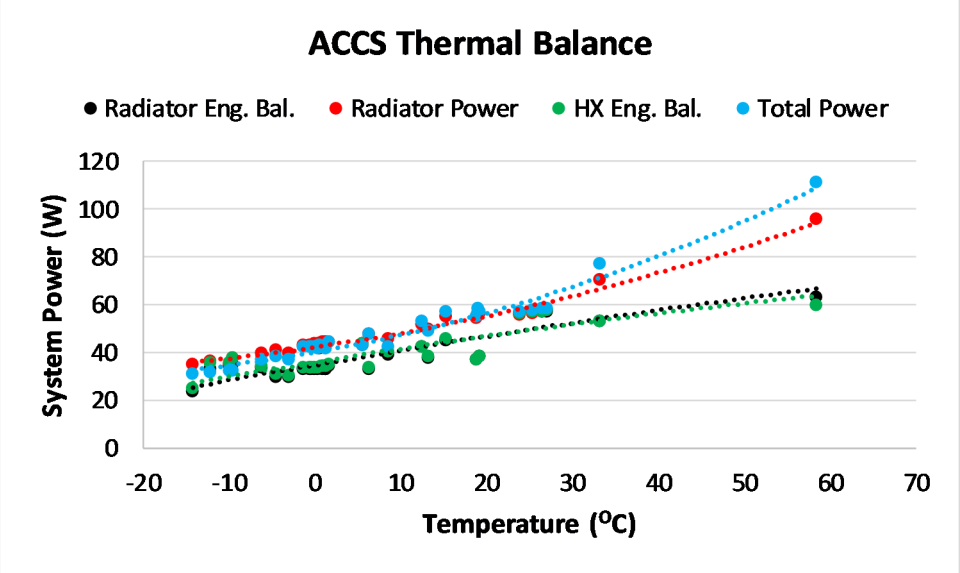

Fig. 10.7: ACCS Power profiles. Total corrected power, radiated power, and energy balance between the heat exchanger and radiator.

Figure 10.8 below compares the total corrected power and a percentage difference/error, assuming that the radiated power is correct. As can be seen, the two agree quite well

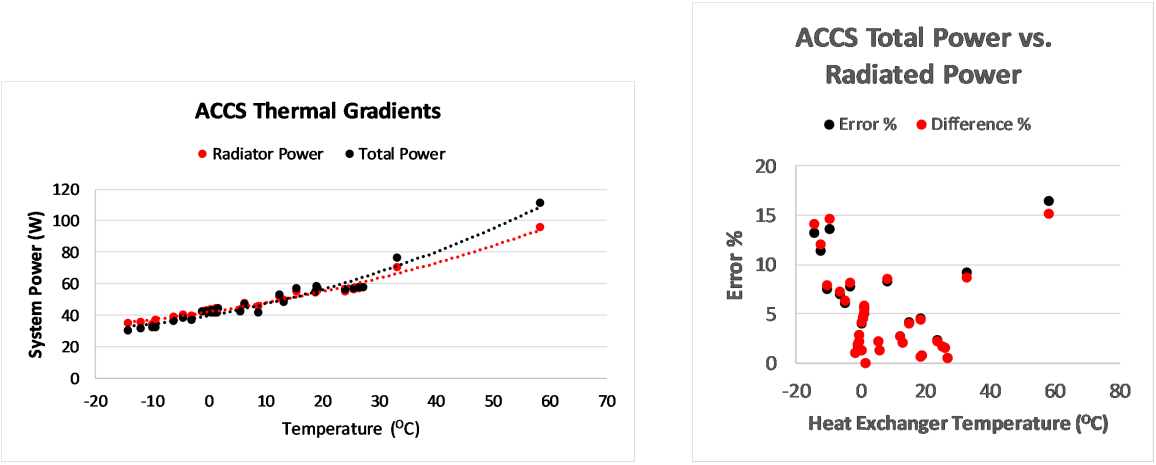

Fig. 10.8: ACCS total power to radiated power comparison and percentage difference.

below 60 W of thermal load and are often within 6% of each other for heat exchanger temperatures between 0 and 30 °C. This indicates that the difference between them is most likely due to power losses and parasitics within the system that become dominant at extreme temperatures.

The total ACCS thermal gradient is the difference in average temperatures between the heat exchanger and the radiator. This gradient dictates the maximum and minimum steady-state temperatures of the ACCS system. It also refers to the ACCS system's effective conductivity with respect to an ideal simplified model. The radiator is the coldest node of the ACCS system and serves as a base for the temperature profile. The flow rate (advective heat transfer) of the working fluid can be used to raise and lower the heat exchanger temperature, similar to a variable conductor, with respect to the radiator temperature. Figure 10.9 below shows the ACCS thermal gradient as a function of power and flow rate. The temperature gradient varies between 2 and 11 degrees C depending on the flow rate, with an average of ∼4 °C. It was determined after TVAC analysis that while the original test plan called for flow rates that varied between laminar and turbulent, the majority of the data collected was turbulent, with the very coldest and slowest flow rates falling within the transitional flow regime. This means the recorded thermal gradients are not nearly as wide as they would be with truly laminar flow. It also means that the full temperature control capability of throttling the pump's flow rate has not been demonstrated. The

performance of the ACCS system in laminar flow will be studied more extensively in future work. Thermal gradients also decrease with thermal load due to the decrease in fluid viscosity with fluid temperature and, therefore an increase in the Reynolds number and turbulence. The thermal gradients shown in figure 10.9 indicate that with the given flow rates, the ACCS heat exchanger temperature could be varied by roughly ∼10 °C with flow throttling. A much larger gradient could be created by toggling the flow on and off in some kind of bang-bang controller. However, a technique like that could easily lower the pump's lifespan.

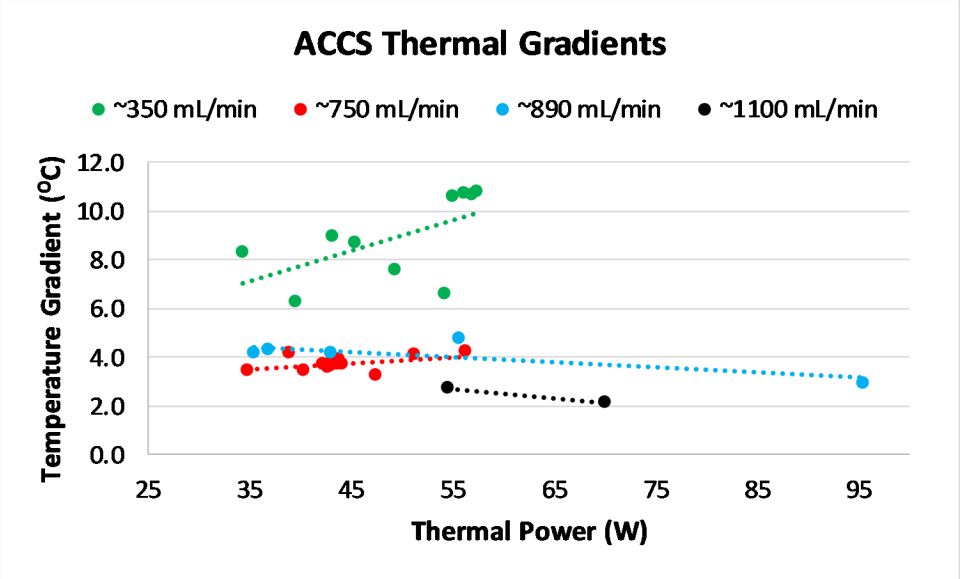

Fig. 10.9: ACCS thermal gradients sorted by flow rate.

The ACCS TVAC characterization tests pushed the 6U radiator and test-cube system to extremes, with heat exchanger temperatures varying between nearly -20 °C and 60 °C. The ACCS radiator was designed to reject nearly 60 W of thermal power while maintaining the heat exchanger rejection temperature around room temperature (25 °C). This can be seen below in figure 9. The radiator temperature forms the cold base of the system, while the fluid and heat exchanger temperatures vary on top of that. The effect of flow rate can be seen in figure 10.10 as variations in the difference between points; this is especially

noteworthy near the 55 W mark. A 3D figure of the ACCS system temperature gradient as a function of system power and flow rate is given below.

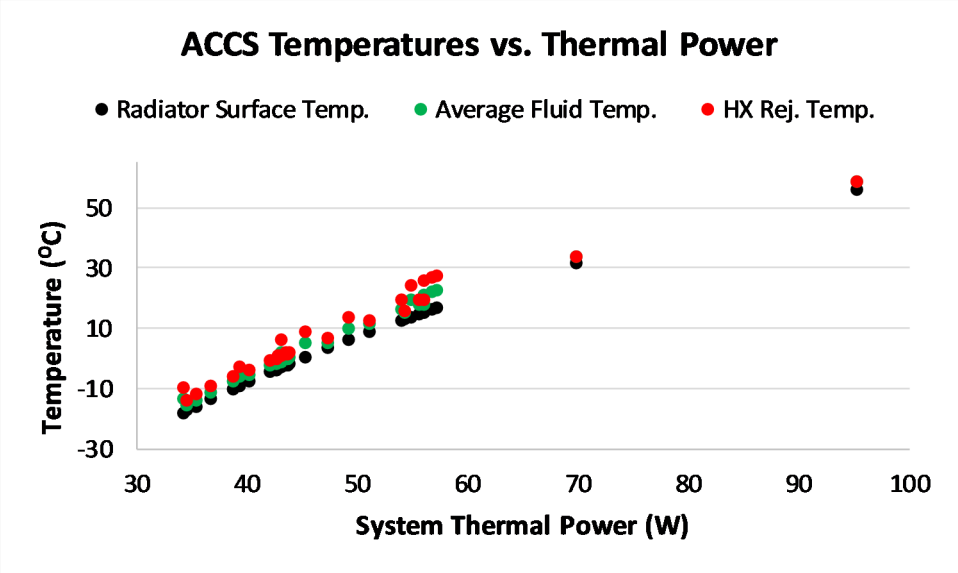

Fig. 10.10: ACCS average temperature profile as a function of system power.

Ultimately, the behavior of the ACCS systems is defined by the theories of single-phase heat exchangers. As such, it is fundamentally controlled by the temperature, system power, and flow rate. Therefore, a 3D representation is required to understand the complete behavior. Figure 10.11 below shows the ACCS heat exchanger rejection temperature as a function of both flow rate and system power.

This graph can be used to define the performance envelope of the ACCS system it can also serve as a design tool to predict the relative temperature of the ACCS. The linear behavior of each flow rate should be noted, rising from bottom right to top left. As thermal power increases, the temperature rises nearly linearly, forming a rising waterfall effect. Additional views of this 3D figure are given in the appendix. The error bars shown represent an average flow rate error of 3.85% and a temperature accuracy of approximately plus or minus 1 °C.

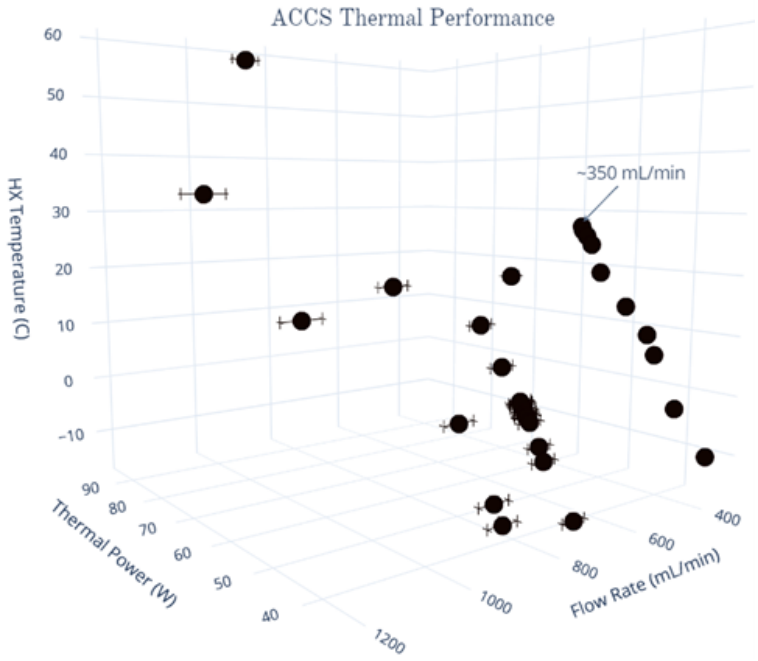

Fig. 10.11: ACCS Performance Envelope. Heat Exchanger temperature as a function of system power and flow rate.

10.2.2 Results: HX, Fluid, & Radiator Temperature Gradients

The Heat Exchanger, working fluid, and radiator each form a node within the ACCS system. Multiple temperature sensors were placed in and throughout all of these nodes for higher fidelity characterization. The heat exchanger featured six surface mount TC's, while the working fluid had four immersion TC's placed at the inlet and outlet of the heat exchanger and radiator. The radiator had five working TC's. Except for the fluid immersion probes, all TC's are small bead high-precision fast response Kapton surface mounts.

The heat exchanger has several thermal zones of interest. The first and arguably most important is the interface for the cryocooler, which serves as the rejection zone for all the thermal load generated by the cold tip, detector, parasitics, and cryocooler itself. All cryocoolers operate more efficiently if their operating environment is kept cool. The UAM HX has several fluid paths embedded directly under the cryocooler to efficiently transfer heat and help keep this zone at an ideal rejection temperature. The next zone of interest is the pump interface. Manifold mounted to the HX, the TCS M510 pump interacts with

the fluid directly. Therefore, all thermal energy generated by the brushless drive motor or generated through friction is deposited directly into the working fluid. Finally, the onboard heat exchanger heaters serve as variable pseudo-thermal loads for the ACCS system as well as guard heaters in case the working temperatures get too cold. Figure 10.12 below shows the temperature distribution across the entirety of the heat exchanger. The coldest temperature recorded was ∼-15 °C near the cryocooler interface and the outlet of the HX. The hottest was ∼74 °C on the surface of the HX heaters. The hottest thermal zone was the HX heaters, followed by the pump and cryocooler interface zones, which swapped depending on the power level for each active system. Overall, the coldest zone was the liquid-to-pump interface, which follows the given system gradients because that would be the closest to the fluid temperature in the HX system.

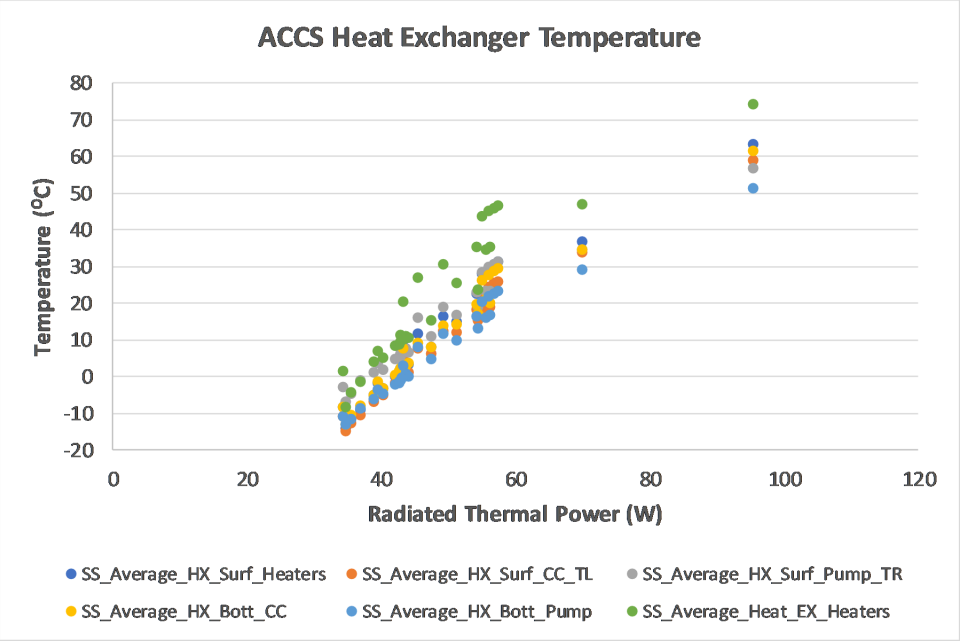

Fig. 10.12: ACCS heat exchanger temperature distribution. See figures 10.3, 6.16 & 6.17 for TC placement and nomenclature.

The working fluid temperatures do not vary internally as much as the rest of the ACCS system. In fact, the temperature difference between the inlet and outlet of the heat exchanger is nearly identical to that of the radiator. This follows the governing energy

balance theory. The majority of the thermal energy absorbed by the heat exchanger is directly transferred to the radiator. Therefore, in a closed-loop system, the temperature differences are nearly identical. Fluid temperatures increase with system load and vary somewhat with flow rate. Slight differences in the heat exchanger to radiator temperature indicate parasitic losses within the test cube tubing and structure. The ACCS working fluid (Novec 7000) is capable of reaching temperatures as low as -122 °C. However, because the radiator plate was not allowed to drop below -20 °C the fluid temperature did not exceed ∼-17 °C. A limitation of Novec 7000 is the heat of vaporization or the boiling point. Novec 7000 boils at only 34 °C. Therefore, under normal circumstances, the system temperature could not exceed this without first causing cavitation within the pump and also drastically increasing the system pressure, potentially to a bursting point. However, because the ACCS system is kept under pressure, the fluid's boiling point is raised to such an extent that the working fluid reached over 60 °C without boiling or causing significant cavitation losses within the pump. The ACCS working fluid temperature profile is shown below in figure 10.13. Plots of the Heat exchanger to radiator temperature gradients for the fluid are given in the appendix. HX and radiator inlet/outlet TC's are called out in figure 10.4 above.

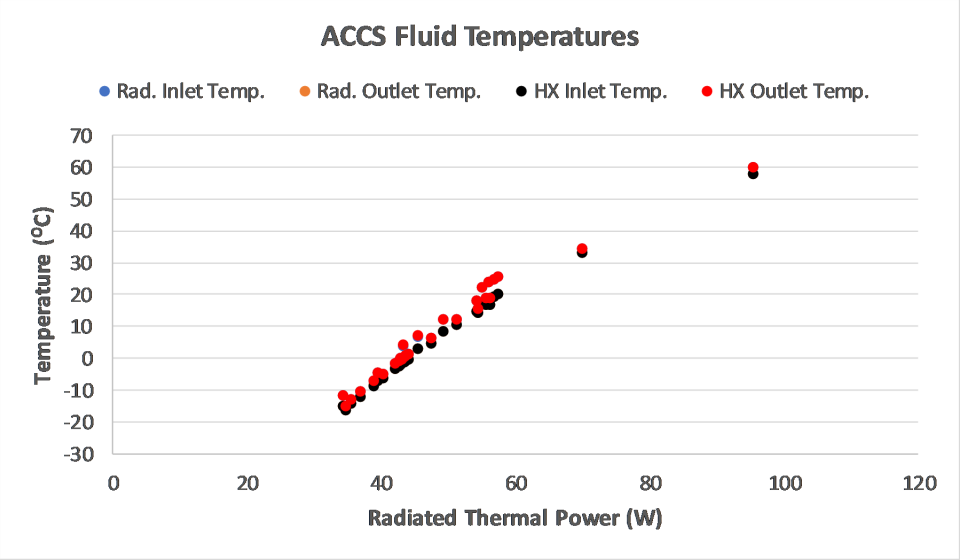

Fig. 10.13: ACCS Working fluid temperatures.

The temperature distribution of the radiator is critical and a direct indication of its efficiency. Ideally, the radiator will operate as an isothermal plate, unlike the heat exchanger, which will have naturally varying temperature zones defined by the payload and satellite bus. The conduction between fluid tubes will dictate the thermal gradients within the radiator. The radiator is additively manufactured from layers of 6061 Aluminum. Therefore, the light weighted webbing of the radiator, along with the placement of the fluid channels, should be designed to transfer as much lateral heat as possible. This can be done by finding the ideal distance between tubes and the thickness of the radiator. Due to the advantages of UAM, different materials can be welded together. Therefore, another option would be to include a thin copper layer to increase the 2D heat transfer within the radiator. The flow rate of the working fluid will set the convective heat transfer coefficient to the radiator. The temperature profile of the ACCS radiator is shown in figure 10.14. TC placement and terminology are given in figure 10.4 above. The radiator temperature gradient follows the flow rate, with the hot-to-cold gradient (right side of the radiator figure 10.4) following the flow path from TC #2 to TC #7 and the outlet surface temperature. Because of conduction, the inlet side of the radiator will always be hotter than the outlet side. To minimize this thermal gradient and improve the efficiency of the radiator the flow rate of the working fluid can be used to set an ideal convective transfer rate to the radiator. The radiator will perform better with fully turbulent flow. However, allowing the radiator to become highly laminar will once again improve the controllability of the ACCS system.

The temperature gradients across the radiator are shown in figure 10.15. A minimum gradient of $\sim$1 °C was measured as a product of a cold case (low thermal load) with high flow rates. On the other hand, when the system was pushed to the opposite extreme, the radiator gradient was nearly 6 °C despite the highest flow rate possible. This indicates that the radiator becomes less isothermal as system power increases. This also implies an ideal radiator size to thermal load (ratio) that will help ensure a near-isothermal and efficient radiator. Modeling combined with TVAC testing can be used to determine this correlation. The average gradient on the radiator is $\sim$3 °C. The vertical variation in the

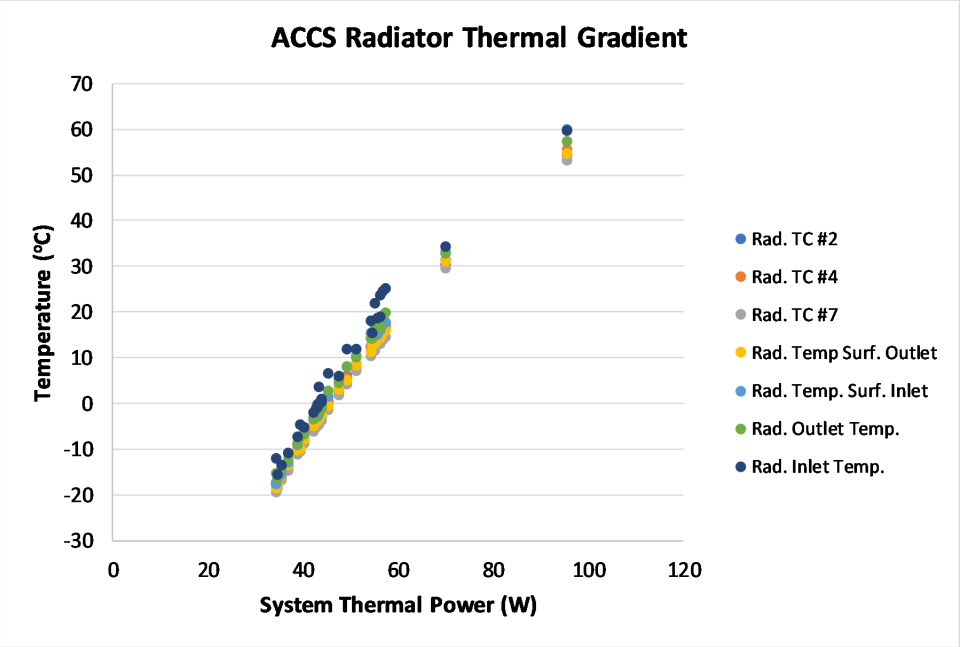

Fig. 10.14: ACCS radiator temperature distribution.

radiator temperature is caused by flow rate/convective heat transfer. However, it should be noted that for most flow rates and thermal power loads, the radiator maintained a lateral gradient of less than ~5 °C over a 6U (20 x 30 cm) size, which is a quite reasonable performance for a low-temperature single-phase heat exchanger system. A 3D model of radiator temperature gradient as a function of system power and flow rate is given in the appendix. Future radiator designs will be optimized for isothermal performance.

10.2.3 Results: TCS M510 Micro-Pump Performance

The TCS M510 centrifugal micro-pump is the heart of the first-stage ACCS MPFL heat exchanger. Therefore, its characterization is critical. The M510 is a brushless DC centrifugal pump with a "Canned" internal design that eliminates all dynamic seals. Canned pumps are highly reliable and ideal for use with the Novec 7000 family of working fluids. For the ACCS TVAC characterization, the flow rate, differential pressure, RPM, and power of the pump were characterized. It should be noted that all of the given results/equations can and should be used to predict pump behavior within the given ACCS or a similar system.

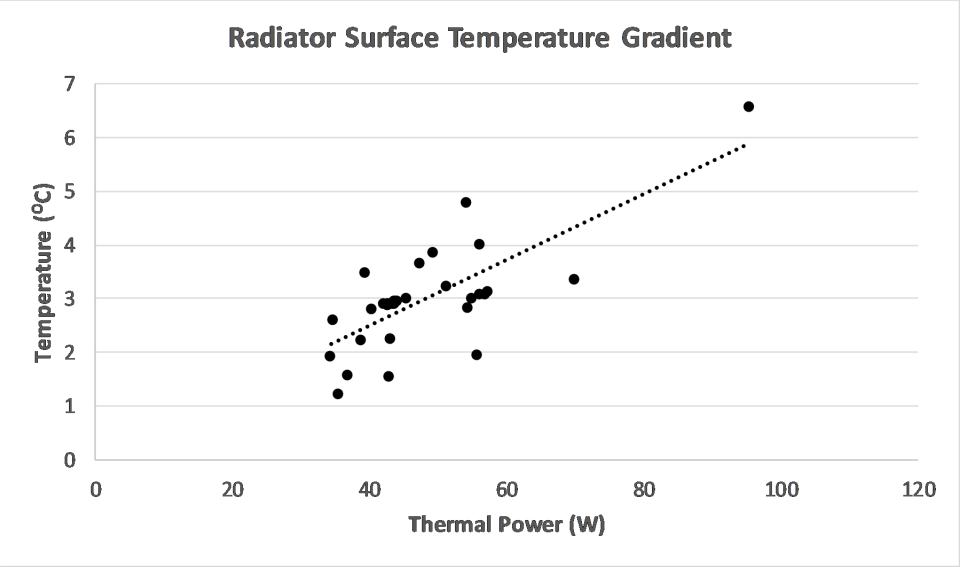

Fig. 10.15: Radiator Temperature Gradient as a function of system power. Vertical variations are indicative of flow rate variation.

However, they would not be valid in a drastically different scenario. Fluid path parameters such as flow path, hydraulic diameter, and overall pressure drop would need to be similar. As will be noted later in the Future Work chapter, a variety of TCS pumps are being fully characterized for use in future ACCS missions. These derived pump curves (affinity law curves) will describe the basic performance and behavior of the TCS pumps and can be used as a predictive model for any MPFL system. Those results will be reported at a later time. Figure 10.16 and 10.17 show the differential pressure of the M510 as a function of power and flow rate.

The ACCS micro-pump generates a forced flow for convective heat transport within the ACCS system. Several parameters govern this heat transfer. The first is the dimensionless Prandtl number. As explained in the Theory chapter, the Prandtl number is the ratio of momentum diffusion to thermal diffusion i.e. the ratio of the fluid velocity boundary layer to the thermal boundary layer. It relates how well a given fluid internally conducts heat compared to convection. For Prandtl numbers lower than one, internal thermal diffusion would dominate. For the ACCS system and Novec 7000 the Prandlt number is much higher than one. This indicates that convective momentum diffusion dominates the heat transfer of

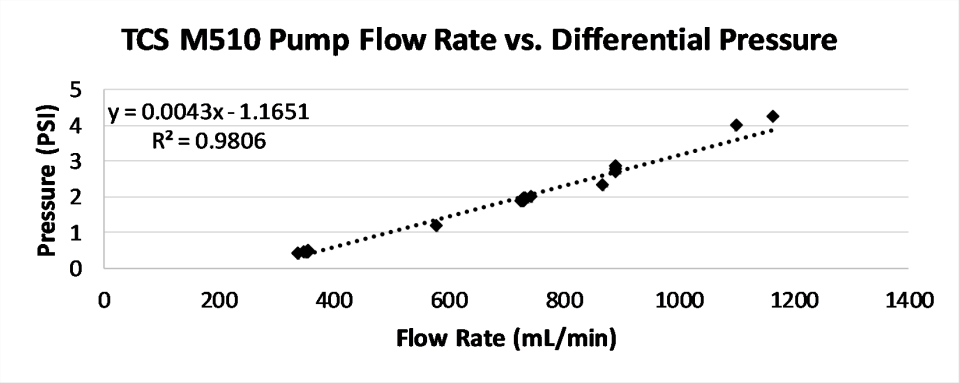

Fig. 10.16: TCS M510 pressure vs. flow rate.

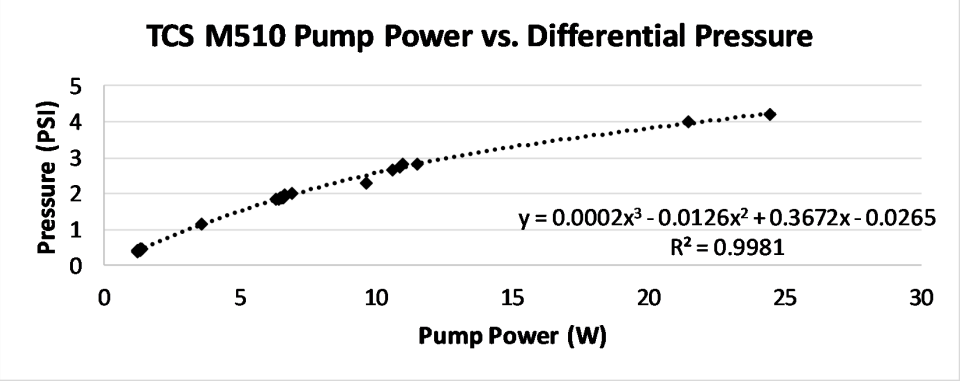

Fig. 10.17: TCS M510 Power vs. pressure.

Novec 7000. Figure 10.18 shows the Prandtl number for the ACCS system. The range varies from ∼10.5 to ∼3.2, with the trend decreasing with temperature. This is consistent with the thermal boundary layer of the internal fluid flow decreasing with increasing temperature.

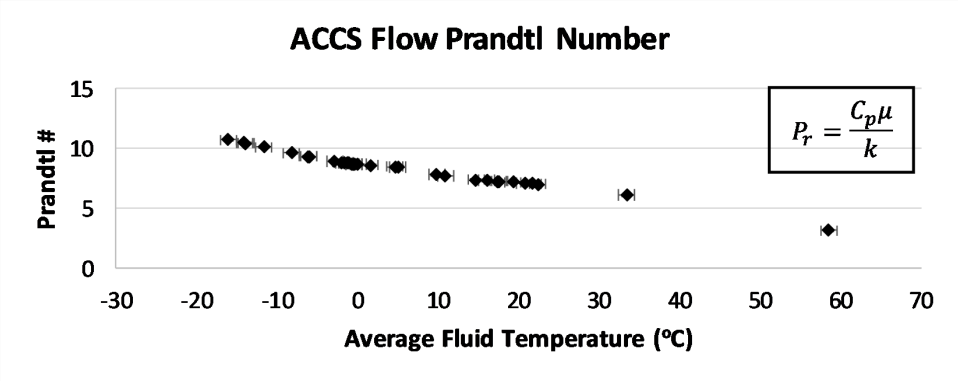

Fig. 10.18: ACCS Prandtl number.

The theory behind convective heat transfer is explained in detail in the Theory chapter. For the purposes of this discussion, the convective heat transfer coefficient is a measure of how much thermal power the working fluid can transfer to and from the HX/Radiator in terms of contact area and temperature gradient. The convective coefficient increases with the flow rate and is often quite large. The actual thermal energy transferred depends on the wetted surface area and length of the UAM flow tubes and the relative temperatures of the heat exchanger and radiator. For the ACCS system, this convective coefficient varies from less than 500 to nearly 1500 W/m^{2}K. Figure 10.19 below shows the experimentally determined convective coefficient for the ACCS MPFL.

Reynolds number is a dimensionless number (see theory chapter) that measures the relative turbulence of a given flow. Generally, for internal (enclosed) flows, Reynolds numbers below 2300 are considered laminar, while greater than 3000 (∼2300 nominal) are turbulent. Reynolds values between these are considered transitional flow in that they have aspects of both laminar and turbulent flow and can easily switch between. The specific Reynolds number of a given flow regime can vary depending on the nature of the flow. However, for the ACCS system with a non-circular (hydraulic diameter) internal flow, figure 10.20 shows

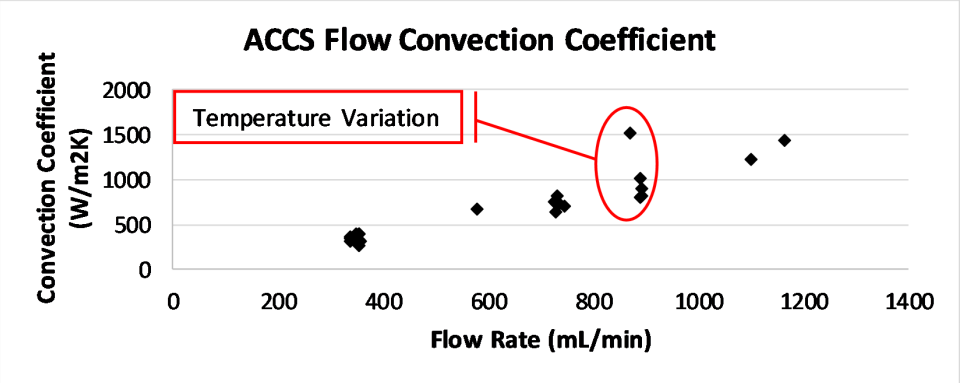

Fig. 10.19: ACCS convection coefficient

the recorded Reynolds numbers. After testing, it was determined that even at the lowest flow rate of ∼350 mL/min, the ACCS flow was transitional. Therefore, in terms of pump performance, the flow rates were never lowered to such an extent as to generate a truly laminar flow regime. From Figure 10.20, it can be inferred that a flow rate of less than ¡300 mL/min would have begun to transition to Laminar. The primary reason the flow rate was not lowered further during TVAC characterization was that the custom-built Venturi flow meter did not have sufficient resolution to read flow rates below ∼300 mL/min accurately. Future tests will further explore the heat transfer capabilities and thermal gradients of the ACCS system during laminar flow regimes. The variations in Reynolds numbers for a given flow rate are due to the relative temperature of the working fluid. The Reynolds number is sensitive to viscosity, which is highly temperature dependent for Novec 7000.

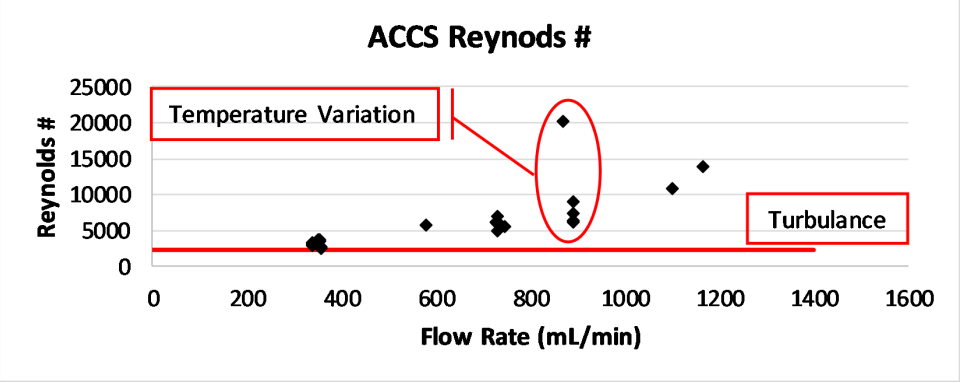

Fig. 10.20: ACCS flow reynolds number.

The temperature profile of the TCS M510 micro-pump is important because it is easy to overheat and burn out the brushless DC drive motor. However, because of the CANNED design of the pump and the fact that the working fluid is directly mixed inside the pump, it is very efficiently cooled and does not deviate far from the working fluid temperature, no matter the drive power. Figure 10.21 shows that the pump motor temperature follows fluid temperature quite closely. In fact, for higher thermal loads, the pump temperature is lower than the working fluid temperature. This is a critical correlation because it means that the average temperature of the pump in future missions can be used as a reasonable approximation for the average fluid temperature.

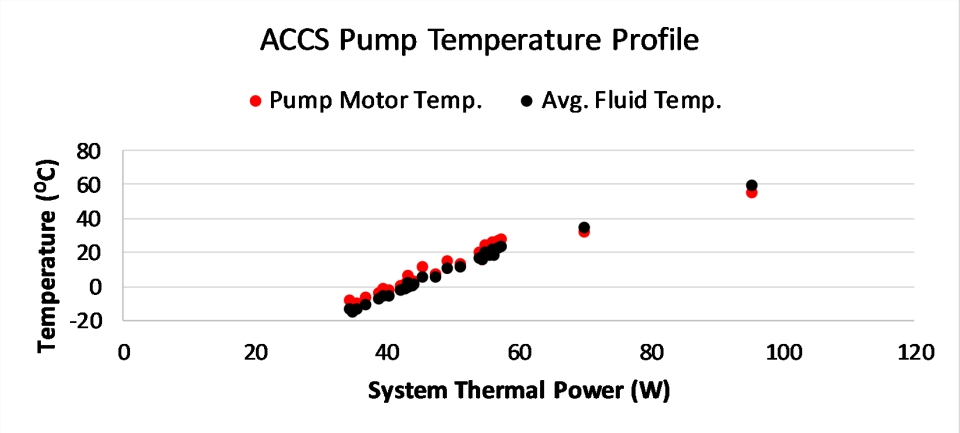

Fig. 10.21: TCS M510 pump motor temperature vs. working fluid temperature.

Centrifugal pumps follow the affinity or similarity laws. These laws state that flow rate, pressure ("Head") and power depend on the pump's RPM or speed and the impeller's physical dimensions, aka the impeller's diameter. See the Theory chapter for more information. This means that for pumps with the same impeller diameter, such as TCS pumps within the same family, a series of performance curves can be generated from experimental data that describe the various pump parameters vs. RPM. These curves can be used to predict the behavior of all M510 pumps but are limited, in this case, by the various testing ranges and limits of the ACCS TVAC characterizations. Figures 10.22 to 10.24 show the pump similarity curves for the M510 micro-pump. Power, differential pressure, and flow

rate as functions of pump RPM. Predictive curve-fit equations are also included. The similarity laws state that the flow rate is linearly related to the RPM, the differential pressure is related to RPM via a second-order polynomial, and the power through a third-order polynomial. This is confirmed by our results, as shown below. Note the accuracy of the R2 value for the regression fit.

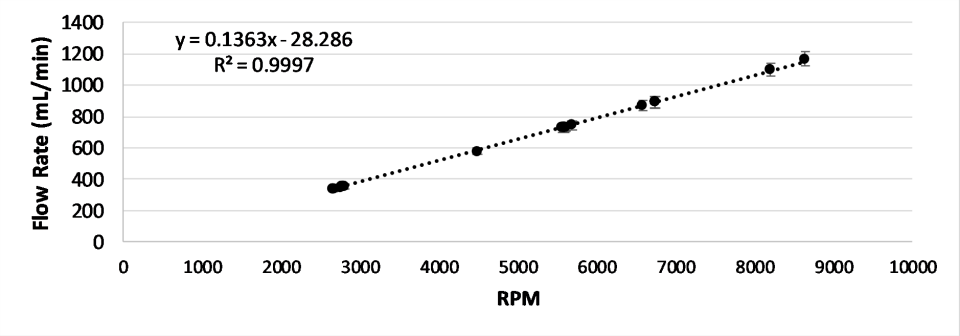

Fig. 10.22: First order similarity law: Linear ACCS flow rate vs. RPM

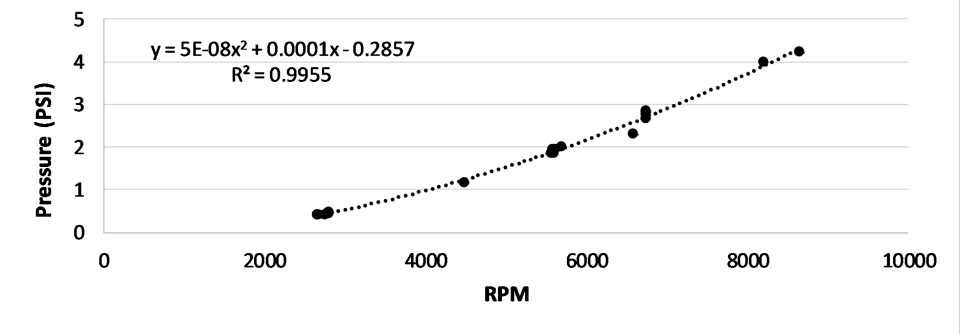

Fig. 10.23: Second order similarity law: Linear ACCS pressure vs. RPM.

10.2.4 Results: Cryocooler Performance

The ACCS Ricor K508N is a miniature, lightweight, tactical cryocooler. Based on a Stirling compression-to-expansion cycle. The basic operation and mechanisms of the K508N as an integral rotary compressor, are simple and robust, which makes it ideal for low-cost satellite missions. The K508N has a long flight history and has been proposed for many

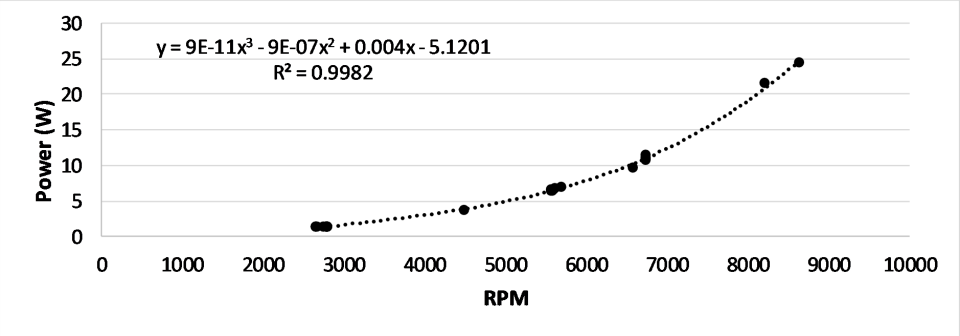

Fig. 10.24: Third order similarity law: Linear power vs. RPM.

CubeSat missions. It was selected for the ACCS system due to its size, low power, and wide thermal operational environment. The cold tip range was also attractive. The K508N is capable of reaching cold tip temperatures below 65 K with not-insignificant thermal loads. The Ricor K508N cryocooler forms the second stage of the ACCS system and directly cools the attached pseudo-instrument focal plane and detector. One of the ACCS system's main operational objectives is to provide an ideal thermal environment for the cryocooler. This allows the primary payload of the satellite to operate without thermal throttling. Thus, improving mission success.

The K508N operates between -40 °C and 85 °C with an ideal room temperature range of <30 °C. The K508N operation is governed by a dedicated internal controller, the Hyb-18. This controller monitors the cold tip setpoint through a balanced bridge feedback loop. The main operating modes of the cryocooler are cooldown, idling and steady state. During cooldown, the K508N can draw up to ∼15 W of power, while steady-state operation often drops below ∼5 W. The ACCS K508N power draw varies widely (∼6 W and ∼15 W) depending on rejection temperature and cold tip thermal load. Figure 10.25 below shows the power profile of the ACCS cryocooler as a function of the heat exchanger rejection temperature. The variation in the required power for a given rejection temperature, data point spread, is caused by thermal loading on the cold tip and set point temperature. The ACCS K508N draws slightly more power than is advertised by the vendor. This is most likely due to heat leaks into the system and the exact tuning of the particular unit.

The K508N cold tip is integrated with the compressor body and isolated from the

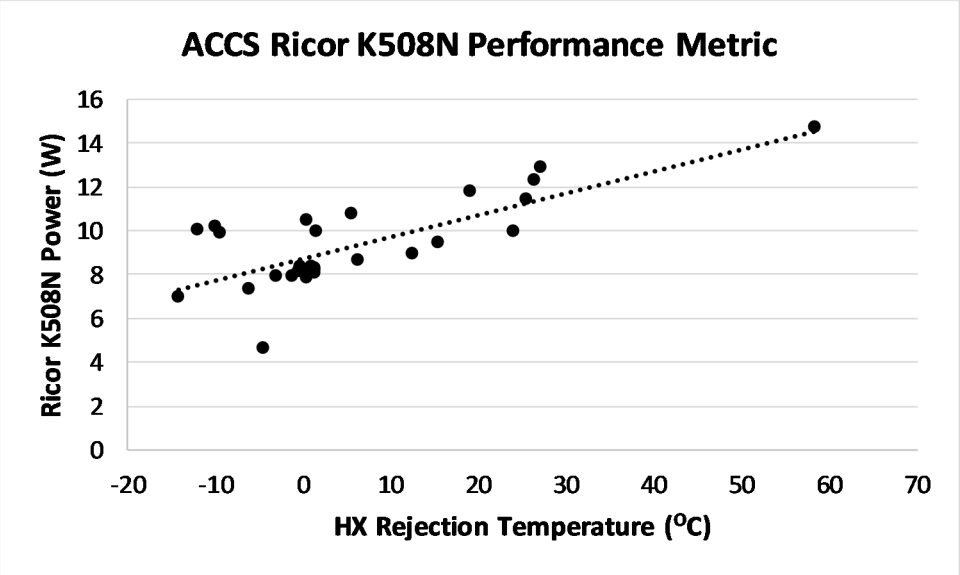

Fig. 10.25: ACCS Ricor K508N cryocooler performance: Power vs. environmental temperature.

environment by MLI. A series of Lakeshore DT-670 cryogenic temperature diodes are used to measure the cold tip temperature. Two in parallel for temperature readout (averaged) and a single diode tied in feedback with the K508N's onboard controller. For the September 2018 TVAC tests, the cold tip was set to ∼85 K, while the January 2019 tests used a more typical ∼115 K setpoint. Most CubeSat-based LWIR instruments require cooling to at least 120 K. The ACCS K508N cryocooler was stable and reliably held set point temperatures despite changes in rejection temperatures. Figure 10.26 shows the cold tip temperature as a function of cryocooler power broken down by thermal load and set point. As can be seen from the highlighted regions, the cold tip temperature did vary, based on thermal load, but was quite consistent when the only parameter changed was rejection temperature. The linear nature of the K508N control for the cold tip temperature is shown in figure 10.27.

The K508N has several thermal zones of importance. The first is the electric motor temperature, which will be the highest in the system due to the majority of the thermal energy of the cryocooler being generated there. The second is the compressor body, followed closely by the junction between the cold finger and the compressor body. This junction is where the thermal load lifted from the cold finger is deposited. The cryocooler motor

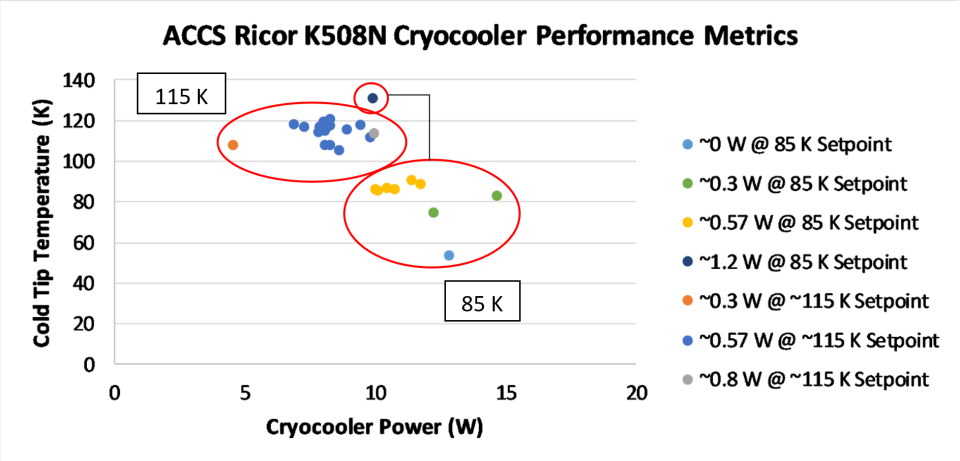

Fig. 10.26: ACCS Ricor K508N cryocooler performance: Cold tip temperature vs. cooler power.

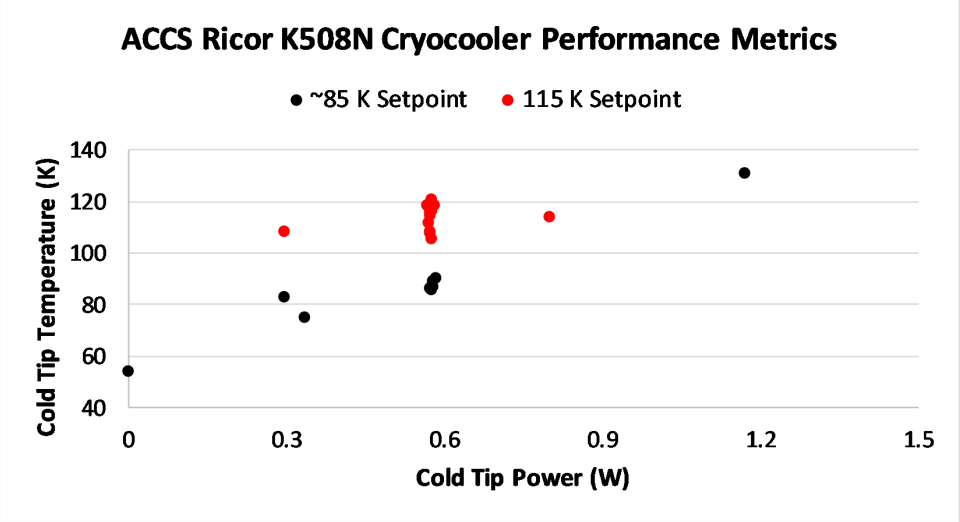

Fig. 10.27: ACCS Ricor K508N cryocooler performance: Cold tip temperature vs. cold tip power.

assembly exhibited some of the hottest temperatures recorded during the ACCS characterization. Reaching temperatures of ∼80 ^{o}C. This highlights the importance of designing the cryocooler thermal rejection system to lift heat from not only the mounting interface but the hottest thermal zone as well. Figure 10.28 below shows the temperatures of the various thermal zones of the K508N cryocooler during TVAC testing.

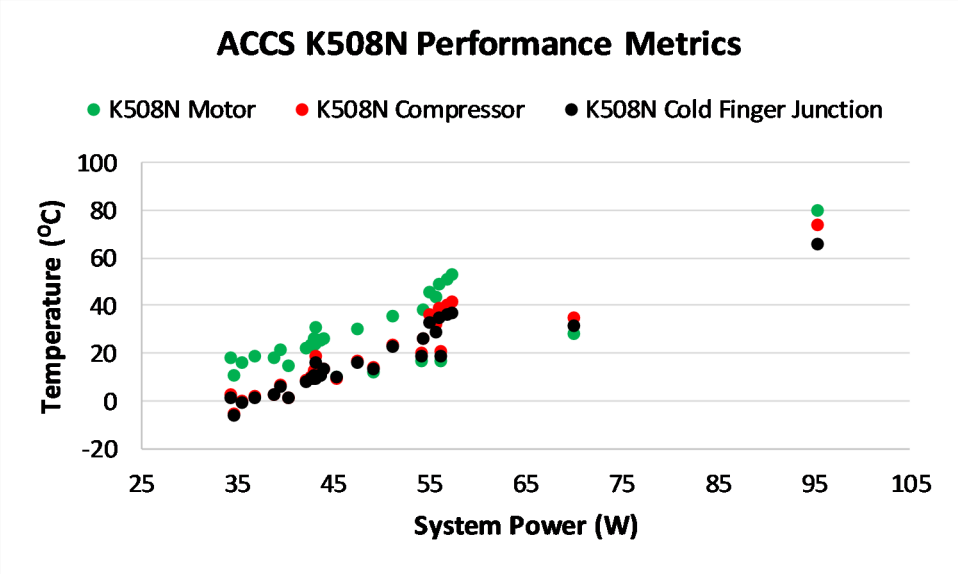

Fig. 10.28: ACCS Ricor K508N body temperature.

The K508N cold tip temperature is actually dependent on four separate variables. The set point, the cold tip thermal load, cryocooler power, and heat exchanger interface temperature. Therefore, to accurately represent this level of dependency, a sorted 3D plot is required. Figure 10.29 shown below, represent the ACCS cryocooler cold tip temperature as a function of all the given variables. Additional views are given in the appendix. The curves show that colder set points and higher thermal loads require more power from the cryocooler. Additionally, increasing the rejection temperature requires more power to maintain the set point. The effect of rejection temperature on cold tip temperature becomes more dominant at lower cold tip temperatures. This is consistent with cryocooler operational theory and a reason to maintain cooler rejection temperatures and minimize thermal loads on the cold tip. Ultimately, however, the ACCS cryocooler was more than capable of maintaining set

point temperatures with realistic thermal loads for a variety of rejection temperatures. The data also demonstrates that the first stage of the ACCS system formed an ideal thermal environment for the K508N.

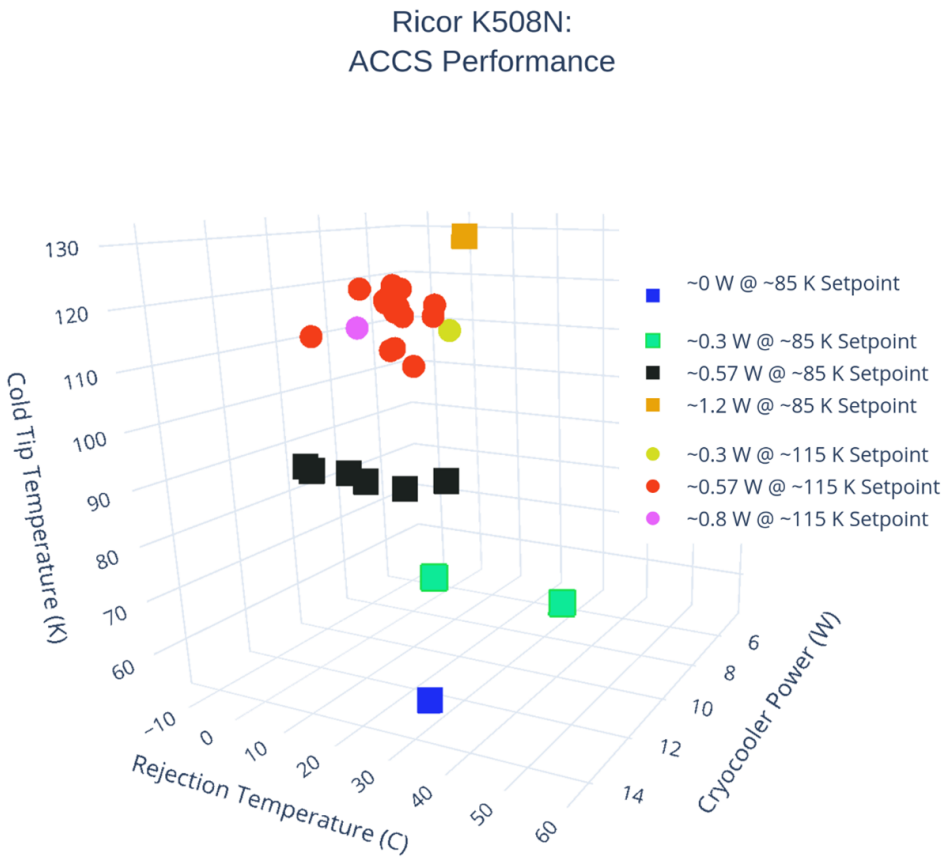

Fig. 10.29: 3D graph of the performance envelope of the ACCS Ricor K508n cryocooler.

10.2.5 Orbital Modeling

The ACCS is designed to operate within the orbital space environment. To demonstrate this capability and characterize the system's transient behavior, the ACCS underwent a series of simulated orbital cycles within the TVAC environment. Patch heaters placed on the radiator were used to simulate the space thermal load and eclipse cycle of the satellite. These simulations helped to raise the ACCS technology readiness level to ∼5 (TBR). The

thermal space environment consists of three primary external sources. The solar input, the planet IR-blackbody input, and the reflected light from the planet, aka the solar Albedo. These three sources vary widely depending on the satellite radiator design, orientation, and orbit. See the analytical modeling chapter for more information. For the ACCS TVAC orbital simulation, a typical near ISS orbit with a 90-minute period (30-minute eclipse) was selected. The environmental inputs were approximated from the analytical model, and the radiator heaters were set to match. Without a control algorithm, the radiator environmental loads were simply toggled on or off depending on the estimated orbital time. The ACCS guard heaters and pump flow rate were cycled in the same way to maintain the average temperature of the heat exchanger. In reality, the environmental thermal load would dynamically change throughout an orbit. Ideally, the built-in, currently under development, PID controller for the ACCS system would throttle the flow rate to compensate. However, that was not possible for these TVAC tests. Three separate orbital tests were performed for the September 2018 TVAC test. Only the last scenario is discussed here. The other two, which varied in terms of orbital load, guard heater response, and flow rate throttling, are described in the appendix.

The total system power was held, on average, at just above 60 W with a heat exchanger temperature of ∼30 °C. The radiator input was varied from ∼25 W to ∼8 W. This typically would result in a temperature change of 20 °C. However, because of the thermal inertia of the ACCS system, a change in temperature of only 8 °C (30 °C to 22 °C) was recorded on the heat exchanger. The pump was throttled from just over 800 mL/min to ∼350 mL/min. The pump power varied from ∼1.25 W to ∼10 W. Therefore, the net change in power was well over 20 W. Because of this large shift and the fact that the pump is capable of generating a differential change in temperature of between ∼7 to 8 °C at the same power level by throttling from 800 to 350 mL/min, the heat exchanger guard heaters were used to supplement power into the system. Throttling the flow rate raised the heat exchanger's temperature in response to the overall drop in system power due to the eclipse. However, without transitioning between off, laminar, and turbulent flow regimes and without an

integrated controller, the large power swings caused by the toggling of the radiator and the thermal momentum of the system made controlling the exact setpoint of the heat exchanger very difficult. The concept of compensating the orbital changes in environmental thermal loading with the ACCS system is demonstrated but will rely on future work to refine the concept. Figures 10.30 through 10.33 show the orbital simulation parameters for the ACCS system.

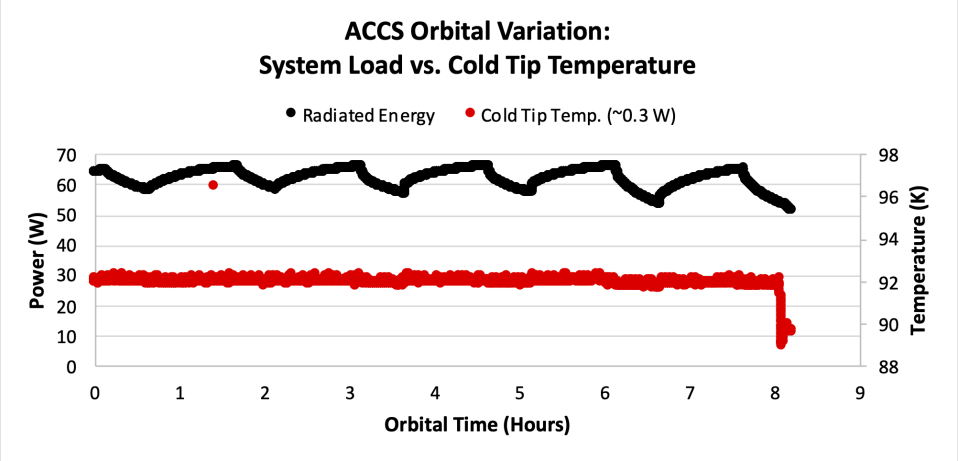

Fig. 10.30: ACCS orbital variation: Radiated energy & cold tip temperature as a function of total thermal load vs orbital time

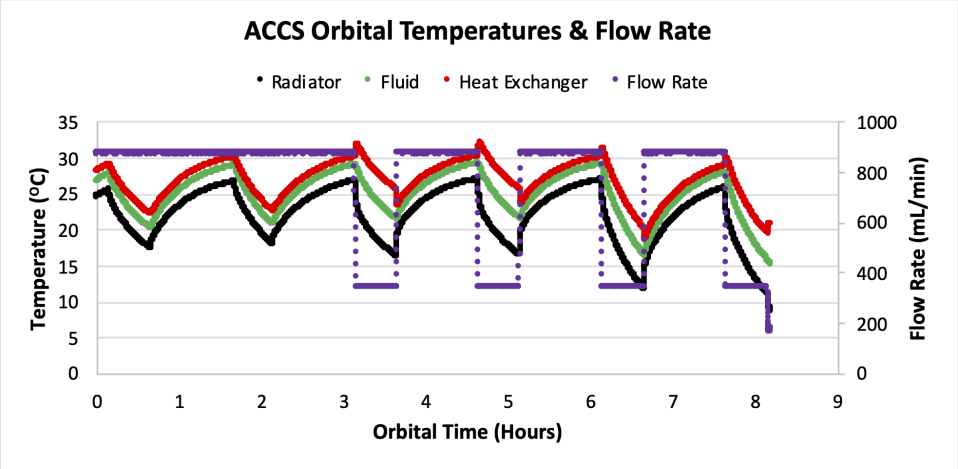

Fig. 10.31: ACCS orbital variation: System temperatures as a function of total thermal load vs orbital time.

The system power profile for the orbital simulation is given in figure 10.32, and the energy balance in 10.33. The radiated power of the radiator in red, figure 10.33, shows that the surface temperature of the radiator does not cool down enough to match the input power levels. This indicates that the system's thermal mass is large enough that it cannot cool down sufficiently during the 30-minute eclipse. During the solar illuminated period, howver, the time is sufficient to warm the radiator to a level that matches the thermal balance (power) of the system. The increase in HX temperature caused by the drop in flow rate is combatted by the radiator's rapid drop in power/temperature. These results highlight the importance of a dynamic PID controller for the ACCS system to account for these hysteresis effects. Figure 10.30 can be used as a design reference for future ACCS missions to predict overall system temperatures for a 6U deployed radiator. If a different radiator design is used, refer to the design tools of this research.

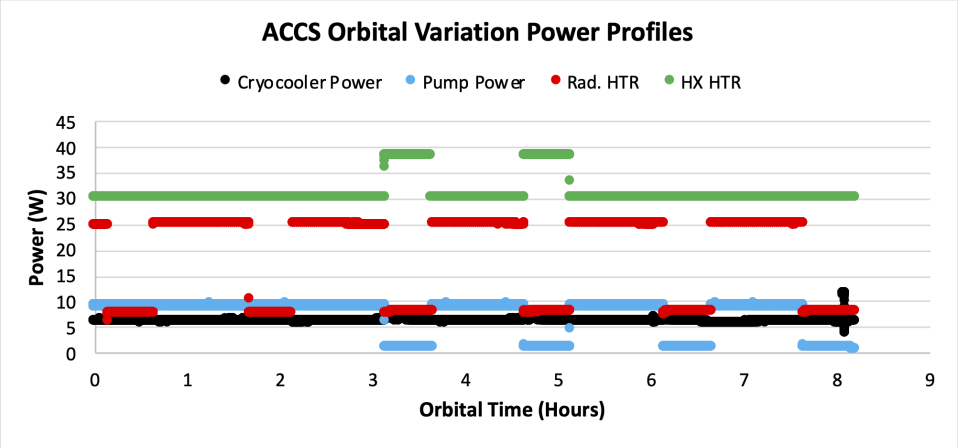

Fig. 10.32: ACCS orbital variation: Operational power profile as a function of total thermal load vs orbital time.

10.2.6 Results: Model Comparison

The final performance metric for the ACCS system is simply the rejection temperature vs. thermal load. This comparison represents how well the single-phase MPFL heat exchanger operates and what temperatures are required to reject a given thermal load. This

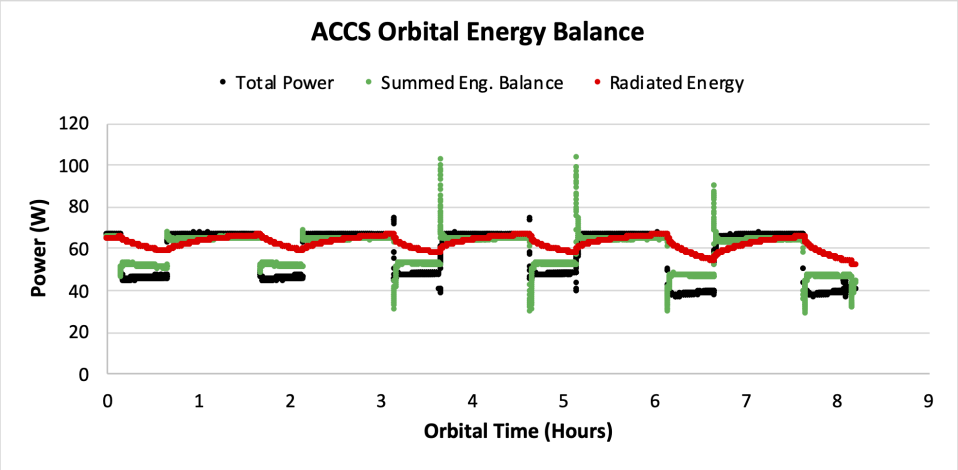

Fig. 10.33: ACCS orbital variation: System energy balance as a function of total thermal load vs orbital time.

data forms the family of ACCS system performance curves shown below in figure 10.34. Lower flow rates will result in higher temperatures. In fact, with enough testing, a whole set of curves can be derived. Two flow regimes can be distinguished from the data shown below; both are labeled and considered turbulent. A laminar curve would demonstrate a much steeper temperature vs. power curve.

The ACCS system is a novel active thermal control technology capable of meeting the thermal needs of a wide variety of satellite and space-born systems. As such, it requires a matching design methodology and a set of tools for rapid development. The analytical and numerical models presented in this dissertation are the beginnings of those tools. The analytical model was used in the preliminary design of the ACCS and helped to predict its behavior and performance. After TVAC characterization, the analytical and numerical models were compared to the experimental data. Each model agreed with the experimental results to a high degree. Figure 10.35 below shows a point-by-point comparison of the analytical and thermal desktop models to the collected experimental data. For each point, the data matched to approximately 0.5%. This is representative of a high level of accuracy and indicates that both the thermal desktop and analytical models are more than capable of predicting the behavior of active thermal control systems like the ACCS. As previously mentioned, because of the long processing times required by Thermal Desktop, only a

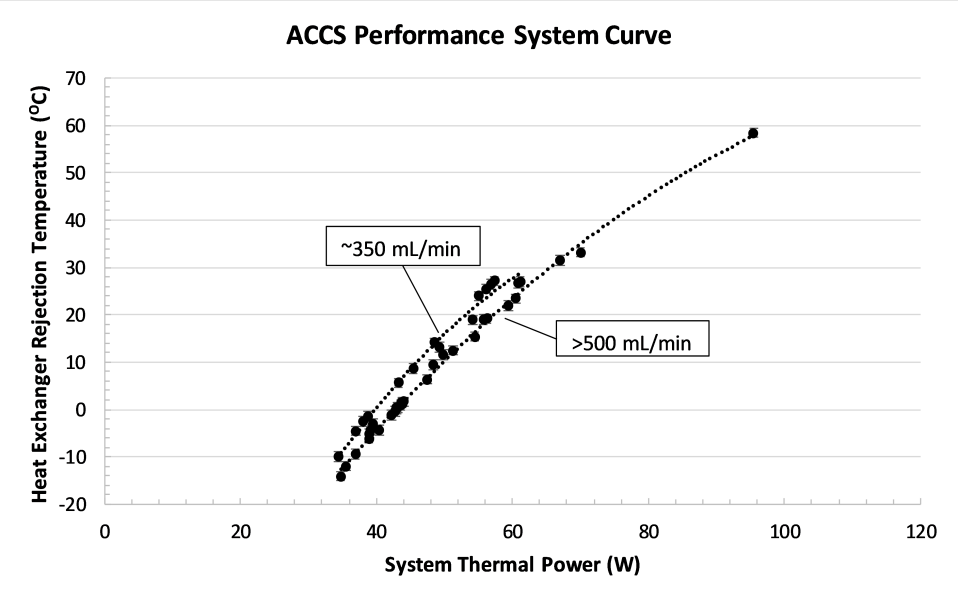

Fig. 10.34: Summary of results. ACCS performance curve, average heat exchanger temperature as a function of total radiated system power.

selection of numerical data points were analyzed. Figures 10.36 and 10.37 show the relative error for both the analytical and numerical models. The models below use radiated power. If the total corrected power is used, similar results are found with slightly larger errors, up to 6%, with an average of less than ∼2%. More information on these results can be found in the appendix for both the analytical and thermal desktop models.

10.3 Summary & Takeaways

Ultimately, the ACCS system has demonstrated a highly linear power vs. temperature response that is consistent with traditional thermal transfer theories. The ACCS can manage >60 W of thermal energy with an average heat exchanger temperature of <30 °C. This is a considerable improvement over conventional passive CubeSat systems. In fact, the ACCS was able to reject approximately ∼95 W of radiated thermal power (∼115 W of inputted power) at <60 °C. The ACCS has also successfully demonstrated the concept of temperature control via pump flow rate throttling. By throttling the working fluid between zero, laminar, transitional, and turbulent flow regimes, the temperature gradients within the ACCS system, aka between HX and radiator, could be reduced to as little as 2 °C. The

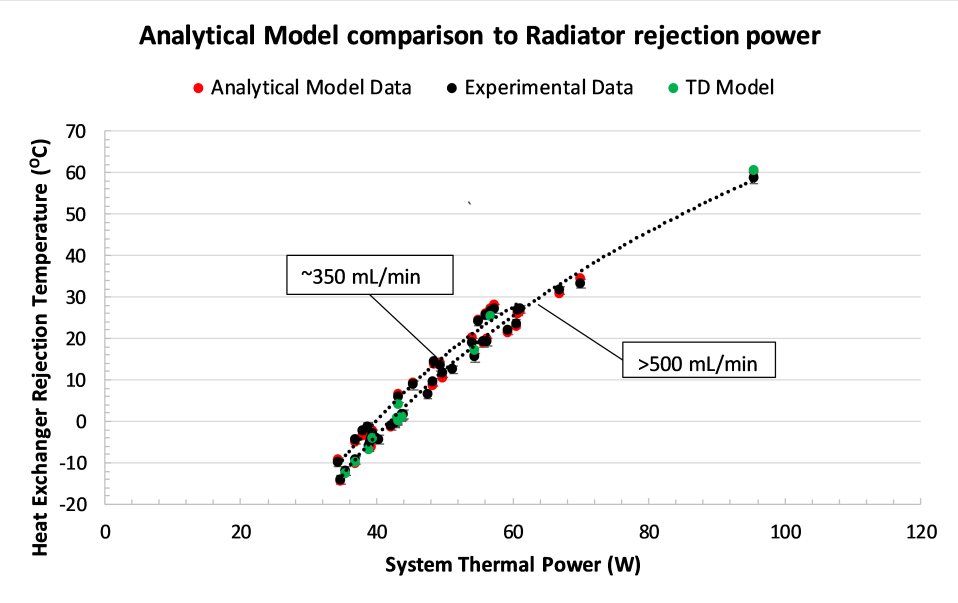

Fig. 10.35: Summary of results. Experimentally determined ACCS performance curve overlaid with predictive data from the ACCS analytical and numerical models.

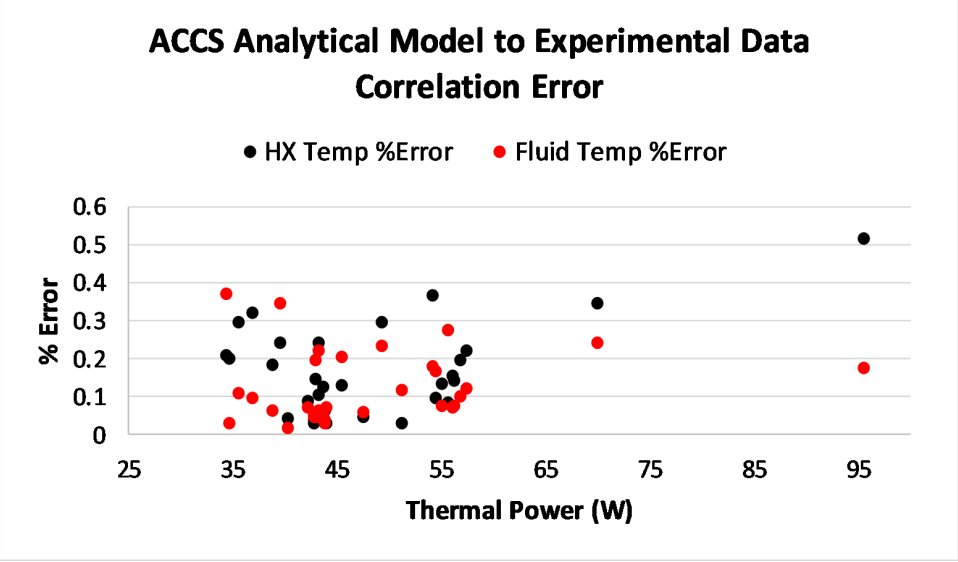

Fig. 10.36: ACCS experimental data vs. analytical model error

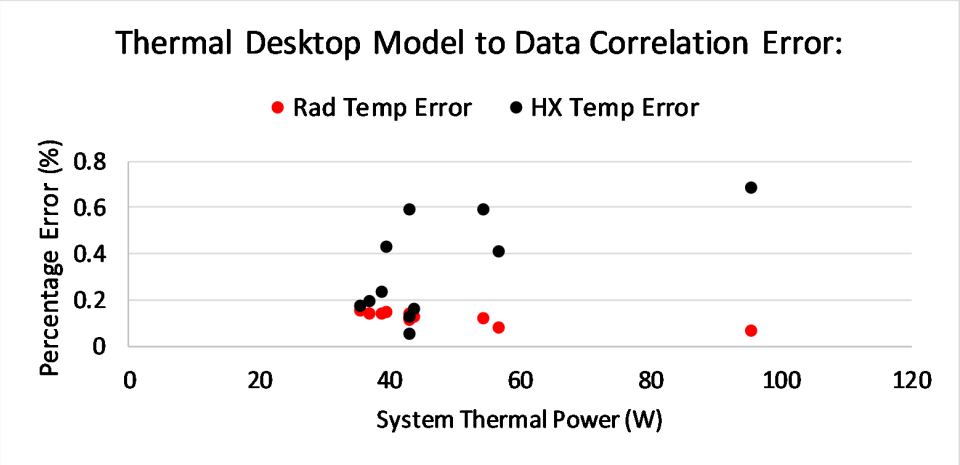

Fig. 10.37: ACCS experimental data vs. numerical model error

system also maintained an ideal thermal environment for the integrated miniature Ricor K508N cryocooler, as was demonstrated by the relative cold tip temperature stability as a function of varying thermal loads, flow rates, and orbital simulations. Finally, the ACCS technology was able to meet all of the given system-level requirements (Table 10.1) and, in many cases, meet or exceed the stated goals/objectives. This level of active thermal control will soon be necessary for advanced CubeSat missions. Future designs will improve and expand the ACCS technology's performance and capabilities.

CHAPTER 11

Future Work

The best way to predict the future is to create it

Abraham Lincoln

11.1 Introduction

As modern CubeSat technology continues to progress, mission requirements and improvements in high-density power generation and storage are driving a thermal management revolution. Passive technologies such as conduction and surface finishes are no longer sufficient to deal with growing power demands, and future missions will require advanced dedicated active thermal solutions. The ACCS technology is just such an active thermal subsystem for both bus and payload thermal management on CubeSats and Small Satellites. Targeted at high-power applications with strict requirements on temperature range, gradients, and stability, the Active CryoCubeSat is a truly novel contribution to this family of new thermal control technologies.

The ACCS is targeted at high-powered satellite bus systems such as antennas, onboard computing, and radar as well as payload-specific systems such as cryogenically cooled electro-optical detectors for IR instrumentation. Advanced CubeSat missions in Earth Science, Heliophysics, and deep space thermal management could also benefit from active thermal control. In fact, lunar orbit CubeSats and lunar rover missions are also being investigated as future applications for a system such as the ACCS. Practically, any mission that requires stable bus temperatures, thermal payload support, high-power thermal rejection, or operates in a difficult thermal environment will require active thermal control technology.

Pumped fluid loops are not new space technology, nor are integrated cryocoolers. In

fact, the Curiosity Mars rover features both. However, a miniaturized two-stage MPFL heat exchanger system like the ACCS that leverages additive manufacturing techniques such as UAM is both novel and unique. The ACCS is a two-stage, single-phase, closed-loop heat exchanger system capable of rejecting more than 100 W while maintaining stable system temperatures below ∼60 °C, within a 6U CubeSat form factor. As such, the ACCS is the first pumped fluid loop active thermal control technology designed specifically for CubeSat platforms and Small Satellite form factors. It is also one of the first thermal systems to specifically accommodate an integrated miniature tactical cryocooler and enable the operation of IR electro-optical system with a 100% duty cycle. Ultimately, the hope of the current research is that the ACCS system will be the beginning of a unique series of technologies that will shape the future of thermal control for small satellites.

11.2 Overview of Current Work

The ACCS system is novel in that a miniaturized single-phase mechanically pumped fluid loop heat exchanger system has never before been developed for Small Satellites. In addition, the ACCS system leverages modern and advanced manufacturing techniques. Specifically, the use of Ultrasonic Additive Manufacturing (UAM). This technology is unique and ideal for embedding fluid loops within mechanical structures. UAM allowed for the miniaturization and simplification of the ACCS system and the direct integration of the MPFL with the CubeSat structure. In addition, UAM allows for iterative design and rapid fabrication, both hallmarks of good systems engineering. Another unique aspect of the ACCS system is the dedicated support of integrated cryocoolers which will enable a new generation of electro-optical infrared instruments and payloads.

This research has succeeded in developing the ACCS active thermal control technology and increasing its TRL to ∼5 (TBR) through the development of a test bed prototype and GEVS TVAC characterization. Dedicated design tools, including an excel based analytical model for rapid design iteration and a numerical Thermal Desktop model for in-depth post-design analysis, were also successfully developed. Finally, a new systems engineering design methodology has been developed that will help to enable future technologies and

advanced Small Satellite missions. The original objectives of the ACCS grant, as given in the introduction of this work, are rewritten here, in Table 11.1, in terms of accomplished objectives.

#	Completed Objectives of the ACCS Research Program
1	1. Developed a miniaturized mechanically pumped fluid loop thermal control subsystem (ACCS) targeted at CubeSats and Small Satellites. 2. Characterized and demonstrated the ACCS in a relevant TVAC environment
2	1. Developed multifunctional structural-thermal components via Ultrasonic Additive Manufacturing (UAM) additive manufacturing 2. Fabricated and tested the ACCS dedicated heat exchanger and 6U radiator.
3	Demonstrated thermal accommodation of a cryocooler (CC) suitable for cryogenic instrumentation on a CubeSat
4	Developed analytical and numerical design tools for rapid iteration and in-depth analysis of ACCS systems.
5	Develop systems-based design methodologies and CONOPS for the rapid development of Active Thermal Control systems for Small Satellites

Table 11.1: Proposed & accomplished goals/objectives of the ACCS research.

The ACCS research project had limits in terms of time and funding. Several aspects would benefit from further work. First among these is a detailed micro-pump trade study and characterization effort. An aspect of the ACCS design that became quite clear early in the research was that, just like the size of the radiator or the design of the fluid channels, the type, size, and performance of the pump should be selected specifically for the application. Larger, more powerful pumps might be required for large systems or high-pressure drop scenarios, but the selected micro-pump can easily be overpowered in many situations. In fact, if the design calls for flow throttling, a pump that can transition from the laminar to

turbulent flow regimes for the given flow path and maintain those flows at less than 50-60% capacity would be ideal. Another aspect of The ACCS design that is important is the required pumping power. Very rarely is power on a CubeSat abundant, and any additional power the pump requires is generally injected right back into the closed-loop system as heat. Therefore, low-power pumps are highly desirable. Or at least pumps that do not waste power. Therefore, a future objective of the ACCS team is to build an on-bench pump characterization system and test each of the relevant TCS micro-pumps currently available, as well as any other suitable pumps. This characterization would be done over the full range of flow, power, and pressure and at extremes of temperature for each of the working fluids of interest. From this data, a series of pump curves could be derived that would enable future designers to down-select appropriate pumps and predict their behavior in any given ACCS design. Another topic of future research would be a numerical analysis of the ACCS deployed radiator and its interactions with the satellite structure. Currently, the ACCS design uses the simplifying assumption that the deployed radiator floats in space with no viewing interactions other than the planet and sun. This is of course, not true. A series of simple Thermal Desktop models could be created to model a variety of CubeSat shapes and sizes, including various solar array designs, and the view factor interactions of the radiator with these bodies could be determined. This view factor analysis would use the built-in Monte Carlo radiation ray tracing capabilities of TD. This would help to create a series of approximate curves and predictive equations that would not only indicate the ideal locations/angles for deployable radiators but also help designers to approximate the thermal loads and solar reflections that the satellite will impose on the radiator and ACCS system. The current working fluid, Novec 7000, is ideal in many ways. However, its low boiling/vapor pressure and chemical compatibility is not ideal. Therefore a more in-depth and updated trade study on currently available working fluids would be appropriate. In fact, the Novec line of fluids includes several promising choices with updated capabilities. Including Novec 7200. Other fluids that should be considered are Paratherm CR, Slytherm, silicone-based fluids, and the Galden and FC series of fluids. Similar to the pump selection,

the working fluid can and should be carefully selected for a given application. The current research was unable to fully explore, due to time and budget, the laminar flow regime of the ACCS system. This is obviously a very important aspect of the ACCS technology and will require more future work. If the current custom venturi flow meter could be replaced with one more sensitive to low viscosities and flow rates, then the ACCS test cube could be further characterized in the CSE TVAC chamber to explore the temperature control of toggling the flow on and off and from fully scaling the flow from a low to high Reynolds number. The TCS pumps should also undergo lifetime testing and failure mode analysis. An aspect of work that USU students are currently undertaking is developing an ACCS PID feedback control algorithm. USU students have used the January 2019 TVAC test data to create a preliminary PID control and feedback algorithm. These control loops are currently waiting to be tested on the ACCS system. Further development of these control algorithms will help the ACCS system to become autonomously controlled.

Finally, future projects should continue to develop analytical rapid design tools and Thermal Desktop numerical modeling for the ACCS system. These models should include transient 2D and 3D analysis, complex radiative heat transfer, orbital analysis, and complex, integrated satellite simulations.

11.3 Future Projects & Missions

The ACCS research was completed in 2019. However, this dissertation was not written until 2021 and published in 2022. During that time, a follow on Small Satellite Technology Partnership grant under the title Active Thermal Architecture was awarded to USU. This research was conducted from 2018 through 2021. At the time of writing this, a follow on flight opportunity was also awarded to USU and Orion Space Solutions of Colorado. Both of these "future" research projects are described in some detail below.

The Active Thermal Architecture (ATA) is a NASA SSTP grant awarded to Utah State University and the Jet Propulsions Laboratory. The primary objective of the ATA project was to create a flight-like ground-based prototype of the ACCS system. This included miniaturizing the ACCS system further to a sub-1U internal volume and developing a

deployable radiator system. The ATA project took this one step further and was able to develop a two-stage deployable tracking radiator. This was made possible through the development of a custom two-axis flexible rotary fluid joint. A novel radiator deployment mechanism was also developed, along with a stepper motor tracking system. The ATA two-stage active control system was integrated with a realistic 6U CubeSat bus, a PGS thermal strap, and a pseudo-electro-optical detector suspended in a novel 3D-printed Kevlar thread isolation mount. The ATA system also featured a series of passive vibration isolation technologies to ensure that any jitter caused by active components was not exported to the bus or payload. The ATA also underwent launch load vibration testing, benchtop deployment, and two separate TVAC characterization tests. One at USU upgraded TVAC facilities and the other as part of a technology demonstration at JPL's Environmental Testing Laboratory (ETL). More information on the ATA project can be found in these publications: [26, 134–143].

The Active Cooling for Multi-Spectral Earth Sensors (ACMES) project is a NASA technology demonstration funded by the Earth Science Technology Office (ESTO) under an InVEST grant. ACMES will start development in 2022 and is projected to launch in late 2024 or early 2025. The ACMES mission will consist of a one-year technology demonstration followed by a possible three-year scientific mission. ACMES will feature a 12U or 16U bus and a full-flight prototype of the ACCS/ATA active thermal control system. The ACCS/ATA will offer payload support to the Hyperspectral Thermal Imager (HyTi) instrument under development by the University of Hawaii. HyTi will demonstrate a high spectral long wave IR (8-10.7 µm) instrument featuring a no-moving parts Fabry-Perot interferometer and JPL's cryogenically cooled HOT-BIRD focal plane technology [144]. The HyTi mission will focus on the derivation of Landsat-like surface temperatures and will study volcanic sulfur dioxide and agriculture emissions [145]. The ACCS/ATA technology will serve as an active thermal control support subsystem for HyTi and will enable a 100% over-land duty cycle of the HyTI instrument, which would be impossible without an active cooling technology. ACMES will regulate payload temperature and provide thermal support

to the HyTi cryocooler and onboard computer. Other instruments included in ACMES are the student-led FINNIS and PLAD payloads [146, 147].

11.4 Long Term Objectives

Long term, the ACCS research teams hope to expand active thermal control technologies in several novel ways. The first would be to expand the heat transfer concept and mechanism to include two-phase thermal control. By allowing the working fluid to undergo a phase change, the thermal gradients within the system could be flipped. Allowing a smaller, hotter, more efficient radiator and lower internal temperatures. A two-phase system would also improve thermal control and temperature stability. However, two-phase systems are challenging and require the development of miniature, power-efficient compressors and thermal control valves. If successful, however, Small Satellite and CubeSat mission designers would have two unique and powerful active thermal control technologies to choose from and, when combined with traditional passive techniques such as heat pipes, would be a powerful set of tools. The current ATA deployable radiator is single-axis tracking, which allows for ideal view factors and a secondary thermal control for the ATA system (radiator view factor). However, future ATA missions would benefit from multi-axis tracking of the radiator and variable area radiators. This would create additional variables of control over the radiative power of the ATA system. These variable area radiators could include foldable radiators, high-efficiency radiators with integrated heat pipes, flexible thin material radiators, articulating deployable radiators, and multifunctional radiators.

CHAPTER 12

Conclusions

The ACCS project successfully developed an active thermal control system targeted at CubeSats and Small Satellite platforms. This technology was demonstrated in a relevant TVAC environment with a final net TRL of ∼5. In addition, the research team established a series of comprehensive systems engineering design methodologies and design tools to allow spacecraft engineers, mission designers, and scientists to tackle spacecraft thermal control from a proactive viewpoint rather than as an afterthought. The future of the ACCS will be to raise the overall technology to TRL 7 and beyond. This will involve refining and optimizing the various technologies and concepts of the ACCS and expanding active thermal control to two-phase systems and beyond. It is the ultimate goal of spacecraft thermal control engineers to achieve end-to-end thermal control of satellites and to enable spacecraft capabilities to operate in the toughest of environments. To achieve this objective, many new technologies will need to be developed along with design tools and systems engineering methodologies. In the end, technology such as the ACCS, ATA, and ACMES hope to enable advanced missions and a new era of Small Satellites.

REFERENCES

[1] C. B. VanOutryve, "A thermal analysis and design tool for small spacecraft," Master's thesis, Utah State University, San Jose State University, 2008.

[2] Fabrisonics. (2022) 3d printing metal without melting? [Online]. Available: https://fabrisonic.com/technology/

[3] L. Martin. (2022) Lm pulse tube cryocooler. [Online]. Available: https://www.lockheedmartin.com/en-us/news/features/2015/clear-vision-optics.html

[4] NASA. (2015) Nasa technology roadmap: 2015. [Online]. Available: https://www.nasa.gov/offices/oct/home/roadmaps/index.html/

[5] Various, *The CubeSat Handbook*. AP Academic Press, 2021.

[6] Wikipedia. (2022) Cubesat. [Online]. Available: https://en.wikipedia.org/wiki/CubeSatHistory

[7] E. Howell. (2018) Cubesats: Tiny payloads, huge benefits for space research. [Online]. Available: https://www.space.com/34324-cubesats.html

[8] R. L. S. et al, "Interplanetary cubesats: Opening the solar system to a broad community at lower cost," *Journal of Small Satellites*, 2012.

[9] Wikepdia. (2022) Lunar icecube. [Online]. Available: https://en.wikipedia.org/wiki/LunarIceCube

[10] N. GSFC. (2022) Lunar ice cube. [Online]. Available: https://nssdc.gsfc.nasa.gov/nmc/spacecraft/display.action?id=L-ICECUBE

[11] J. P. Laboratory. (2018) Marco. [Online]. Available: https://www.jpl.nasa.gov/missions/mars-cube-one-marco

[12] N. S. S. S. Exploration. (2018) Marco: Mars cube one. [Online]. Available: https://solarsystem.nasa.gov/missions/mars-cube-one/in-depth/

[13] B. C. Technologies. (2022) Xb6 spacecraft. [Online]. Available: https://storage.googleapis.com/blue-canyon-tech-news/1/2022/04/BCTDataSheetSpacecraftXB6.pdf

[14] M. Design. (2022) Hawk solar arrays. [Online]. Available: https://mmadesignllc.com/products/solar-arrays/

[15] N. S. Institute. (2021) Nasa: State-of-the-art of small spacecraft technology. [Online]. Available: https://www.nasa.gov/smallsat-institute/sst-soa

[16] NASA. (2021) Nasa: State-of-the-art of small spacecraft technology: 7.0 thermal control. [Online]. Available: https://www.nasa.gov/smallsat-institute/sst-soa/thermal-control

[17] Ricor. (2022) K508n. [Online]. Available: https://www.ricor.com/products/k508n/

[18] B. Moshe and A. F. et al, "Ricor's k508n highly reliable integral rotary cryogenic cooler," *Ricor Online*, 2022.

[19] Wikipedia. (2022) Ultrasonic consolidation. [Online]. Available: https://en.wikipedia.org/wiki/Ultrasonicconsolidation

[20] NASA. (2015) Nasa technology roadmaps ta 14: Thermal management systems. [Online]. Available: https://www.nasa.gov/sites/default/files/atoms/files/2015nasatechnologyroadmapsta14thermalmanagementfinal.pdf

[21] S. Selvadurai, A. Chandran, and D. Valentini, "Challenges involved in implementing pumped fluid loop thermal control systems in high power nano and microsatellites," *International Conference on Environmental Systems*, 2021.

[22] P. B. Anthony D Paris and G. Birur, "High temperature mechanically pumped fluid loop for space applications — working fluid selection," *SAE Transactions*, vol. 113, pp. 892–898, 2004.

[23] T. v. d. B. e. a. J. van Es1, "Mini mechanically pumped loop modelling and design for standardized cubesat thermal control," *International Conference on Environmental Systems*, 2020.

[24] A. Ghosh and D. B. et all, "Cubesat active thermal control via microvascular carbon fiber channel radiator," *The Small Satellite Conference*, 2017.

[25] P. Hawaii. (2022) Epet 400: Spacecraft mission design. [Online]. Available: https://pressbooks-dev.oer.hawaii.edu/epet302/chapter/8-6/

[26] B. Mattos, L. Anderson, R. Christenson, and C. Swenson, "The active cryocubesat project: System modeling and control design," *SmallSat Archives*, 2021.

[27] NASA. (2022) The cubesat standard. [Online]. Available: https://www.cubesat.org/about/

[28] E. Mabrouk. (2015) Nasa: What are smallsats and cubesats. [Online]. Available: https://www.nasa.gov/content/what-are-smallsats-and-cubesatsf

[29] G. Nikolovska. (2022) What are cubesats and other small satellites? [Online]. Available: https://www.nasa.gov/content/what-are-smallsats-and-cubesatsf

[30] P. Labs. (2022) Innovation, iteration, and automation. [Online]. Available: https://www.planet.com/company/approach/

[31] J. P. Laboratory. (2018) Rain cube. [Online]. Available: https://www.jpl.nasa.gov/missions/radar-in-a-cubesat-raincube

[32] UniBap. (2021) Nasa hyti: Unibap. [Online]. Available: https://unibap.com/en/our-offer/space/projects/hyti-mission/

[33] F. Bruhn. (2022) Unibap ix 10 and ix 5. [Online]. Available: https://unibap.com/en/

[34] Y. A. Cengel and M. A. Boles, *Thermodynamics and Engineering Approach*. McGraw Hill, 2008.

[35] Incropera, Dewitt, Bergman, and Lavine, *Fundamentals of Heat and Mass Transfer*. John WIley and Sons, 2007.

[36] S. Struck. (2022) Conduction, convection, and radiation – 3 modes of heat transfer. [Online]. Available: https://sciencestruck.com/3modes-of-heat-transfer-conduction-convection-radiation:text=Modes20of20Heat20Transfer20120Conduction.20E2978F20Conduction,420Heat20Transfer20Co-efficient.20...20520Applications.20

[37] W. Conduction. (2022) Thermal conduction. [Online]. Available: https://en.wikipedia.org/wiki/Thermalconduction

[38] W. Convection. (2022) Convection. [Online]. Available: https://en.wikipedia.org/wiki/ConvectionMechanisms

[39] W. Radiation. (2022) Thermal radiation heat transfer. [Online]. Available: https://en.wikipedia.org/wiki/Thermalradiation

[40] K. Academy. (2022) What is the first law of thermodynamics? [Online]. Available: https://www.khanacademy.org/science/physics/thermodynamics/laws-of-thermodynamics/a/what-is-the-first-law-of-thermodynamics

[41] A. A. Science. (2022) Second law of thermodynamics. [Online]. Available: https://www.allaboutscience.org/second-law-of-thermodynamics.htm

[42] W. Advection. (2022) Advection. [Online]. Available: https://en.wikipedia.org/wiki/Advection

[43] W. M. Transfer. (2022) Thermal mass transfer. [Online]. Available: https://en.wikipedia.org/wiki/Thermalmass

[44] Carslaw and Jaeger, *Conduction of Heat in Solids*. Oxford At The Clarendon Press, 1959.

[45] W. Kays, M. Crawford, and B. Weigand, *Convective Heat and Mass Transfer*. McGraw Hill, 2005.

[46] J. Howell, M. P. Menguc, and R. Siegel, *Thermal Radiation Heat Transfer*. CRC Press, 2016.

[47] CRTech. (2022) Thermal desktop. [Online]. Available: https://crtech.com/videos/welcome-thermal-desktop

[48] R. S. Web. (2022) Design of the first artificial satellite of the earth. [Online]. Available: http://www.russianspaceweb.com/sputnikdesign.html

[49] C. Tate. (2013) International space station's cooling system: How it works (infographic). [Online]. Available: https://www.space.com/21059-space-station-cooling-system-explained-infographic.html.

[50] R. Galvez. (2022) The space shuttle and its operations. [Online]. Available: https://www.nasa.gov/centers/johnson/pdf/584722main_Wings-ch3a-pgs53-73.pdf

[51] S. Gribben. (2018) The parker solar probe. [Online]. Available: https://solarsystem.nasa.gov/missions/parker-solar-probe/in-depth/text=What20is20Parker20Solar20Probe,the20Sun20than20any20spacecraft.

[52] NASA. (2022) Webb space telescope. [Online]. Available: https://webb.nasa.gov/

[53] ——. (2022) Webb inovations: Infrared detectors. [Online]. Available: https://webb.nasa.gov/content/about/innovations/infrared.html

[54] NASA-JPL. (2022) Webb innovations: Cryocooler. [Online]. Available: https://webb.nasa.gov/content/about/innovations/cryocooler.html

[55] NASA-Northrop-Grumman. (2022) Webb innovations: Sunshield. [Online]. Available: https://webb.nasa.gov/content/observatory/sunshield.html

[56] J. E. Keese, "Spacecraft thermal control systems," *Online Lecture*, 2022.

[57] D. G. Gilmore, *Spaceccraft Thermal Control Handbook*. Aerospace Press, 2002.

[58] M. Donabedian, *Spaceccraft Thermal Control Handbook*. Aerospace Press, 2002.

[59] TWI. (2022) At what temperature do conventional electronics packages fail? [Online]. Available: https://www.twi-global.com/technical-knowledge/faqs/faq-at-what-temperature-do-conventional-electronics-packages-fail

[60] Various, *Space Mission Engineering: The New SMAD*. Englewood Cliffs, NJ: Prentice-Hall, 2011.

[61] V. L. Pisacane, *Fundamentals of Space Systems*. Oxford University Press, 2005.

[62] P. Fortescue, G. Swinerd, and J. Stark, *Spacecraft Systems Engineering*. John Wiley and Sons, 2011.

[63] Various, "Satellite thermal control engineering," *ESA SME 2004*, 2004.

[64] A. Kashani, J. Maddocks, F. Nellis, and Y. Gianchandani, "Technologies for cooling of large distributed and deployable loads," *SPIE*, vol. 6678, 2007.

[65] V. L. Pisacane, *The Space Environment and Its Effects on Space Systems*. AIAA, 2008.

[66] J. M. Palmer, "The measurement of transmission, absorption, emission, and reflection," *University of Arizona*, 2022.

[67] F. E. Swalley, "Thermal radiation incident on an earth satellite," *NASA*, 1962.

[68] I. Martinex, "Spacecraft thermal modeling and testing," *Isidoro Martinez*, 2016.

[69] OReilly. (2022) Prevost's theory of exchanges. [Online]. Available: https://www.oreilly.com/library/view/heat-and-thermodynamics/9789332511231/xhtml/ch12sec3.xhtml

[70] P. B. et al, "Mechanically pumped fluid loops for spacecraft thermal control: Past, present and future," in *TFAWS*, Oct. 2004.

[71] W. S. Janna, *Design of Fluid Thermal Systems*. PWS Publishing, 1998.

[72] V. P. D. Technologies, "Mechanically pumped fluid loops: Components and systems for space applications," *TFAWS*, 2012.

[73] Boing. (2022) Active thermal control system (atcs) overview. [Online]. Available: https://www.nasa.gov/pdf/473486mainissatcsoverview.pdf

[74] P. Bhandari and G. B. et al. (2022) Performance of the mechanically pumped fluid loop rover heat rejection system used for thermal control of the mars science laboratory curiosity rover on the surface of mars. [Online]. Available: https://trs.jpl.nasa.gov/bitstream/handle/2014/44145/13-2330_A1b.pdf?isAllowed=ysequence=1

[75] P. Bhandari and Gajanana. (2022) Performance of the mechanically pumped fluid loop rover heat rejection system used for thermal control of the mars science laboratory curiosity rover on the surface of mars. [Online]. Available: https://trs.jpl.nasa.gov/bitstream/handle/2014/44145/13-2330_A1b.pdf?isAllowed=ysequence=1

[76] P. Bhandari and G. B. et all, "Mars science laboratory mechanically pumped fluid loop for thermal control - design, implementation, and testing," *SAE International Journal of Aerospace*, vol. 4, pp. 299–310, 2011.

[77] NASA. (2018) Europa thermal control design. [Online]. Available: https://dataverse.jpl.nasa.gov/file.xhtml?fileId=60318&version=1.0

[78] H. O. et al. (2022) Thermal control architecture trade study for the europa clipper pre-project study. [Online]. Available: https://tfaws.nasa.gov/wp-content/uploads/TFAWS2015-PT-10-Paper.pdf

[79] Boing. (2009) Development of a mechanically pumped fluid loop for 3 to 6 kw payload cooling. [Online]. Available: https://www.sae.org/publications/technical-papers/content/2009-01-2350/

[80] P. Bhandari and G. B. et al. (2006) Mechanically pumped fluid loop (mpfl)technologies for thermal control of future mars rovers. [Online]. Available: https://pdfs.semanticscholar.org/d066/082ad1843eefac27f2135d1e9f7e859effed.pdf

[81] A. T. Fluids. (2022) Galden heat transfer fluids. [Online]. Available: https://www.appliedthermalfluids.com/product-category/solvay-solexis/galden-heat-transfer-fluid/text=Galden

[82] M. H. T. Fluids. (2022) Fc heat transfer fluids. [Online]. Available: https://www.3m.com/3M/en_US/p/c/electronics-components/specialty-fluids/heat-transfer-fluids/

[83] Paratherm. (2022) Paratherm cr htf. [Online]. Available: https://www.paratherm.com/heat-transfer-fluids/paratherm-cr-htf/

[84] BCN3D. (2020) When was 3d printing invented? the history of 3d printing. [Online]. Available: https://www.bcn3d.com/the-history-of-3d-printing-when-was-3d-printinginventedtext=The20first20documented20iterations20of,was20polymerized20by20UV20light.

[85] S. R. Scholars. (2020) Charles hull and the rise of 3d printing. [Online]. Available: https://stmuscholars.org/charles-hull-and-the-rise-of-3d-printing/

[86] M. Ahart. (2019) Types of 3d printing technology. [Online]. Available: https://www.protolabs.com/resources/blog/types-of-3d-printing/

[87] SPC. (2017) What materials are used for 3d printing? [Online]. Available: https://www.sharrettsplating.com/blog/materials-used-3d-printing/

[88] GE. (2022) What is additive manufacturing? [Online]. Available: https://www.ge.com/additive/additive-manufacturing?utmsource=googleutmmedium=paidadvertisingutmcampaign=campaignutmterm=metal203d20printerutmcontent=manufacturinggclid=EAIaIQobChMItefp1t73-QIVSR6tBh1ffgaqEAAYAiAAEgKNbfDBwE

[89] A. Hehr and M. Norfolk, "A comprehensive review of ultrasonic additive manufacturing," *Rapid Prototyping Journal*, vol. 26, pp. 445–458, 2019.

[90] J. D. (2022) What are the applications for 3d printing in space? [Online]. Available: https://www.3dnatives.com/en/top-10-3d-printing-space/

[91] Windform. (2019) Solving the challenges of long duration space flight with 3d printing. [Online]. Available: https://www.nasa.gov/missionpages/station/research/news/3d-printing-in-space-long-duration-spaceflight-applications

[92] W. et al. (2022) Propelling the field of small sats forward with pbf 3d printing and windform® xt 2.0 carbon fiber filled composite material. [Online]. Available: https://www.windform.com/case-studies/3d-printed-3u-demonstrator-space-ready-cubesat/

[93] C. S. UPEC. (2013) Ogms-sa cubesat. [Online]. Available: https://www.csu.u-pec.fr/en/cubesats/ogms-sa-cubesat/

[94] Wikipedia. (2022) Cryocooler. [Online]. Available: https://en.wikipedia.org/wiki/Cryocooler

[95] S. Miller, R. Ross, and J. Raab, *Cryocoolers*. ICC Press, 2018.

[96] Wikipedia. (2022) Closed cycle cryocooler principles of operation. [Online]. Available: https://www.arscryo.com/cryocooler-principles-of-operation

[97] A. K. Diab, "Modeling and optimization of a hybrid cryocooler," Master's thesis, University of Wisconsis Madison, 2004.

[98] R. Ross, "Aerospace coolers: a 50-year quest for long-life cryogenic cooling in space," *JPL NASA*, 2022.

[99] K. Penanan. (2013) Northrop grumman miri cryocooler. [Online]. Available: https://www2.jpl.nasa.gov/advtech/coolers/ACTDP_MIRI.htm

[100] I. McKinley, D. Johnson, and J. Rodriguez, "Characterization testing of lockheed martin standard micro pulse tube cryocooler," *JPL NASA*, 2016.

[101] W. Gully, D. Glaister, P. Hendershott, V. Kotsubo, J. Lock, and E. Marquardt, "Vall aersoapce next generation two stage 35k cryocoolers: The sb235 and sb235e," *International Cryocoolers Conference*, vol. Cryocoolers 14th, 2007.

[102] M. Barr, K. Price, and G. Pruitt, "Raytheon rs1 cryocooler performance," *Springer Science*, vol. Cryocoolers 13th, 2004.

[103] J. M. Russell, M. G. Mlynzcak, and L. L. Gordley, "An overview of the saber experiment for the timed mission," *SPIE*, vol. 2266, 2013.

[104] R. Esplin and L. Z. et al, "Saber instrument design update," *Space Dynamics Lab Publications*, 1995.

[105] NASA. (2001) Saber a pioneer in atmospheric science. [Online]. Available: https://www.nasa.gov/centers/langley/news/factsheets/SABER.html

[106] M. G. Mlynczak and T. D. et al, "Radiometric stability of the saber instrument," *DOI AGU*, 2020.

[107] M. G. Mlynczak, "Energetics of the mesosphere and lower thermosphere and the saber experiment," *Adv. Space Res*, vol. 20, pp. 1177–1183, 1997.

[108] C. Rodgers, "Retrieval of atmospheric temperature and composition from remote measurements of thermal radiation," *Reviews of Geophysics and Space Physics*, vol. 14, 1976.

[109] D. R. et al, "The thermal infrared sensor (tirs) on landsat 8: Design overview and pre-launch characterization," *Remote Sensing*, 2015.

[110] T. Pagano and H. A. et al, "Cubesat infrared atmospheric sounder (ciras)," *Californnia Polytechnical Institute Lecture Series*, 2016.

[111] E. Portal. (2061) Ciras. [Online]. Available: https://www.eoportal.org/satellite-missions/ciras

[112] D. Mamula and T. P. et al, "Noaa eon-ir cubesat study for operational infrared soundings," *Californnia Polytechnical Institute Lecture Series*, 2017.

[113] M. Watson. (2020) Engineering an elegant system. [Online]. Available: https://www.nasa.gov/sites/default/files/atoms/files/nasatp20205003644interactive2.pdf

[114] C. D. Brown, *Elements of Spacecraft Design*. AIAA, 2002.

[115] F. Shah. (2022) What is a system. [Online]. Available: https://www.scribd.com/document/161380682/A-System-is-a-Collection-of-Elements-or-Components-That-Are-Organized-for-a-Common-Purpose

[116] S. Sinek. (2022) The golden circle for beginners. [Online]. Available: https://simonsinek.com/private-classes/the-golden-circle-for-individuals/

[117] P. Venture. (2022) Strategic vs. tactical vs. operational. [Online]. Available: https://www.profitableventure.com/strategic-plan-operational-tactical-difference/

[118] NASA. (2022) Appendix c: How to write a good requirement. [Online]. Available: https://www.nasa.gov/seh/appendix-c-how-to-write-a-good-requirement

[119] JPL. (2022) Nasa jpl team-x. [Online]. Available: https://jplteamx.jpl.nasa.gov/

[120] ESA. (2022) European space agency cdf. [Online]. Available: https://www.esa.int/Enabling_Support/Space_Engineering_Technology/CDF

[121] K. Institute. (2022) What is kaizen. [Online]. Available: https://www.kaizen.com/what-is-kaizen

[122] L. M. Jiji, *Heat Conduction*. Springer, 2009.

[123] S. Kakac and Y. Yener, *Heat Conduction*. Taylor and Francis, 1993.

[124] S. P. Ketkar, *Numerical Thermal Analysis*. ASME Press, 1999.

[125] Quote. (2022) 2nd law of thermodynamics. [Online]. Available: https://en.wikipedia.org/wiki/Second_law_of_thermodynamics#cite_ref-28

[126] Nuclear-Power. (2022) Planck's law-hypothesis. [Online]. Available: https://www.nuclear-power.com/nuclear-engineering/heat-transfer/radiation-heat-transfer/plancks-law-plancks-hypothesis/

[127] L. Geeks. (2022) Nusselt number: Its importance and relations. [Online]. Available: https://www.nuclear-power.com/nuclear-engineering/heat-transfer/radiation-heat-transfer/plancks-law-plancks-hypothesis/

[128] P. Talukdar, "Internal forced convection," *Class Notes*, 2022.

[129] Various, "Heat exchangers: The effectivness ntu method," *Class Notes*, 2022.

[130] McCrometer, "Permanent pressure loss comparison among various flowmeter technologies," *McCrometer White Paper*, 2010.

[131] Socomore and Ring. (2022) Aeroglaze z306. [Online]. Available: https://www.socomore.com/media/

[132] SpaceMatdb. (2022) Aeroglaze z306 flat black absorptive polyurethane low outgassing. [Online]. Available: https://www.spacematdb.com/spacemat/manudatasheets/Aeroglaze

[133] NASA. (2022) Systems engineering principles. [Online]. Available: https://www.nasa.gov/consortium/SystemsEngineeringPrinciples

[134] L. A. et al, "Measurement considerations for exported force and torque (eft) testing of the ricor k508n cryocooler," in *Proc. of the American Mechanism Conference*, Oct. 2022.

[135] L. A. et al., "Developments in cubesat active thermal control: A review of the active cryocubesat (accs) and advanced thermal architecture (ata) projects for the jpl cubesat community," in *JPL Internal CubeSat Forum*, Oct. 2021.

[136] L. A. et al, "Cubesat active thermal control: A review of the active cryocubesat (accs) and advanced thermal architecture (ata) projects," in *Thermal Fluids Analysis Workshop*, Oct. 2021.

[137] ——, "Random vibration, exported vibration, and passive isolation testing of the ricor k508n cryocooler," in *Cryocooler Engineering Conference*, Oct. 2021.

[138] ——, "Cubesat active thermal control in support of advanced payloads: The active thermal architecture project," *SPIE*, 2021.

[139] ——, "The active thermal architecture: Thermal control for small-satellites," *SmallSat*, 2021.

[140] ——, "The active thermal architecture: Active thermal control for small satellites," *NASA STP*, 2021.

[141] ——, "An overview of the design, analysis, and testing of a novel support structure for electro-optical detectors," *AIAA*, 2021.

[142] ——, "Active thermal architecture design & status," *SmallSat*, 2021.

[143] ——, "Active thermal architecture for cryogenic optical instrumentation," *SmallSat*, 2018.

[144] H. S. F. Laboratory. (2021) Hyti: Hyperspectral thermal imager. [Online]. Available: https://www.hsfl.hawaii.edu/missions/hyti/

[145] R. W. et al, "Hyti: Thermal hyperspectral imaging from a cubesat platform," *SmallSat*, 2019.

[146] S. et al, "The active cooling for multispectral earth sensors (acmes) mission," in *4S Conference*, May 2022.

[147] A. et al, "Active thermal control for the multispectral earth sensors (acmes) mission," in *Small Satellite Conference*, Aug. 2022.

APPENDICES

APPENDIX A

ACCS: Additional Resources

This chapter will provide additional resources to compliment and expand the written ACCS dissertation. Further resources are available online in the form of excel/VBA codes, Matlab models & Analytics, and Thermal Desktop simulations. A comprehensive database of the various datasets generated & experimentally derived are also provided. Further information on the ACCS technology is available in published journal and conference papers.

This appendix will focus on figures and tables with detailed captions. Explanatory text will be kept to a minimum.

A.1 Additional Calibration Data

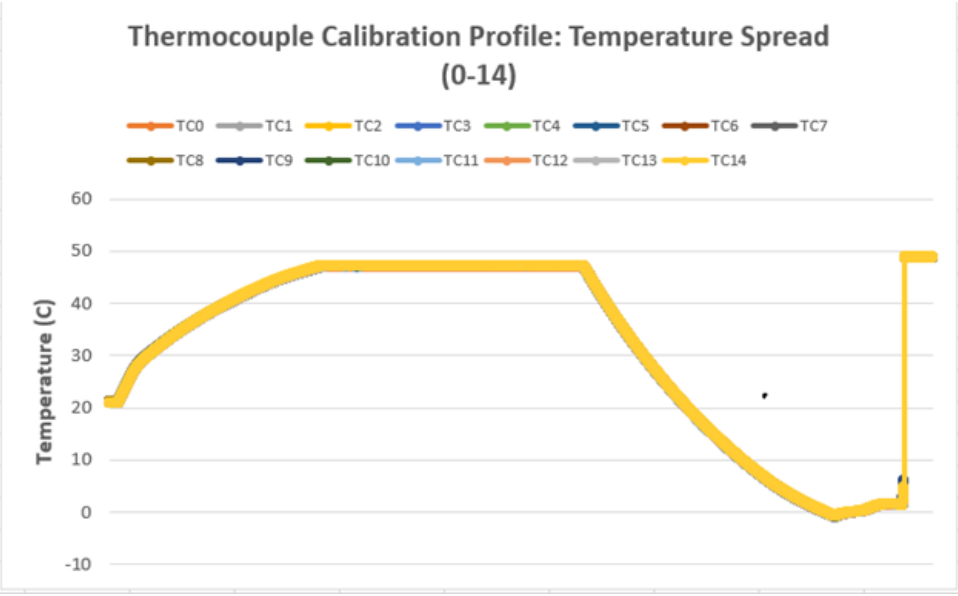

Fig. A.1: ACCS calibration data. TC's 0 through 14.

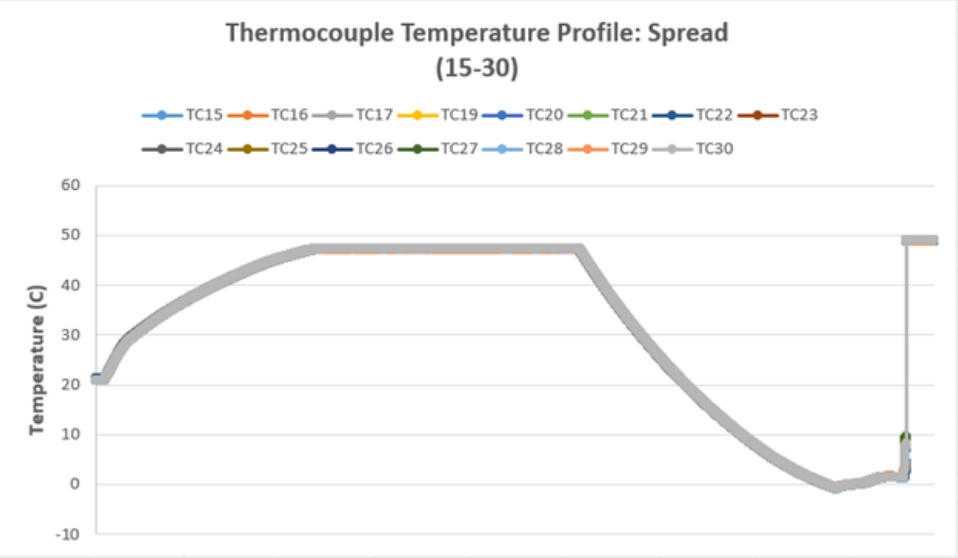

Fig. A.2: ACCS calibration data. TC's 15 through 30.

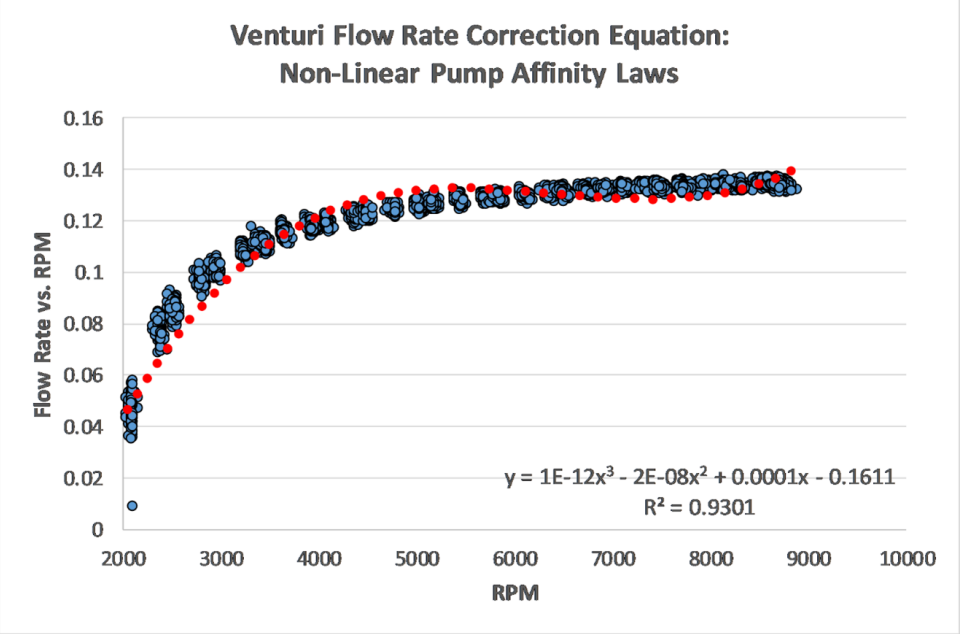

Fig. A.3: Venturi flow meter calibration data. Curvature & curve-fit eq for the entire ACCS flow regime.

A.2 2D Conduction Shape Factors

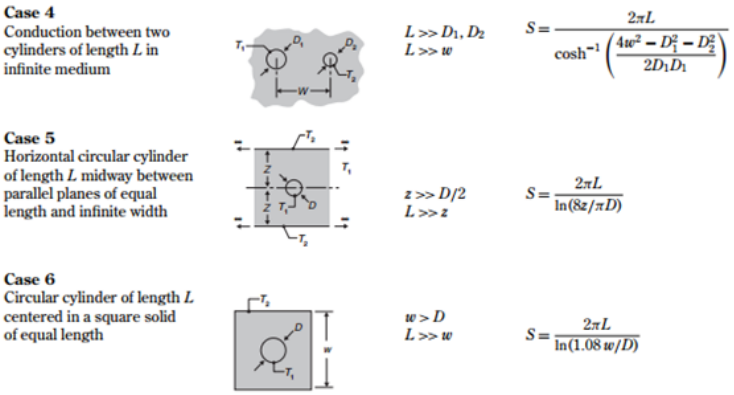

Fig. A.4: Various 2D shape factors used by the ACCS analytical model

APPENDIX B

ACCS Analytical Model Comparison

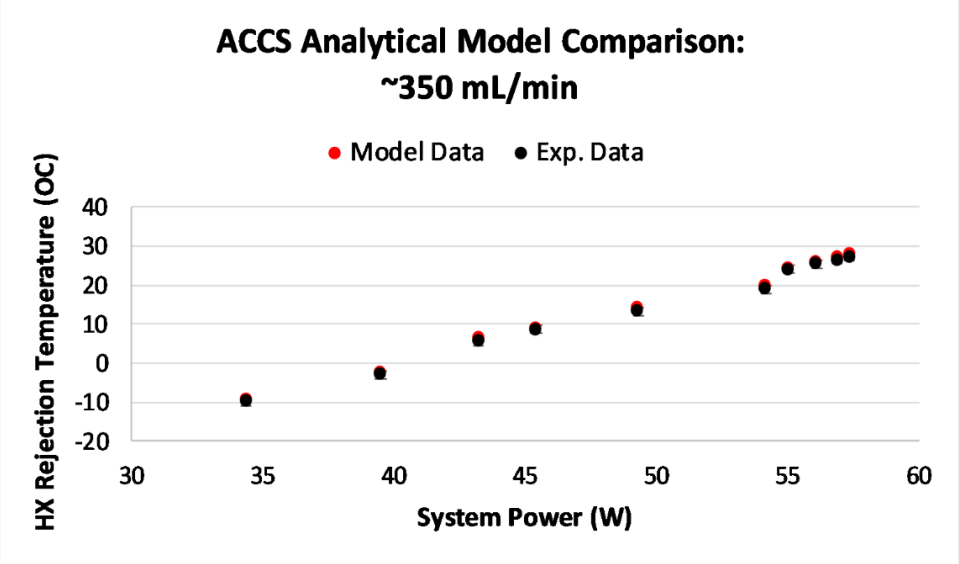

Fig. B.1: Comparison of the ACCS analytical model to TVAC performance data. ~350 mL/min. Considering total radiated power.

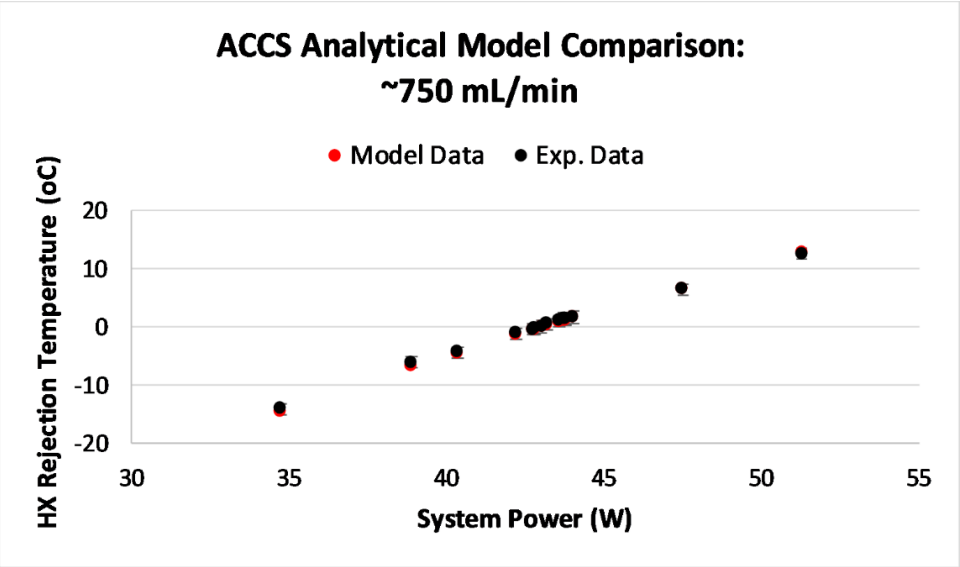

Fig. B.2: Comparison of the ACCS analytical model to TVAC performance data. ~750 mL/min. Considering total radiated power.

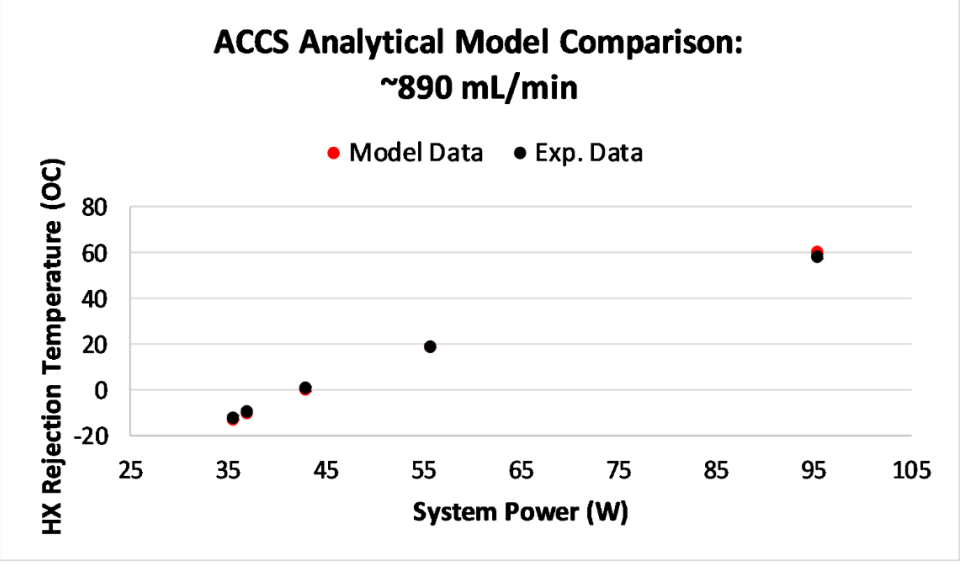

Fig. B.3: Comparison of the ACCS analytical model to TVAC performance data. ~890 mL/min. Considering total radiated power.

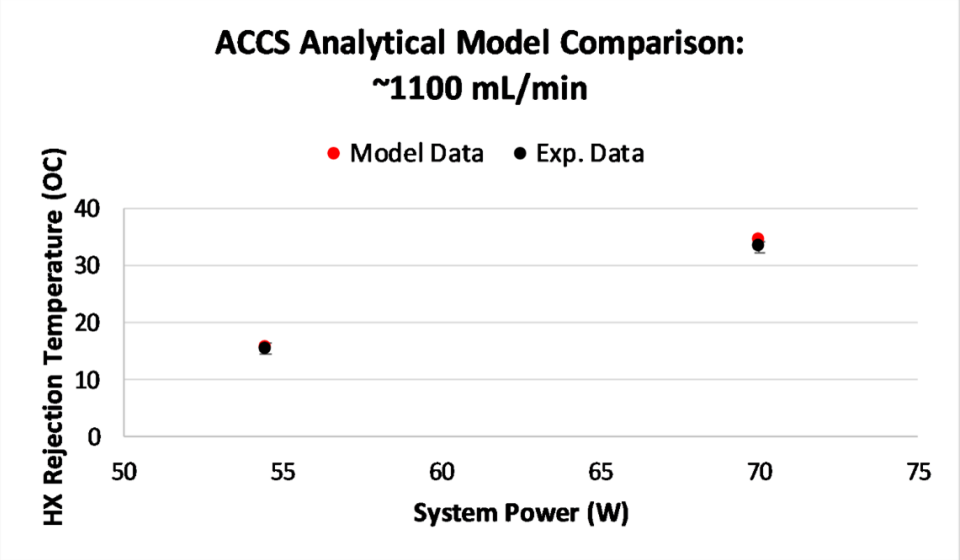

Fig. B.4: Comparison of the ACCS analytical model to TVAC performance data. ~1100 mL/min. Considering total radiated power.

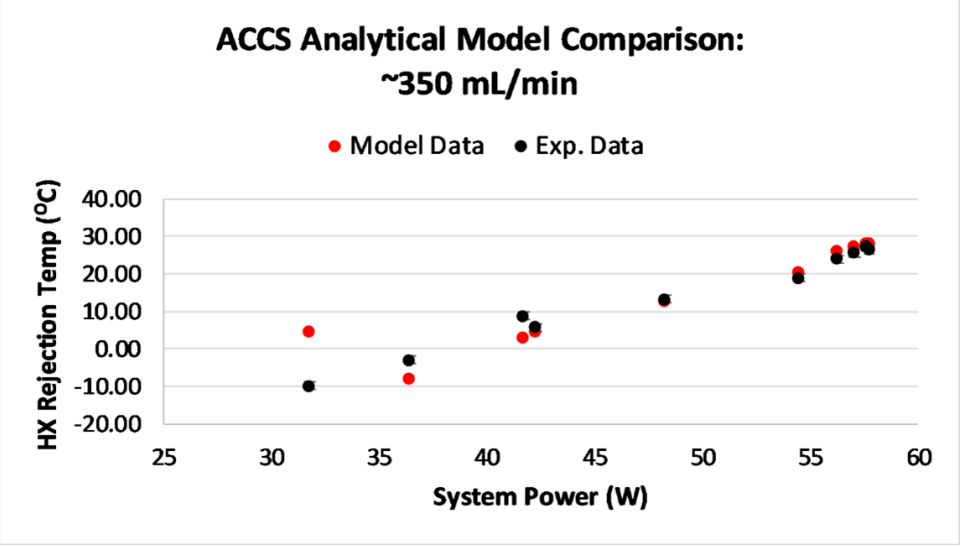

Fig. B.5: ACCS predicted performance (analytical model) to TVAC characterization data. Considering total input power ~350 mL/min.

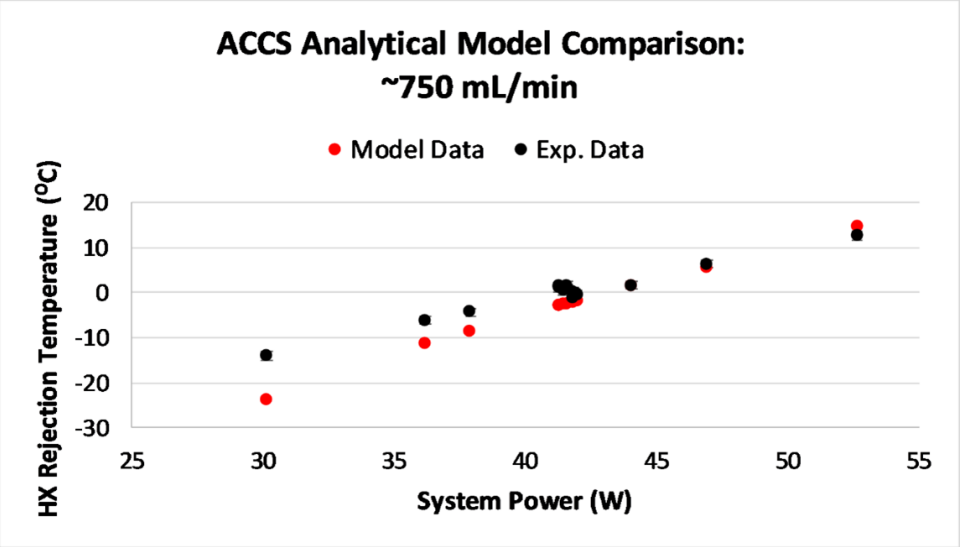

Fig. B.6: ACCS predicted performance (analytical model) to TVAC characterization data. Considering total input power ~750 mL/min.

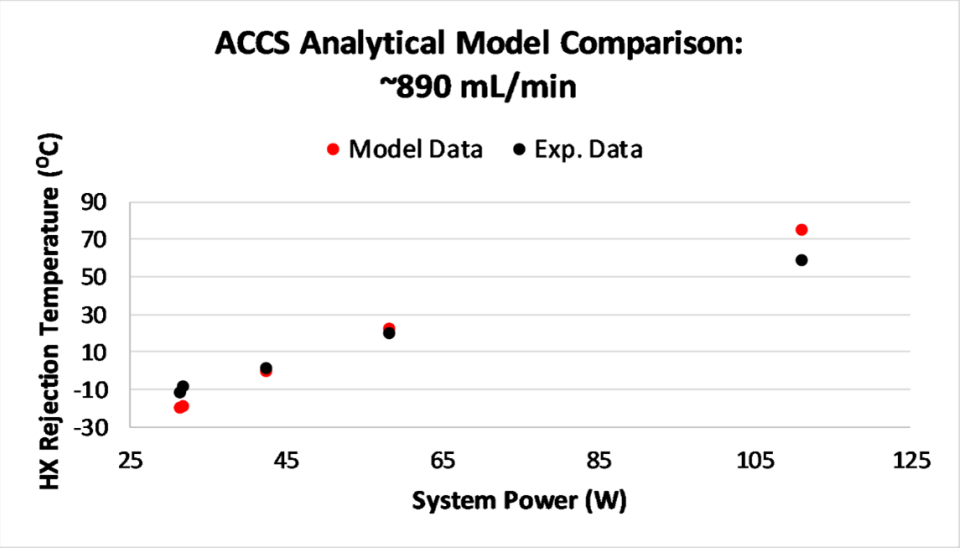

Fig. B.7: ACCS predicted performance (analytical model) to TVAC characterization data. Considering total input power ~890 mL/min.

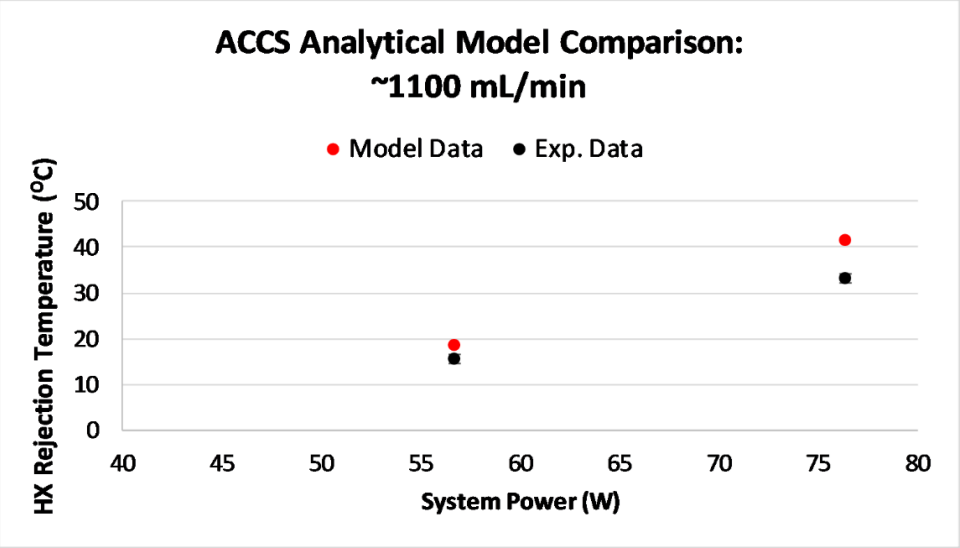

Fig. B.8: ACCS predicted performance (analytical model) to TVAC characterization data. Considering total input power ~1100 mL/min.

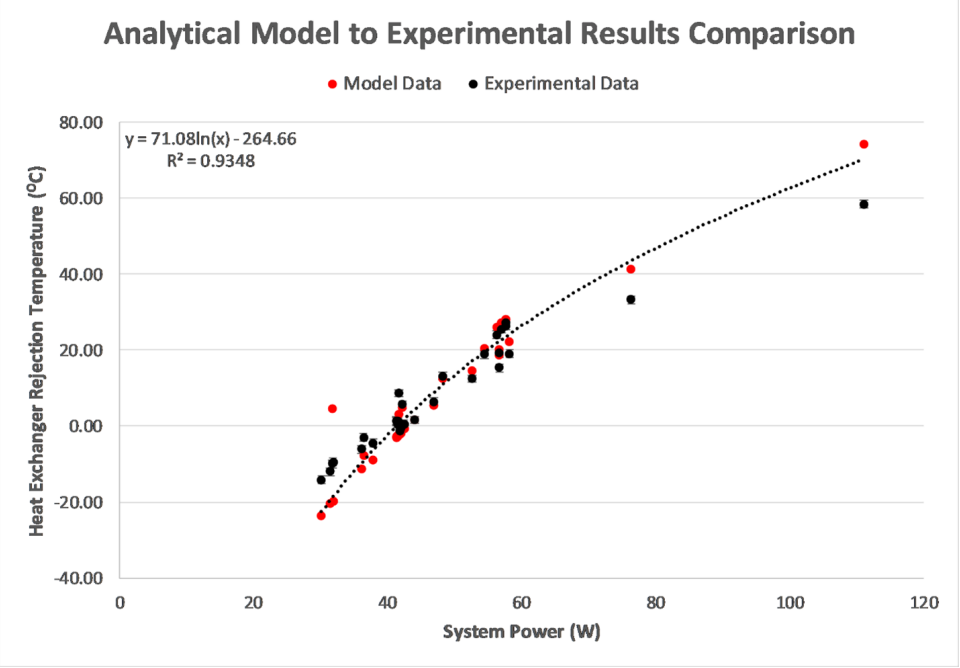

Fig. B.9: ACCS predicted performance (analytical model) to TVAC characterization data. Considering total input power.

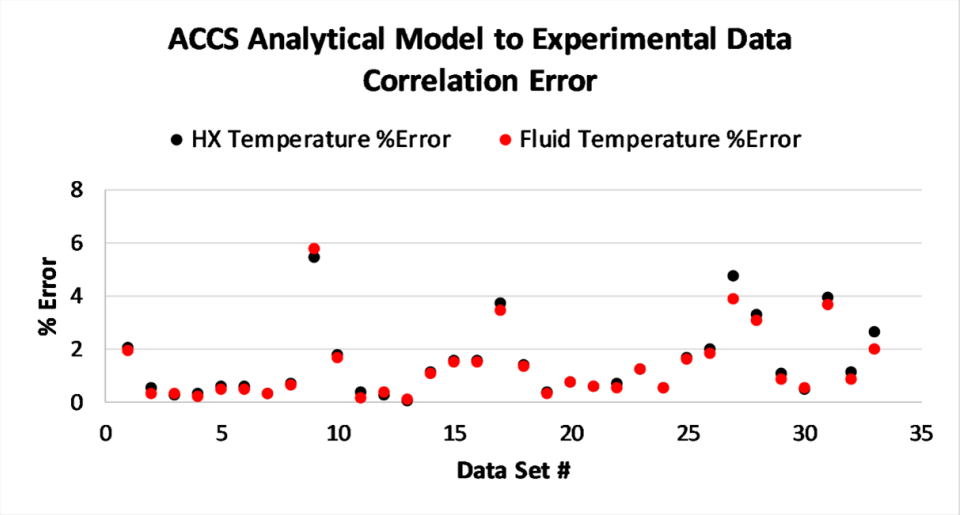

Fig. B.10: ACCS analytical model vs. TVAC performance data error as a function of data set case #. Considering total input power.

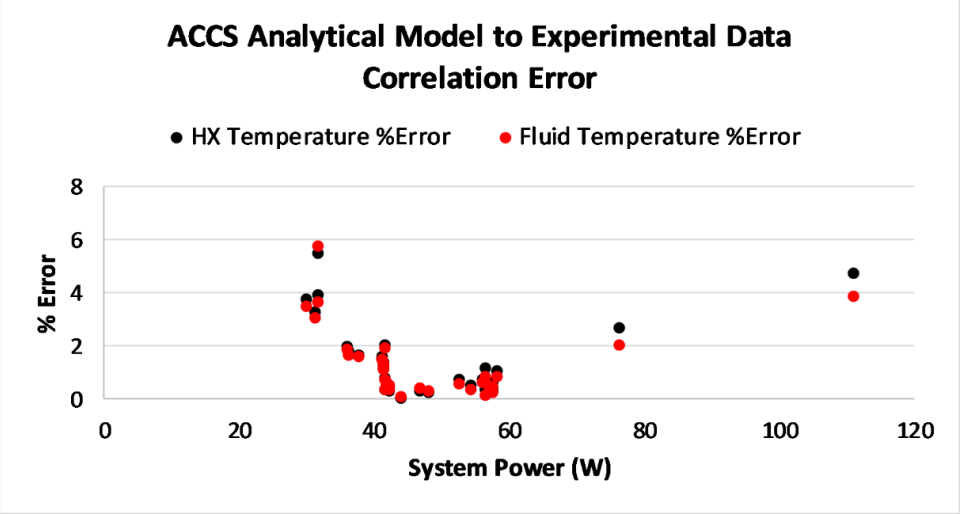

Fig. B.11: ACCS analytical model vs. TVAC performance data error as a function of total input power.

APPENDIX C

Thermal Desktopo Numerical Model Comparison

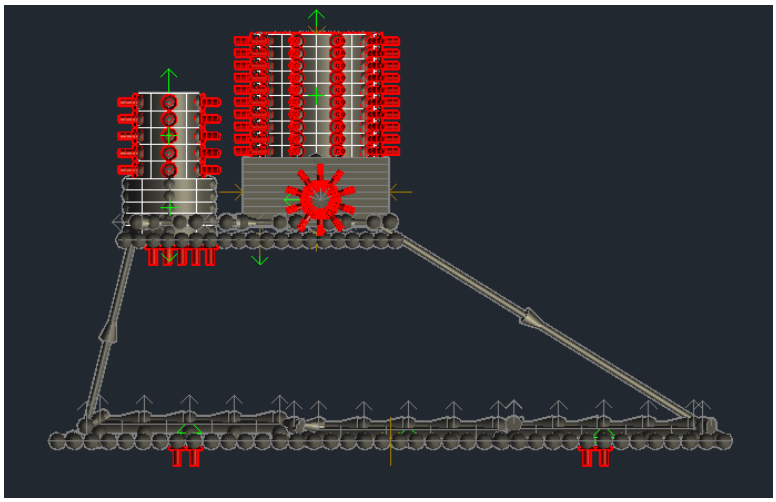

Fig. C.1: Additional views of the ACCS Thermal Desktop model. Front view of the total assembly.

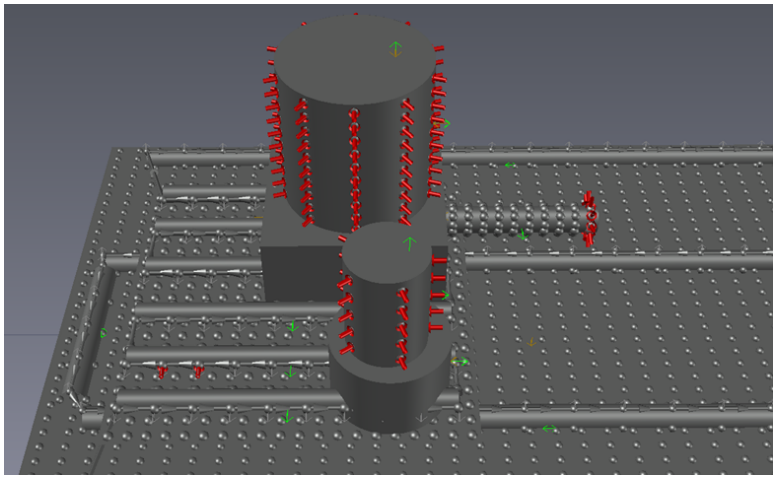

Fig. C.2: Additional views of the ACCS Thermal Desktop model. Iso-Top view of the total assembly.

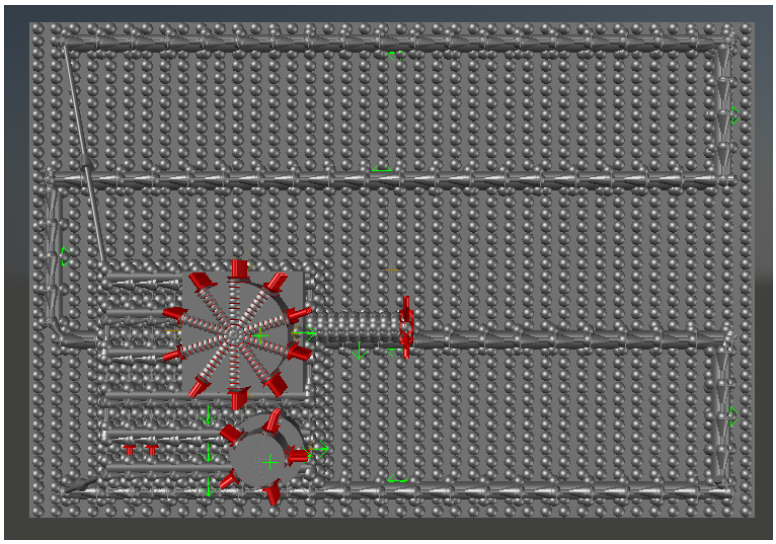

Fig. C.3: Additional views of the ACCS Thermal Desktop model. Top view of the total assembly.

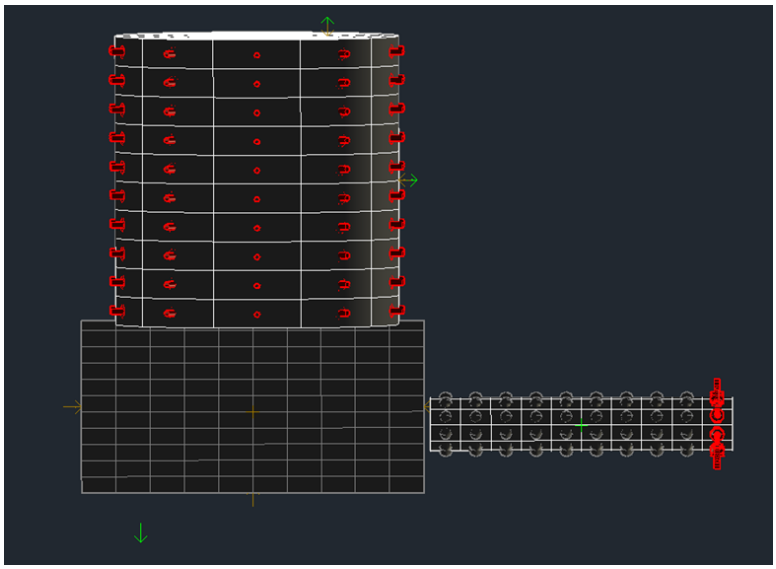

Fig. C.4: Additional views of the ACCS Ricor K508N Thermal Desktop model. Side view of the cryocooler.

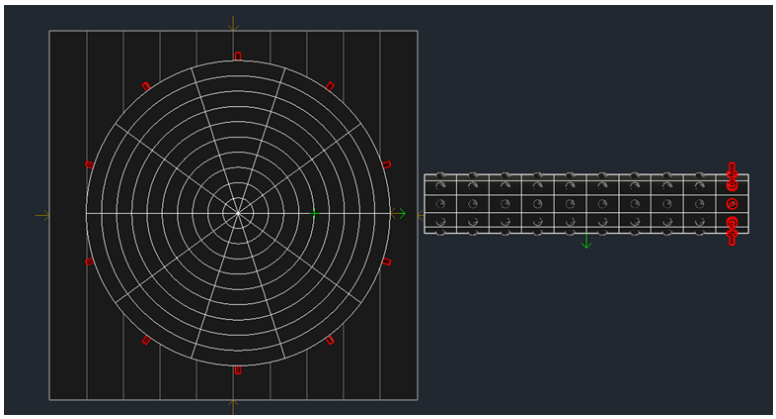

Fig. C.5: Additional views of the ACCS Ricor K508N Thermal Desktop model. Top view of the cryocooler.

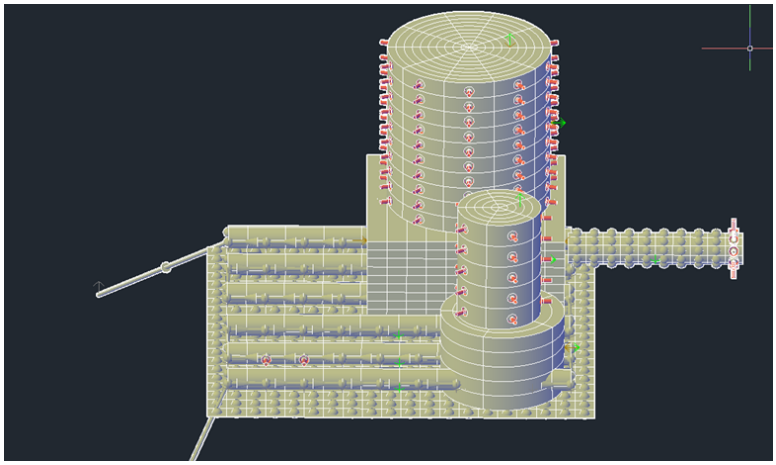

Fig. C.6: Additional views of the ACCS Ricor K508N Thermal Desktop model. Top-iso view of the cryocooler.

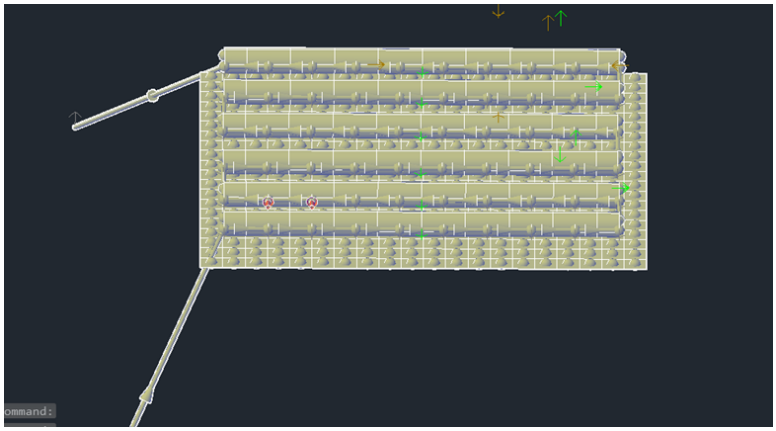

Fig. C.7: Additional views of the ACCS heat exchanger Thermal Desktop model. Top-iso view.

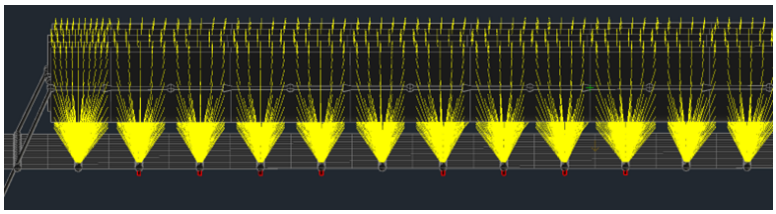

Fig. C.8: Additional views of the ACCS heat exchanger Thermal Desktop model. Plate to tubing contactors shown.

Case # + Notes		Heat Exchanger Rejection Temperature (°C)				Radiator Surface Temperature (°C)			
		TD Model		Exp. Data		TD Model		Exp. Data	
1	Thermal Power (W) 35.52 Fluid Flow Rate (mL/min) 890.05	Average				Average			
		-16.71		-12.00		-19.8		-16.14	
		Min	Max	Min	Max	Min	Max	Min	Max
		-17.56	-15.71	-13.12	-10.99	-20.68	-18.68	-16.95	-15.73
		Error: 1.80%				**Error: 1.42**			
2	Thermal Power (W) 43.0 Fluid Flow Rate mL/min 890.55	Average				Average			
		3.34		0.52		-0.79		-3.64	
		Min	Max	Min	Max	Min	Max	Min	Max
		2.23	4.5	-1.32	1.92	-1.96	0.7	-4.64	-3.09
		Error: 1.03%				**Error: 1.06%**			
3	Thermal Power (W) 43.23 Fluid Flow Rate (mL/min) 354.66	Average				Average			
		5.95		5.62		-1.24		-3.29	
		Min	Max	Min	Max	Min	Max	Min	Max
		4.81	8.51	2.75	8.03	-3.05	1.35	-4.75	-2.48
		Error: 0.12%				**Error: 0.76%**			
4	Thermal Power (W) 56.9 Fluid Flow Rate (mL/min) 352.67	Average				Average			
		30.3		26.42		20.5		15.76	
		Min	Max	Min	Max	Min	Max	Min	Max
		28.71	34.33	22.17	30.14	18.03	24.02	13.89	16.98
		Error: 1.29%				**Error: 1.64%**			
5	Thermal Power (W) 95.46 Fluid Flow Rate (mL/min) 868.43	Average				Average			
		72.63		58.41		66.44		55.51	
		Min	Max	Min	Max	Min	Max	Min	Max
		71.01	75.51	50.85	62.98	62.79	74.62	53.21	59.77
		Error: 4.29%				**Error: 3.33%**			

Table C.1: Part 1: ACCS heat Exchanger & radiator Thermal Desktop model comparison. Considering the total input power.

Case # + Notes		Heat Exchanger Rejection Temperature (°C)				Radiator Surface Temperature (°C)			
		TD Model		Exp. Data		TD Model		Exp. Data	
6	Thermal Power (W) 36.89 Fluid Flow Rate (mL/min) 890.94	Average				Average			
		-16.37		-9.42		-19.48		-13.70	
		Min	Max	Min	Max	Min	Max	Min	Max
		-17.22	-15.3	-10.73	-8.48	-20.35	-18.36	-14.66	-13.07
		Error: 2.64%				**Error: 2.23%**			
7	Thermal Power (W) 39.51 Fluid Flow Rate mL/min 355.94	Average				Average			
		-6.99		-2.98		-11.49		-9.26	
		Min	Max	Min	Max	Min	Max	Min	Max
		-7.71	-5.64	-4.24	-1.73	-13.08	-8.9	-10.73	-7.25
		Error: 1.48%				**Error: 0.084%**			
8	Thermal Power (W) 54.5 Fluid Flow Rate (mL/min) 1099.73	Average				Average			
		23.75		15.38		19.21		12.65	
		Min	Max	Min	Max	Min	Max	Min	Max
		22.1	26.1	12.81	16.89	17.54	21.49	11.36	14.21
		Error: 2.90%				**Error: 2.29%**			
9	Thermal Power (W) 43.74 Fluid Flow Rate (mL/min) 729.39	Average				Average			
		-0.27		1.40		-3.34		-2.51	
		Min	Max	Min	Max	Min	Max	Min	Max
		-1.02	0.66	0.44	2.46	-4.72	-3.07	-3.74	-0.83
		Error: 0.61%				**Error: 0.31%**			
10	Thermal Power (W) 43.19 Fluid Flow Rate (mL/min) 729.14	Average				Average			
		0		0.45		-3.1		-3.59	
		Min	Max	Min	Max	Min	Max	Min	Max
		-0.76	0.96	-0.66	1.52	-4.47	-0.81	-4.58	-1.66
		Error: 0.165%				**Error: 0.09%**			
11	Thermal Power (W) 38.89 Fluid Flow Rate (mL/min) 743.88	Average				Average			
		-8.87		-6.12		-11.93		-10.29	
		Min	Max	Min	Max	Min	Max	Min	Max
		-9.62	-7.91	-7.20	-5.26	-13.07	-10.59	-11.37	-9.14
		Error: 1.03%				**Error: 0.62%**			

Table C.2: Part 2: ACCS heat Exchanger & radiator Thermal Desktop model comparison. Considering the total input power.

Case # + Notes		Ricor K508N Cryocooler Body Temperature (°C)				TCS M510 Micro-Pump Body Temperature (°C)			
		TD Model		Exp. Data		TD Model		Exp. Data	
1	Thermal Power (W) 35.52 Fluid Flow Rate (mL/min) 890.05	Average				Average			
		1.67		4.46		-7.98		-11.84	
		Min	Max	Min	Max	Min	Max	Min	Max
		-12.4	19.78	-1.51	16.64	-10.63	-5.05	-13.42	-10.27
		Error: 1.01%				**Error: 1.47%**			
5	Thermal Power (W) 95.46 Fluid Flow Rate (mL/min) 868.43	Average				Average			
		73.69		72.43		66.26		56.45	
		Min	Max	Min	Max	Min	Max	Min	Max
		60.78	82.89	64.87	79.12	61.95	66.75	54.32	58.57
		Error: 0.37%				**Error: 2.97%**			
8	Thermal Power (W) 54.5 Fluid Flow Rate (mL/min) 1099.73	Average				Average			
		30.01		29.69		26.39		15.34	
		Min	Max	Min	Max	Min	Max	Min	Max
		16.82	47.75	25.27	37.95	21.2	31.95	15.06	15.62
		Error: 0.11%				**Error: 3.82%**			
10	Thermal Power (W) 43.19 Fluid Flow Rate (mL/min) 729.14	Average				Average			
		12.2		14.04		2.53		0.26	
		Min	Max	Min	Max	Min	Max	Min	Max
		0.08	30.9	8.96	23.73	0.94	4.24	-0.93	1.45
		Error: 0.64%				**Error: 0.83%**			

Table C.3: ACCS Ricor K508N & TCS M510 micro-pump Thermal Desktop model comparison. Considering the total input power.

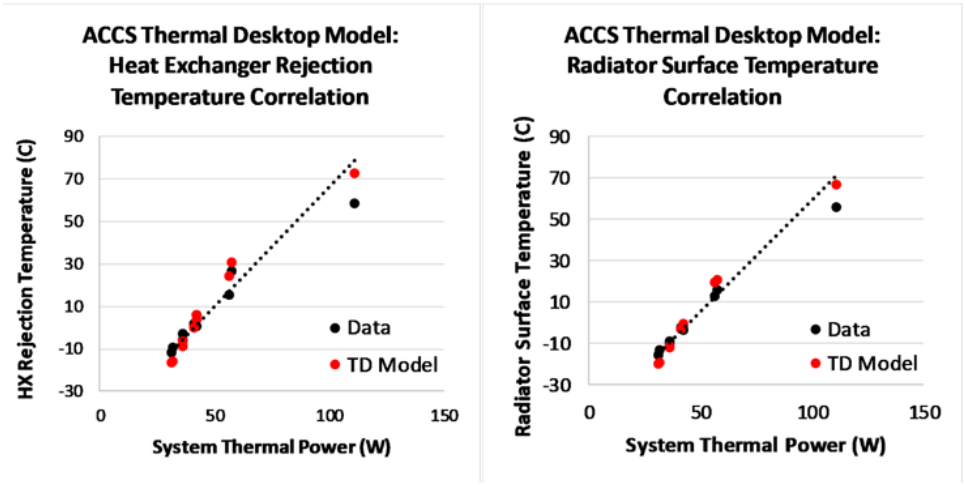

Fig. C.9: ACCS Thermal Desktop predicted performance (numerical model) to TVAC characterization data. Considering total input power.

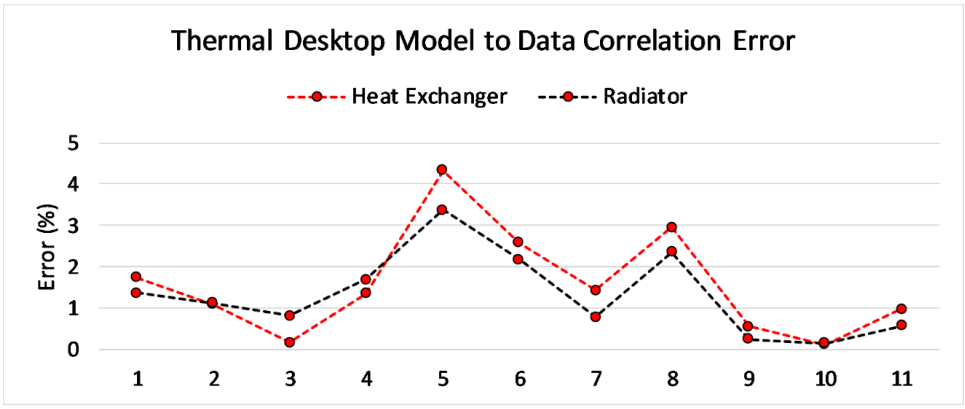

Fig. C.10: ACCS analytical model vs. TVAC performance data error as a function of data set case #. Considering total input power.

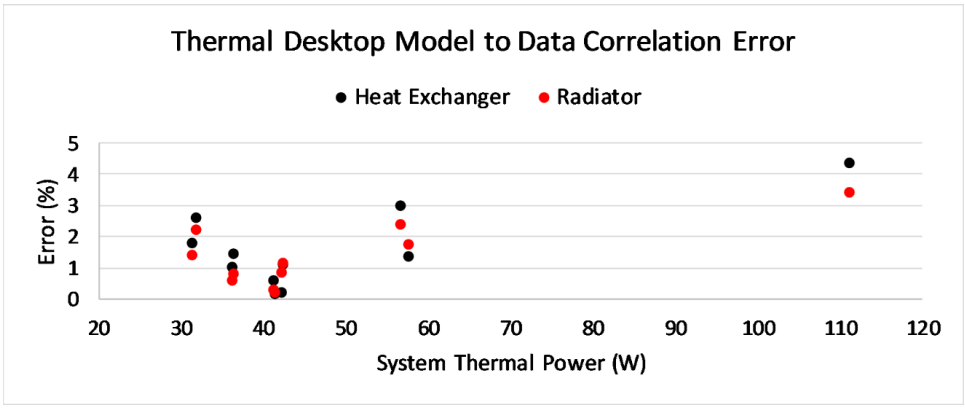

Fig. C.11: ACCS analytical model vs. TVAC performance data error as a function of total input power.

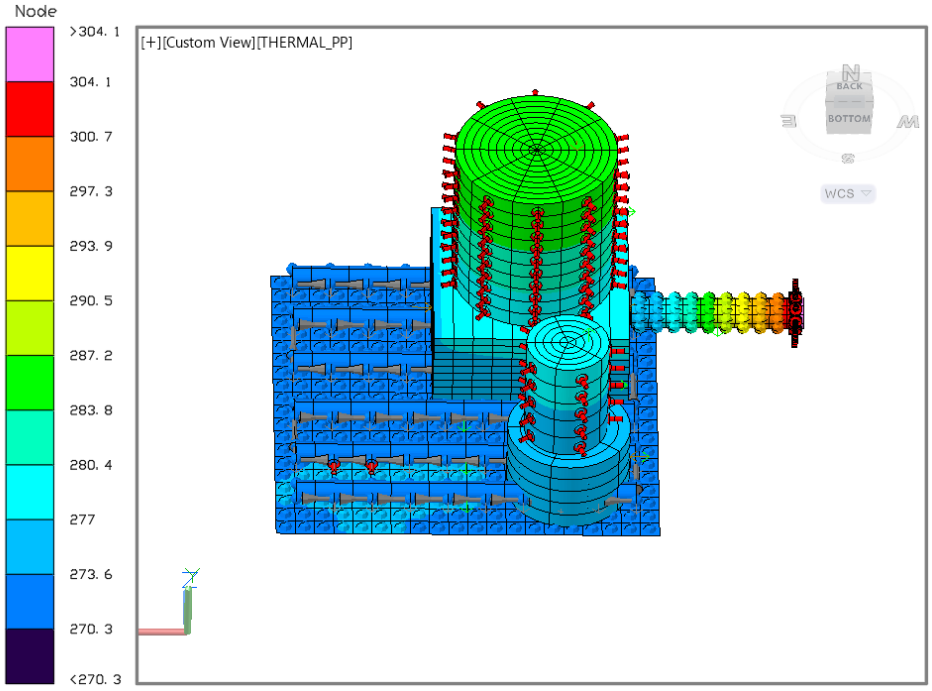

Fig. C.12: Thermal Desktop colormap of the ACCS heat exchanger assembly. 41.5 W of total power with a nominal flow rate of 730 mL/min.

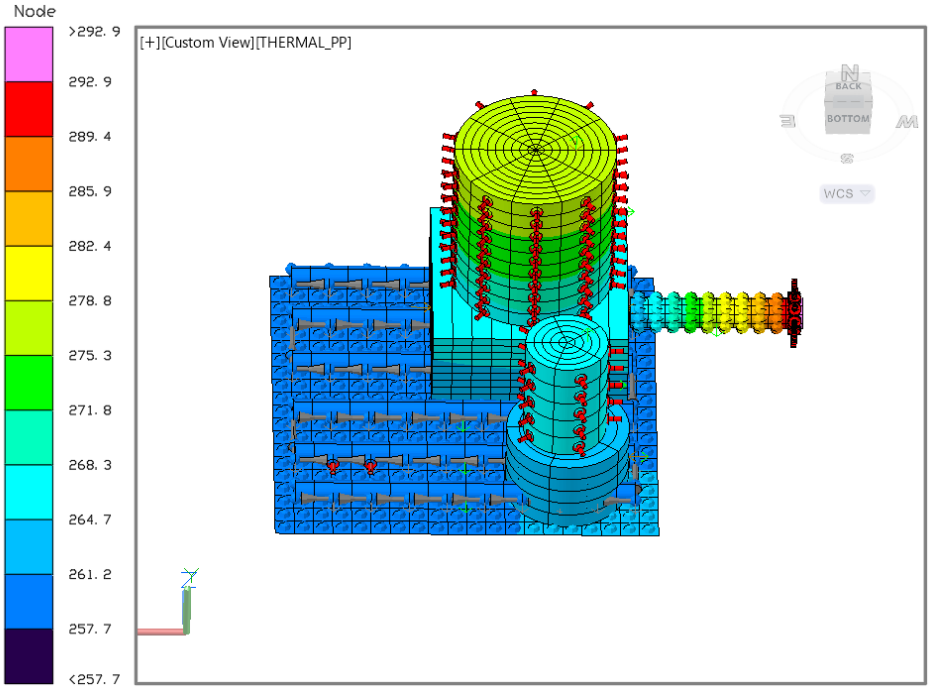

Fig. C.13: Thermal Desktop colormap of the ACCS heat exchanger assembly. 31.5 W of total power with a nominal flow rate of 890 mL/min.

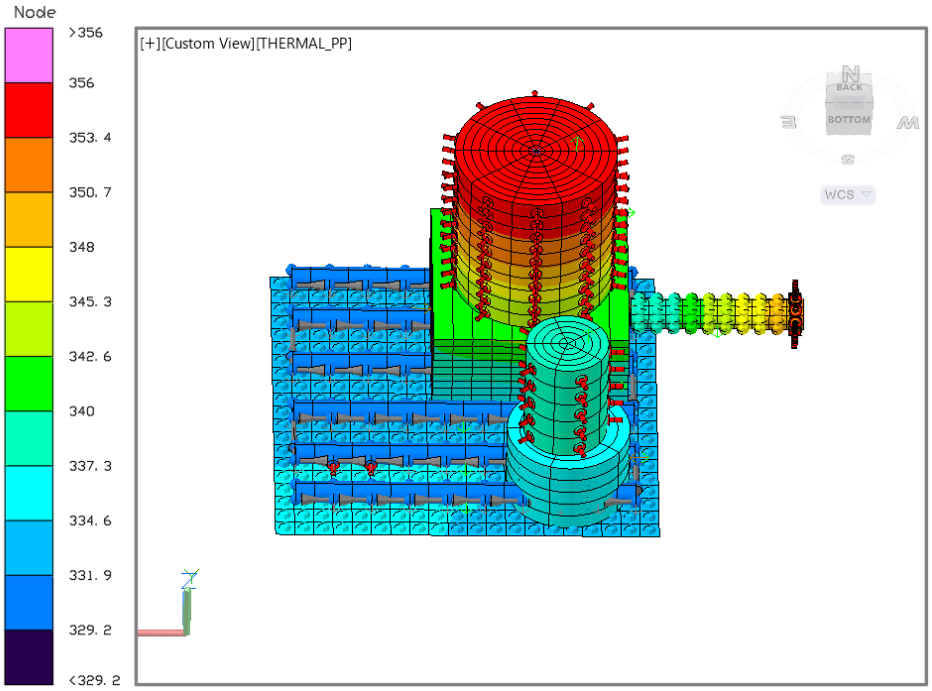

Fig. C.14: Thermal Desktop colormap of the ACCS heat exchanger assembly. Hot case: 111.1 W of total power with a nominal flow rate of 890 mL/min.

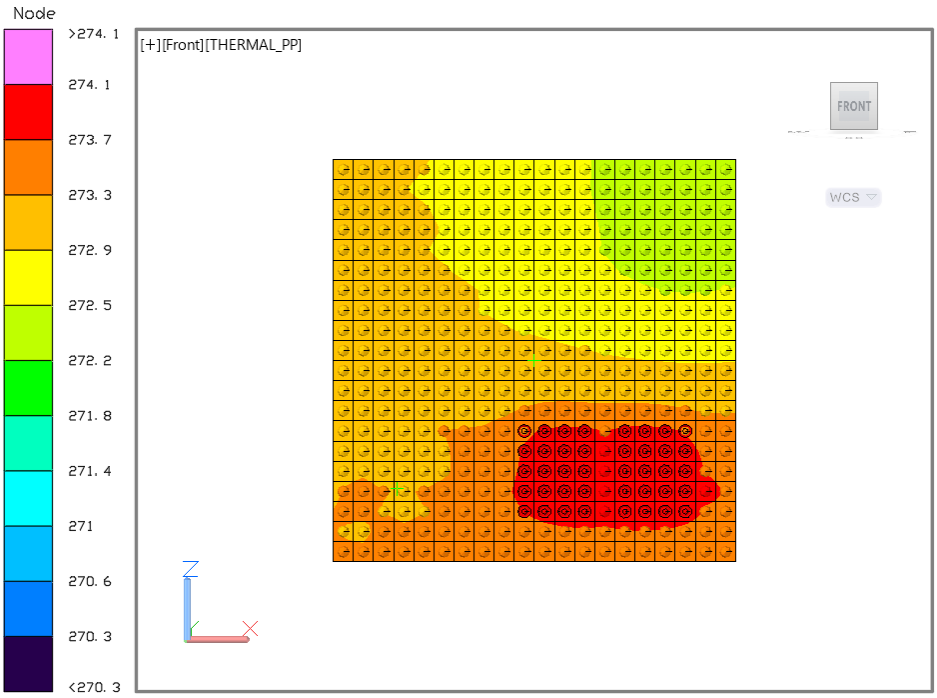

Fig. C.15: Thermal Desktop colormap of the ACCS heat exchanger. 41.5 W of total power with a nominal flow rate of 730 mL/min.

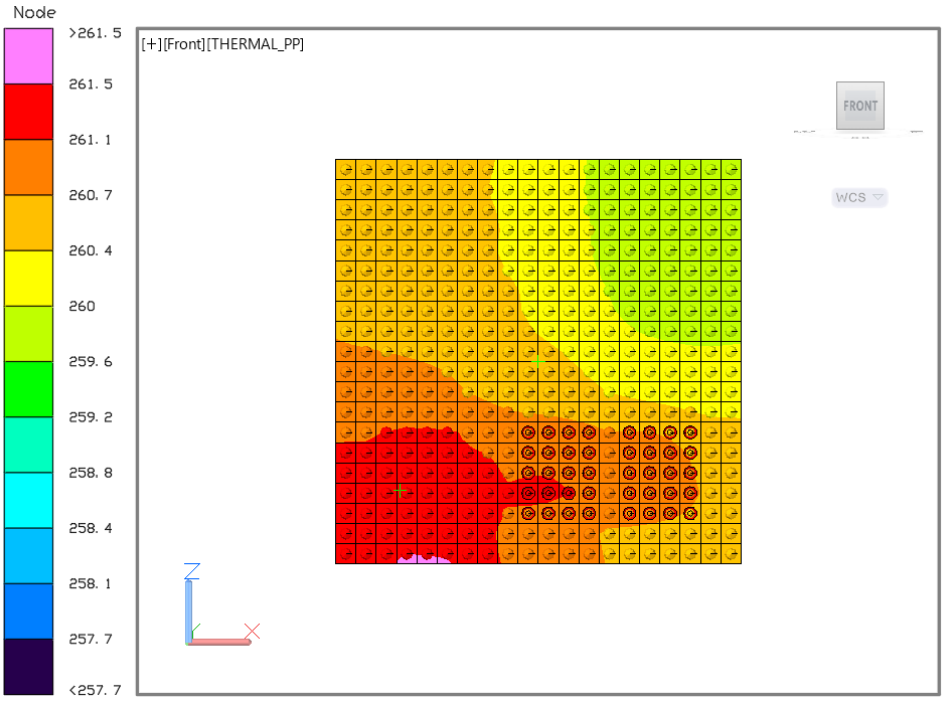

Fig. C.16: Thermal Desktop colormap of the ACCS heat exchanger. 31.5 W of total power with a nominal flow rate of 890 mL/min.

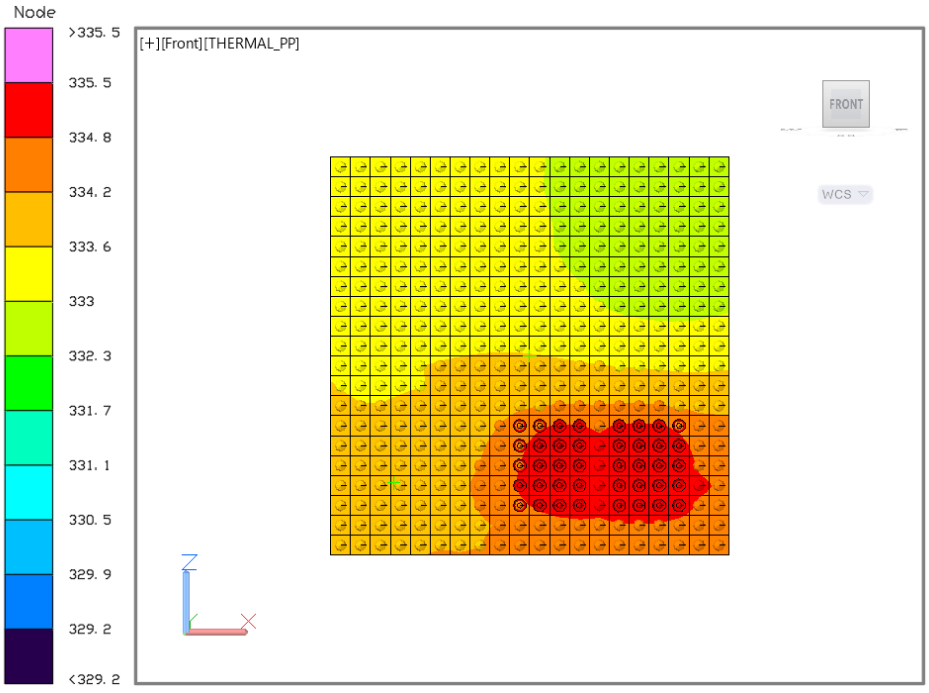

Fig. C.17: Thermal Desktop colormap of the ACCS heat exchanger. Hot case: 111.1 W of total power with a nominal flow rate of 890 mL/min.

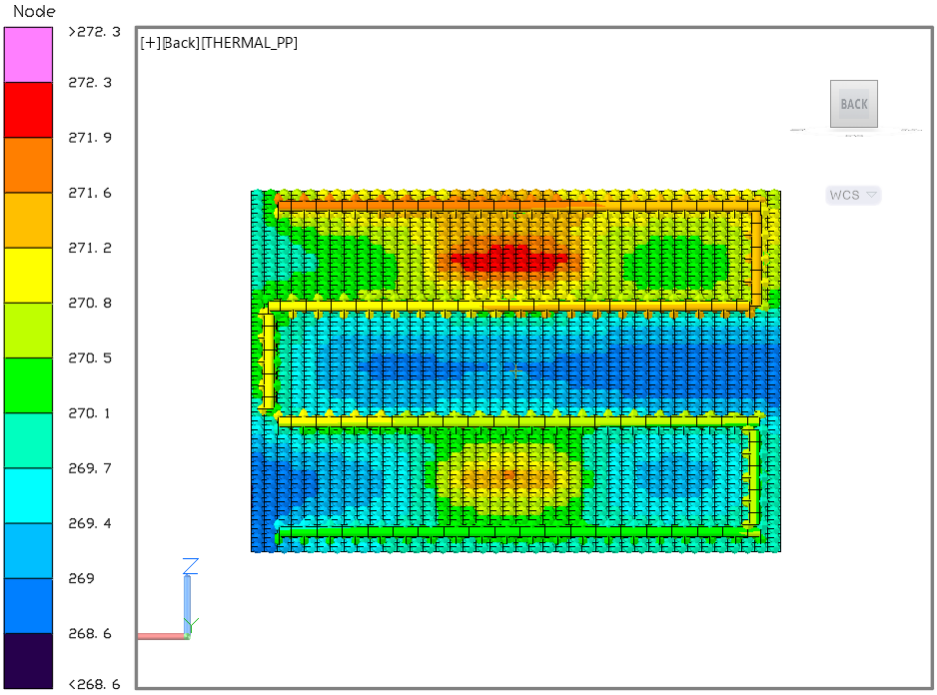

Fig. C.18: Thermal Desktop colormap of the ACCS radiator. 41.5 W of total power with a nominal flow rate of 730 mL/min.

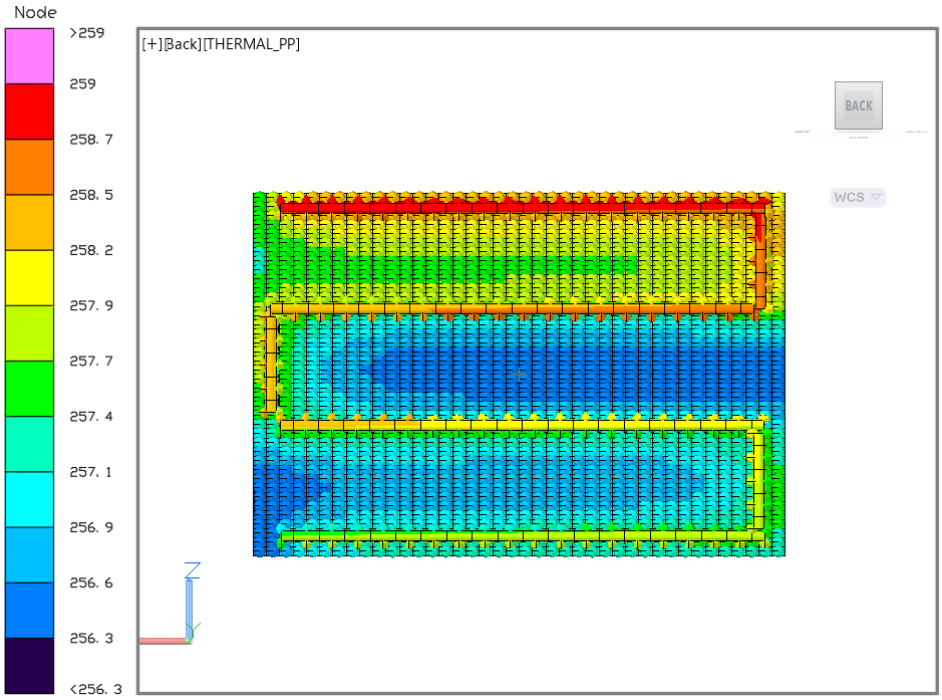

Fig. C.19: Thermal Desktop colormap of the ACCS radiator. 31.5 W of total power with a nominal flow rate of 890 mL/min.

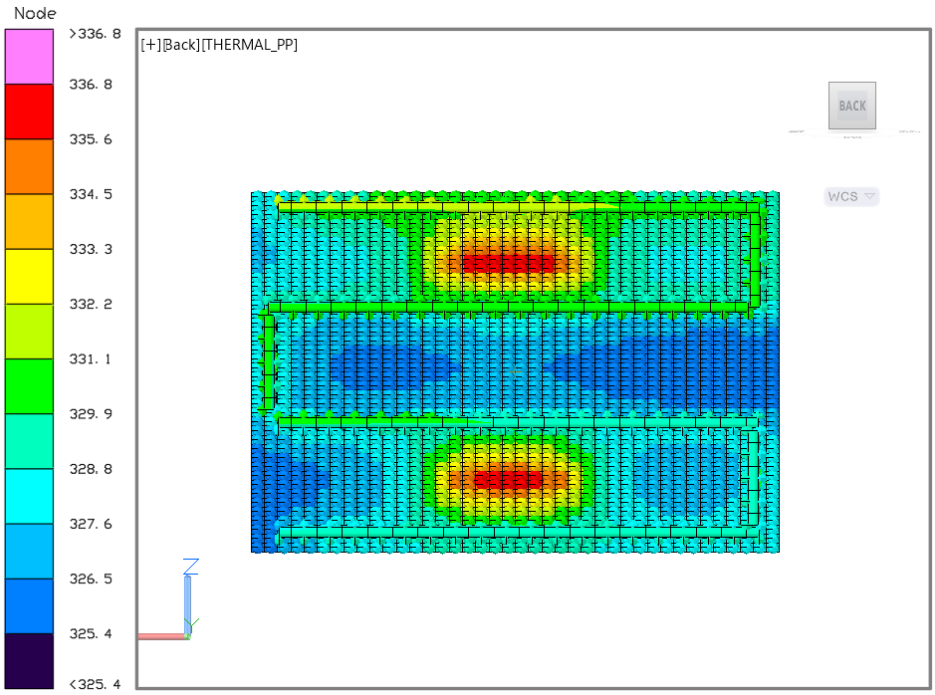

Fig. C.20: Thermal Desktop colormap of the ACCS radiator. Hot case: 111.1 W of total power with a nominal flow rate of 890 mL/min.

APPENDIX D

Additional ACCS TVAC Characterization Data

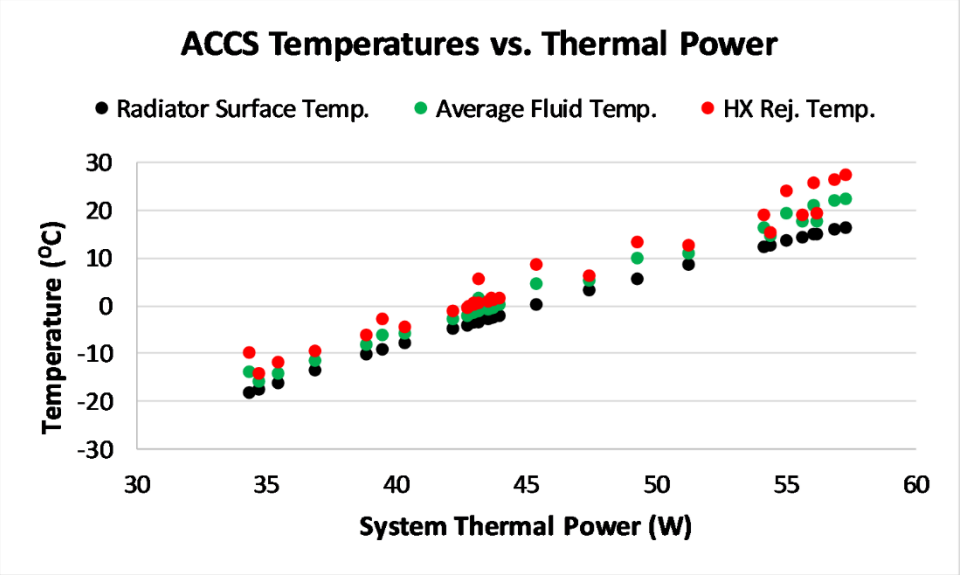

Fig. D.1: Average ACCS system temperatures as a function of total thermal power. Note the apperant thermal gradients between the heat exchanger, fluid, and radiator. These values seem to increase with power and decrease with flow rate.

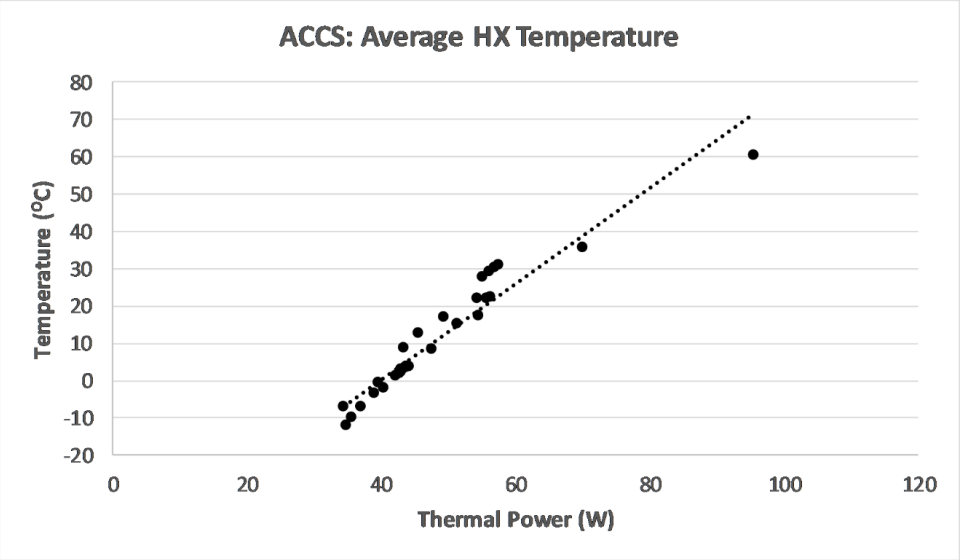

Fig. D.2: Average heat exchanger temperature as a function of total power. Note the relative spread from linear.

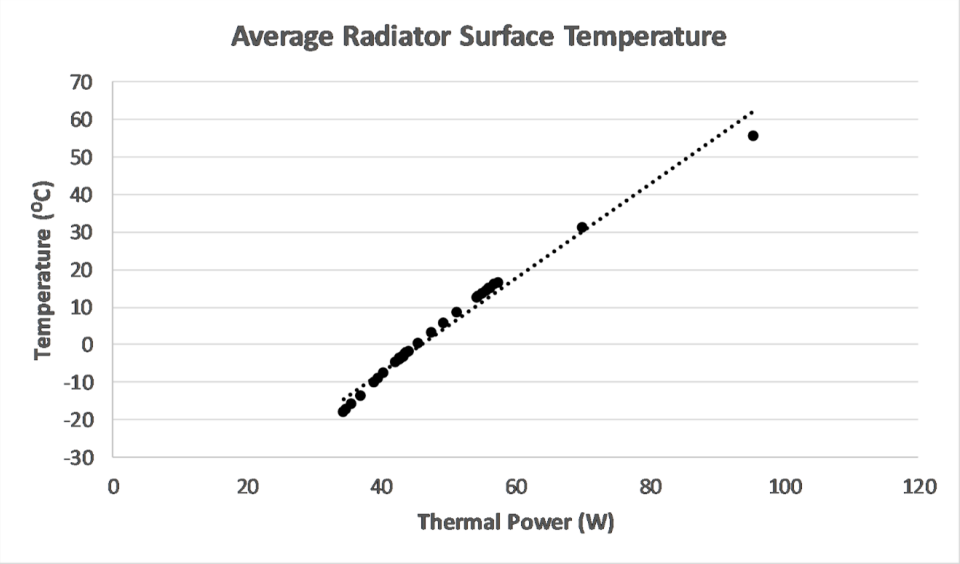

Fig. D.3: Average radiator temperature. Note the linearity of the curve, which implies that the radiator performance is governed by its physical characterisitcs, rather than the ACCS MPFL.

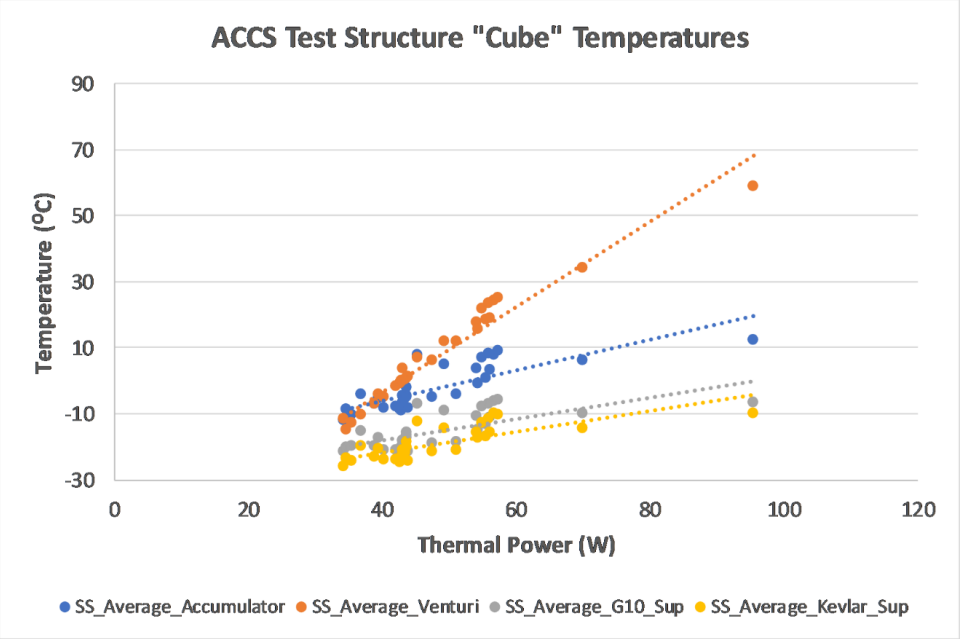

Fig. D.4: System temperatures of the ACCS Test-Cube as a function of thermal power. These temperatures indicate the relative gradients within the test-bench & help to identify parasitics within the system.

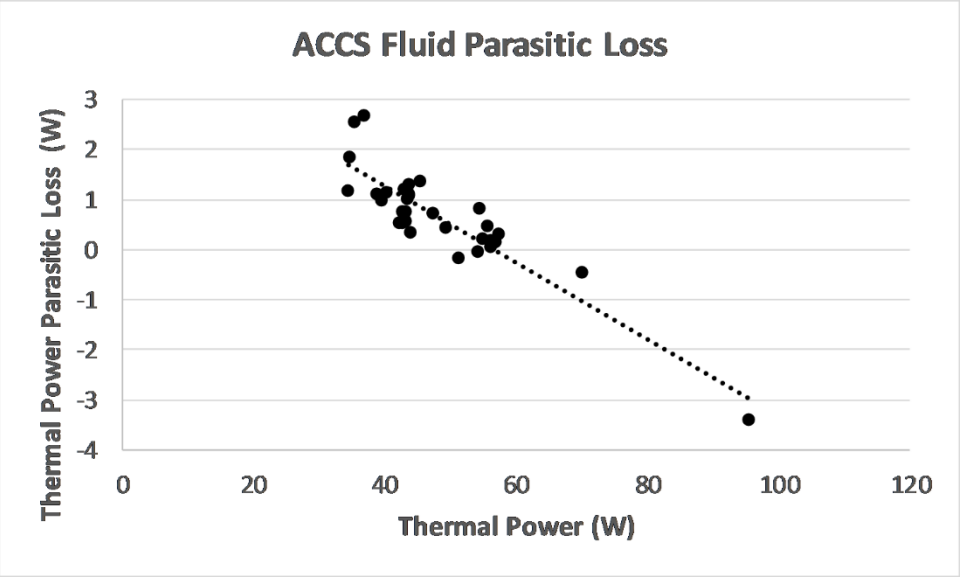

Fig. D.5: Parasitic losses within the ACCS MPFL. These are determined by comparison of the advective fluid balance (flow rate, emmersion TC's, and fluid properties) between the heat exchanger, radiator, and fluid lines.

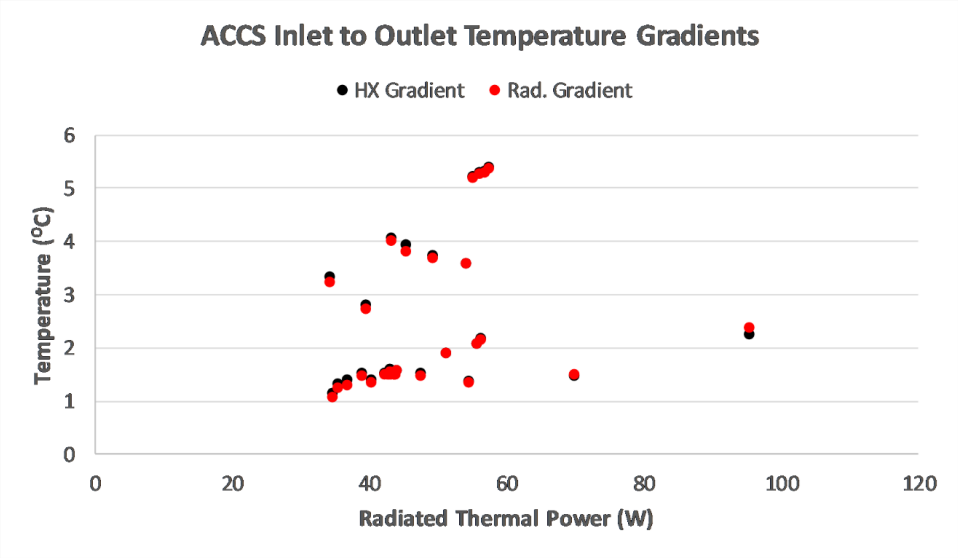

Fig. D.6: Thermal gradients within the ACCS heat exchanger & radiator. These indicate the relative isothermality of each component as a function of radiated thermal power.

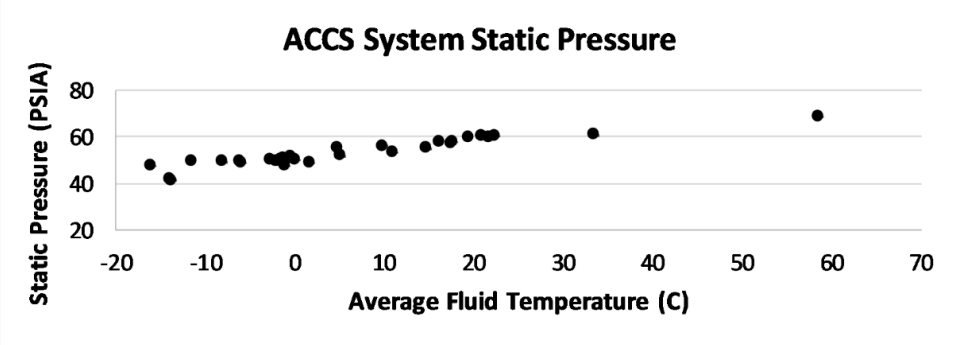

Fig. D.7: ACCS Test-Cube system static pressure as a function of temperature. Note the linearity, which indicates that the fluid accumulator was successfully balancing the internal pressure of the system.

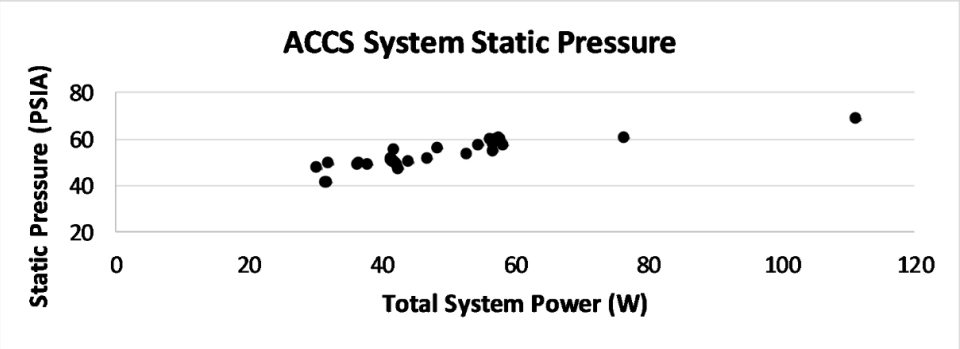

Fig. D.8: ACCS Test-Cube system static pressure as a function of total power. Note the linearity, which indicates that the fluid accumulator was successfully balancing the internal pressure of the system.

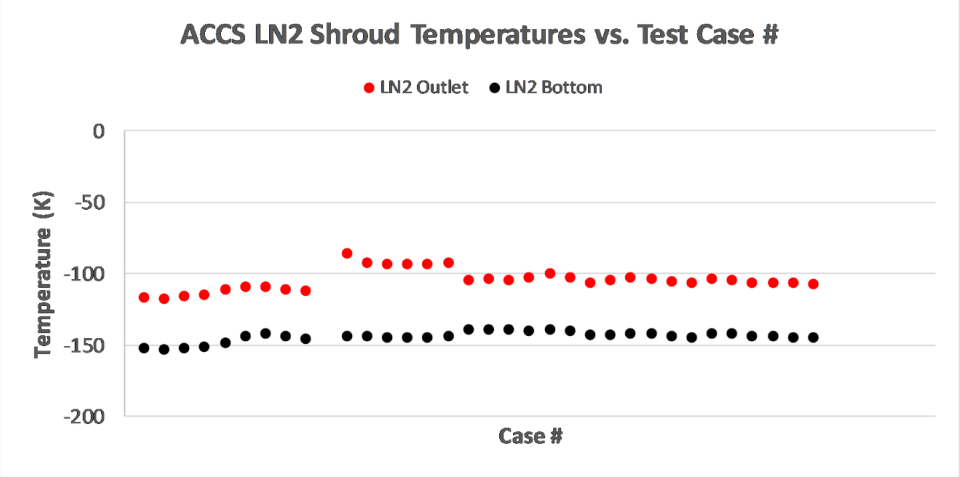

Fig. D.9: LN2 shroud temperature as a function of time (aka data set case #). The two shrouds were stable and fairly consistent in temperature. A gradient of approximately 30 degrees (on average) existed between them.

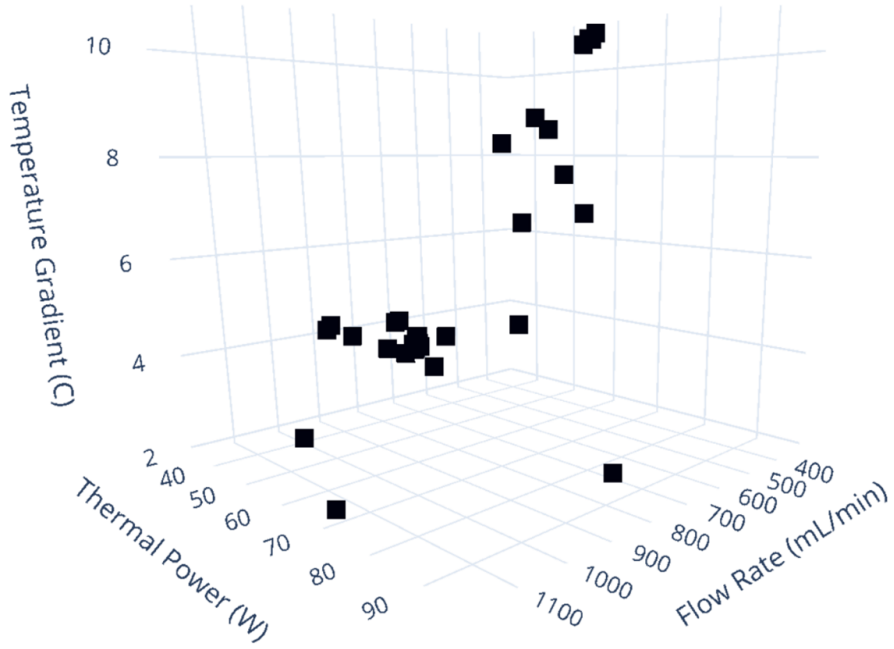

Fig. D.10: 3D chart of the radiator performance envelope. Given as a function of thermal power, flow rate, and surface temperature gradient (isothermality).

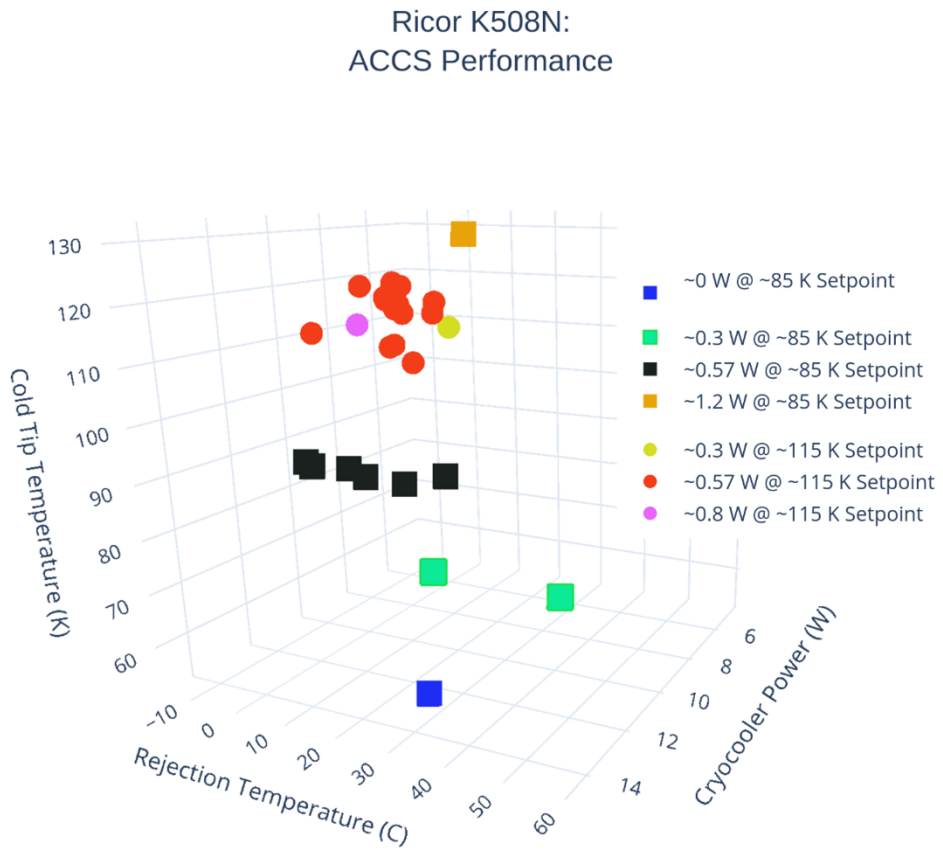

Fig. D.11: Secondary view of the Ricor K508N performance envelope as a 3D function.

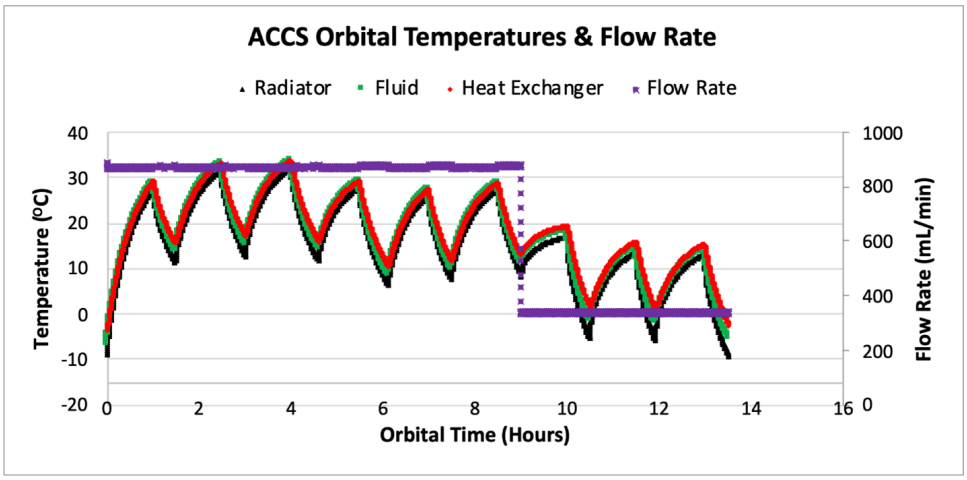

Fig. D.12: Second orbital simulation of the ACCS technology. Temperatures vs. orbital time & flow rate.

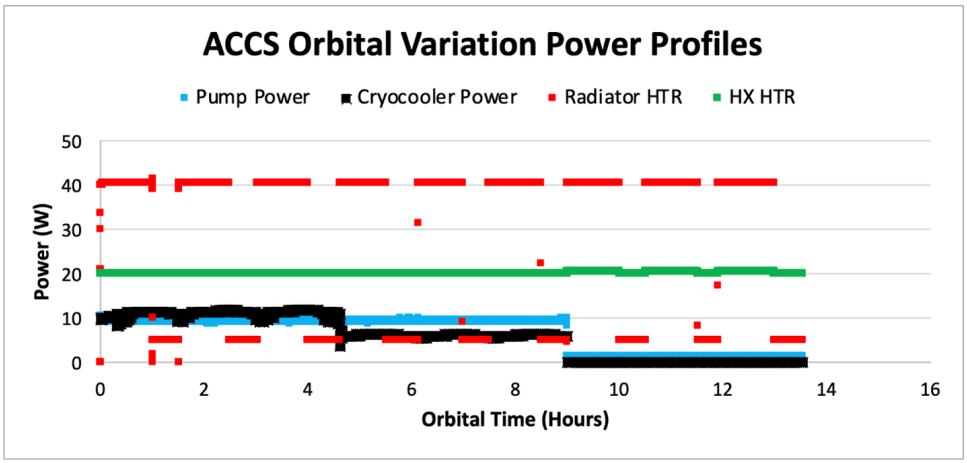

Fig. D.13: Second orbital simulation: Power values for active components.

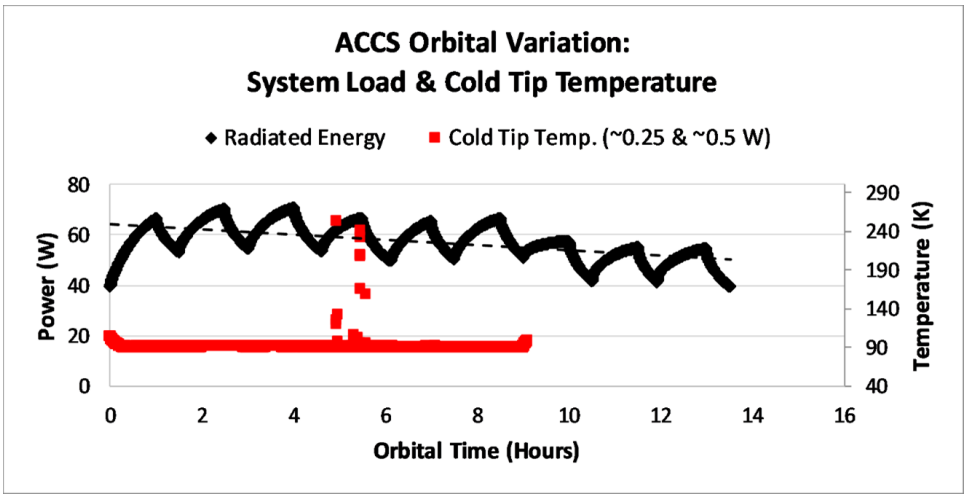

Fig. D.14: Radiated energy of the ACCS UAM radiator as a function of time. Cryocooler cold tip temperature.

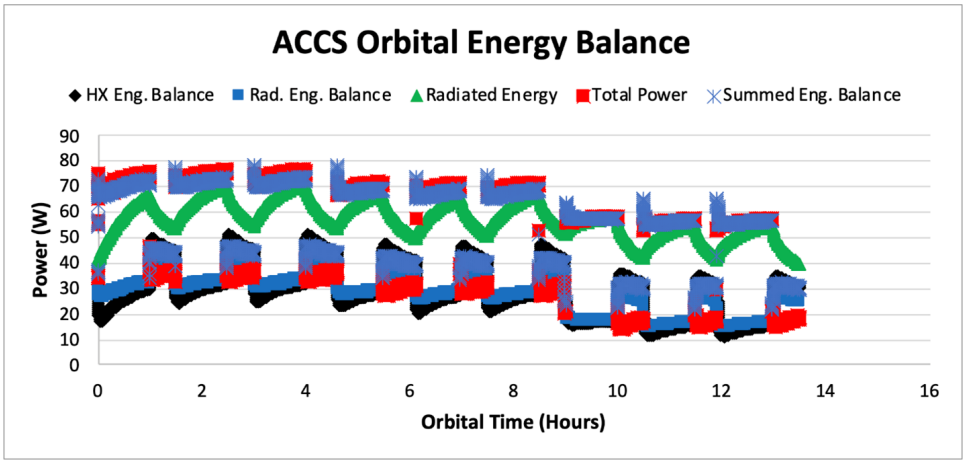

Fig. D.15: Orbital energy balance. Second orbital simulation.

CURRICULUM VITAE

Lucas S. Anderson

Published Conference Papers

- NASA LEARN: Forum Active Cooling for Multispectral Earth Sensors, Lucas Anderson, Charles Swenson, and Chad Fish, in *NASA LEARN Forum*, 2022.
- Active Thermal Control for the Multispectral Earth Sensors (ACMES) Mission, Lucas Anderson, Charles Swenson, and Chad Fish, Miguel Nunes, Robert Wright, in *Proc. SmallSat Conf.*, 2022.
- FINIS: New Methane Detector Technology for Point-Source Detection and Leak Rate Measurements, Bruno Mattos, Alan Marchant, Charles Swenson, Michael Kirk, Steve Brezenski, Lucas Anderson, Chad Fish, John Noto, Jason Powell, Nicholas Wallace, Mark schoeberl, in *Proc. SmallSat Conf.*, 2022.
- The Active Cooling for Multispectral Earth Sensors (ACMES) Mission, Charles Swenson, Lucas Anderson, Chad Fish, Bruno Mattos, Robert Wright, Mark Schoeberl, in *4S Int. Conf. Small Satellites*, 2022.
- Measurement Considerations for Exported Force and Torque (EFT) Testing of the Ricor K508N Cryocooler, Bill Zwolinski, Pascal Erne, Lucas Anderson, Joel Mork, Ian McKinley, in *Proc. American Mechanisms Conference*, 2022.
- Developments in CubeSat Active Thermal Control: A Review of the Active CryoCubeSat (ACCS) and Advanced Thermal Architecture (ATA) Projects for the JPL CubeSat Community, Lucas Anderson, Charles Swenson, A.J. Mastropietro et al, in *Proc. Internal "NASA" CubeSat forum (ICF))*, 2021.

- CubeSat Active Thermal Control: A review of the Active CryoCubeSat (ACCS) and Active Thermal Architecture (ATA) projects, Lucas Anderson, Charles Swenson, A.J. Mastropietro, Jonathan Sauder, Ian McKinley, and Mason Mok *Proc. NASA Thermal Fluids Analysis Workshop (TFAWS)*, 2021.

- Random Vibration, Exported Vibration, and Passive Isolation testing of the Ricor K508N Cryocooler, Lucas Anderson, Joel Mork, Charles Swenson, Bill Zwolinski, A.J. Mastropietro, Jonathan Sauder, Ian McKinley, *Proc. Cryogenic Engineering Conf. and Int. Cryogenic Materials Conf.*, 2021.

- CubeSat Active Thermal Control in Support of Advanced Payloads: The Active Thermal Architecture Project, Lucas Anderson, Joel Mork, Charles Swenson, Bill Zwolinski, A.J. Mastropietro, Jonathan Sauder, Ian McKinley, and Mason Mok, *SPIE Optics & Photonics Conf.*, 2021.

- The Active Thermal Architecture: Thermal Control for Small-Satellites, Lucas Anderson, Charles Swenson, A.J. Mastropietro, Jonathan Sauder, in *Proc. SmallSat Conf.*, 2021.

- The Active CryoCubeSat Project: System Modeling and Control Design, Bruno Mattos, Lucas Anderson, Randy Christenson, Charles Swenson, in *Proc. SmallSat Conf.*, 2021.

- The Active Thermal Architecture: Active Thermal Control for Small-Satellites, Lucas Anderson, Charles Swenson, A.J. Mastropietro, Jonathan Sauder, in *NASA Satellite Technology Partnership (STP)*, 2021.

- An Overview of the Design, Analysis, and Testing of a Novel Support Structure for Electro-Optical Detectors, Joel Mork, Lucas Anderson, Charles Swenson, in *wasatch Aerospace & Systems Engineering Conf.*, 2021.

- Active Thermal Architecture: Design and Status, Lucas Anderson, Charles Swenson, A.J. Mastropietro, Jonathan Sauder, in *Proc. SmallSat Conf.*, 2020.

- The Active Thermal Architecture: Active Thermal Control for Small-Satellites, Lucas Anderson, Charles Swenson, A.J. Mastropietro, Jonathan Sauder, in *NASA SSTP*, 2020.

- Active Thermal Control System With Deployable Tracking Radiator, Russell Babb, Lucas Anderson, Sarah Abdel-Motaleb, Charles Swenson, A.J. Mastropietro, Simon Luong, Elham Maghsoudi, Ian McKinley, Stefan Cappucci, in *Proc. SmallSat Conf. Poster Session*, 2019.

- CubeSat Active Thermal Management in support of cooled electro-optical instrumentation for advanced atmospheric observing missions, Lucas Anderson, Charles Swenson, Alan Marchant, A.J. Mastropietro, Elham Maghsoudi, Simon Luong, Ian McKinley, in *SPIE Optics & Photonics Conf.*, 2018.

- Enabling critically cooled instrumentation via active thermal management for CubeSats: The active CryoCubeSat Project, Lucas Anderson, Charles Swenson, Randy Davidson, A.J. Mastropietro, Elham Maghsoudi, Simon Luong, Ian McKinley, Stefano Cappucci, *Cryocooler Engineering Conf.* , 2018.

- The Active CryoCubeSat Project: Testing and Preliminary Results, Lucas Anderson, Ryan Davidson, Charles Swenson, A.J. Mastropietro, Elham Maghsoudi, Simon Luong, Ian McKinley, Stefano Cappucci, in *Proc. SmallSat Conf.*, 2018.

- Active Thermal Architecture for Cryogenic Optical Instrumentation, Sarah Abdel-Motaleb, Russell Babb, Lucas Anderson, Ryan Davidson, Charles Swenson, A.J. Mastropietro, Simon Luong, Elham Maghsoudi, Ian McKinley, Stefano Cappucci, in *Proc. SmallSat Conf. Poster Session*, 2018.

- The Active CryoCubeSat Project: Design and Status Lucas Anderson, Charles Swenson, A.J. Mastropietro, Elham Maghsoudi, Simon Luong, Douglas Hofmann, Scott Roberts, in *Proc. SmallSat Conf.*, 2017.